FORSCHUNGSZENTRUM
ROSSENDORF e.V.

FZR

FZR-65
February 1995

Proceedings of the
FOBOS workshop '94

Cracow, Poland

June 28 - 30, 1994

Edited by W. Wagner

Forschungszentrum Rossendorf e.V.
Postfach 51 01 19 · D-01314 Dresden
Bundesrepublik Deutschland

Telefon (0351) 591 3376
Telefax (0351) 591 3700
E-Mail wagner@fz-rossendorf.de

Fotos Yuri Tumanov, Dubna

FOBOS - collaboration

Proceedings of the

FOBOS workshop '94

held at the

Henryk Niewodniczansky Institute of Nuclear Physics

in

Cracow, Poland

June 28 - 30, 1994

Edited by W. Wagner

Rossendorf, Germany, 1995

Preface

The beautiful old king's town Cracow in Poland really was a nice place for the in the mean time fourth FOBOS workshop.

From June 28th till 30th the Henryk Niewodniczansky Institute of Nuclear Physics, the youngest member of the "DUBNA-ROSSENDORF-SOFIA-BERLIN-MOSCOW-CRACOW" - collaboration, was a kind host for scientists not fearing the long way, as from Iowa (USA) as from Cheboksary (Chuvashia), to meet in the centre of Europe for reviewing recent investigations in heavy ion physics and discussing on problems related to the scientific programme of the newly commissioned 4π - Fragment spectrometer FOBOS.

After coming into operation at the Flerov Laboratory of Nuclear Reactions (FLNR) of the JINR Dubna in March 1993, FOBOS has been tested round about during the first runs at the heavy-ion beam of the U-400M cyclotron in September and December 1993. For that reason, in continuation of the First International Conference on Set-up FOBOS held in Sofia(1990) and the FOBOS workshops held in Dresden (1991,1992) and in Dubna (1993), it anew was the time to invite people also from outside for an evaluation of the possibilities of this further child within the family of 4π-detector arrays for nuclear research.

Fifty participants from Armenia, Bulgaria, France, Germany, Poland, Russia and the USA took note of the first experimental results presented by H.-G. Ortlepp, the spokesperson of the FOBOS - collaboration, by C.-M. Herbach, J. Krueger, Yu. V. Pyatkov and W. Wagner. The apparatus parameters reached and the development of main subsystems of FOBOS were outlined in nine methodical talks. Certain advantages of FOBOS in comparison with respective multi - detector arrays, like, e.g., its relatively low detection threshold for heavy fragments, the excellent time-, angular-, energy- and charge resolutions within a broad dynamic range, etc., make FOBOS well-suited for basic research in heavy-ion physics, yet especially for the investigation of nuclear fission.

Ten review-lectures were given by invited speakers. It can be concluded that, in particular, the fragmentation of hot nuclei is a topic of high actuality, namely at intermediate energies, i.e., in the transitional

region of the Fermi-energy domain. Refined theoretical approaches for the description of the dynamics of heavy-ion induced reactions developed in recent time predict unexpected properties of hot nuclear matter waiting for its experimental proof. No wonder that several proposals made for further experiments at FOBOS are directed to the investigation of such phenomena. Other interesting ideas are related to the property of FOBOS to effectively register charged reaction products from events of medium multiplicity.

Generally new possibilities for the study of the mechanism of heavy-ion induced reactions will be opened in near future by the production of radioactive secondary beams at the U-400M. An important upgrade of this basic accelerator for FOBOS will be the installation of an ECR ion source now already in progress. Using the continuous beam than available, the operating efficiency of the FOBOS spectrometer will be increased substantially. Therefore, at present great efforts are made to complete the full configuration of FOBOS. The FOBOS forward-array is planned to be mounted early in 1995.

It is opportune to note here that an inalienable material and personnel support of these works is given by the Detector Laboratory of the Institute of Nuclear and Hadronic Physics (INHP) of the Research Centre Rossendorf Inc. and by the Henryk Niewodniczansky Institute of Nuclear Physics in Cracow. The FOBOS project is financially supported by the Federal Ministry for Education, Science, Research and Technology, Germany, under the contract Nr. 06 DR 671.

Since the edition of these proceedings was finished at a time when a further experimental run at FOBOS had been carried out (September 1994) and the Meeting of the Advisory Committee for Nuclear Physics of the JINR Dubna had taken place (November 1994), works carried on and the up-to-date collection of proposals for experiments at FOBOS are included. Hence, one can take these Proceedings of the FOBOS workshop '94 as a state-of-the-art report of the FOBOS collaboration.

Dubna, December 1994 *Wolfgang Wagner*

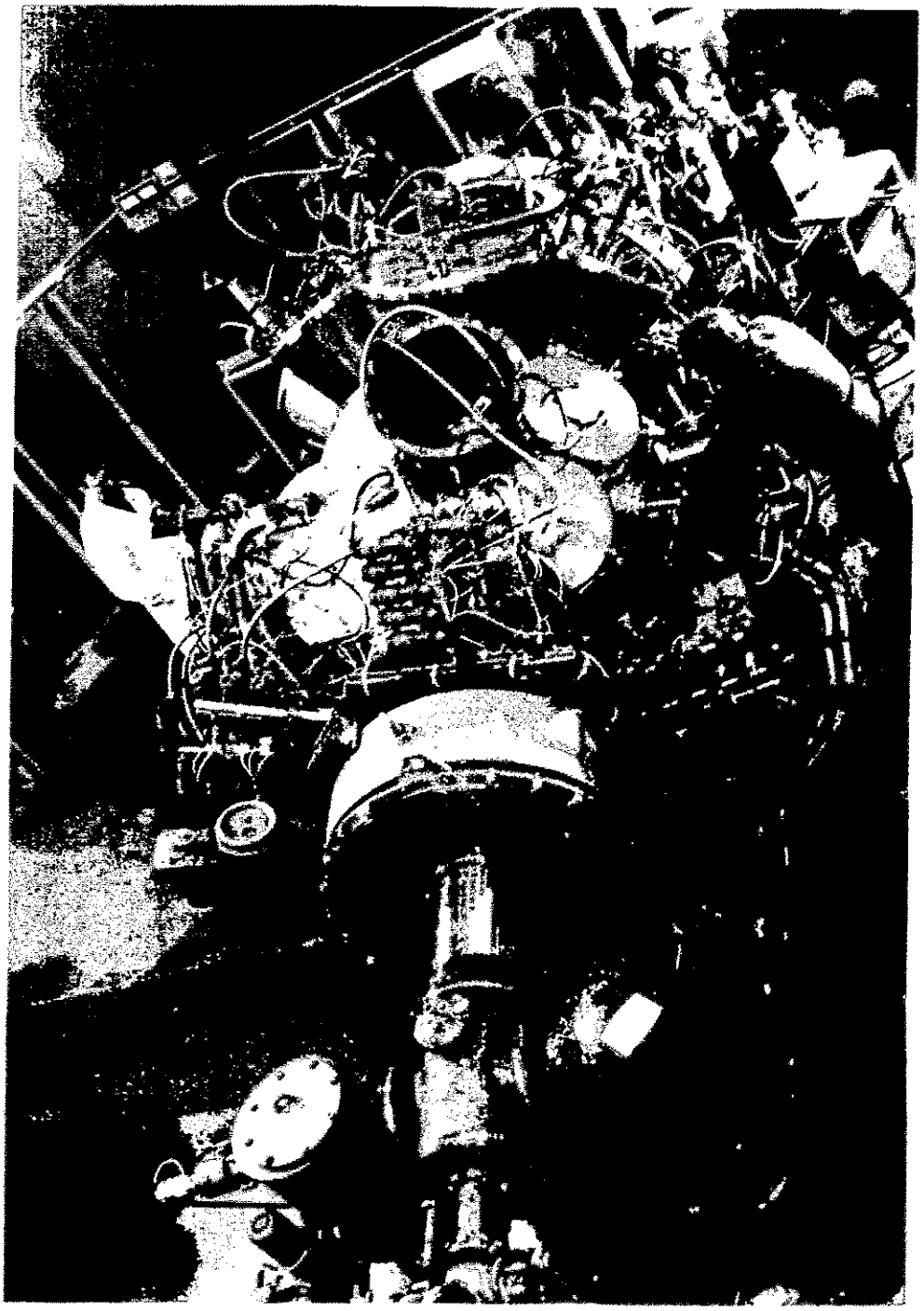

CONTENTS

II. Experiments at FOBOS in 1993 ÷ 1994
(First results obtained at FOBOS)

III. Experiment proposals for FOBOS

IV. Lectures given on the FOBOS workshop '94

V. References (Publications starting from 1991) 201

FOBOS WORKSHOP '94

Cracow, June 28 - 30 1994

PROGRAMME

Tuesday, June 28 1994

Chairman : A. Gobbi

9:00 - 9:10	A. Budzanowski	Opening of the FOBOS workshop
9:10 - 9:35	H.-G. Ortlepp	Present status of the FOBOS array
9:35 - 10:10	Yu.E. Penionzhkevich	Facilities of the Flerov Laboratory of Nuclear Reactions of the JINR Dubna
10:10 - 10:35	V.B. Kutner	Heavy ion beams from the U-400M cyclotron
Coffee break		

Chairman : A.A. Ogloblin

11:30 - 12:05	C.-M. Herbach	IMF emitted before and during fission studied in the reaction ^{7}Li (43 AMeV) + ^{232}Th at FOBOS
12:05 - 12:40	Yu.V. Pyatkov	Cold spontaneous fission of ^{244}Cm measured at FOBOS
12:40 - 13:05	W. Wagner	Alpha particles from ^{244}Cm ternary spontaneous fission measured at FOBOS
Lunch		

Chairman : H. Oeschler

15:30 - 15:55	G. Pausch	Activities of the Detector Laboratory of the INHP Rossendorf for FOBOS - Possible ancillary detectors for FOBOS
15:55 - 16:20	W. Wagner	The FOBOS scintillator shell and the phoswich forward array
16:20 - 16:35	A. Matthies	The FOBOS ionization chambers
16:35 - 16:50	A.A. Aleksandrov	The position sensitive avalanche counters of FOBOS (not held)
16:50 - 17:05	V.M. Doronin	The gas-handling equipment of FOBOS (not held)
17:05 - 17:20	G. Renz	The gas-vacuum system of FOBOS
17:20 - 17:45	Z. Sosin	A multianode gas ionization chamber
Coffee break		

Chairman : K.-D. Schilling

17:45 - 18:00	C. Umlauf	Computer control of the vacuum and gas status of FOBOS (not held)
18:00 - 18:15	S.I. Ivanovski	The computer network of the FLNR (not held)
18:15 - 18:30	H.-G. Ortlepp	Upgrade of the FOBOS data acquisition system
18:30 - 18:45	D.V. Vakatov	Upgrade of the FOBOS data acquisition software
18:45 - 19:00	D.V. Kamanin	Light charged particle multiplicities in the reaction ^{32}S (30 AMeV) + ^{197}Au studied at VICKSI - Some aspects of data analysis
19:00 - 19:15	H.-G. Ortlepp	Recent results obtained at FOBOS for the reaction ^{14}N (34 AMeV) + ^{197}Au

Wednesday, June 29 1994

Chairman : Yu. E. Penionzhkevich

9:00 - 9:35	A. Gobbi	Dissipative collisions at 20 - 200 AMeV
9:35 - 10:10	K. Grotowski	Thermodynamics of hot nuclei
10:10 - 10:45	J. Peter	Production and decay of hot nuclei in HIC

Coffee break

Chairman : K. Grotowski

11:30 - 12:05	V.I. Zagrebaev	The mechanism of light particle formation and the nucleus - nucleus interaction
12:05 - 12:40	A.A. Ogloblin	Deep quasielastic mechanism in nuclear reactions
12:40 - 13:15	C. Le Brun	Times from large fragment correlations
13:15 - 13:40	Yu.A. Muzychka	On the possibility of using (HI,αf) reactions for investigation of fission

Lunch

Chairman : H.-G. Ortlepp

15:30 - 16:05	H. Oeschler	Deep inelastic collisions in the reaction ^{40}Ar (31 AMeV) + ^{232}Th
16:05 - 16:30	J. Lukasik	CHIMERA - Microscopic description of heavy ion collisions at intermediate energies
16:30 - 16:55	R. Planeta	Missing momentum vector in the reaction ^{20}Ne (15 AMeV) + ^{197}Au

Coffee break

Chairman : E. Norbeck

17:30 - 17:55	A. Siwek	Multifragmentation in the reaction ^{32}S (30 AMeV) + ^{58}Ni studied at VICKSI
17:55 - 18:20	J. Krüger	Projectile fragmentation and fission in the reaction ^{32}S (30 AMeV) + ^{197}Au studied at VICKSI

Conference dinner

Thursday, June 30 1994

Chairman : J. Peter

9:00 - 9:35	E. Norbeck	Exotic decay channels in HIC : $^{12}C + ^{12}C \rightarrow 6\,\alpha$
9:35 - 10:10	V.D. Toneev	HIC - subthreshold production of heavy and strange mesons
10:10 - 10:45	N.V. Antonenko	Possible mechanism of light nuclei production in fusion

Coffee break

Chairman : W. Wagner

11:30 - 11:55	K.O. Oganessian	Experimental investigation of fast light particles from HIC
11:55 - 12:20	H.-W. Barz	Flow effects in intermediate energy HIC at 50 - 400 AMeV
12:20 - 12:45	A. Wieloch	The random walk model for quasielastic and damped collisions
12:45 - 13:10	K. Grotowski	Nuclear multifragmentation - the Coulomb focusing effect

Lunch

Chairman : P. Gippner

15:30 Round table discussion : New experiments at the FOBOS set-up

Moderators : K. Grotowski, A. A.Ogloblin, H.-G. Ortlepp, Yu.E. Penionzhkevich

Friday, July 1 1994

Excursion to the Wieliczka Salt Mine

Minutes of the FOBOS-workshop '94

held in June 28 - 30, 1994
at the IFJ Cracow, Poland
under the chairmanship of Prof. A. Budzanowski

The first experiments with FOBOS have been provided according to the decisions of the last collaboration meeting from May 1993 and the first results have been published /1,2/. The present state of development of FOBOS enables to continue the physical programme.

The lectures given at the workshop by all the invited speakers as well as the contributions of the members of the FOBOS collaboration are highly acknowledged. They were very helpful for the discussion of the further experimental programme at FOBOS. It is planned to publish the Proceedings of the FOBOS workshop '94. Therefore the authors are asked to send their camera-ready manuscripts (without page numbers) till Sept. 1, 1994 to H.-G.Ortlepp, FLNR, JINR Dubna, 101000 Moscow, Head Post Office, P.O.Box 79, Russia. Ready LATEX files can be sent per e-mail to:

Ortlepp@LJAR11.JINR.Dubna.SU
or by fax to:
(+7) (09621) 40594

Special attention has been paid to the following directions of investigation at FOBOS, where the specific features of this detector array are especially appropriate to obtain new physical information :

1. Competition and correlation between fission fragments and emitted particles (IMF, LCP) in asymmetric heavy ion collisions in the energy range of 30 - 60 AMeV.

2. Deep inelastic reaction processes at relatively high bombarding energy.

3. New possibilities to study reaction mechanisms by use of secondary (radioactive) beams at the U-400M.

4. Cold spontaneous fission.

The full geometry of the gas detector array of FOBOS will be available at the end of 1994. Further 10 FOBOS modules will be equipped with 70 CsI scintillation counters.
This configuration can be operated only if a sharp time reference signal (e.g. from the cyclotron RF) is available to provide time-of-flight measurement with a resolution of about 1ns. Otherwise the use of special START-detectors is necessary. This considerably decreases the geometrical acceptance of FOBOS.

The installation of an ECR-source at the U-400M cyclotron planned to be provided in the period from Oct. 1994 till Feb. 1995 will essentially improve the beam parameters, namely the present disadvantageous duty cycle (now about 10%) and the extraction coefficient (now less than 20%). This will result in an overall increase of the detection efficiency of FOBOS by at least a factor of 10.

The further completion of the FOBOS forward array is proposed to be provided by the Institute of Nuclear Physics, Cracow. It has been considered that the forward array is a necessary tool for FOBOS to enable a complete event reconstruction by the analysis of moment and energy balances.

The last experiment before the shut down of U-400M for its upgrade is planned to be provided in Sept. 15-30, 1994. The investigation of fission induced by ^{6}He ions is preferred if the parameters of the secondary ^{6}He beam achieved at that time at FOBOS allow the measurement of an angular distribution.
Otherwise the continuation of the investigation of the reaction ^{14}N (34 AMeV) on ^{197}Au will be prepared.

For the period of U-400M upgrade a measurement of the cold spontaneous fission of ^{250}Cf is planned.

The following experiment proposals for FOBOS have been discussed :

H.-G. Ortlepp et al. "Fission and IMF emission in the reactions ^{14}N and ^{20}Ne on ^{197}Au and ^{232}Th at energies of 35 - 50 AMeV." (beam 1 nA, 10 mm^2 beam spot, 20 FOBOS modules, 2 START-detectors, 200 h beam time per reaction or 5 nA continuous beam, no leading detector, 100 h beam time)

Yu.E. Penionzhkevich, S.V. Stepantsov "Investigation of fission at secondary ^{6}He beam." (beam 10^5 - 10^6 ^{6}He per second, 150 mm^2 or 400 mm^2 beam size at FOBOS, geometry and beam time not defined)

Yu.V. Pyatkov "Investigation of cold spontaneous fission." (50 μg/cm^2 ^{250}Cf source combined with a START-detector and shielded to avoid contamination, statistics 5*10^5 fissions, measurement time about 10 days)

Yu.A. Muzychka "Excitation functions (barriers) of fission in the (HI,αf) reaction." (beam 10^{10} ^{20}Ne per second, target 200 μg/cm^2 ^{176}Hf, forward detector to register coincident alpha particles, geometry and beam time not defined)

Yu.A. Muzychka "Fission modes in the reaction ^{20}Ne on ^{204}Pb." (beam 6 AMeV ^{20}Ne, geometry etc. not defined)

R. Wolski "Investigation of alpha particle induced reactions :
$\alpha + {}^{24}Mg \rightarrow {}^{12}C + {}^{16}O$
$\alpha + {}^{28}Si \rightarrow {}^{16}O + {}^{16}O$
$\rightarrow {}^{20}Ne + {}^{12}C$."
(E_α = 24 - 28 AMeV, no further comments)

A.A. Ogloblin "New deep quasielastic reaction mechanism in ^{16}O on ^{12}C at 30 AMeV." (no further comments)

Prof. A. Budzanowski (presently head of the JINR Programme Advisory committee for Nuclear Physics) asked all authors to send their proposals in time to this committee, which will meet in Nov. 1994 in Dubna.

/1/ Yu.V. Pyatkov et al., "Two-Velocities Measurement of Fragment Spectra in ^{244}Cm Cold Spontaneous Fission on the FOBOS Spectrometer " Proc. of the Workshop on Nuclear Fission and Fission - Product Spectroscopy, Chateau de la Baume, Seyssins, France, May 2-4, 1994

/2/ - A.A. Aleksandrov et al., "First Experiments with FOBOS" Proc. Fifth Int. Conf. on Nucleus - Nucleus Collisions, Taormina, Italy, May 30 - June 4, 1994: Ed. by M. di Toro and E. Minesco (Special issue of Nucl. Phys. A)

H.-G. Ortlepp (spokesperson of the FOBOS collaboration)
W. Wagner

FOBOS WORKSHOP '94

LIST OF PARTICIPANTS

N.V. Antonenko	Bogoliubov Laboratory of Theoretical Physics, JINR, Dubna, Russia
H.W. Barz	INHP, Research Centre Rossendorf Inc., Germany
A. Budzanowski	Henryk Niewodniczansky Institute of Nuclear Physics, Cracow, Poland
N.A. Demechina	Institute of Physics, Jerewan, Armenia
S. Dshemuchadse	INHP, Research Centre Rossendorf Inc., Germany
L. Freindl	Henryk Niewodniczansky Institute of Nuclear Physics, Cracow, Poland
W. Gawlikowicz	Henryk Niewodniczansky Institute of Nuclear Physics, Cracow, Poland
P. Gippner	INHP,Research Centre Rossendorf Inc., Germany and FLNR JINR Dubna
A. Gobbi	GSI Darmstadt, Germany
K. Grotowski	Henryk Niewodniczansky Institute of Nuclear Physics, Cracow, Poland
C.-M. Herbach	INHP, Research Centre Rossendorf Inc., Germany
S.I. Ivanowsky	Flerov Laboratory of Nuclear Reactions, JINR, Dubna, Russia
D.V. Kamanin	Flerov Laboratory of Nuclear Reactions, JINR, Dubna, Russia
S. Kliczewski	Henryk Niewodniczansky Institute of Nuclear Physics, Cracow, Poland
J. Krüger	INHP, Research Centre Rossendorf Inc., Germany
V.B. Kutner	Flerov Laboratory of Nuclear Reactions, JINR, Dubna, Russia
C. Le Brun	National Institute for Nuclear and Particle Physics, Caen, France
J. Lukasik	Henryk Niewodniczansky Institute of Nuclear Physics, Cracow, Poland
A. Matthies	INHP, Research Centre Rossendorf Inc., Germany and FLNR JINR Dubna
Yu.A. Muzychka	Flerov Laboratory of Nuclear Reactions, JINR, Dubna, Russia
E. Norbeck	Dept. of Physics and Astronomy, University of Iowa, Iowa City, USA
H. Oeschler	Technical University Darmstadt, Germany
K.O. Oganessian	Laboratory of Nuclear Problems, JINR, Dubna, Russia
A.A. Ogloblin	Kurchatov Institute of Atomic Energy, Moscow, Russia
H.-G. Ortlepp	INHP, Research Centre Rossendorf Inc., Germany and FLNR JINR Dubna
G. Pausch	Detector Laboratory, INHP, Research Centre Rossendorf Inc., Germany
Yu.E.Penionzhkevich	Flerov Laboratory of Nuclear Reactions, JINR, Dubna, Russia
J. Peter	National Institute for Nuclear and Particle Physics , Caen, France
R. Planeta	Henryk Niewodniczansky Institute of Nuclear Physics, Cracow, Poland
Yu.V. Pyatkov	Moscow Physics Engeneering Institute, Russia
G. Renz	INHP, Research Centre Rossendorf Inc., Germany and FLNR JINR Dubna
I. Sandrev †	Base for Development and Application,Bulgarian Academy of Sciences,Sofia
K.-D. Schilling	INHP, Research Centre Rossendorf Inc., Germany
R. Siudak	Henryk Niewodniczansky Institute of Nuclear Physics, Cracow, Poland
A. Siwek	Henryk Niewodniczansky Institute of Nuclear Physics, Cracow, Poland
I. Skwirczynska	Henryk Niewodniczansky Institute of Nuclear Physics, Cracow, Poland
Z. Sosin	Henryk Niewodniczansky Institute of Nuclear Physics, Cracow, Poland
S.V. Stepantsov	Flerov Laboratory of Nuclear Reactions, JINR, Dubna, Russia
A. Szczurek	Henryk Niewodniczansky Institute of Nuclear Physics, Cracow, Poland
V.D. Toneev	Bogoliubov Laboratory of Theoretical Physics, JINR, Dubna, Russia
C. Umlauf	INHP, Research Centre Rossendorf Inc., Germany and FLNR JINR Dubna
D.V. Vakatov	Laboratory of Computing Techniques and Automation, JINR, Dubna, Russia
W. Wagner	INHP, Research Centre Rossendorf Inc., Germany and FLNR JINR Dubna
A. Wieloch	Henryk Niewodniczansky Institute of Nuclear Physics, Cracow, Poland
T. Wilpert	Free University Berlin, Germany
R. Wolski	Henryk Niewodniczansky Institute of Nuclear Physics, Cracow, Poland
V.I. Zagrebaev	Chuvash State University, Cheboksary, Russia

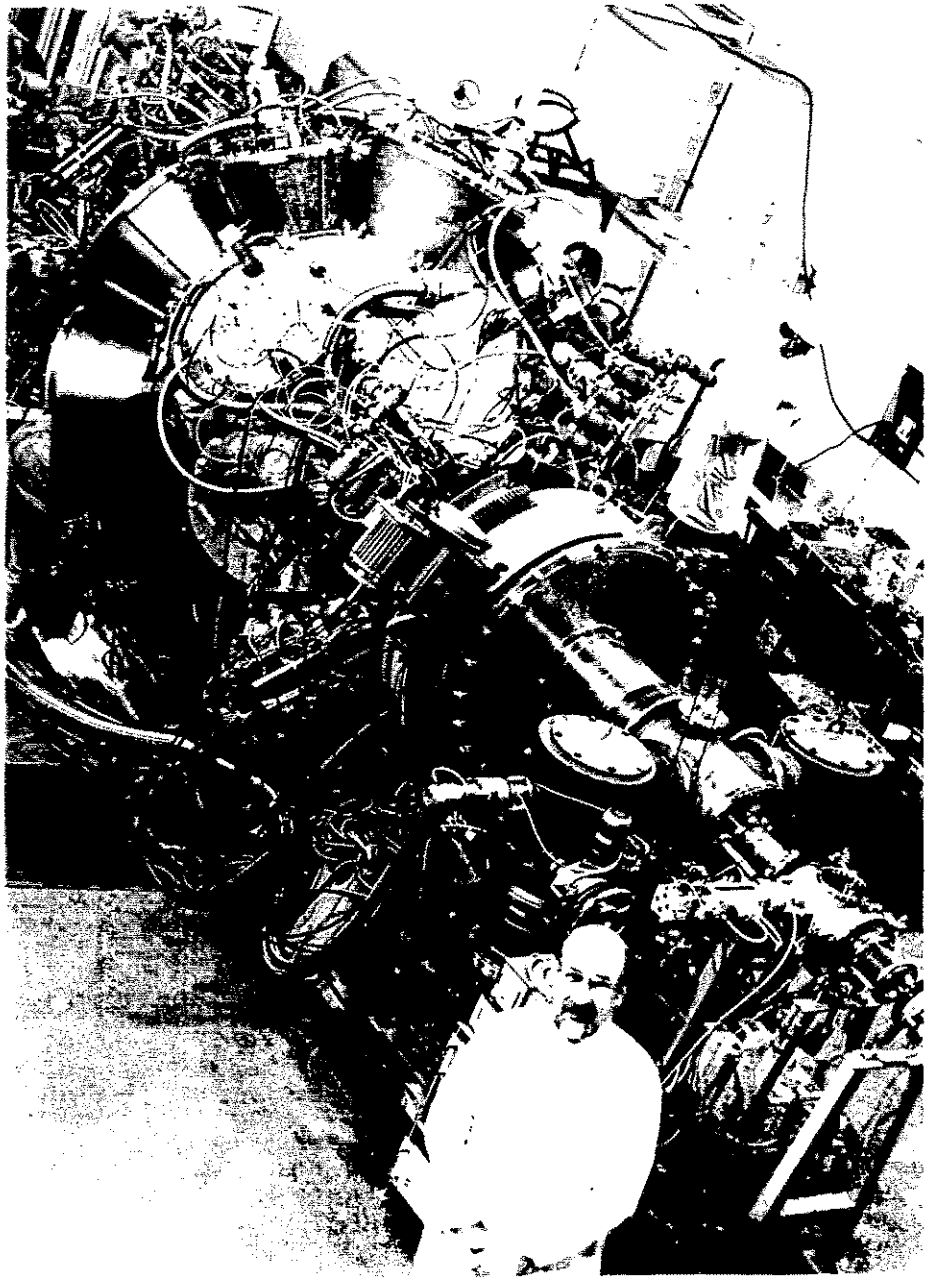

FLNR- Meeting , Ratmino, October 27 - 28 1994
"THE RESEARCH PROGRAMME OF THE FLNR IN 1995"

PLANNED RESEARCH ACTIVITIES AT FOBOS IN 1995

The FOBOS collaboration
DUBNA-ROSSENDORF-BERLIN-MOSCOW-CRACOW at the FLNR JINR Dubna

Spokesperson : Hans-Georg Ortlepp

Permanent address : Forschungszentrum Rossendorf e.V.
Institut für Kern- und Hadronenphysik
01314 Dresden / Germany
PF 51 01 19

Present address : JINR Dubna
Flerov Laboratory of Nuclear Reactions
141980 Dubna (Moscow region) / Russia

1. Upgrade of the FOBOS array

- Design and installation of a new target mechanism
- Installation of the phoswich forward array

2. Beam experiments

- Investigation of the competition and correlations between fission fragments (IMF), heavy residues and intermediate mass fragments as well as light charged particles in asymmetric heavy ion collisions in the energy range of 30 - 60 AMeV (400 h beam time)
- Search for new phenomena in deep-inelastic reactions at energies of 15 - 50 AMeV (300 h beam time)
- Study of direct reactions at 30 - 50 AMeV (150 h beam time)

3. Source experiments

- Study of cold spontaneous fission of ^{250}Cf

4. Simulations and data analysis

- Analysis of the data taken in the $^{14}N + ^{197}Au$ experiment BUU-, BNV- and QMD-simulations of heavy ion collisions
- Investigation of the response of FOBOS to different sources of LCP
- Calibration procedures for the FOBOS scintillator shell

5. The programme for FOBOS in 1995

The beam experiments at FOBOS have been started at the U-400M cyclotron in October 1993. In the first configuration 10 of altogether 30 detector modules were in operation. In 1994 FOBOS has been upgraded to 18 modules.

Events with two or three fragments have been recorded from the reactions ^{7}Li (43 AMeV) + ^{232}Th and ^{14}N (34 AMeV) + ^{197}Au. First results concerning correlations between fission and intermediate mass fragments have always been published but data analysis is by far not finished.

The remaining part of detector modules will be equipped until the end of 1994. In full configuration 30 modules each consisting of a position sensitive avalanche counter, an axial ionization chamber and 7 CsI(Tl) scintillator crystals will be available in 1995. In connection with a considerable upgrade of the cyclotron U-400M by the installation of an ECR source this allows continuation of the experiments at FOBOS with one order of magnitude higher efficiency.

The FOBOS forward array consisting of 92 phoswich detectors is planned to be mounted in the first half of 1995. The mechanics of this device has been designed by the INP Cracow and the detectors have been delivered by the HMI Berlin. The HV-supply has been developed in Dubna. Since the funding for this array was stopped by the German side the remaining part should be shared between INP Cracow (electronics and target mechanism) and FLNR Dubna (modification of the existing backward part of FOBOS).

The beam time considering the proposal for further investigation of massive fragment correlations in the reaction ^{14}N + ^{197}Au should be sufficient to record enough statistics of three-body events both at 34 and 55 AMeV. New information is expected concerning IMF emission after incomplete fusion (yields, spectra, time scales) in dependence on the excitation energy of the emitting system. The possibility to reconstruct the mass and the velocity of the intermediate system after incomplete fusion and the primary evaporation cascade is essential.

Further proposals concern other aspects of reaction mechanism. Analyzing the same raw data new understanding of the IMF emission as a very asymmetric fission or a cluster evaporation as well as concerning the competition between fission and survival of hot heavy residues is expected.

A new interesting problem proposed to be studied at FOBOS is the occurrence of large fluctuations in the hot neck region of the reseparating nuclei after deep inelastic collisions at 20 - 50 AMeV. Unusual dispersions of all observables have been predicted. Recording the target- and projectile-like fragments as well as the IMF emitted from the neck region such effects should be observable at FOBOS.

The study of exotic direct reactions like ^{24}Mg + ^{24}Mg $\rightarrow$ 3 ^{16}O is the topic of the first external proposal for FOBOS.

Further simulations are necessary to favor one of the last two experiments.

SOME POSSIBILITIES FOR EXPERIMENTAL RESEARCH AT THE FOBOS SETUP AT THE U-400M BEAMS

Yu. E. Penionzhkevich

The Flerov Laboratory of Nuclear Reactions, JINR

Heavy ion beams have opened wide prospects for investigating the properties of nuclear matter in its extreme state - at high values of the isotopic spin, deformation, angular moment and excitation energies. Such exotic states of nuclei are being studied at the Flerov Laboratory of Nuclear Reactions with the use of beams of heavy ions in the 5 MeV/A≤E≤100 MeV/A range. The Laboratory has three heavy ion cyclotrons - U-200, U-400 and U-400M. Their characteristics are given in Table I. The high beam intensity , up to $2\text{-}4\times10^{13}$ pps, is worth noting. It allows investigating processes with a cross-section approaching 10^{-35} cm^2. The FLNR accelerator facilities are constantly being developed. A tandem combining the U400 and U400M cyclotrons has been designed, extending the range of accelerated particles up to uranium and increasing the energy of the heavy Xe-U nuclei.

Table I.

Characteristics of the FLNR heavy-ion accelerator facilities

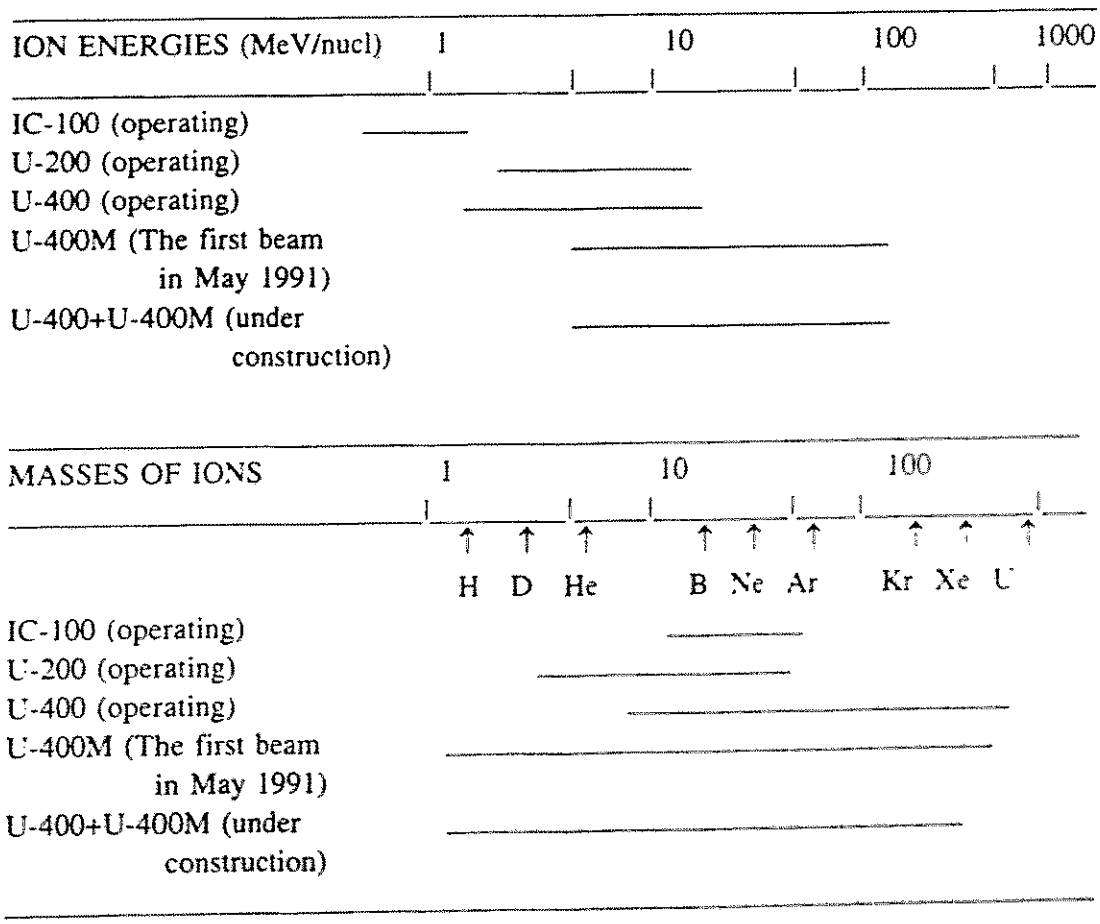

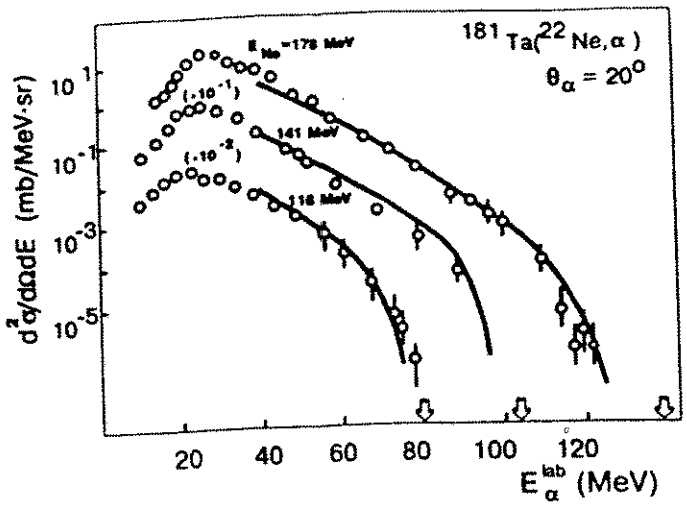

Fig. 1. Inclusive energy spectra of α-particles from the reaction $^{181}Ta(^{22}Ne,\alpha)$ measured at θ_α=20° for the beam energies 116, 141 and 178 MeV. The arrows indicate the maximum possible energies assuming a two-body reaction mechanism. The solid lines represent the result of theoretical calculations within the dissipative massive transfer model [2].

The U-400 cyclotron has been in operation over 10 years. It has been used for research in fields traditional for FLNR involving low energy physics(E≤20 MeV). Primarily, these are fusion reactions producing new trans-fermium elements. Hence, the Flerov Laboratory of Nuclear Reactions carries out experiments involving synthesis of trans-actinide nuclei in cold and hot fusion reactions [1].

It can be seen that for the fissioning nuclei the probability of survival of the compound nuclei with high excitation energy is relatively high. Of great interest are direct measurements of the cross-section of compound nuclei formation at beam energies of up to 40 MeV/A (E^*≈ 400 MeV). Such measurements are expected to be performed on the U-400M cyclotron in the $^{186}W(^7Li,xn)Ir^{175-169}$ reaction (where x=18-24). In this reaction compound Ir nuclei will be measured by means of registering their α-decay. The experiment is expected to be performed in collaboration with Lanzhou Institute of Physics (China).

Simultaneously with further increase of the energy of the bombarding particle the cross-section of the reactions producing compound nuclei begins to decrease dramatically due to the competitive emission of pre-equilibrium charged particles. This process takes place even at energies close to the Coulomb barrier. At energies of 10 MeV/A the cross-section of pre-equilibrium α-particle emission comprises a significant part of the total reaction cross-section. With the use of a magnetic spectrometer having high momentum resolution and multi-layer scintillating detectors, systematic investigation of energy spectra of light charged particles has been performed at FLNR in a wide range of energies up to the maximum available for a given reaction and determined by the energy conservation laws supposing a two-body nature of the mechanism for the production of fast particles (breakup-fusion) [2].

Fig. 1 displays the energy spectra for light particles produced in the ^{181}Ta +^{22}Ne reaction. The arrows in the diagram indicate the value of the two-body kinematic limit

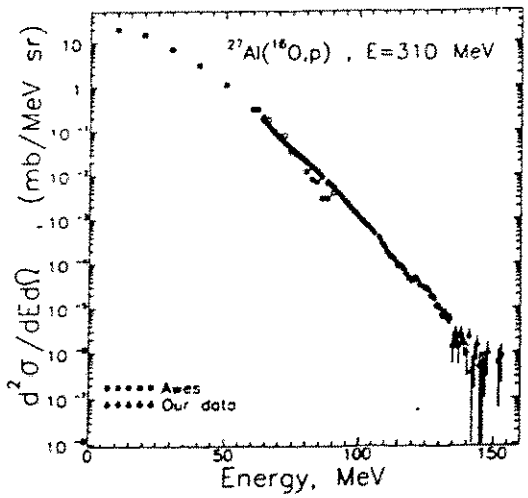

Fig. 2. Energy spectrum of protons produced in the reaction $^{27}Al(^{16}O,p)$ at E=310 MeV [3].

corresponding to the fusion of the projectile residue (I-LP) and the target and producing a final nucleus in the ground state. Application of a multi-layer scintillation telescope improved the sensitivity of such experiments. Fig. 2 presents the energy spectrum of protons measured with the aid of the telescope. It shows that at bombarding beam energies of 20 MeV/A, protons with energies up to 160 MeV are observed in the spectrum [3].

The following conclusions about the properties of energy spectra of light charged particles were made:

An increased yield for α-particle emission was observed in comparison to other particles, even to protons. The maximum of the energy spectrum is lying at light particle velocities less than the beam velocity, which provides evidence for a significant role of the relaxation processes at the stage of light particle emission. With an increase in the beam energy the peak of the double differential emission cross-section of light particles shifts in the direction of the energies corresponding to the beam velocity. However, even at energies a few tens of MeV/A in the spectrum of forward- peaked light particles there is a considerable dissipative contribution (E_c^b (α)<E_α<E_α^{beam}).At a smaller projectile mass A_1 the peak in the spectrum approaches V_{beam} which implies a decrease in the 'dissipative' part of the spectrum. With an increase in the projectile energy the maximum value of the differential cross-section $\frac{d^2\delta}{d\Omega dE}$ ($\frac{opt}{LP}$) at first rapidity rises(by a factor of ten at the transition from E_1=5 MeV/A to E_1=20 MeV/A), and then a saturation is observed. And finally, for low energies ~ 10 MeV/A the energy spectrum of light particles extends up to the two-body kinematic limit, corresponding to the fusion of the projectile residue (I-LP) and the target accompanied by the production of a final nucleus in the ground state, an abrupt change being observed at the very end of the spectrum. The analysis of these data as well as the results of other experiments show that the energy spectra of light charged particles reflect all possible interaction mechanisms between ions and nuclei at low and medium energies. In ref.[2] are pointed out 4 basic mechanisms for light particle production (Fig. 3).

1. The process of complete fusion of the nuclei with subsequent evaporation of light particles from the compound nucleus or from fission fragments. A distinctive feature of the evaporating particles is their low energy and isotropic angular distribution.

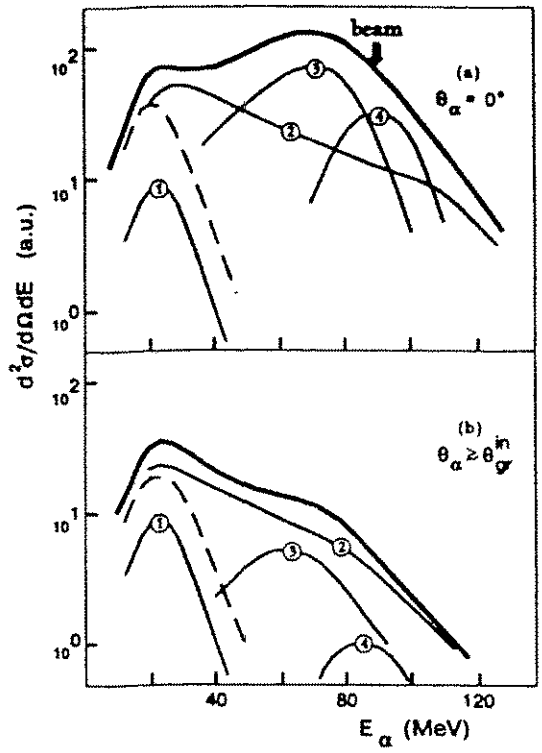

Fig. 3. Schematic picture of the α-particle energy spectra and of expected contributions of the four mechanisms of their formation at beam energies ~20 MeV/A: (1) - evaporation from the compound nucleus, (2) - incomplete fusion reaction, (3) - inelastic breakup, (4) - elastic breakup. The dashed line corresponds to the total yield of evaporative α-particles (from process (1) and from any other heavy residues formed in processes (2) and (3).

2. The initial two-body process of incomplete fusion with emission of only one pre-equilibrium particle . The light particles produced in this process can be fast (up to energies corresponding to the two-body kinematic limit E_{RP}^{max}) or slow. They can be formed both from the projectile nucleons (massive transfer) and the target nucleons (knock-on processes). These particles cannot be accompanied by other particles, however, they may be accompanied by slow (evaporation) light particles, neutrons or fission fragments.

3. The two-body primary process of few-nucleon transfer inelastic excitation (ΔN=0) followed by decay of the excited projectile-like nucleus. This process produces both fast and slow light particles. The former are accompanied by fast projectile-like fragments or other fast particles, the latter (when the dissipation is high) are accompanied only by slow fragments. This group of the mechanisms should also include the deep-inelastic excitation of the target and the projectile either without any mass transfer (ΔN=0) or with mutual exchange of an equal number of nucleons.

4. The quasi-inelastic break-up process of the incident ion and the quasi-inelastic process of knocking out a light particle from the target. It is rather difficult to experimentally discriminate between these processes , because the evaluation of the total cross-section of a three-body process requires integration over all the angles of the complementary fragment which can be performed only by means of a 4-π detector.

Naturally, this differentiation of the processes is purely conventional. Besides, it depends on the mass and energy of the incident ion. However, it points to the possibilities for investigating the light particle emission mechanism. This investigation should be performed with the aid of detectors allowing high-sensitivity measurement (geometrical efficiency, capability to use high intensity in the initial beam) of the energy spectra and cross-sections, as well as granularity and geometry close to 4-π making it possible to measure the correlations, the multiplicity and angular distributions. FLNR has two facilities with these features - the 4-π detector of multiple events FOBOS and the system of multilayer scintillation telescopes in conjunction with the BGO-ball from LAMPF (Los Alamos) to be installed at the beam of the U-400M cyclotron.

Table II. Characteristics of the FOBOS facility.

Table II
Characteristics of the FOBOS facility.

Particle	PPAC + BIC		CsI Shell *[15mm]*		ARGUS array *BGO [20mm]*		Array "O-deg." *CsI [150mm]*	
	E min MeV/A	E max MeV/A	E min MeV/A	E max MeV/A	E min MeV/A	E max MeV/A	E min MeV/A	E max MeV/A
H	---	---	1.5	63.0	2.0	100.0	5.0	250.0
He	0.2	4.0	2.0	65.0	2.0	101.0	5.0	253.0
Li	0.2	5.0	2.0	82.0	3.0	125.0	7.0	320.0
IMF (Z<15)	0.15	10.0	----	----	4.0	150.0	----	----
FF	0.15	10.0	----	----	----	----	----	----

Taking into account the characteristics of the 4π-setup FOBOS it seems possible to solve the following physical problems:

1. Investigation of the induced binary, ternary and multiple fission of heavy nuclei in reactions with ions from ^{7}Li to ^{40}Ar at energies E_I<30 MeV/A, including light nuclei fission with emission of two clusters ($Si^{28} \rightarrow O^{16}+C^{12}$, $Mg^{24} \rightarrow {}^{12}C+{}^{12}C$).
2. Investigation of the emission mechanism for fast charged particles in coincidence with residual nuclei decay products at $E_I \leq 30$ MeV/A. In that case the charged particle may act as a trigger for the selection of a defined state of the residual nucleus according to its excitation energy and angular momentum.
3. Investigation of the target nucleus fragmentation and measurement of the particle multiplicities and their correlations, including those for backward angles. These experiments can provide an explanation for the characteristics of the transformation processes with

complete momentum transfer and complete fragmentation New mechanisms are expected to be revealed here, including the semiperipheral mechanism of deep-inelastic transfer with the formation of intermediate mass fragments from the neck region at the energy of $E_l \approx 40$ MeV/A, predicted by M. Di Toro [5].

4. Investigation of the multifragmentation process near the $E_l \geq 40$ MeV/A threshold.
5. Reactions with radioactive beams.

One of the topical tasks pursued at many heavy ion research centres of the world is investigation with radioactive beams. FLNR also has a programme in this field. With the advent of radioactive nuclei beams it has become possible not only to study their properties, but also to study reactions induced by them. The main problem of producing secondary beams is linked with the synthesis of radioactive nuclei. At present, direct reactions producing radioactive nuclei at energies up to 20 MeV/A and projectile fragmentation reactions at energies of $E_b \geq 50$ are the most effective. In the first case neutron and proton stripping and pickup reactions are used, as well as transfer reactions and (p,2p), (p, 3p) and (p, He^3) reactions on hydrogen targets using inverse kinematics. In these reactions the energy resolution of the secondary beam can be 1-3%. Using the maximum intensity of low energy ions (10^{13} 1/s), beams of ^{6}He,^{9}Li, ^{12}Be, etc. can be produced with intensities up to 10^6 1/s.

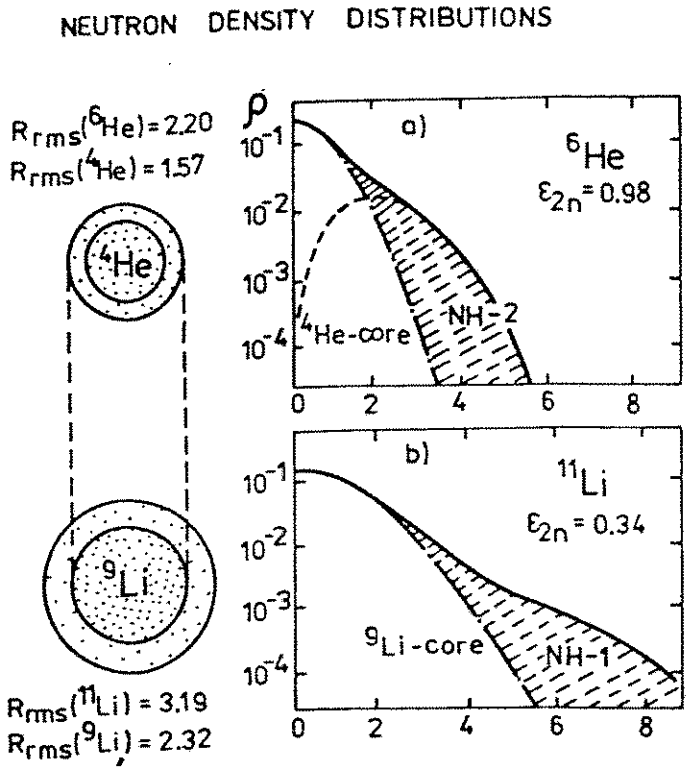

Fig. 4. A presentation of the neutron density distributions for ^{6}He and ^{11}Li, showing the difference between two types of halo (1st type - ^{11}Li, 2nd type - ^{6}He).

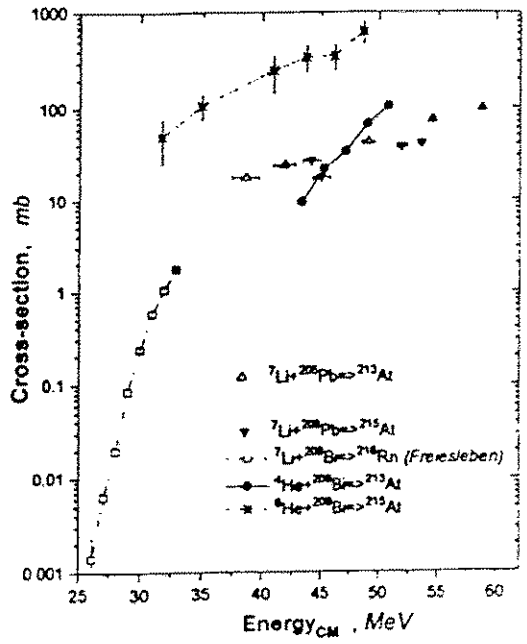

Fig. 5. Excitation function for the fusion-fission reactions ^{6}He + ^{209}Bi for $E_{c.m.}$=30-50 MeV. Other reactions cross sections are shown for comparison.

Radioactive beams of secondary low energy particles are of great interest in investigating nuclear reactions induced by them close to the Coulomb barrier. A few years ago it was demonstrated that in the very neutron-rich nuclei of light elements, such as ^{11}Li, ^{14}Be and others, there can be neutron halos characterised by a large root-mean-square radius of the neutron distribution (Fig. 4) [6]. Thus, for the ^{11}Li nucleus this radius proved to be close to the neutron distribution radius of the uranium nucleus (~13 fm). This allowed a number of predictions to be made about the peculiarities of interactions of such nuclei - a relatively high cross-section of the sub-barrier nuclear fusion of halo nuclei producing weakly-excited compound nuclei, sub-barrier valence neutron transfer and excitation of the soft mode of giant resonances. At the U-400M cyclotron in FLNR radioactive beams of ^{6}He, ^{9}Li and $^{11-12}$Be have been produced with energies of ~10 MeV/A. They have been used to investigate elastic scattering and fusion-fission reactions.

With the use of the secondary ^{6}He beam the excitation function of the fusion-fission reaction ^{6}He +^{209}Bi in the $E_{C.M.}$= 30-50 MeV was studied [7] (Fig. 5). A comparison of the cross-section data for ^{209}Bi fission by ^{4}He and ^{6}He nuclei shows that at the same excitation energy the cross-section of ^{209}Bi fission by ^{6}He nuclei is about 5 times larger than that for ^{4}He nuclei. A large energy shift (~15 MeV) between the thresholds of these reactions also attracts attention. It is indicative of an increase of the Coulomb barrier of the fusion for the nuclei having the neutron halo (^{6}He). Unfortunately, the restrictions imposed by the target thickness in the case of using low-energy primary beams do not allow a large yield of secondary nuclei, particularly in the mass range of A≥10. Fragmentation reactions are used for such radioactive beams at primary ion beam energies of $E_{I.}$=50-100 MeV/A. For producing a secondary beam of exotic nuclei it is necessary to use beams of highly-neutron-rich or

neutron-rich nuclei, such as ^{36}Ar, ^{36}S, ^{48}Ca and others. At FLNR experiments are under way using reactions with ^{6}He nuclei produced in the $^{7}Li(40\ MeV/A)+CH_2$ reaction. With the aid of the transport system of the primary nucleus it has become possible to shape a ^{6}He beam with an energy resolution of 1%. The fragment-separator COMBAS project [8] is under way. Fragmentation reactions of the high-intensity primary beam of the U400M cyclotron will be used to produce beams of radioactive nuclei. The parameters of this separator are given in Table III.

Table III. Expected Parameters of the COMBAS fragment-separation with other existing separators.

Comparison of Fragment Separators.

Device	Ω[msr]	Δp/p[%]	Max.[T-m]	Res. Power
LISE	1.0	5.0	3.2	800
FRS	0.7-2.5	2.0	9-18	240-1500
A 1200	0.8-4.3	3.0	5.4	700-1500
RIPS	5.0	6.0	5.76	1500
COMBAS	6.4	20	4.5	4360

REFERENCES

1. Yu.Ts Oganessian, in: Classical and Quantum Mechanical Aspects in Heavy Ion Collisions. Lecture Notes in Physics, v.33, Springer, Heidelberg, 1975.
2. V. Zagrebarev, Yu. Penionzhkevich. Preprint GANIL P 93 20. 1993.
3. K.O. Oganessian et al., in: Contributed Papers 5th Int. Conf. on Nucleus-Nucleus Collisions, Taormina, Italy, 1994, p.65.
4. M.K. Jones et al., Phys. Rev., C48 (1993) 2800.
5. M. Colonna, M. Di Toro et al., Preprint LNS 03-03-94, Catania, 1994.
6. A.A. Ogloblin, in: Proc. Int. School-Seminar on Heavy Ion Physics (Eds. Yu.Ts. Oganessian, Yu.E. Penionzhkevich R. Kalpakchieva), Dubna 1993, v.1, p.28.
7. N.K. Skobelev et al., in: Proc. Int. School-Seminar on Heavy Ion Physics (Eds. Yu.Ts. Oganessian, Yu.E. Penionzhkevich R. Kalpakchieva), Dubna 1993, v.1, p.51.
8. A.G. Artukh et al., Nucl. Instr. Meth. A306 (1991) 123.

THE U-400M CYCLOTRON EQUIPPED WITH AN ECR ION SOURCE

G.G. Gulbekian, V.B. Kutner

Joint Institute for Nuclear Research, FLNR, Dubna, Russia

The cyclotron complex U-400 + U-400M [1] was designed to produce ion beams from protons to uranium with energies of 100 ÷ 20 AMeV. Recent progress in the development of intense ECR ion sources changed this project. The main reason is that heavy- ion beams up to about Xe can be produced with similar energy and even higher intensity at the U-400M by using an ECR ion source. Ions heavier than Xe would have a slightly lower energy.

In fig. 1 the maximum reachable ion energies are compared for the cyclotron-tandem U-400 + U-400M with a PIG ion source and for the U-400M with an ECR ion source.

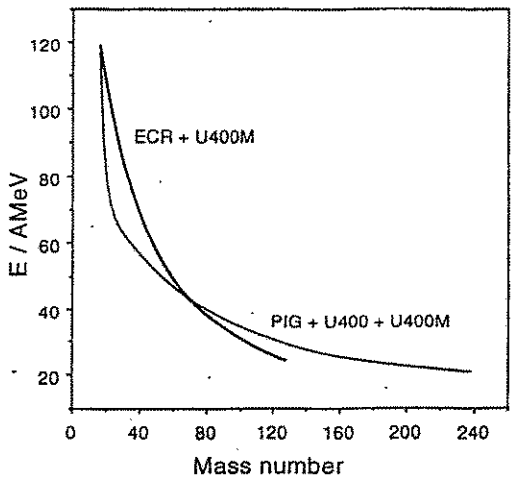

Fig. 1 Maximum ion energies for the cyclotron-tandem with a PIG and for the U-400M with an ECR ion source.

The development of the DECRIS-14 ECR ion source was started in the FLNR at JINR, Dubna, in 1989. The main configuration is that of the MINIMAFIOS source [2]. The clystron-based UHF generator works in a frequency range of 14.0 - 14.5 GHz with maximum output power up to 2 kW [3]. The DECRIS-14 has been tested with N_2, O_2 and Ar. Some typical ion currents obtained in 1993 are given in tab. 1. Further efforts have been made to increase the charge state and the intensity as well.

Tab. 1 Ion currents (eμA) from the DECRIS-14 at an extraction voltage of 10 kV.

Ion / Charge state	4+	5+	6+	7+	8+	9+	11+	Support gas
N	270	92	17					
O		160	87	26				
Ar					70	24		Helium
Ar				120	110	70	15	Oxygen

The axial injection into the U-400M was developed by the end of 1994. The mounting of the DECRIS-14 to the cyclotron is in progress now and is planned to be finished by the end of the first quarter in 1995. A second ECR ion source developed in collaboration with the GANIL Research Centre, France, will be installed at the U-400M in the course of 1995.

The dependence of the U-400M ion energy on the ratio of the ion charge to its mass number (q/A) is drawn in fig. 2.

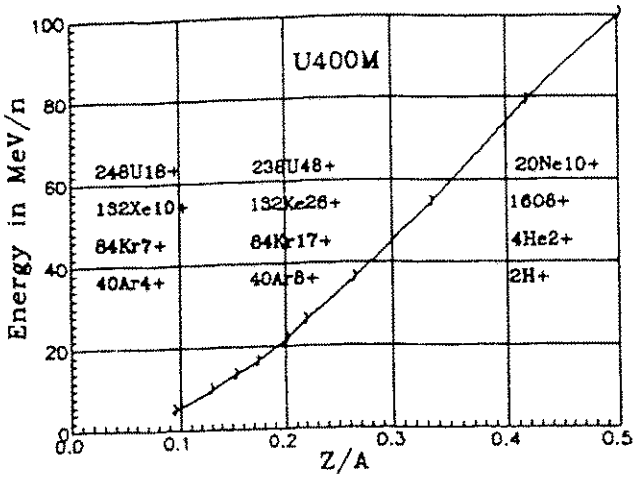

Fig. 2 . The dependence of the U-400M ion energies on the q/A ratio.

The beam parameters of the U-400M using a PIG ion source are listed in tab. 2.

Tab. 2 Beam parameters of the U-400M + PIG (1994).

Ion	Energy (AMeV)	Intensity (pps)
$^{4}He^{1+}$	30	$1 \cdot 10^{14}$
$^{6}Li^{2+}$	50	$1 \cdot 10^{12}$
$^{7}Li^{2+}$	44	$6 \cdot 10^{12}$
$^{12}C^{3+}$	30	$2 \cdot 10^{13}$
$^{14}N^{3+}$	26	$2 \cdot 10^{13}$
$^{14}N^{4+}$	40	$2 \cdot 10^{12}$
$^{14}N^{5+}$	60	$6 \cdot 10^{11}$
$^{16}O^{3+}$	15	$2 \cdot 10^{13}$
$^{16}O^{+4}$	30	$3 \cdot 10^{12}$
$^{16}O^{5+}$	48	$2 \cdot 10^{12}$
$^{20}Ne^{2+}$	6	$5 \cdot 10^{13}$
$^{20}Ne^{4+}$	20	$5 \cdot 10^{12}$
$^{20}Ne^{5+}$	30	$3 \cdot 10^{12}$
$^{20}Ne^{6+}$	46	$1 \cdot 10^{12}$
$^{40}Ar^{4+}$	6	$2 \cdot 10^{13}$
$^{40}Ar^{5+}$	10	$1 \cdot 10^{13}$

Evaluated parameters of the U-400M equipped with the ECR ion source are given, for comparison, in tab. 2.

Tab. 2 Source intensities (pps), beam intensities (pps) and energies (AMeV) of heavy-ion beams of the U-400M upgraded with DECRIS-14.

Ion	ECR intensity	Beam intensity	Energy
$^{7}Li^{2+}$	$3\cdot10^{13}$	$6\cdot10^{12}$	41
$^{12}C^{4+}$	$8\cdot10^{14}$	$5\cdot10^{13}$	54
$^{12}C^{6+}$	$1\cdot10^{12}$	$2\cdot10^{11}$	98
$^{14}N^{5+}$	$8\cdot10^{14}$	$5\cdot10^{13}$	61
$^{16}O^{5+}$	$(2\div5)\cdot10^{15}$	$2\cdot10^{13}$	49
$^{20}Ne^{6+}$	$2\cdot10^{14}$	$2\cdot10^{13}$	45
$^{36}S^{10+}$	$3\cdot10^{13}$	$4\cdot10^{12}$	49
$^{40}Ar^{14+}$	$(2\div7)\cdot10^{12}$	$1\cdot10^{12}$	58
$^{48}Ca^{14+}$	$5\cdot10^{12}$	$1\cdot10^{12}$	44
$58Ni^{6+}$	$1\cdot10^{13}$	$2\cdot10^{12}$	6.5
$^{84}Kr^{17+}$	$1\cdot10^{13}$	$2\cdot10^{12}$	22
$^{129}Xe^{26+}$	$(1\div3)\cdot10^{12}$	$6\cdot10^{11}$	22
$^{181}Ta^{29+}$	$(2\div4)\cdot10^{11}$	$8\cdot10^{10}$	15
$^{238}U^{24+}$	$2\cdot10^{12}$	$4\cdot10^{11}$	6

References

[1] G.N. Flerov et al., Report JINR 9-84-55, Dubna, Russia, 1984 (in Russian).
[2] R. Geller et al., Rev. Sci. Instrum. 56(8) (1985) 1505
[3] A. Efremov et al., Proc. of the Internat. School-Seminar on Heavy Ion Physics, Dubna, May 10-15, 1993, JINR E7-93-274, Dubna, Russia, 1993, v.2., p.506.

I. The 4π - Fragment spectrometer FOBOS

at the Flerov Laboratory of Nuclear Reactions of the JINR Dubna

Status and methodical contributions

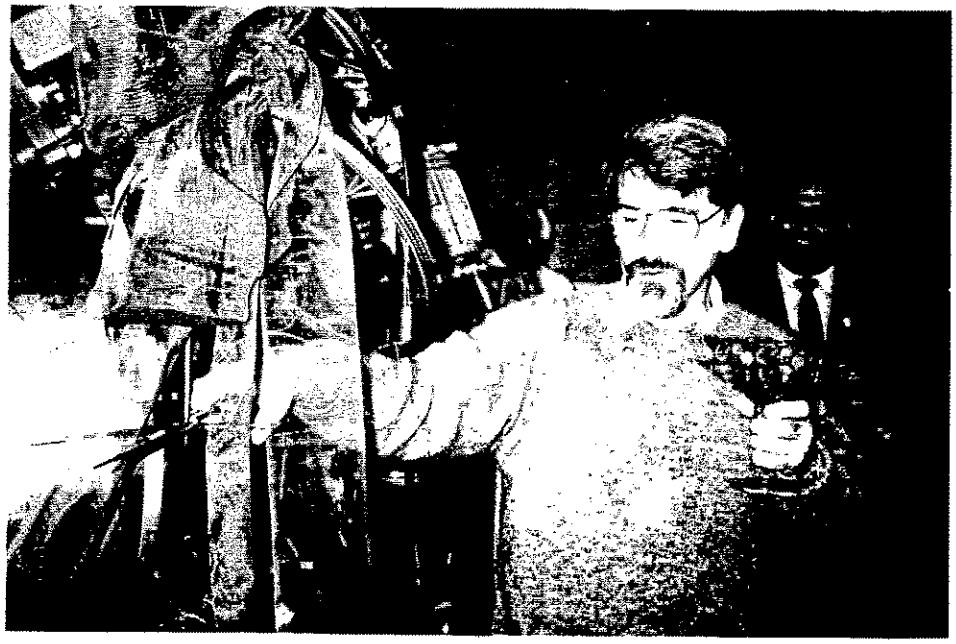

THE 4π -FRAGMENT SPECTROMETER FOBOS - STATUS AND FIRST PRELIMINARY RESULTS

H.-G.Ortlepp[1], M.Andrassy[1], G.G.Chubarian, M.Danziger[2], L.Dietterle[1], A.S.Fomichev, P.Gippner[1], C.-M.Herbach[1], A.I.Ivanenko, I.V.Kolesov, A.Matthies[1], D.May[1], Yu.Ts.Oganessian, Yu.E.Penionzhkevich, V.N.Pokrovskij, G.Renz[1], L.A.Rubinskaja, V.E.Shuchko, O.V.Strekalovski, V.V.Trofimov, V.M.Vasko W.Wagner[1]

Joint Institute of Nuclear Research, Dubna
P.O. Box 79, 101000 Moscow, Russia

[1] *On leave from: Research Center Rossendorf inc., Institut für Kern- und Hadronenphysik*
[2] *On leave from: TU Dresden, Sektion Physik*

K.Heidel, K.D.Schilling, W.Seidel, H.Sodan[3]
Research Center Rossendorf inc., Institut für Kern- und Hadronenphysik
PF 19, 0-8051 Dresden, FRG
[3] *Zentralinstitut für Kernforschung Rossendorf*

H.Fuchs, D.Hilscher, H.Homeyer, W.v.Oertzen, P.Ziem
Hahn-Meitner-Institut Berlin, Bereich Schwerionenphysik
1000 Berlin 39, Glienicker Strasse 100

G.Pausch
Hahn-Meitner-Institut Berlin, Freie Universität Berlin

B.A.Burova, S.V.Radnev, I.D.Sandrev
Laboratory for Technical Developments-Physics
1184 Sofia, Bulgaria

1 Introduction

The 4π detector of multiple events FOBOS (ref. 1,2) is dedicated to heavy ion induced reaction studies in the projectile energy range of 10 - 100 AMeV. At such energies a wide variety of questions concerning energy, momentum and angular momentum transfer, as well as the formation and decay mechanisms of hot nuclear systems call for exclusive correlation measurements in 4π geometry. Presently several 4π systems are being or have been installed at different laboratories (see e.g. ref. s 3-5). The FOBOS detector was proposed for the planned U400 + U400M cyclotron complex as a universal spectrometer for the expected energy range. After several modifications the following concept was chosen: as the intermediate energy range may be reached at the U400M only for relative low mass heavy ions, the experiments will be performed in "direct kinematics". The products to be registered may be roughly divided into three groups - light penetrating evaporation products and heavier fragments, both emitted in all directions of the laboratory frame, and forward emitted products from early reaction stages. Respectively, the FOBOS detector (fig.1) is devided into three subsystems - an array of 210 scintillation detectors, 30 combinations of position sensitive avalanche counters with axial ionization chambers and a forward array of phoswich counters.
Prototypes of all detectors have been tested with radioactive sources and in several runs at the U-400 cyclotron of the FLNR. For this purpose a small reaction chamber ("mini-FOBOS") has

been installed at one U-400 beam line. In march '93 a beam of 34AMeV ^{14}N ions has been extracted from the new U-400M cyclotron and transported to a Ni target in the FOBOS setup. From two operating chambers first data have been taken. Presently (may '93) FOBOS is being prepared for the first experiment devoted to ternary fission.

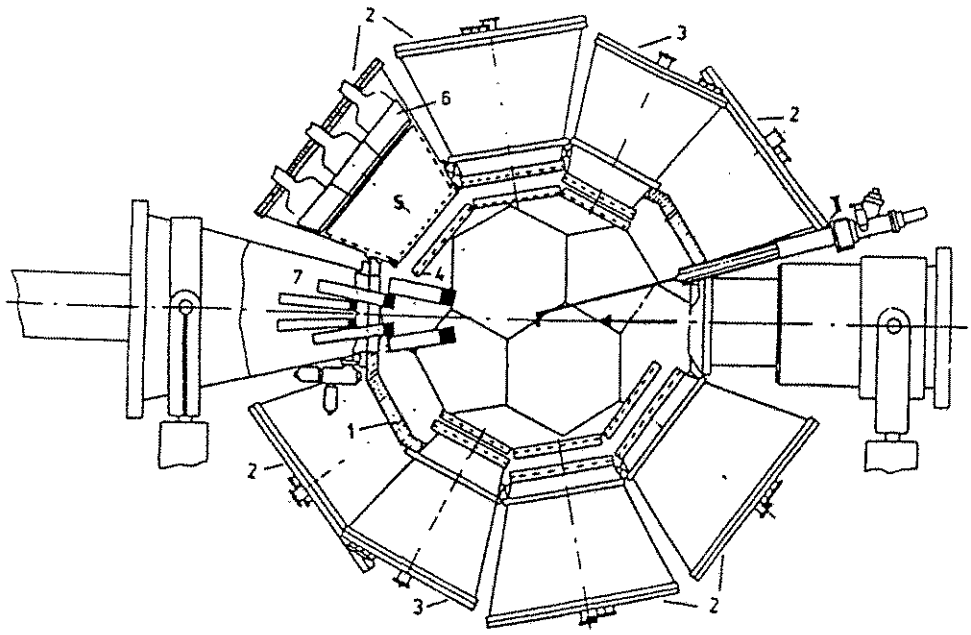

Fig. 1: Cut of the FOBOS Detector

1- Vacuum camber
2,3- Detector module cases
4- Position sensitive avalanche counters
5- Bragg ionization chamber
6- Scintillation counter
7- Forward array

2 Basis concept

The main task of FOBOS is to identify as many as possible charged particles from multiple events and to determine their velocity vectors. A multi-detector principle was chosen with such detector cells which can handle only one particle of a certain multiple event. As it is impossible to cover the whole expected dynamic ranges of particle masses and kinetic energies with one shell of counters of a certain type, different types have been combined.
The granularity is governed by the expected multiplicities: 30 position sensitive avalanche counters (PSAC) and 30 axial ("Bragg") ionization chambers (BIC) will registrate 2...6 heavy and intermediate mass fragments. To stop also penetrating light charged particles 210 scintillation counters are placed behind the BIC's.
For projectile fragments and preequilibrium particles emitted under very forward angles ($< 15^0$) parts of the ARGUS detector (ref.6) are foreseen to be moved to Dubna.
The counters are arranged in 30 modules placed on the facettes of a polyeder (12 regular pentagons and 20 regular hexagons). Two pentagons are used for the beam input and exit, the last containing also the forward detectors in an extended cone.
The physical quantities of the detected particles are derived from the counter signals as shown in fig. 2. The flight path (target-PSAC) amounts to 50 cm and the depth of the BIC to 25 cm.

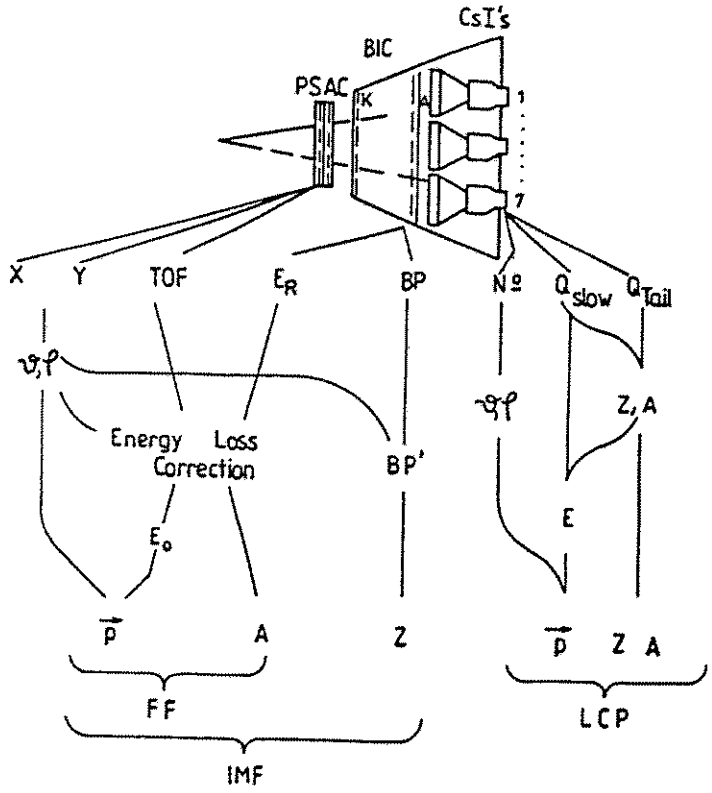

Fig. 2: Derivation of measured quantities from the detector signals

3 Mechanical construction, evacuation and gas supply

All conical detector modules are held in their position by a central support frame acting also as a vacuum chamber (fig. 1). The input beam pipe and the exit cone rest on pillars. The whole construction may be turned by $\pm 90^0$ to set every module, if necessary, in a horizontal position where it may be put in or out with the help of a manipulator.

Every counter gas volume is connected through two valves with collector rings, through which evacuation and gas supply is performed (fig. 3). To compensate the gas deterioration a pressure stabilized flow - through regime is utilized. The pressure ranges amount to 200...800 Pa of pentane for the avalanche counters and to 10...100 kPa of P-10(90% argon + 10% methan) for the ionization chambers. The maximum possible gas flow foreseen corresponds to one exchange in three hours.

The evacuation part was successfully tested. A vacuum of $2 \cdot 10^{-6}$Torr within the FOBOS ball has been achived using four turbo molecular pumps. All Bragg ionization chamber cases and the manipulator for handling them were delivered from Bulgaria. All the gas flow and pressure control units including supporting valves and pumps of the gas supply system are mounted mechanically and electrically. A system for on-line gas mixing for the Bragg chambers was mounted and added to the FOBOS setup.

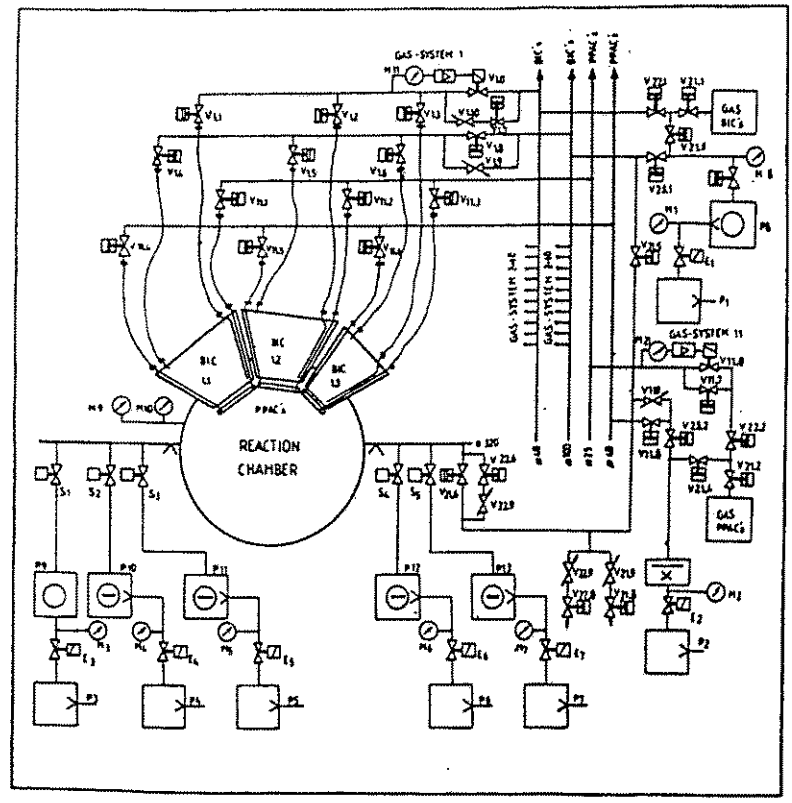

Fig. 3: Scheme of the evacuation and gas supply system of FOBOS. Only three modules are shown, the others are connected with the collectors in parallel

All these components can be controlled either manually or remotely by the SIEMENS SX automation system /7/ (fig.4), which was successfully installed and tested in 1992. Basic software for process visualisation on X-terminals of the changing status of the evacuation and gas supply system has been developed (fig.5). The actual pressure values can be observed at 64 different positions of the system. The valves and pumps can be switched over in a simple manner by mouse clicks.

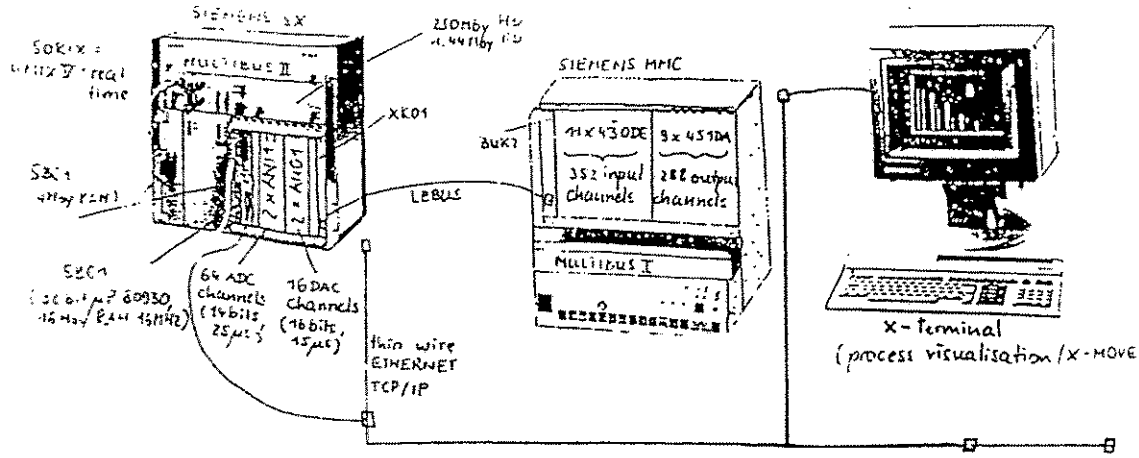

Fig. 4: SIEMENS SX automation system hardware

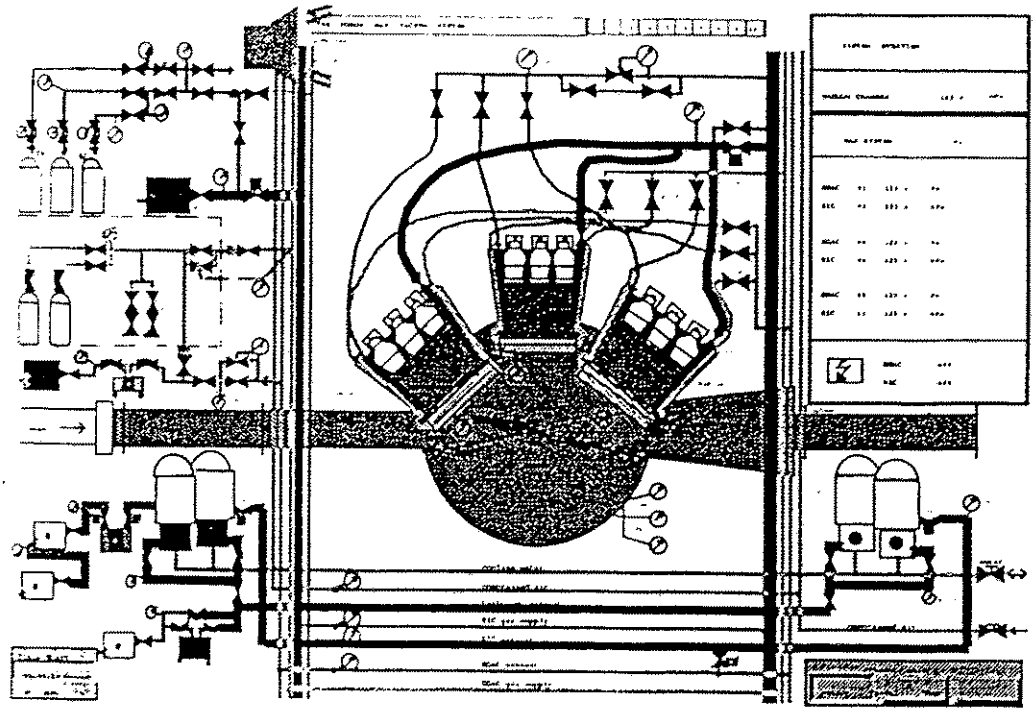

Fig. 5: FOBOS process visualisation X-graphic display

4 The Gas-Filled Detectors

The PSAC's are based on the principles described in ref.7. One cathode foil delivers the timing signal and two anode wire planes serve as coordinate grids. Three $120\mu g/cm^2$ polyester foils are utilized, the outer ones acting as windows and the central one with $40\mu g/cm^2$ gold layers on both sides as cathode. The counter frames have pentagonal and hexagonal outer shapes and leave open circular sensitive areas of 243 mm and 327 mm diameter, respectively. The sensitive gaps amount to 3.0 mm with a maximal tolerance of $\pm 50\mu m$, $30\mu m$ Cu - Be wires 1.0 mm spaced serve as anodes. Every two neighbouring wires are connected with one conductive strip capacitively coupled with a delay line. The two lines with 1.4 ns/mm specific delay and 560Ω impedance are matched with resistors at one end and coupled to readout amplifiers with 560Ω "cold" dynamical input resistance and 800 fold current amplification at the other end. The detector bias is fed to the cathode. The cathode readout circuit deliveres an 80 fold amplified current signal for timing and a charge signal of 150 mV/pC sensitivity for pulse height analysis needed for checking purposes. All channels are protected against damage in the case of spark discharges in the gas. The circuits are placed directly on the counter frame.

Every counter is being tested with an alpha source. A small transmission avalanche counter is used as time reference to determine the time resolution and the dependence of the PSAC timing signal on the position. This dependence (fig. 6, left) is stored in an individual correction file for each PSAC. After correction (fig. 6, right) the remaining time shift does not exceed ±100ps. A PSAC is accepted if the overall time resolution (including the reference counter) does not exceed 750ps FWHM and the leakage rate is less than 10^{-4}Torr l s^{-1}.

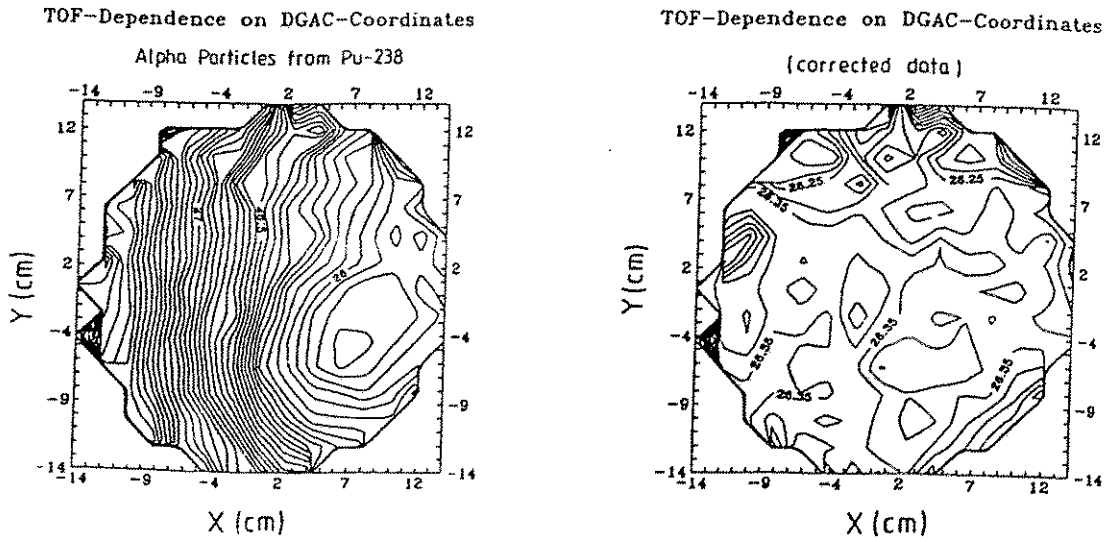

Fig. 6: Position dependence of the PSAC timing signal before (left) and after (right) correction

The axial ionization chambers cover cones of $\pm 13.8^0$ and $\pm 17.4^0$ with entrance window diameters of 285 mm and 385 mm, respectively. The window foils are supported by a twofold structure - a heavy carrier of 94% transparency and an etched nickel mesh with 2.7 mm cells of 66% transparency. As the last number causes the most serious solid angle restriction, better solutions for this mesh are being developed. Cells smaller than 3 mm are necessary, because otherwise the foil would not withstand 100 kPa gas pressure needed to stop most of the intermediate mass fragments within 25 cm depth. The field shaping is performed by copper strips coated every 5 mm on a teflon insulator cone. The voltage devider provides equal potential steps e.g. a homogenious field.

The advantages of a homogenious field, also for chambers with large apertures, was shown in ref. 9. The Frisch grid consists of two perpendicular planes of 1 mm spaced $50\mu m$ thick CuBe wires. This solution has been chosen to compensate the mechanical tension deforming the carrying ring. The anode placed 10 mm behind the Frisch grid is made of $10\mu m$ aluminized mylar which may be penetrated by light charged particles to be registered in the scintillation counters.

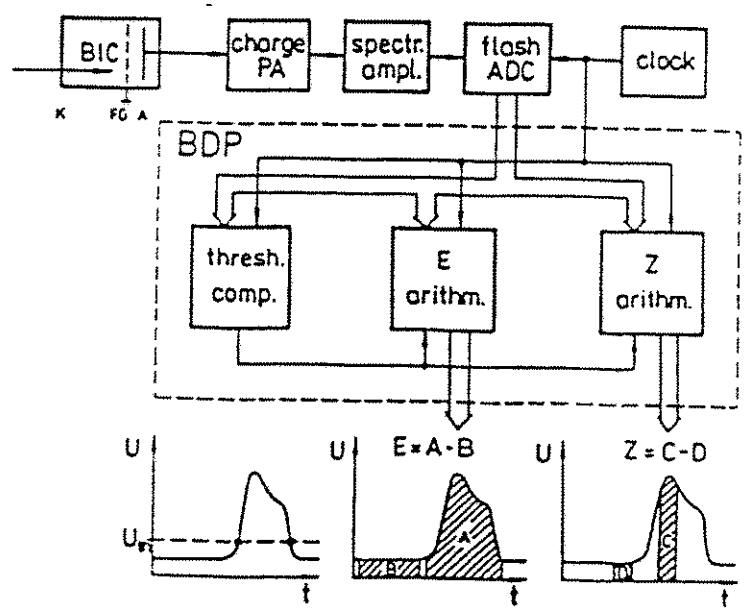

Fig. 7: Pinciple of the new signal processing method for Bragg peak spectroscopy

At a gas pressure of 100 kPa an anode potential of + 8kV is necessary (the entrance

window acts as cathode and is grounded). The electron drift time of up to $4\mu s$ would cause large ballistic deficit in the case of conventional pulse shaping. Therefore a digital processing method is utilized which derives the energy and Bragg peak height from digitized signal samples. The principle is illustrated schematically in fig. 7, more details are given in ref. 10.

5 Scintillator Shell

The gas-filled detectors of the FOBOS array are not able to registrate penetrating light charged particles (LCP). Therefore the gas detector part of FOBOS will be surrounded by scintillation counter [11]. The CsI(Tl) scintillator shell consists of 210 hexagonal crystals (200 mm and 150 mm diameter) placed behind the Bragg ionizations chambers covering them with a geometrical efficiency of 73.4%. The number of scintillators joined together in one module is equal to seven. Scintillator thicknesses of 1.5 cm and 1 cm have been chosen for the angles $\theta = 16^0 - 52^0$ and $\theta = 53^0 - 164^0$ respectively.

The crystals polished at the front side and rough at the back side are coupled via hollow conical light guides to the photomultipliers of type FEU 173 ($\oslash$ 150 mm) and FEU 167 ($\oslash$ 100 mm). Efforts have been made to enhance the light collection efficiency and to avoid inhomogenities due to the large dimensions of the crystals. Typical energy resolutions for Pu alpha particles of 6 - 7% have been achieved.

LCP were discriminated up to Z = 3 by a pulse shape analysis method [12] integrating the current pulse of the photomultiplier with the help of two charge-to-digital converters (QDC) within the time gates of δt_1 = 0-400 ns and δt_2 = 1600-3600 ns (fig. 8). The reaction shown in this example is 9.1 AMeV ^{20}Ne + ^{58}Ni. The detector was placed at 45^0 with respect to the beam direction.

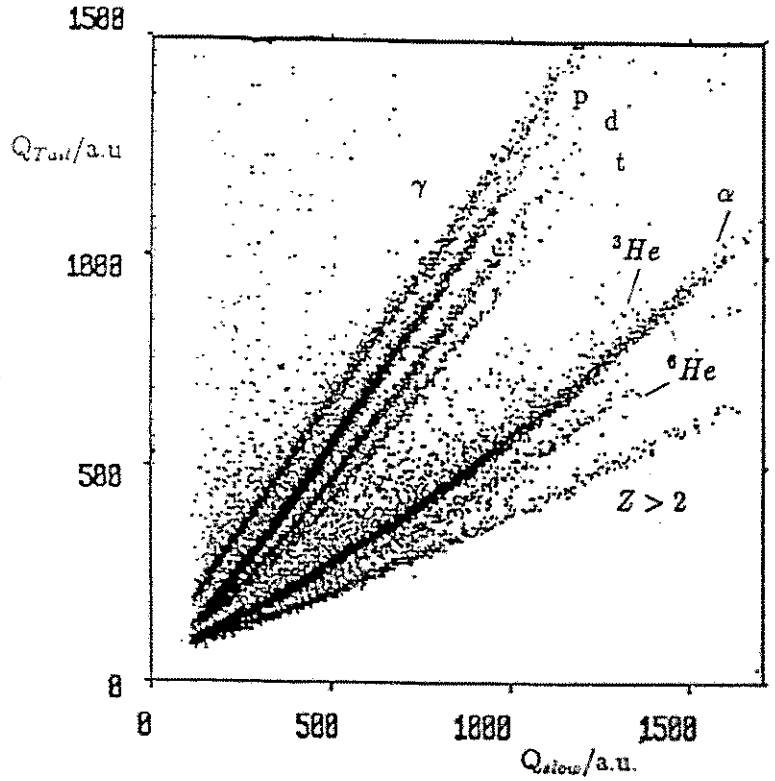

Fig. 8: Pulse shape discrimination of light charged particles with a 15 mm thick CsI(Tl)

6 Electronics and Data Acquisition

The front-end electronics of one PSAC + BIC - module (fig. 9, upper part) occupy 5 CAMAC stations and deliver 5 parameters: Bragg peak height and energy derived from the

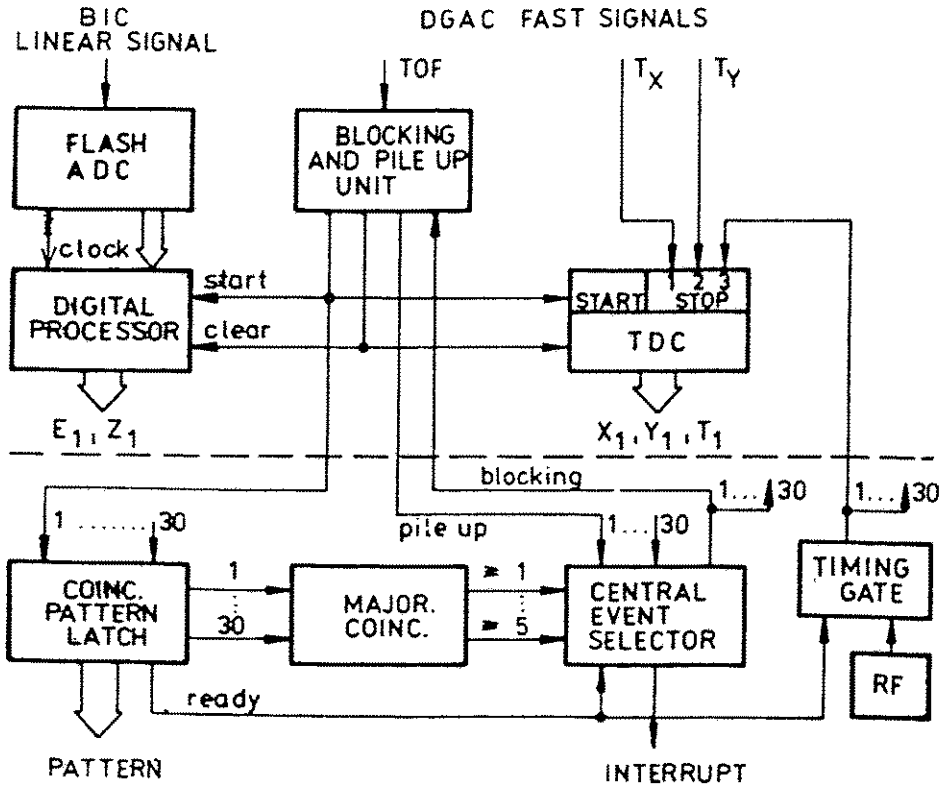

Fig. 9: Front-end electronics of one PSAC + BIC module (above) and first level trigger (below) of the FOBOS gas part

BIC signal (fig. 6) as well as two coordinates and time of flight from the PSAC. As time reference serves the cyclotron RF fed via the timing gate which is opened by a "ready " signal, into stop 3 of the TDC (fig. 9). In experiments on "mini-FOBOS" instead of the RF the delayed signal of a small transmission start avalanche counter has been used. The pattern of PSAC's fired within an interval of 200 ns is stored in the coincidence pattern latch. An event is accepted if the multiplicity exceeds a certain level and if no pile-up has been detected. A pile-up is recognized if either another PSAC signal occures within 12μs before or 6μs after the event, the BIC threshold (fig. 6) was exeeded within 10μs before the event or the trailing edge of the BIC signal (which is time-significant in this type of chambers) does not fall in a certain time window relative to the PSAC signal. This effort is necessary because our BIC's are rather slow (4μs electron collection time) due to their large dimensions. An accepted event causes an interrupt starting the data readout procedure, a rejected event leads to fast reset of the whole system without any dataway access. The coincidence pattern determines which addresses have to be read out via the CAMAC dataway. The gas-ball front-end electronics occupy 9 CAMAC crates connected via VDB bus with an Eurocom-6 VME station. The software for CAMAC access and data transfer from the VME station via Ethernet to a VAX computer has been developed and implemented into the HOOPSY (ref. 13) data acquisition system. This new hard- and software has been applied successfully in an experiment at VICKSI in the HMI Berlin and allowed us to increase the data accumulation rate up to 1200 multi-parameter events per se-

cond. For the CsI detectors FASTBUS QDC's with common gates are utilized. The FASTBUS crate is connected to the same VDB bus. Presently this part of the data acquisition system is not yet finished.

In the test experiments performed 1991/92 at the "mini-FOBOS" setup, the data acquisition based on the CAMDA (ref. 14) program package running on a PC. This package has been extended considerably to allow interactive control of the signal processing CAMAC modules.

7 The Fragment Mass Determination Procedure

In the FOBOS spectrometer the mass determination is based on measured time-of-flight, kinetic energy and emission angles (fig. 2) of particles and fragments from fission-like reactions. Test runs with single modules have been carried out by detecting fission fragments from a ^{248}Cm source and recoils produced by elastic scattering of Kr(3AMeV)-ions. The experimental set-up consists of a FOBOS PSAC + BIC-module and a small parallel-plate avalanche counter (PPAC) to generate the start signal. The particles have to pass through a total areal density of about 1.3 mg/cm^2, which is mainly caused by layers of mylar and gold. Therefore, the mass determination has to take into account the dependence of the residual energy measurement on the energy losses.
The task of mass-identification under these conditions is to solve a system of two equations, which represent kinetic energy Eo at the START of the time-of-flight (TOF) path as a function of the fragment mass A. Thereby the measured TOF and the energy-signal EBIC of the ionization chamber (BIC) are given as fixed parameters.

$$\text{Eo (TOF,A)} = \text{A/2(L/TOF)}^2 + \text{dE1 (E,Z(A))}$$
$$\text{Eo (EBIC,A)} = \text{Er(EBIC)} + \text{dE2(Er,Z(A),gi)}$$

The value dE1 considers the energy losses within the path L up to the STOP, dE2 summarizes all losses from the START up to the entrance of the fragment into the BIC.
The following points have been regarded by the solution principle:

- in dependence on the actual position, where the particle crosses the layer, the foil thickness gi can be influenced by the entrance angle, nonplane surfaces and nonuniformities of the foil;

- electronic dependence of the TOF-signal on the position at the DGAC, where the particle passed through (see fig. 6)

- the calculation of the energy losses was performed by using the range-energy-relation. Thereby the access to a data set R(E,Z,A) is a fast method of numerical processing. In order to simplify the range data the A-dependence was eliminated by creating the array R/A = r(E,Z);

- by deducing the Er-value from the EBIC-signal nuclear stopping was considered. This ionization defect was calculated for the chamber gas (90% Ar, 10% CH4) by using the formula from ref 15. The fragment energy corrections are 2-3 MeV.

If Z is not determined via Bragg peak spectroscopy charge-mass-correlation must be introduced as a known function Z(A).

these events turns out to be positive.

For the measurement at 10 AMeV, the mean values of the relative fission fragment velocity v_{rel} result in 2.31 $\pm$ 0.15 cm/ns (2.46) and 2.51 $\pm$ 0.15 cm/ns (2.61) concerning the event groups with small and large momentum transfer (fig. 16). The values in brackets are estimates using the VIOLA systematics [24]. The mean number of evaporated neutrons deduced event by event from the mass, energy and momentum conservation was compared with the estimates of the massive transfer model using the TKE from [24]. Our respective experimental values of 3 $\pm$ 6 and 9 $\pm$ 6 are smaller than the theoretical estimates by about 6 units. However, although it seems to be difficult to obtain the predicted absolute values, the difference of the neutron numbers between the two groups is reproduced correctly. This is of particular importance for the analysis of events with higher multiplicities, where the folding angle method cannot be applied, namely to possess a filter of excitation energy.

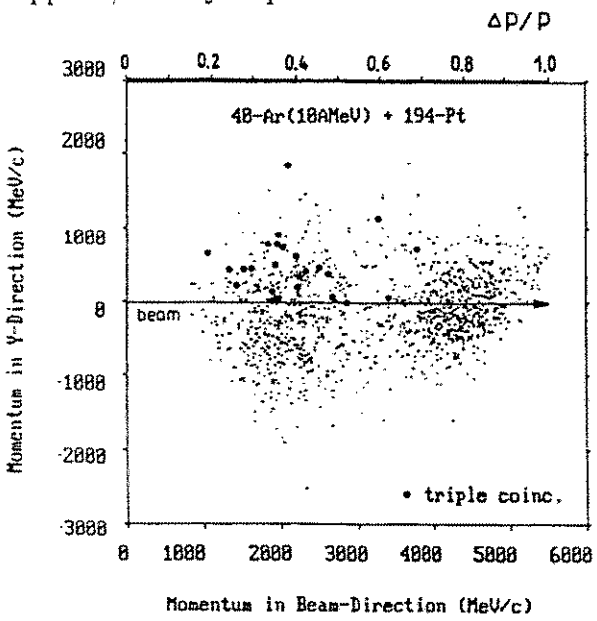

Fig 13: Total fragment momentum distribution

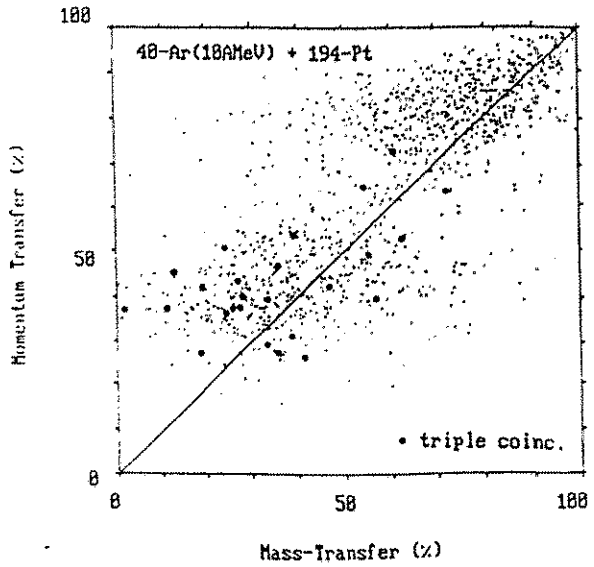

Fig. 14: Mass and momentum transfer correlation

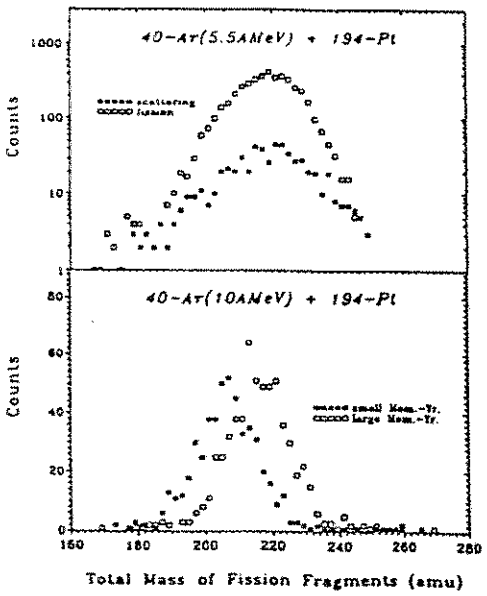

Fig. 15: Total mass distributions

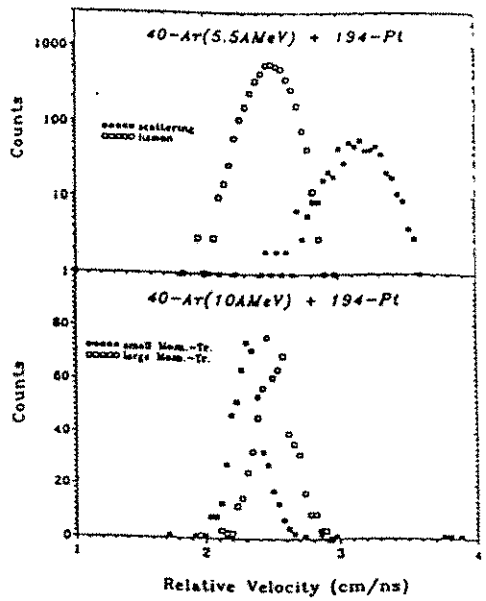

Fig. 16: Relative fragment velocities

References

[1] A.G. Akhperdshanian et al.,JINR Communication **P13-87-760** (Dubna 1987)

[2] H.-G- Ortlepp et al., Print ZfK - **734**, Rossendorf 1990 Status Report FZR 92-11, Rossendorf 1992

[3] G.D. Westfall et al., Nucl. Instr. and Meth. in Phys. Res. **A238** (1985) 347

[4] R.T. Souza et al., Preprint MSU **CL-720** (East Lausing 1989)

[5] E. Plagnol, Proc. of Me XXVII. International Winter Meeting on Nuclear Physics, Bormio 1990, (Ricerca Scien. ed Eduz, Perm., supplemento N. 78, 1990), p. 181

[6] W. Terlau et al., HMI Bericht **482** (1990) 93

[7] G. Renz, M. Andrassy, Annual Report 1991 (FZ Rossendorf, Institut für Kern- und Hadronenphysik) FZR 92-09 (1992) 64

[8] W. Seidel et al., Nucl. Instr. and Meth. in Phys. Res. **A273** (1988) 536

[9] A. Matthies et al., Contr. to the Symposium on Correlation Experiments on Heavy Ion Beams, Dresden 1988, **JINR D7-88-299** (Dubna 1988) p.11

[10] H.-G. Ortlepp and A. Romaguera, Nucl. Instr. and Meth. in Phys. Res. **A276** (1989) 500

[11] A.S. Fomichev et al., Preprint JINR, P15-92-50, Dubna 1992

[12] J. Alarja et al., Nucl. Instr. and Meth., **A242** (1986) 352

[13] G. Roeschert et al., HMI Bericht **436** (Berlin 1986)

[14] H. Stelzer, CAMDA a CAMAC - PC Data Acquisition System, Introduction and Short Manual, Messel 1989

[15] S.Kalbitzer et al., Z.Physik A278 (1976)233

[16] H.B.Bogdanova et al.,; Phys. of El. Part. and At.Nucl. 17/5(1986) 1022.

[17] J.Henninger et al., Report JINR Dubna 6-84-366 (1984)

[18] J.S.Forster et al., Nucl. Instr. Meth. 136(1976)349

[19] Banjerjee et al., Nucl. Instr. Meth. B136(1986)527

[20] R.Brandt eat al., Phys. Rev. 131(1963)2617

[21] H.G. Ortlepp et al., Annual Report 1992, Institute of Nuclear and Hadronic Physics, FZR 93-10 (1993) 97

[22] M. Fatyga et al., Phys.Rev.Lett. **55** (1985) 1376

[23] U. Jahnke et al., Report HMI-B 463 (Berlin, 1988)

[24] V.E. Viola, Nucl.Data Sect. **A1** (1966) 391;
V.E. Viola et al., Phys. Rev. **C31** (1985) 1550

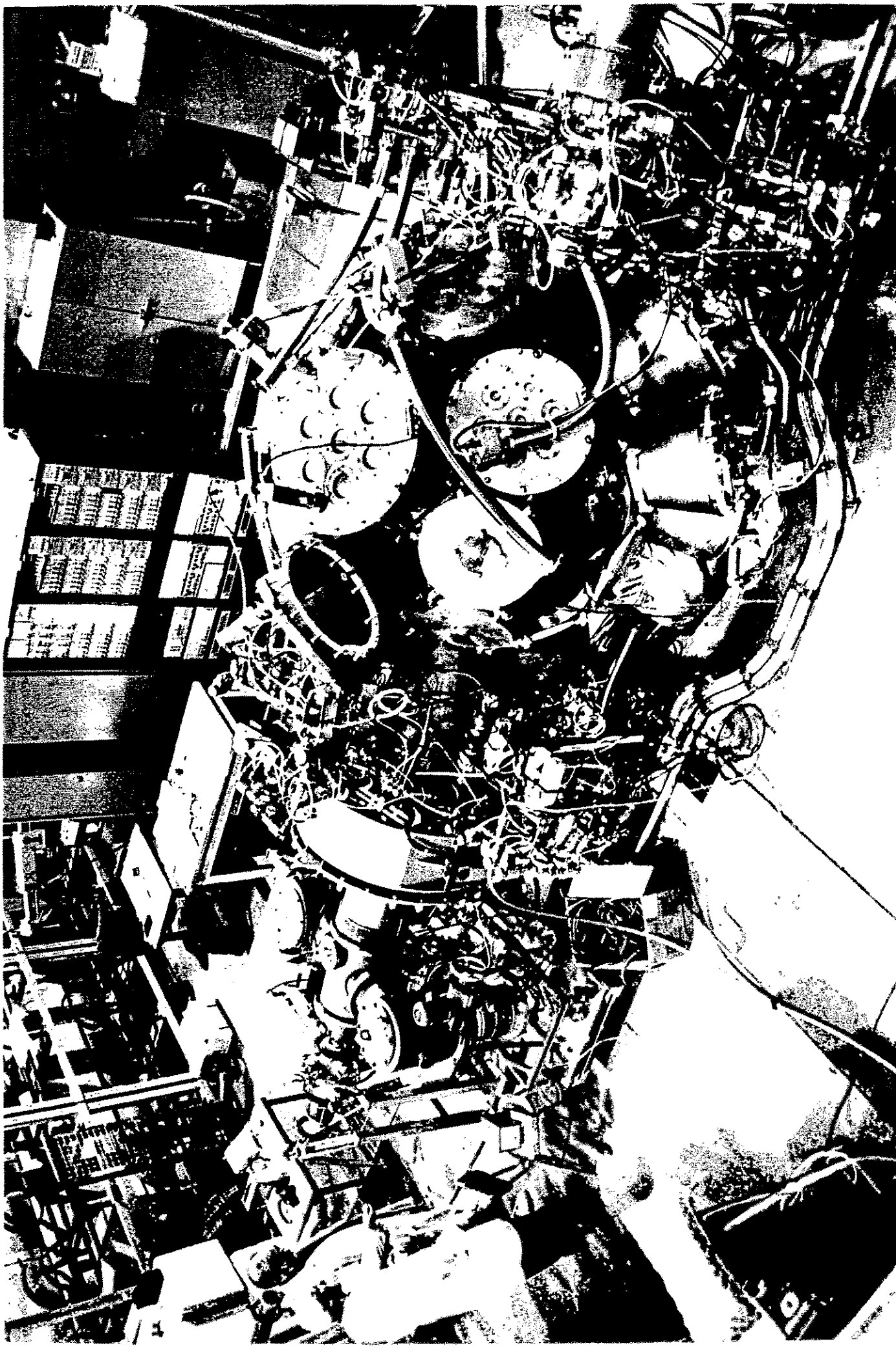

STATUS OF THE FOBOS SCINTILLATOR SHELL

W. Wagner[1], H.-G. Ortlepp[1], D.V. Kamanin, A. Matthies[1], O.V. Strekalovsky, V. E. Zhuchko

[1] Research Centre Rossendorf Inc., GERMANY

The scintillator shell of the FOBOS array consists of 210 CsI(Tl) counters arranged behind the gas detectors to register light charged particles (LCP) and penetrating light fragments [1] . All the crystals will be delivered by MONOCRYSTAL Kharkow, Ukraine, till the end of 1994. The photomultipliers, hollow light guides and biases as well as the high voltage supplies are at hand.

80 scintillation detectors have been installed at FOBOS . They were operated in the experiment ^{14}N (34 AMeV) + ^{197}Au in September 1994. To apply pulse-shape discrimination method [2] (fig. 1) and to match the timing conditions of the first level trigger [3] of FOBOS the scintillator signals have to be split and delayed. Therefore a special multichannel splitting-and-delay box has been developed at the RC Rossendorf which realizes output magnitude attenuation and a delay of 200 ns on the base of delay-line microchips.

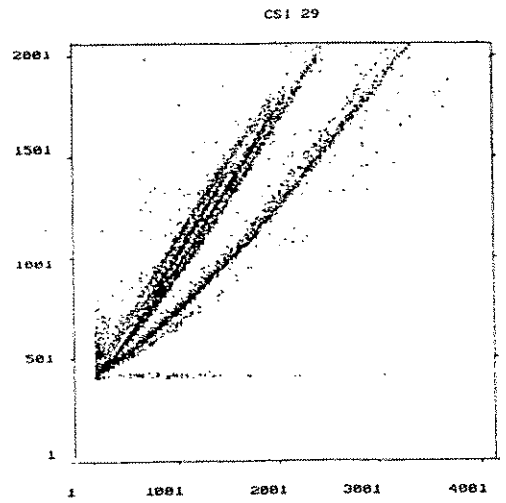

Fig.1 Pulse-shape discrimination matrix of a CsI(Tl) detector positioned at an angle ϑ=37.4°.

The FOBOS electronics has been upgraded by a FASTBUS minicrate containing four 96-channel current integrating ADCs (C.A.E.N. CIAFB F683C) and by control logics for the scintillator shell (fig. 2).

New control software has been developed to include the FASTBUS electronics into the VDB branch of the FOBOS data acquisition system [4] .

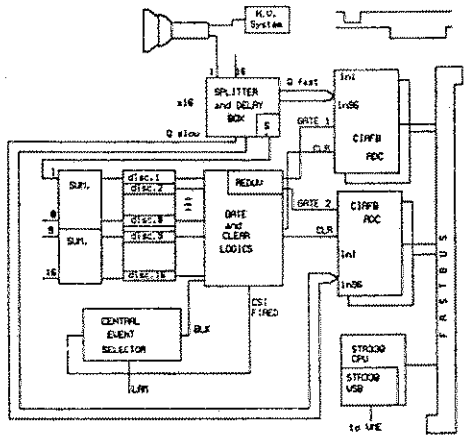

Fig.2 Blockscheme of the scintillator shell electronics.

Fig. 3 shows the image of one of the hexagonal shaped CsI(Tl) crystals of the scintillator shell when the coordinate information of the position sensitive avalanche counter (PSAC) of the respective FOBOS module has been recorded in coincidence with the scintillator signal.

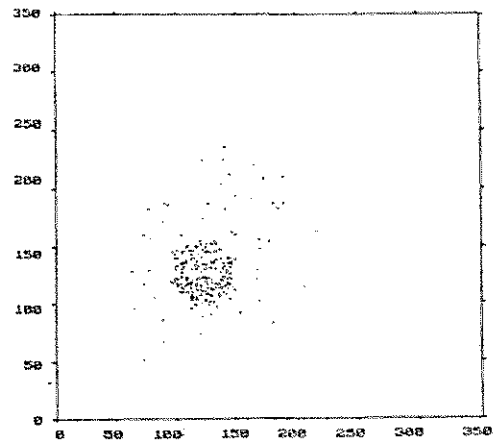

Fig.3 Coordinates matrix of the PSAC for events correlated with one of the scintillation detectors.

For penetrating light fragments particle discrimination was performed applying the ΔE-E-method to the energy loss (ΔE) of the fragments in the FOBOS ionization chamber

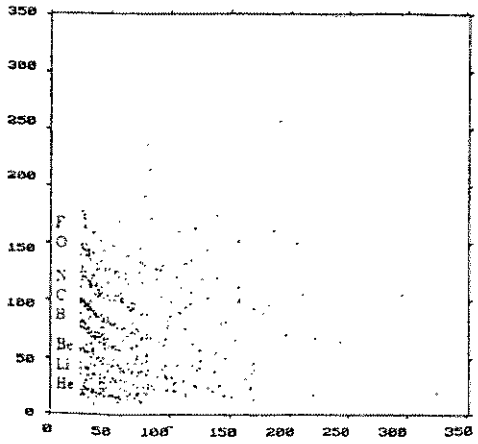

Fig. 4 Particle identification matrix for fragments penetrating the BIC and stopped in the scintillator

(BIC) together with the light output of the fragments stopped in the scintillator (E) (fig. 4). By this way the dynamical range of the FOBOS detector is increased considerably.

Furthermore this method can be used for energy calibration of the nonlinear response of CsI(Tl).

REFERENCES

1) Wagner, W. et al., Scientific Report 91/92, Flerov Laboratory of Nuclear Reactions, JINR Dubna, Russia, 1992 , p.244.
2) Alarja, J. et al., Nucl. Instr. and Meth. A242, 1986, p.352.
3) Ortlepp, H.-G. et al., Proc. of the Internat. School-Seminar on Heavy Ion Physics, v.2, JINR Dubna, Russia, 1993, p.466 (ed. Yu. Ts. Oganessian et al.).
4) ibid. [1] , p.249 .

THE FOBOS FORWARD ARRAY

W. Wagner [1], A. Budzanowski [2], B. Czech [2], D . Hilscher [3], J. Holik [2], H. Homeyer [3], W. Janczur [2], H.-G. Ortlepp [1], G. Pausch [1], O.V. Strekalovsky, L. Zrodlowski [2]

[1] *Research Centre Rossendorf Inc., GERMANY*
[2] *Institute for Nuclear Physics, Cracow, POLAND*
[3] *Hahn-Meitner Institute Berlin, GERMANY*

For geometrical reason the minimum acceptance angle of the FOBOS spectrometer[1] is $\vartheta \approx 21°$. Mainly forward directed reaction products such like quasi-inelastic or projectile-like fragments, preequilibrium particles or heavy residues are not or ineffectively registered. On the other hand these particles carry valuable information about the transferred linear momentum in the nuclear reaction, the reaction plane, the excitation energy of the intermediate system, the recoil velocity etc.

Therefore it has been proposed to modify part of the former ARGUS detector [2] of the HMI Berlin for use as forward array at FOBOS.

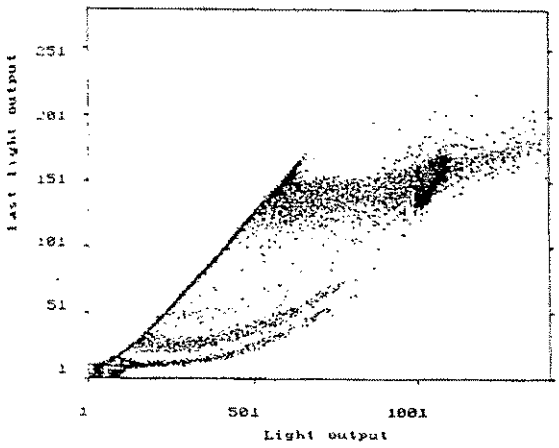

Fig. 1 Scatterplot of a phoswich detector of the forward array applying pulse processing .

Six rings of altogether 92 phoswich detectors consisting of 0.5 mm Pilot-U fast scintillator and 20 mm BGO are prepared to be installed into the forward cone of FOBOS.

The geometrical conditions are given in tab. 1. The thickness of the scintillators allows to stop protons (alpha particles) with energies up to ≈ 100 AMeV. Particle charge identification is possible up to Z ≈ 15 with a threshold for light charged particles (LCP) (≈ 5 AMeV).

Tab. 1 Geometry of the FOBOS forward array

Ring	Detectors	ϑ
1	12	5 °
2	16	8 °
3	16	10.5 °
4	16	14 °
5	16	18.5 °
6	16	23.5 °

The mechanics for adaptation of the forward array to FOBOS has been designed and produced at the INP Cracow and delivered to FLNR Dubna. The high voltage supply developed in CAMAC standard at Dubna is computer controlled under WINDOWS.

To include the forward array into the FASTBUS data acquisition system of the FOBOS scintillator shell [3] a simple pulse processing concept [4] has been modified for application to phoswich detectors and tested at a ^{14}N beam.

It is planned to use the full configuration of the FOBOS array in the next beam experiment in 1995.

REFERENCES

1) Ortlepp, H.-G. et al., Proc. of the Internat. School-Seminar on Heavy Ion Physics, v.2, JINR Dubna, Russia, 1993, p.466.
2) Terlau, W. et al., Annual Report 1989, HMI 482, Berlin, Germany, 1990, p.93.
3) Wagner, W. et al., Scientific Report 91/92, Flerov Laboratory of Nuclear Reactions, JINR Dubna, Russia, 1992, p.244.
4) Tõke, J. et al., Report UR - NSRL - 394, University of Rochester, USA, 1993.

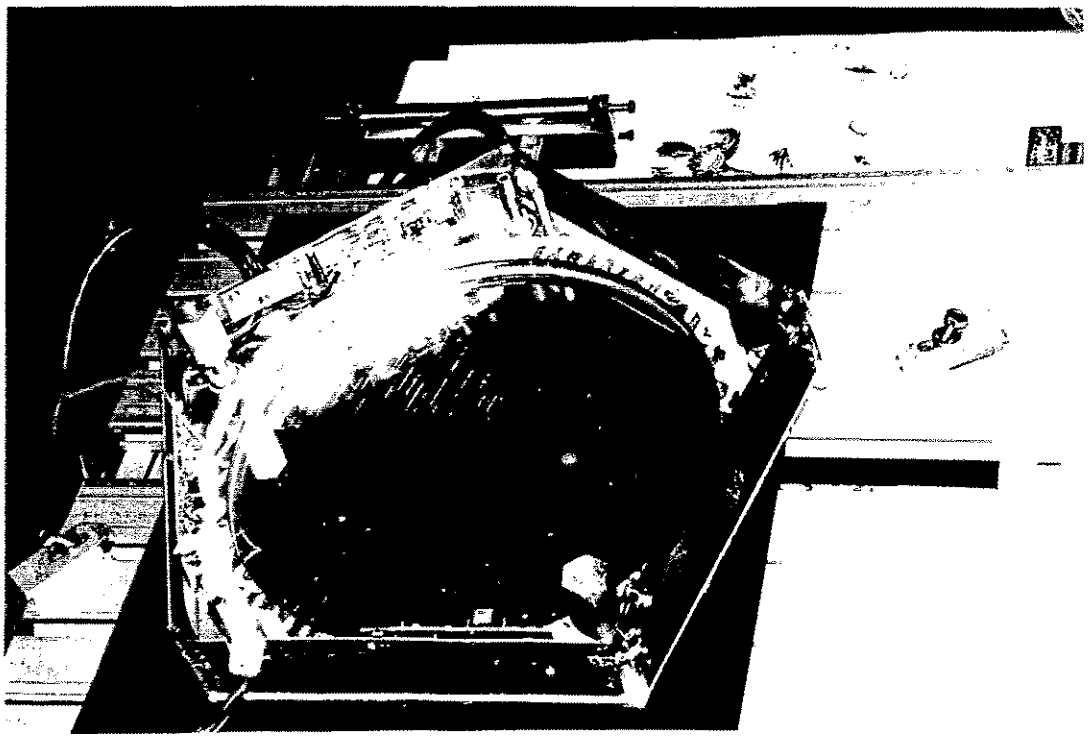

TEST MEASUREMENTS PERFORMED WITH A BRAGG IONIZATION CHAMBER *

M. Gebhardt [3], V.N. Doronin [1], P. Gippner [1,2], H.-G. Ortlepp [1,2], G. Renz [1,2], D.I. Shishkin [1], W. Wagner [1,2]

[1] *Joint Institute for Nuclear Research, Dubna, RUSSIA*
[2] *Forschungszentrum Rossendorf e. V., GERMANY*
[3] *Johann Wolfgang Goethe Universität, Frankfurt, GERMANY*

An ionization chamber with the electric field parallel to the particle trajectory, well known as a Bragg ionization chamber (BIC) is presented. Bragg-curve spectroscopy (BCS) was first proposed by Gruhn et. al. [1]. It is a well established method for nuclear charge identification of heavy-ion reactions products. The BIC allows to dertermine the nuclear charge and the energy of low energetic heavy ions ($E / A \approx 0.8 \div 2.0$ AMeV).

In contrast to the customary technique of pulse-shaping by a long and a short time constant the real-time digital processing of the BIC was used. The basic idea of this method is shown in fig. 1 and the principle is described in ref. [2]. The results obtained in this work are useful for the operation of the detector modules of the 4π - spectrometer FOBOS built up at the cyclotron facility U-400M of the JINR Dubna [3] for the study of medium energy ($E / A \approx 10 \div 30$ MeV) heavy-ion reactions.

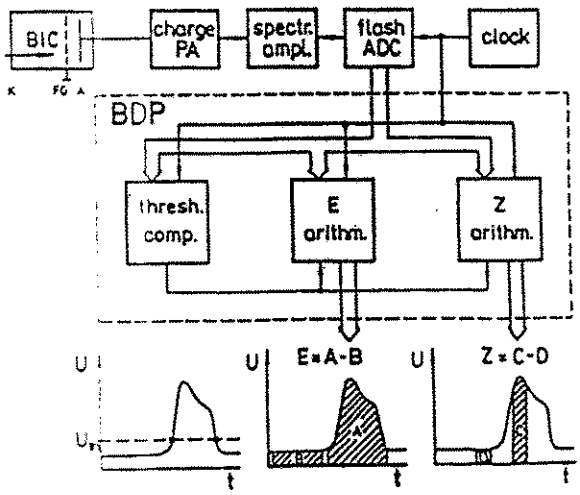

Fig. 1 Principle of the real - time digital processing of the BIC

First tests have been performed by use of a trifold alpha-particle source (^{238}Pu, ^{239}Pu and ^{244}Cm). All measurements were carried out at a BIC without the entrance window foil. Therefore, it was not necessary to correct for energy straggling. The BIC consists of a cathode (K), a Frisch-grid (FG) and an anode (A). The distance between K and FG (FG and A) amounted to 24.8 cm (1 cm) respectively. Fig. 2 shows the BIC and illustrates the principle of the drift-time measurement.

The BIC is usually operated in a flow-though regime with P 10 gas (a mixture of 90 % Ar + 10% CH_4) at a pressure of $\approx$ 200 Torr. In the first run we realized a stationary regim using gas from a ballon because at that time the device for on-line gas mixing was yet not ready. This resulted in a gas mixture P 5 what has been estimated from a drift-time measurement. Furthermore, we analysed the gas by the help of a mass spectrometer that confirmed the estimation made.

The drift-velocity v_D was measured for different gas mixtures. Fig. 3 shows the v_D- measurement for P 10 at a pressure of 200 Torr. Fig. 4 shows the measured energy spectrum.

The goal was to analyze the behavior of the BIC energy signal over a measurement time of 5 weeks. We expected a decrease of the pulse-magnitude (energy) as resulting from the out-gasing of the inner BIC walls and from the leakage rate.

* The project is supported by the BMFT, Germany, under contract Nr. 06 DR 671

Fig. 5 shows the decrease of the magnitude in dependence on time t. The decrease was about 1.25 % within a time intervall of 18 hours.

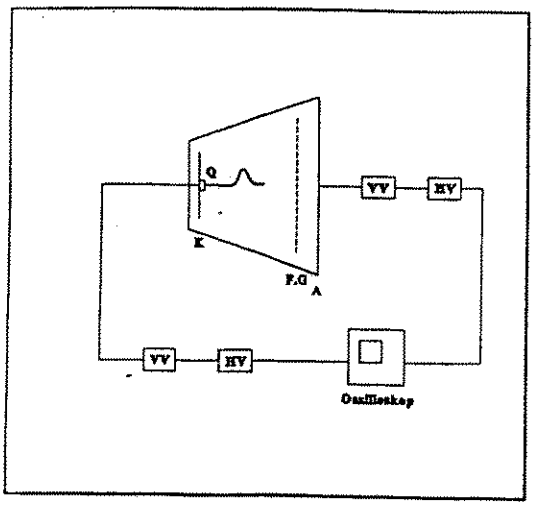

Fig. 2 Principle of drift-time measurement

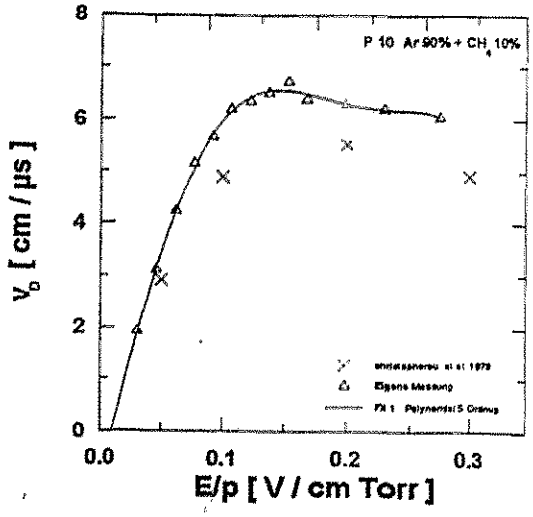

Fig. 3. Drift-velocity (v_D) measurement for a gas mixture P10

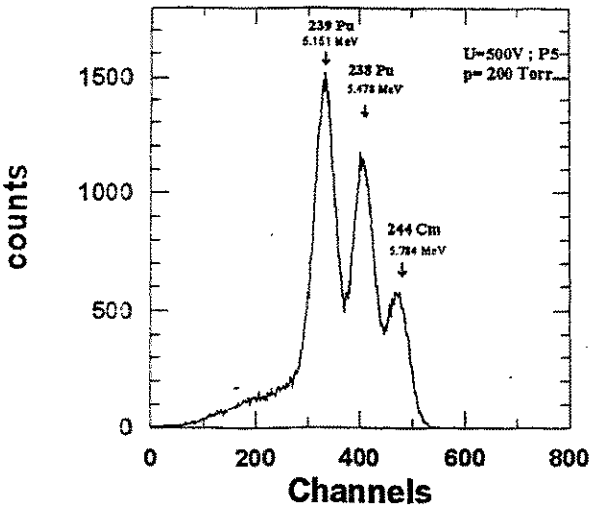

Fig. 4 Energy spectrum of the applied trifold alpha-particle source

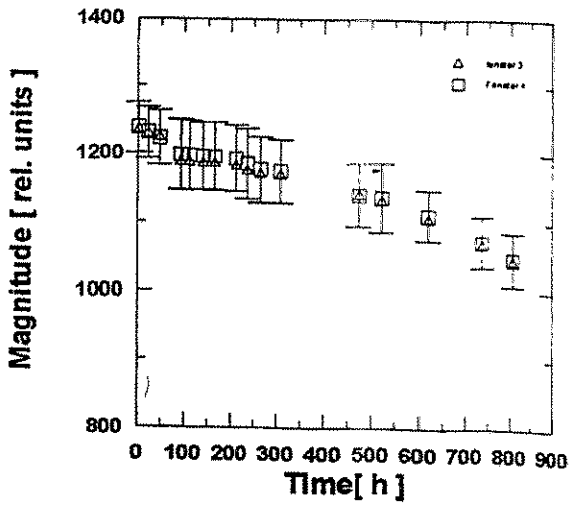

Fig. 5 Decrease of the magnitude of the energy signal in dependence on time

Furthermore, we analysed the change of the BIC signal due to mixing of a defined amount of air to the chamber gas. These experiments have been done using alpha particles from a ^{239}Pu source. The chamber gas was P10 and we estimated the concentration of air by the help of a mass spectrometer.

Fig. 6 shows the decrease of the magnitude in dependence on the concentration of air. By addition of altogether 10 Torr of air in steps of 2 Torr to the actual gas pressure we optained a mean value for the decrease of the energy signal of 0.68 %. Fig. 7 shows the measured energy spectrum.

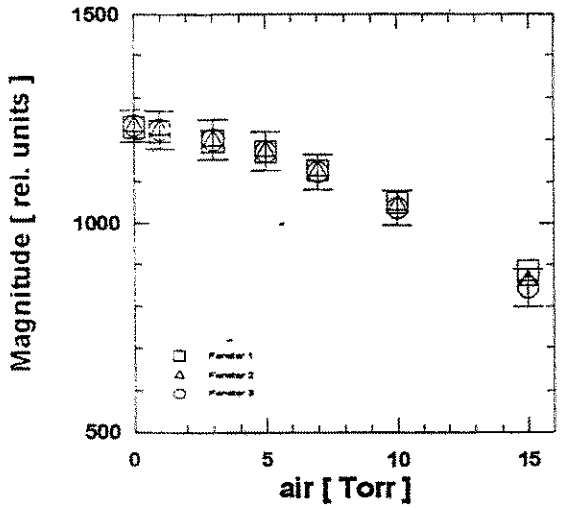

Fig. 6 Decrease of the magnitude of the energy signal in depence on the concentration of air

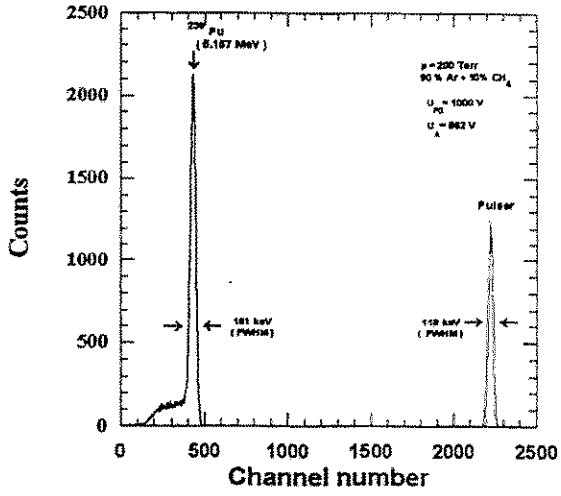

Fig. 7 Energy spectrum of alpha particles from ^{239}Pu

Subtracting the electronic noise $\Delta E = 110$ keV ($\Delta E/E = 0.85$ %) from the measured width $\Delta E =$ 161 keV ($\Delta E/E = 2.9$ %) we obtained a value for the intrinsic energy resolution of the BIC of $\Delta E = 51$ keV ($\Delta E/E = 2$ %).

References

1) C.R. Gruhn et al., Nucl. Instr. and Meth. A196, 1982, p.33.
2) H.-G. Ortlepp and A. Romaguera, Nucl. Instr. and Meth. A276, 1989, p.500.
3) H.-G. Ortlepp et al., "First experiments with FOBOS", Proc. Internat. Conf. on Nucleus - Nucleus Collisions, Taormina, Italy, 1994 (to be published in Nucl. Phys. A)

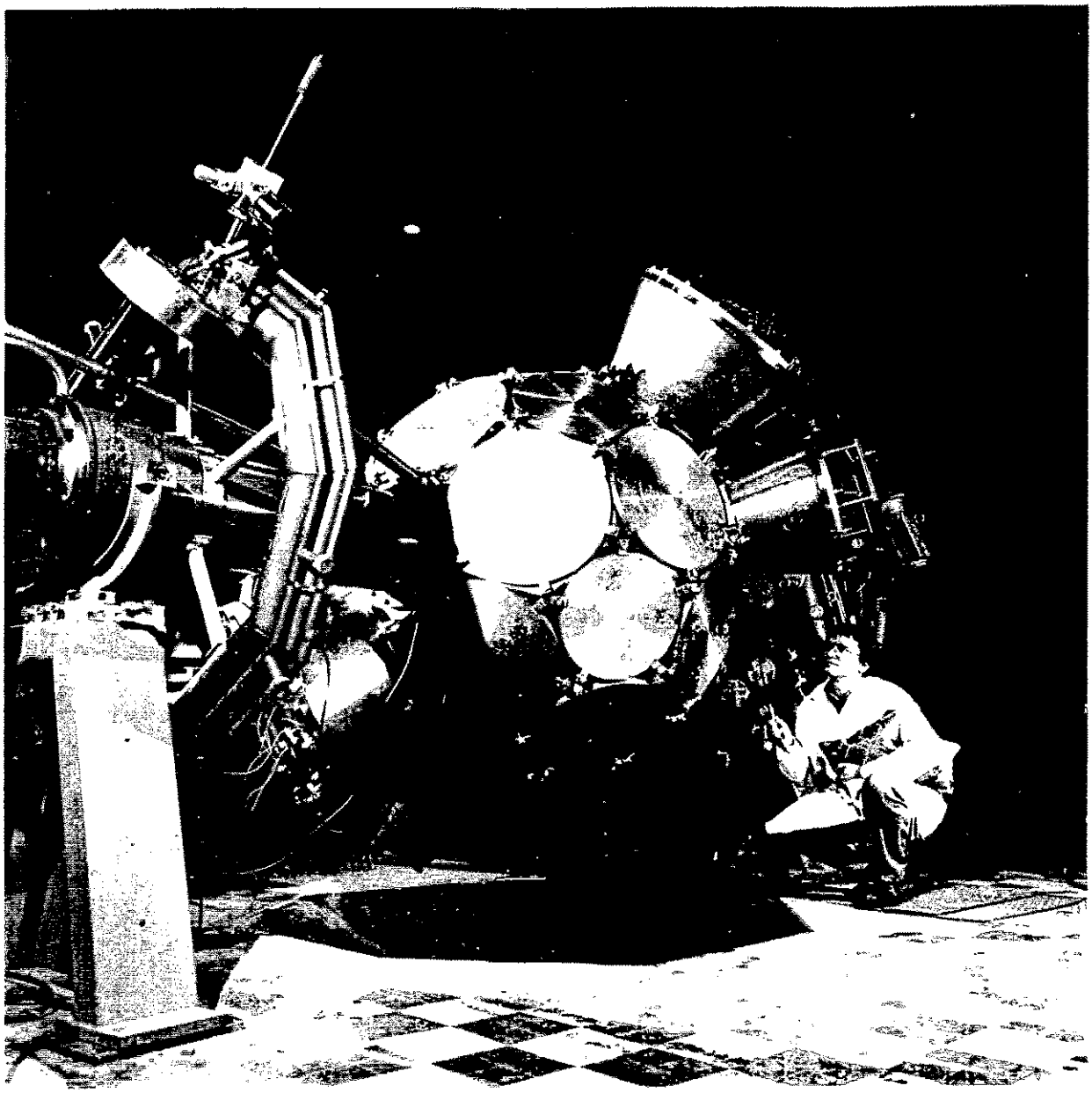

STATUS OF THE EVACUATION AND GAS SUPPLY SYSTEM OF FOBOS

G. Renz [1], V.M. Vasko, P. Gippner [1], A. Matthies [1], V.N. Doronin, D.I. Shishkin, C. Umlauf [1], M. Gebhardt [2]

[1] *Research Centre Rossendorf Inc., GERMANY*
[2] *Physical Institute of the Johann Wolfgang Goethe University Frankfurt, GERMANY*

The gas supply and exchange system of the FOBOS position sensitive avalanche counters (PSAC) [1] and Bragg ionization chambers (BIC) [2] worked very well during several weeks of the FOBOS experiments in 1994. Providing a full gas exchange inside the gas detector volumes within several hours a pressure stabilization accuracy of better than 1% has been achieved.

The transition to the on-line mixing method for the preparation of the P10 (90% Ar + 10% CH_4) gas mixture guaranteed us a good long-time stability of the gas mixture composition and, therefore, of the electron drift time in the BIC. The gas is mixed by automatic control of two independent electronic mass flow controllers for the gas components (fig.1).

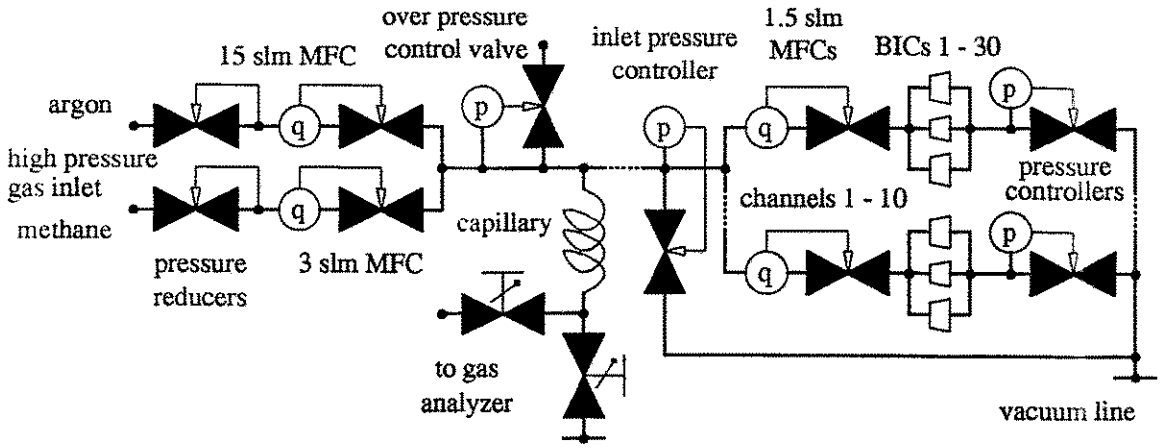

Fig. 1 Scheme of the BIC on-line gas mixing and control system

We also have the possibility to make an on-line check of the gas composition by means of a LEYBOLD Transpector gas analyzer [3]. For tuning the mixer output mass flow to the gas flow through the BIC regulation system we used an additional controller at the BIC inlet collector.

A crucial problem of the FOBOS facility is the leakage rate Q through the thin entrance window foils of the great number of gas detectors. We have to find a compromise between foil thickness and quality, sensible effective pumping speed S_{eff} and reachable ultimate pressure p_E inside the central chamber of FOBOS.

The gas diffusion rate of 1.5 µm thick DuPont Mylar foils was measured at the FLNR Dubna in 1992. We found, for unsupported test foils (area A = 13 cm^2) at a difference pressure of 2.67 mbar a value of

$$Q/A = 3.7 \cdot 10^{-8} \text{ mbar l/s cm}^2 .$$

Extrapolating to a working gas pressure of 267 mbar we, therefore, expected a leakage rate of $Q = 4.2 \cdot 10^{-3}$ mbar l/s for a BIC with an active window area of A = 1104 cm^2 and a value of $Q = 2.2 \cdot 10^{-3}$ mbar l/s for a BIC with A = 594 cm^2.

Summing over all 30 BIC modules at 267 mbar yields a total value of Q= 0.1 mbar l/s for the theoretical leakage rate of the whole FOBOS facility. The contributions of the PSAC foils is negligible because of the much lower working pressure within the PSAC. Table 1 shows that the real leakage rates measured during the FOBOS experiments in 1993/1994 were much higher than the expected value of Q.

At nearly 2.7 mbar l/s (per pump) the overload threshold for automatic switch-off of a turbomolecular pump O1 AB - 1500 is reached.

In order to avoid this risk and to increase the total pumping speed we decided to replace these turbomolecular pumps situated at the beam entrance and exit of FOBOS by cryopumps HBK - 3.2 A-P (S = 2600 l/s). In connection with the LEYBOLD TURBOVAC 1000 (S = 1000 l/s) set-up [2] directly mounted to the central chamber of FOBOS this resulted in an effective pumping speed of altogether 5000 l/s (fig.2). This pump combination was carefully tested under different load conditions using calibrated leakage rates, generated by special mounted gas flow controllers. We showed, that we can manage now long-time leakage rates of even 13.3 mbar l/s supporting under this condition an ultimate vacuum of $p_E = 3 \cdot 10^{-3}$ mbar.

Table 1 Vacuum values within the central chamber of FOBOS during the different experiments

Experiment	foils [µm]	number of BIC	p (P10) [mbar]	pumps in use	S_{eff} [l/s]	Q [mbar l/s]	p_E [mbar]
9 /93	1.2	6	117	4 O1 AB - 1500	1500	0.2	$1.3 \cdot 10^{-4}$
10/ 93	1.2	12	267	3 O1 AB - 1500	1100	1.7	$1.6 \cdot 10^{-3}$
12/ 93	1.2	12	267	3 O1 AB - 1500 3 Turbovac 1000	3100	6.7	$2.1 \cdot 10^{-3}$
6/ 94	1.5	8	267	3 Turbovac 1000 4 HBK - 3.2 A-P	5000	0.3	$6.0 \cdot 10^{-5}$
9/ 94	1.5	16	333	3 Turbovac 1000 3 HBK - 3.2 A-P	4250	0.9	$2.1 \cdot 10^{-4}$

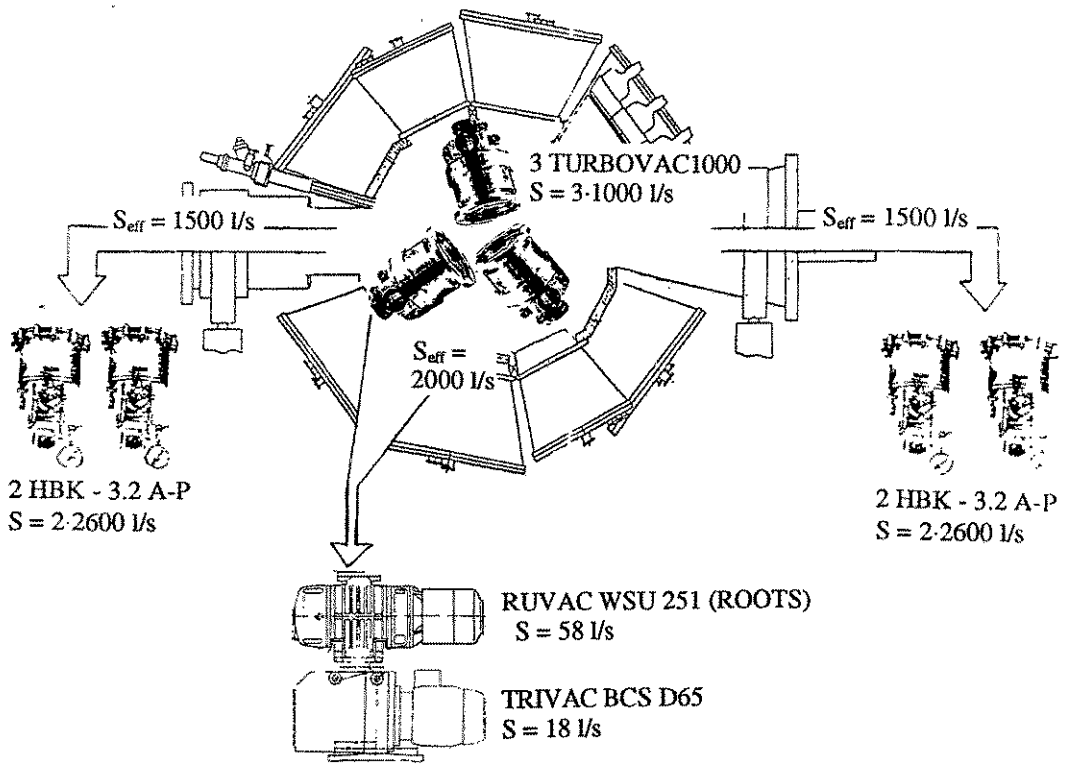

Fig. 2 The improved FOBOS evacuation system

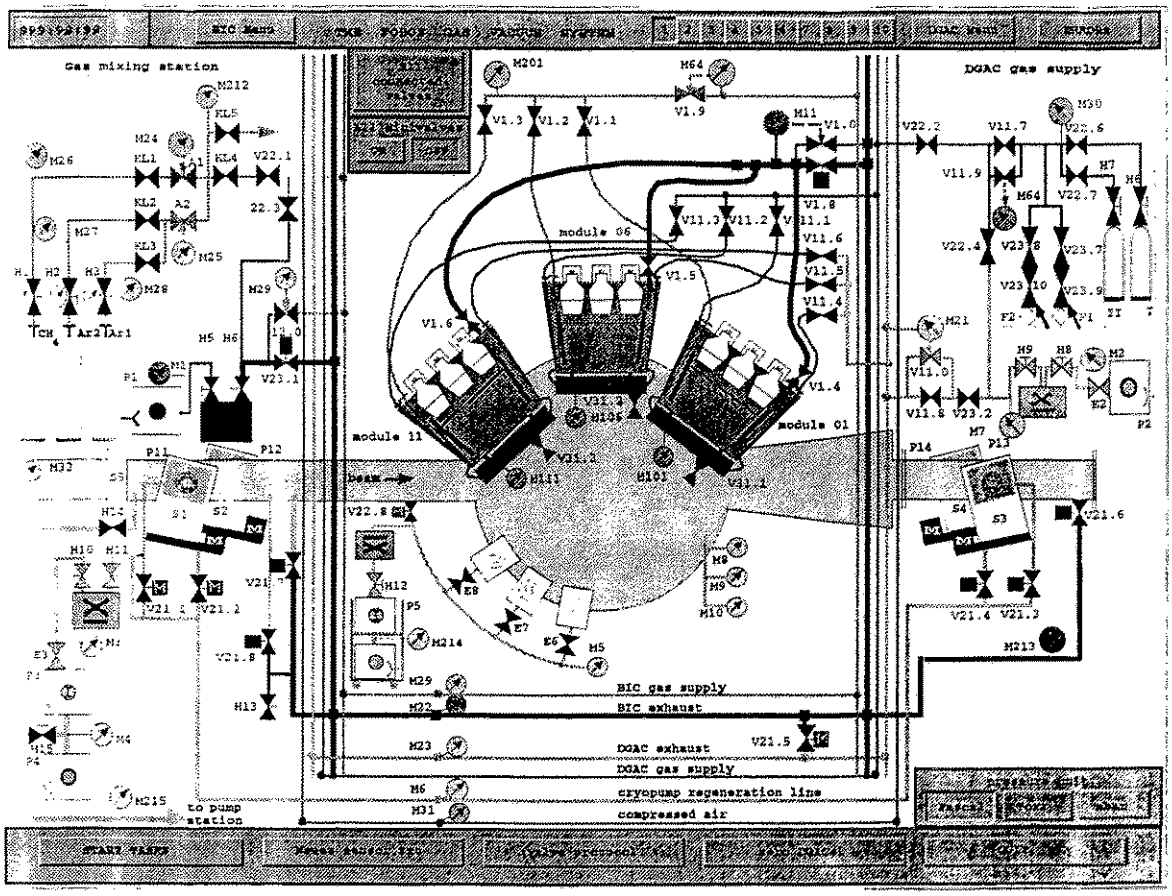

Fig. 3 Visualization of the status of the FOBOS gas vacuum system on a X-terminal

In parallel many efforts were made to reduce the leakage rate of the BIC entrance windows increasing the quality of the foils and of the supporting grids. For preliminary checks of the BIC windows under real experimental conditions and in order to study the phenomenon of foil-aging a special test facility was built-up. We tested 12 BIC with new 1.5 μm thick Mylar foils at a pressure of p = 267 mbar.

If we excluded the worst BIC with Q = 14....40 mbar l/s we found an average leakage rate for the foils of $Q = 3.8 \cdot 10^{-3}$ mbar l/s in good agreement with the expected values.

The existing control software [4] working on a SIEMENS SX automation system [5] including the graphical visualization on an X - terminal (fig. 3) was adapted to the new evacuation system. A supervision of the turbopump diagnostic signals (pump status, current, frequency) via RS232 interfaces from the TURBOVAC NT20 control blocks [6] was included. Additionally to the pressure at 63 measuring points we now measure and visualize all analog signals from the 11 mass flow controllers by multiplexing them to one DAC channel. In order to increase the safety of the FOBOS gas-vacuum system under all conditions several hardware tests and diagnostic routines were supplemented. The state of the whole system is recorded continuously.

REFERENCES

1) Renz, G., et al., Annual Report FZR - 35, Rossendorf, 1994, p.90.
2) Renz, G., et al., Annual Report FZR - 35, Rossendorf, 1994, p.91.
3) LEYBOLD INFICON Inc., Transpector Gas Analysis System, Manual, 2/1993.
4) Renz, G., et al., Annual Report FZR 93 - 10, Rossendorf, 1993, p.122.
5) Renz, G., et al., JINR LNR Scientific Report, 1992, p.15.
6) LEYBOLD AG, Operating Instructions, TURBOTRONIK NT20, 1992.

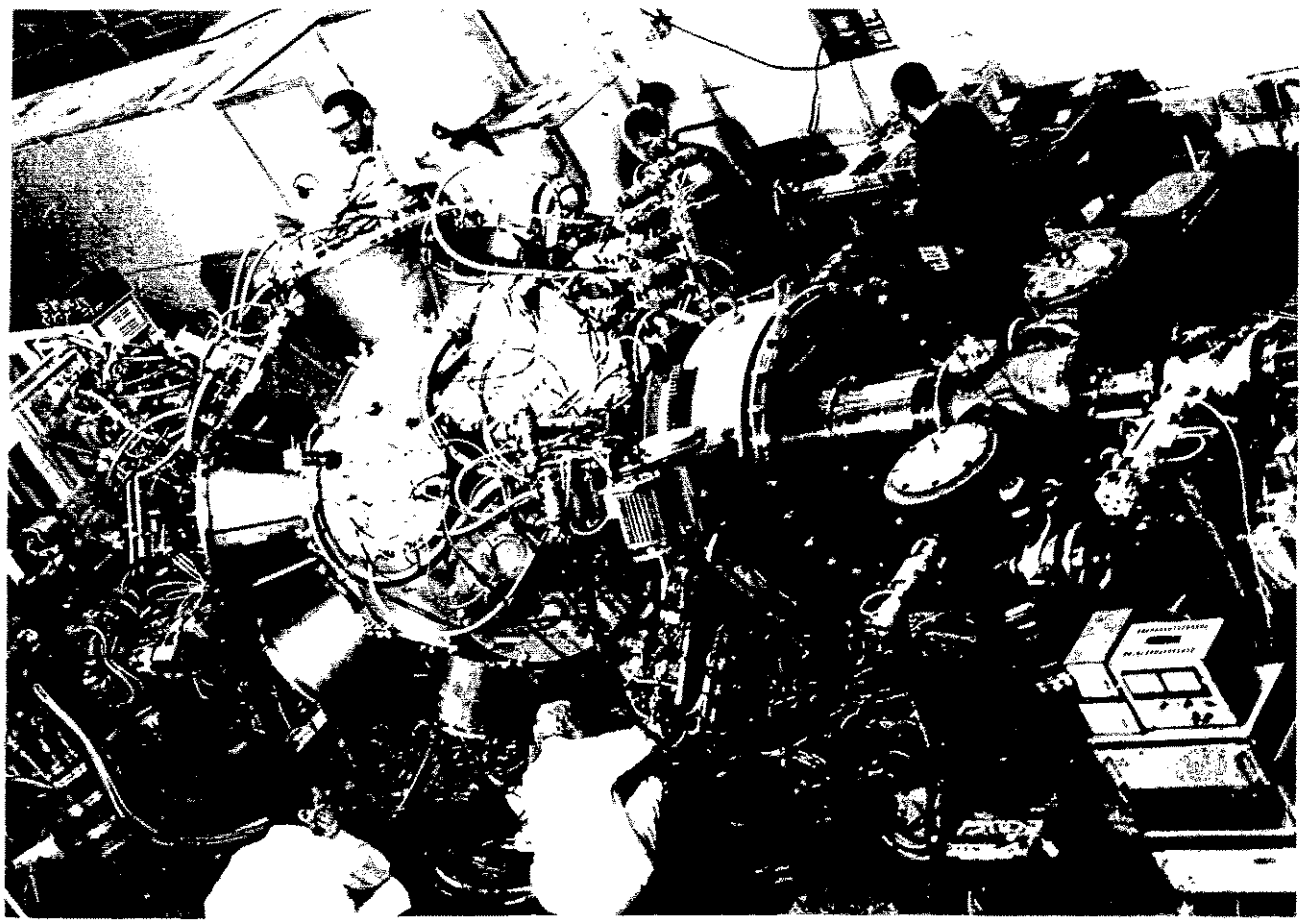

THE FRONT-END ELECTRONICS AND THE DATA ACQUISITION SYSTEM OF THE FOBOS 4π - ARRAY

O.V. Strekalovsky [1], K. Heidel [2], S.I. Ivanovsky [1], D. May [2], H.-G. Ortlepp [2], G. Pausch [2], G. Renz [2], V.V. Trofimov [1], I.P. Tsurin [1], W. Wagner [2], V.E. Zhuchko [1]

[1] Joint Institute for Nuclear Research, Dubna, RUSSIA
[2] Research Centre Rossendorf Inc., GERMANY

1. Introduction

The FOBOS spectrometer /1/ built up at the FLNR of the JINR Dubna is intended for heavy ion reaction studies in the bombarding energy range of 10...100 AMeV. In its final stage it will consist of a gas detector ball of 30 position sensitive avalanche counters (PSAC) and 30 (Bragg) axial ionization chambers (BIC) behind them. A shell of 210 CsI(Tl) scintillation counters /2/ surrounds the gas detector ball. In addition 92 phoswich counters of the former ARGUS array /3/ of the HMI Berlin will be used as a forward detector.

The counters are arranged in 30 modules placed on the facets of a polyeder of 12 regular pentagons and 20 regular hexagons. Two pentagons are used for the beam input and exit, the last containing the forward detector in an extended cone.

2. The position sensitive avalanche counter channel

The PSAC are based on the principles described in ref. /4/. One central cathode foil delivers the timing signal and two outer anode wire planes serve as coordinate grids (fig.1). Three 120 $\mu g/cm^2$ thick polyester foils are utilized, the outer ones acting as the counter windows and the central one depleted with 40 $\mu g/cm^2$ gold layers on both sides as the cathode. The counter frames have pentagonal or hexagonal shapes leaving circular sensitive areas of diameters 243 mm and 327 mm respectively. The sensitive gap amounts to 3.0 mm. 30 μm thick Cu-Be wires spaced by 1.0 mm serve as anodes.

Every two neighboring wires are connected with a conductive strip capacitively coupled to a wound delay-line. The two lines have 1.4 ns/mm specific delay and 50 Ω impedance. They are matched with resistors at one end and coupled to read-out amplifiers 5027-30 with 560 Ω "cold" dynamical input resistance and 800 fold current amplification at the other end.

The negative detector bias is fed to the cathode. The cathode read-out circuit delivers an 80 fold amplified current signal (Avalanche-Counter-Amplifier 5027-40) for timing and a charge signal of 150 mV/pC sensitivity for pulse-height analysis needed for checking purposes. The amplifier is isolated from high voltage (bias 1.5 kV, filter time 0.5s). The timing signal may be directly fed into a trigger. All channels are protected against damage for the case of spark discharges in the gas. The circuits are placed directly on the counter frame.

The three constant-fraction discriminators (CFD) are housed in a single CAMAC module FZR 5386 (fig. 4). Their thresholds are CAMAC-controlled. The wide dynamic range (1000:1) allows to cover all experimental conditions without changing the amplification factor of the preamplifiers. The delays necessary for formation of zero-crossing must be realized by external cables. The time walk is ± 50 ps for step pulses of 2 ns risetime in the range 10 mV ÷ 2V.

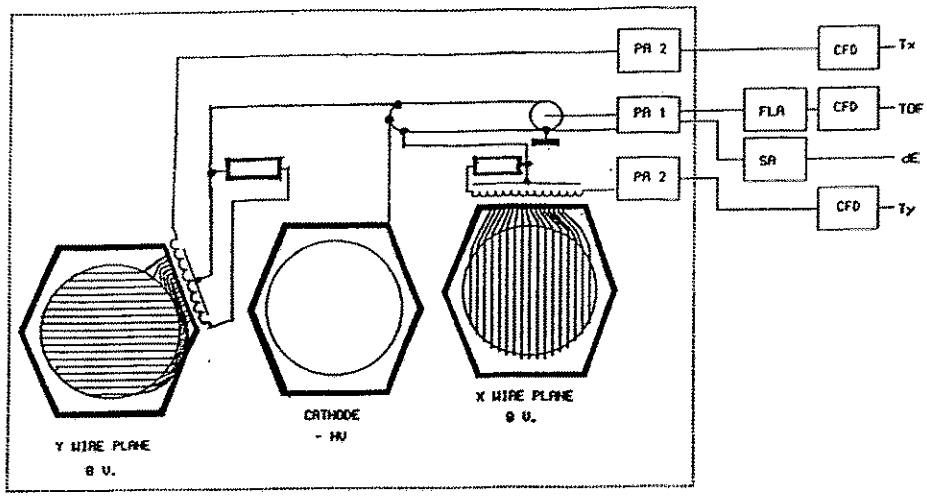

Fig. 1 Read-out principle of the position sensitive avalanche counter

3. The ionization chamber channel

The axial ionization chambers cover cones of $\pm 13.8^{\circ}$ and $\pm 17.4^{\circ}$ with entrance window diameters of 285 mm and 385 mm respectively. The window foils are supported by a twofold structure - a main carrier with 94 % transparency and an etched nickel mesh of $\varnothing$ 2.7 mm cells with 66 % transparency. Since the last number causes the most serious restriction to the solid angle a better solution for this mesh is being developed. However, cells smaller than $\varnothing$ 3 mm are necessary because otherwise the foil would not withstand a gas pressure of 100 kPa needed to stop most of the intermediate mass fragments within the depth of the BIC of 25 cm.

The field shaping is performed by copper strips coated on the Teflon insulator cone in a distance of 5 mm. The voltage devider provides equal potential steps , e.g. a homogeneous field.

The Frisch grid consists of two perpendicular planes of 1 mm spaced 50 µm thick Cu-Be wires. This solution has been chosen to compensate the mechanical tension deforming the carrier ring.

The anode placed 10 mm behind the Frisch grid is made of a 10 µm thick aluminized Mylar foil which may be penetrated by the light charged particles to be registered in the scintillation counters. At a gas pressure of 100 kPa an anode potential of + 8 kV is necessary (the entrance window acts as cathode and is grounded).

The electron drift time of up to 4 µs would cause large ballistic deficit in the case of conventional pulse shaping. Therefore a digital processing method /5/ has been utilized which derives the energy and Bragg-peak height from digitized signal samples. The principle is illustrated in fig. 2. The read-out system of the BIC consists of a charge sensitive preamplifier 5027-10 and two CAMAC modules - the Bragg-curve digitizer BCD 5387 and the Bragg digital processor BDP 5385 /6,7/. The Bragg-curve signal is shaped by a spectroscopy amplifier with short time constant 0.2/0.4 µs and digitized by an 8-bit flash ADC with a quartz stabilized sampling frequency of 10 MHz. When a signal is recognized by the threshold comparator two arithmetic units calculating E and Z are activated. The algorithms are schematically displayed in the bottom of fig. 2. The shadowed areas indicate sums of digitized values. A digital comparator determines the threshold for pulse recognition

and a pile-up inspector rejects erroneous results. The control of the working conditions and the data transfer is performed via the CAMAC dataway. The control logics (not shown in fig. 2) realizes the

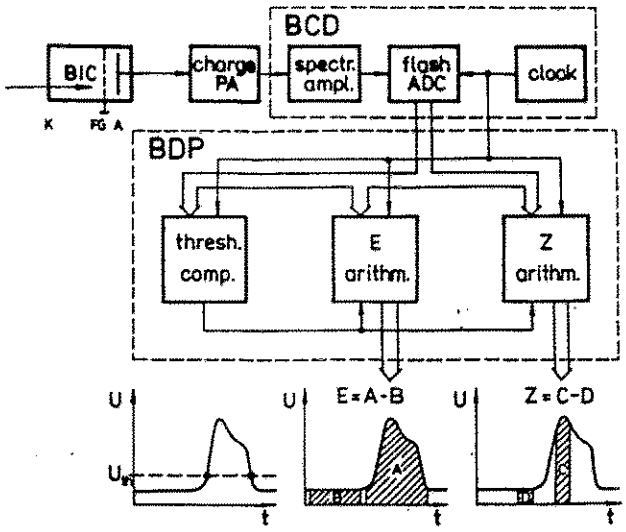

Fig. 2 Principle of the new signal processing method for Bragg-peak spectroscopy

coincidence conditions with the PSAC, the pile-up inspection and the connection with the first-level trigger logics. The digital processing system is faster by a factor of 10 and about two times cheaper than a conventional one and very simple to operate.

4. The first-level trigger

Fig. 3 shows a block diagram of the electronics of the PSAC plus BIC subsystem

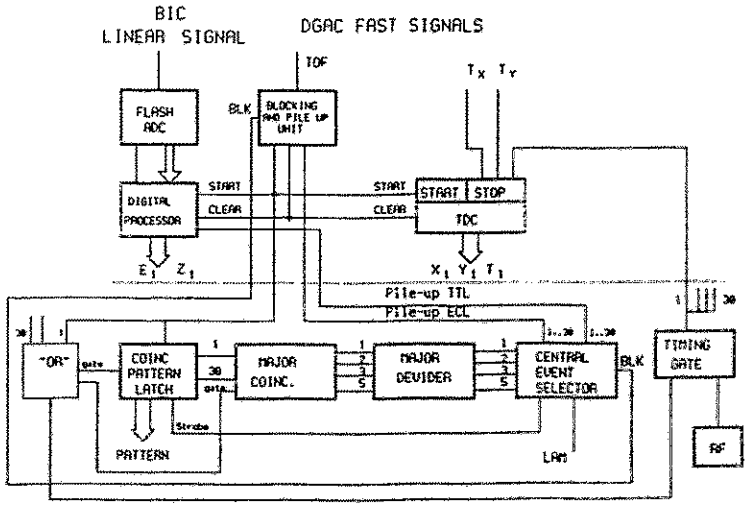

Fig. 3 Front-end electronics of a gas detector module and part of the first-level trigger

If the BDP is not busy the PSAC timing signal pass a blocking and pile-up unit (LBIN module in fig. 4) which is connected with the control logics of the BDP and reaches the coincidence pattern latch register KR13K. The pattern is analyzed by a majority coincidence unit KL360 the outputs of which are connected with the central event selector. If the multiplicity condition is fulfilled and there was no pile-up signal the central event selector indicates a "good " event and sets a LAM. To provide an effective pile-up rejection the following conditions must be fulfilled to allow an event for registration: (i) no avalanche counter signal 12 μs before and 6 μs after the event

(ii) no threshold comparator response 10 μs before the event

(iii) trailing edge of the threshold comparator within a certain time window relative to the avalanche counter signal.

The computer first reads the coincidence register and then the conversion results of the TDC's and BDP's fired. Then the blocking signal is removed and the system is ready again.

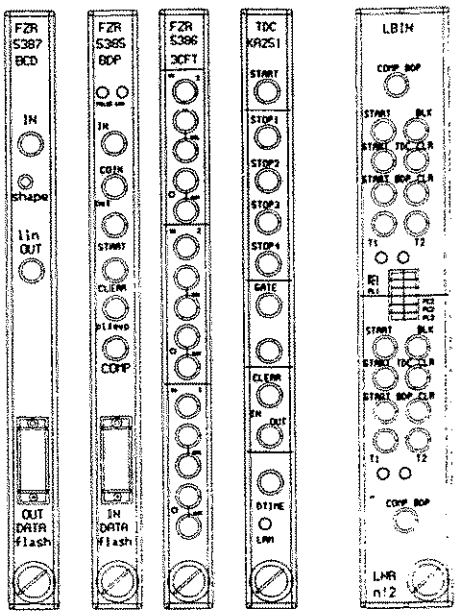

Fig. 4 CAMAC modules for FOBOS

5. The scintillation counter channel

The avalanche counters and ionization chambers are not sensitive to low ionizing high energetic light charged particles (LCP). Therefore a shell of 210 CsI(Tl) scintillators was decided to be arranged behind the gas detectors.

Fig. 5 shows a diagram of the electronics of the CsI(Tl) detectors. For the purpose of pulse-shape discrimination the anode signals of the photomultipliers are split by a passive splitting-and-delay box into a "fast" and a "slow" branch. The "fast" signals are delayed by 200 ns delay-line chips FLOETH PD24-20051D.

The branches are directly connected with the respective CIAFB analog-to-digital converters. The CIAFB /8/ is a 96 channel 12/15 bit gated charge integrating ADC housed in a single width FASTBUS module. The signals Gate-1 (400 ns) for Q_{fast} and Gate-2 (2 μs) for Q_{slow} are delivered by a REDUV gate-and-delay generator /9/. For every 16 scintillator channels a sum signal is provided which is fed via a buffer to a discriminator. From the discriminator outputs a simple first-level trigger signal of the scintillator shell is derived and fed into a gate-and-clear logics. A signal "CsI-fired" is sent to the central event selector.

Getting a LAM the EUROCOM-6 VME CPU after reading the front-ends of the gas detectors looks for the "CsI-fired" bit. If it is set, data from the FASTBUS modules are transferred after conversion (conversion time ≈ 1 ms for the 96 channels of CIAFB ADC) to a VME buffer. Then all conversion results are scanned and those exceeding a given threshold are added to the event data. If there is an event in the gas detectors but not in the CsI shell or the event has been rejected by the fast trigger of the gas detectors , a "Fast Clear" prevents the conversion in the CIAFB thus excluding the 1 ms dead-time.

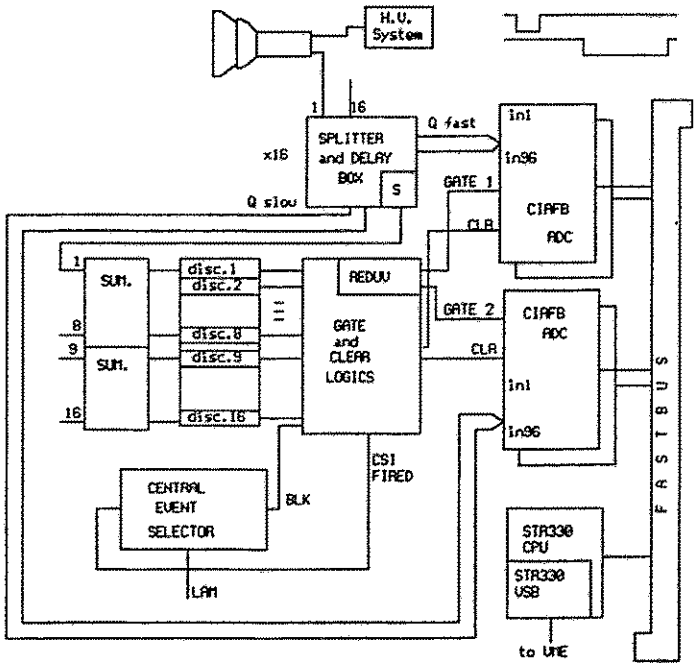

Fig. 5 The data acquisition system of the CsI(Tl) detectors

5. The system for data acquisition and analysis of FOBOS

Fig. 6 shows the status of the FOBOS data acquisition system in the middle of 1994. Seven CAMAC crates for digitizing and control are connected with the main VME crate by means of the parallel VSB Differential Bus Extension (VDB bus) /10/. The VDB bus is well suited for multi-crate systems where different bus standards have to be controlled.

In the main VME crate a single-board computer EUROCOM-6 with 68030 CPU builds the separate data to the event data block. The STR 723 VSB / VDB converter /11/ is placed in the ELTEC VME crate at the rear side. It connects VSB bus to VDB bus. The STR 723 works in the VSB-Master / VDB-Slave mode.

The CAMAC-to-VSB interface is a single width CAMAC crate controller STR 610 / CBV /11/ driven from the VME Subsystem Bus (VSB) via the VSB Differential Cable. The specification of the STR 610 / CBV is similar to the A1-type CAMAC crate controller. The CBV occupies the CAMAC station N=24 and requires a connection to station N=25 via an other CAMAC module, e.g. STR 611 / DMS (CAMAC Dataway-Display and Dummy crate controller). The STR 610 / CBV maps a portion of the VSB address space to the CAMAC "C,N,A,F" and generates single CAMAC cycles from each proper VSB cycle.

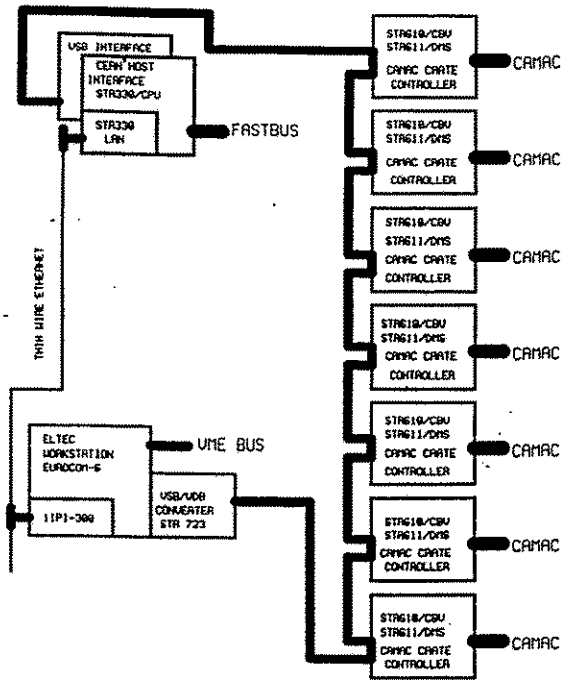

Fig. 6 Configuration of the data acquisition system of FOBOS

Four F683C FASTBUS ADC's /8/ are used for the photomultiplier read-out. In a FASTBUS Mini-Crate there are the STR 330 / CPU CERN Host Interface FASTBUS processor board, the STR330 / VSB I/O-Port and the STR 330 / LAN Ethernet module /11/. The STR 330 is a 68030-based processor system. The STR 330 / VSB I/O-Port provides an efficient interface between the CHIPS and the ELTEC VME workstation. The STR 330 / VSB operates in VDB Slave mode. The CHIPS data memory is directly mapped into the local VSB address space and the VME EUROCOM-6 processor module is treated by the same manner as any local memory.

The ELTEC VME workstation is connected to a special Ethernet segment and further by a fiber-optic link to the μVAX and SUN computers in the computer center (fig. 7).

The real-time operating system OS-9 (professional) released by Microware is used for the 68030 based VME and FASTBUS CHIPS modules. All time-critical tasks of the data acquisition are moved to the VME and FASTBUS processors.

The HOOPSY data acquisition software system /12/ resident at the μVAX has been modified for VME EUROCOM-6 and successfully applied in a the first FOBOS experiments. The data collected on the disk of the SUN Sparcstation-10 can be stored on Exabyte tape.

Quasi on-line monitoring of recorded data is performed by several PC's with the help of the ATHENE data analysis software /13/ having access via LAN to the data just written on disk. The data file structure is characterized by sequential event storage into closed blocks of fixed length. All events are stored completely. The information about the data file structure is assigned to the program by header blocks.

The evacuation and gas supply system of FOBOS /14/ is based on a SIEMENS-SX-Multibus II system and a SUN Sparcstation SLC computer. It controls 64 ADC and 16 DAC channels and 352 digital input and 288 output channels within a Multibus I crate. The necessary cyclic data transfer to the SUN station is realized via special TCP/IP socket programming. The pressure-time behavior of any of the 64 measuring points can be displayed on the screen of the SUN. Each on-line diagram shows the pressure trend at one of a measuring points during the past 30 minutes. Programs for error handling have been implemented. In case of an error a message window with explaining text is opened and an acoustic signal is warning the user. If some pressure exceeds

its permitted range the high voltage is switched off automatically. A DECbridge-90 has been installed to connect the FOBOSNET segment with the Ethernet segment of the evacuation and gas supply system. For control of the high voltage channels of the C.A.E.N. SY 403 and SY 127 systems they have been connected to a DECserver-200.

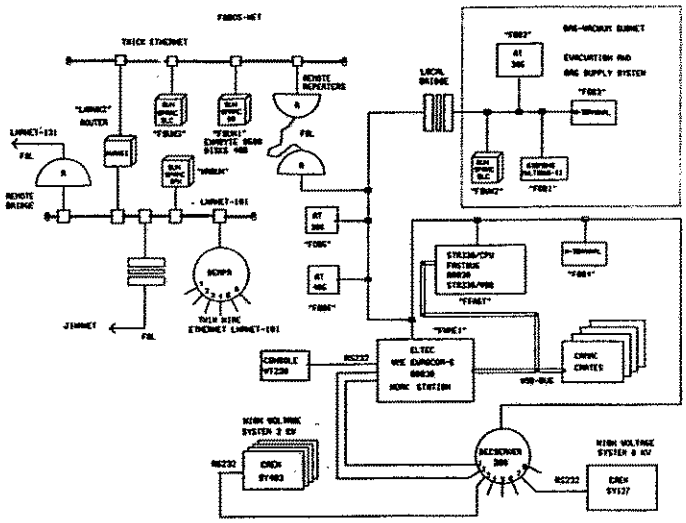

Fig. 7 Architecture of the FOBOS network in 1994

7. Performance

The first experiments at the FOBOS multidetector array using the VME-based data acquisition system have been started last year /15/. They are directed to study the fission process of nuclei as in the case of cold fission in ^{244}Cm(sf) as at the heavy ion beam of the cyclotron U-400M of the FLNR at JINR Dubna.

References

/1/ H.-G. Ortlepp et al., Proc. Int. School-Seminar on Heavy Ion Physics, v.2, JINR Dubna, Russia, 1993, p.466.
/2/ W. Wagner et al., FLNR Scientific Report 1991/92, JINR Dubna, Russia, 1992, p.244.
/3/ W. Terlau et al., Report HMI - 482, Berlin, 1990, p.93.
/4/ W. Seidel et al., Nucl. Instr. and Meth. A273, 1988, p.536.
/5/ H.-G . Ortlepp and A. Romaquera , Nucl. Instr. and Meth. A273, 1989, p.500.
/6/ W. Fromm et al., JINR Scientific Report 1989-1990, E7-91-75, Dubna, 1991.
/7/ K. Heidel and H.-G. Ortlepp, Annual Report 1992, FZR 93 - 10, Rossendorf, 1993, p.136.
/8/ C.A.E.N. General Catalogue 1993.
/9/ REDUV Manual, Institut de Physique Nucléaire, Orsay, France.
/10/ P. Ziem et al., Report FZR 92 - 11, Rossendorf, 1992, p.19.
/11/ STRUCK Product Summary 1990, Hamburg, Germany, 1990.
/12/ G. Röschert et al., Report HMI - 436, Berlin, 1986.
/13/ C.-M. Herbach, C. Umlauf, FLNR Scientific Report 1991/92, JINR E7-93-57, Dubna, 1993, p.250.
/14/ G. Renz et al., Annual Report 1992, FZR 93 - 10, Rossendorf, 1993, p.122.
/15/ A.A. Aleksandrov et al., Proc. of the Int Conf. on Nucleus-Nucleus Collisions, Taormina, Italy, 1994 (to be published in Nucl. Phys.).

UPGRADE OF THE FOBOS DATA ANALYSIS SOFTWARE

C.-M. Herbach [1] , D.V. Vakatov [2]

[1] *Research Centre Rossendorf Inc., GERMANY*
[2] *Joint Institute for Nuclear Research , Dubna, RUSSIA*

1 UPGRADE OF THE DATA ANALYSIS PROGRAM ATHENE

1.1 Introduction

The ATHENE code for IBM PC was originally designed at the Flerov Laboratory of Nuclear Reactions by C.-M. Herbach and C. Umlauf /1/ to analyze the data obtained from the experimental set-up "Mini-FOBOS". Since December 1992 the adaptation of the ATHENE code to the NDP /2/ environment on IBM PC-386/486 and its further improvement has been performed in the collaboration with the Laboratory of Computing Techniques and Automation .

The program allows to read data written in the formats of the programs CAMDA, OLYMP and HOOPSY. It is foreseen to read data written in other formats as well as to use additional special data transformation algorithms.

The user has the possibility to accumulate and to visualize both ordinary histograms (fig.1) or.

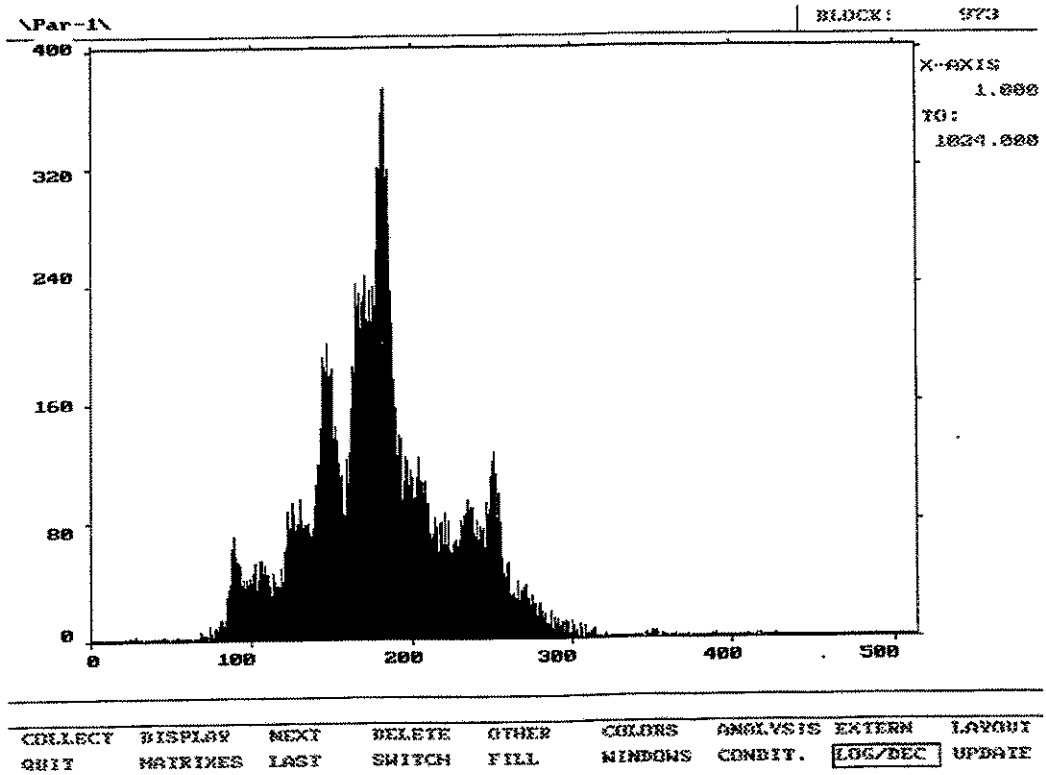

Fig. 1 The one-dimensional histogram working space

color scatter-plots (fig.2). He also can produce new data files reduced in the event dimension and/or selected by some condition in the formats of CAMDA or OLYMP.

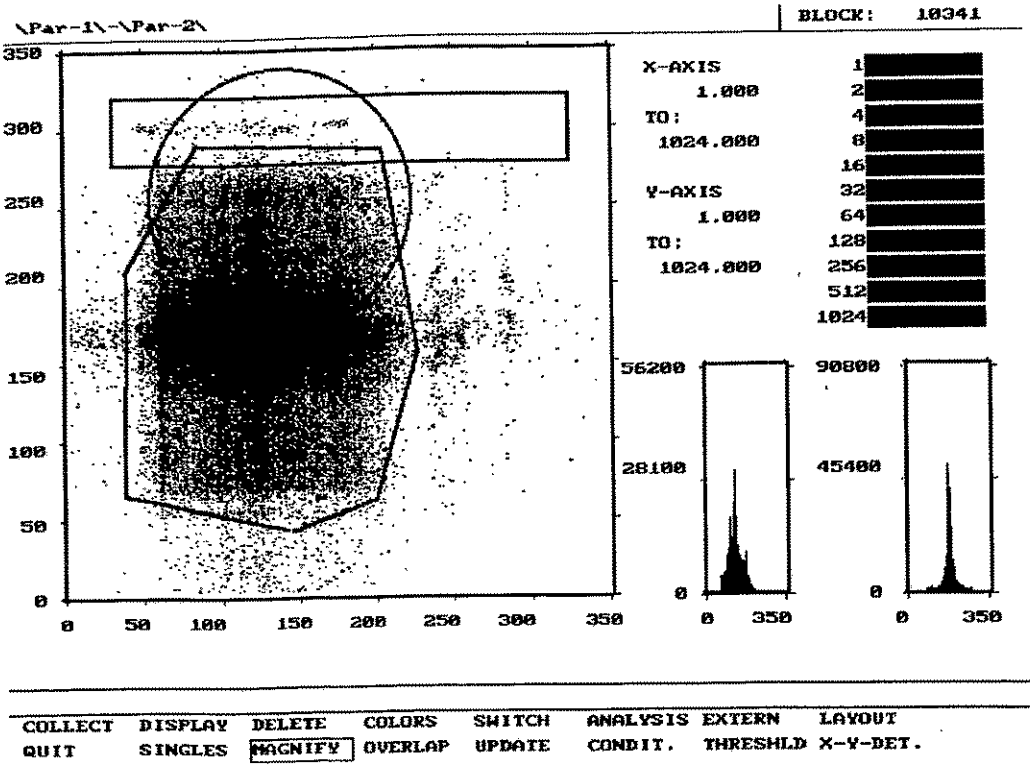

Fig. 2 The scatter-plot and three graphical gates

During the data accumulation the user can observe and switch between any of 20 histograms and 10 scatter-plots. He can execute some operations acting to these histograms such as simultaneous displaying (in XOR mode) of several histograms, linear/logarithmic scaling, setting gates within the histograms (graphically by use of the mouse), calculating some statistics concerning these gates, etc. He also can interactively drive the process of data accumulation by setting both parameters to be gathered and relevant selection criteria for every histogram, scatter-plot or output data file.

All configuration conditions concerning the parameters, histograms, gates, selection criteria and colors used in the program can be easily saved to a disk file and retrieved just so the content of any histogram or a scatter-plot.

The user drives the program with the help of a system of menus. He can use both the keyboard and the mouse to manage the menus.

1.2 Data reading, selection and accumulation

The common idea of processing the data within the program is shown in fig. 3. Experimental data are extracted from the data source event by event At the first stage their parameters may be transformed with some user-defined algorithm embedded into the program code in advance. The user can interactively determine lower and upper limits of each of these parameters with the aid of a menu.

The next step is the filling of all declared accumulation units (histograms, scatter-plots and the output data-file) with parameters of the latest event. Here also a personal event selection for each accumulation unit can be made which determines whether the event must be used to update the content of this accumulation unit.

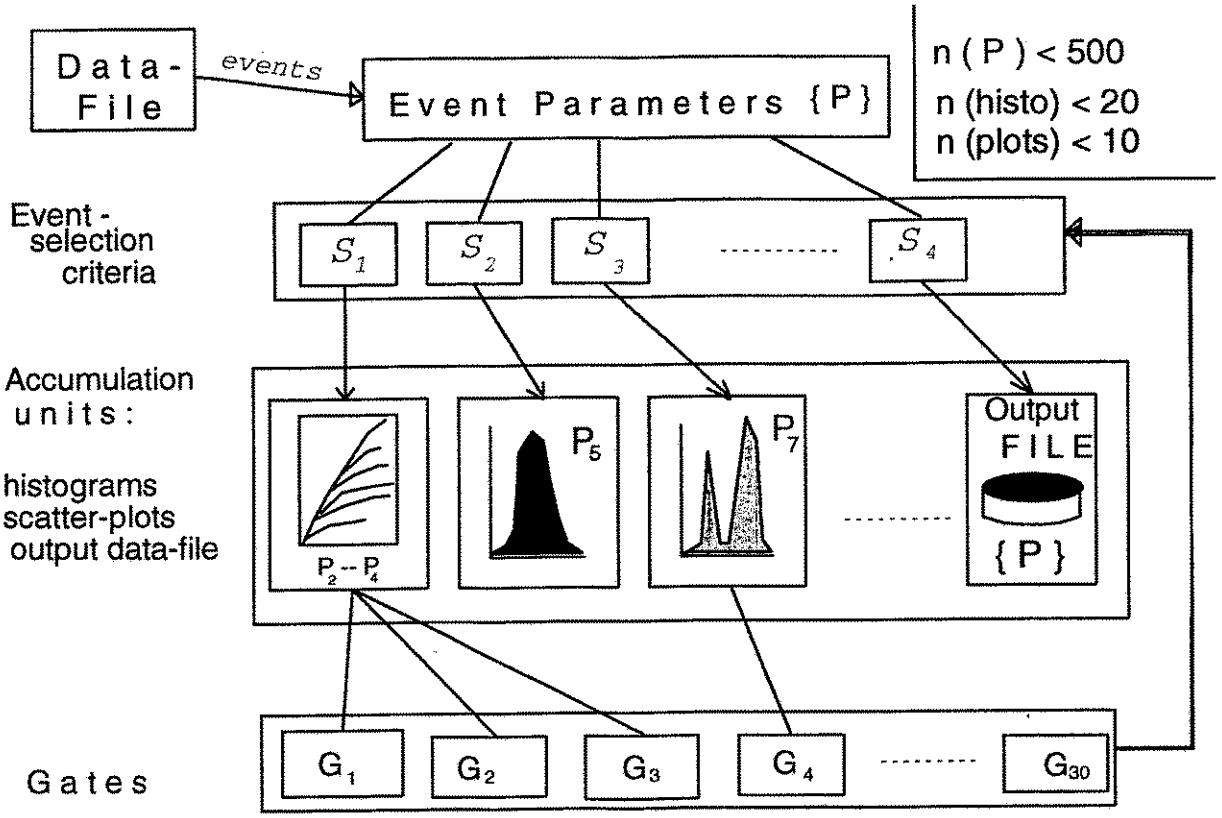

Fig. 3 General schedule of the data processing in ATHENE

Any selection criterion is built on the base of a set of gates. There are four predefined types of gates in the program - a ring, a box and a polygon area in the space of two parameters and an interval for single parameters. The user can set up to 30 gates interactively. The gates can be applied by using either the appropriate graphical tool, the relevant menu or both them In fig. 2 an example is shown of how to determine three different gates for the parameters "Par-1" and "Par-2" by using the (color) scatter-plot of these parameters.

The selection criterion is a logical expression combining the gates. It may be false or true depending on the validity of the event parameters as regards to gates used in the expression . The user can determine these logical expressions for each accumulation unit with the help of the relevant menu. The common form of such an expression is as follows:

$$S = (G_i \text{ .AND. } \overline{G}_j \text{ .AND. } ...) \text{ .AND. } (G_k \text{ .OR. } G_l \text{ .OR. } ...) \text{ .AND. } (\overline{G}_m \text{ .OR. } G_n \text{ .OR. } ...) \text{ .AND. } ...$$

where $\overline{G}_*$ means the negation of the gate G_*

Although the gates can be determined with the help of a histogram or a scatter-plot they do not depend on any histogram or scatter-plot because the gates are imposed directly to the event parameters.

1.3 Upgrading in 1993 - 1994

Some of the most significant advantages of the new version of ATHENE in comparison with the original one are the following :

- The new version works in the protected mode of the processor i80386(486) and, therefore, it can use all (extended) memory of the computer to store both code and data of the program. This feature significantly decreases the required size (150K instead of former 600K) of conventional memory. It also dramatically increases the size of the memory used by the program and allows to keep (and accumulate) simultaneously several scatter-plots in the memory (e.g. $10 \div 15$ plots of $350 \cdot 350$ cells at a computer with 8 Mb RAM). In this turn, it allows one to easily manipulate with accumulated scatter-plots (e.g. adding or multiplying them by each other) even if one of them is located in the disk file.

- The basic graphic routines have been rewritten using the graphics library so to operate now in the VGA graphic mode (instead of the former EGA mode).

- The mouse control has been implemented in addition to the keyboard. This provides a faster and more convenient way of setting gates graphically by using histograms and scatter-plots. It also facilitates handling menus in the program.

- The possibility of magnifying selected parts of histograms or scatter-plots has been provided what allows to set gates more precisely.

- Some of the data processing and visualization algorithms have been improved to speed up the execution of the program.

- Algorithms have been added to process data in OLYMP, HOOPSY and some other formats what enables us to use ATHENE for the complex quasi on-line monitoring of experimental data.

1.4 Quasi on-line data monitoring

During the last experiments at the FOBOS set-up we used the schedule of data transferring and monitoring as shown in (fig.4).

The delay from the real-time of the experiment was $2 \div 5$ s. All functions of the program can be used as in the quasi on-line as in the off-line mode (e.g. data conversion and selection). The only restriction is the power of the PC.

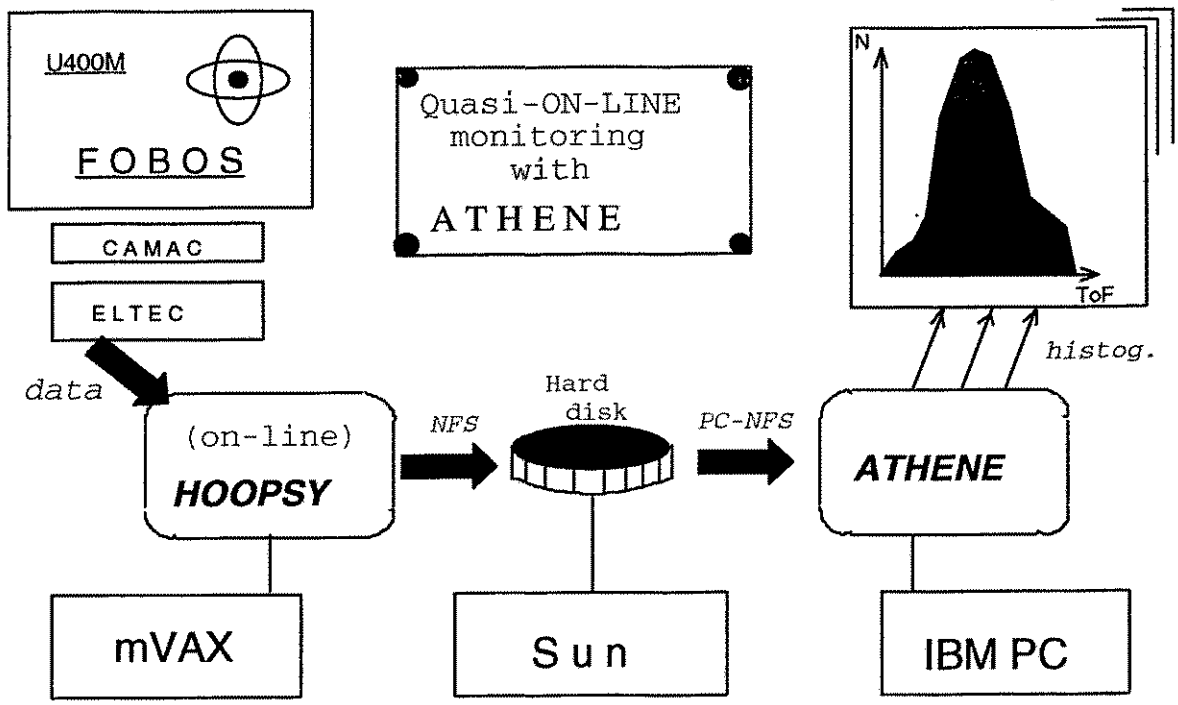

Fig. 4 The quasi on-line data monitoring with ATHENE

2 CREATION OF A NEW DATA-PROCESSING PROGRAM ATHENE94

The new version of the ATHENE program is able to process more complex and voluminous data what allows to analyze the current FOBOS data. However, the size of data obtained from the experiment increases dramatically if the dimension of the event becomes larger. Qualitative improvements of the ATHENE algorithm and even use of more powerful PC, eventually, can not satisfy the requirements of the user completely.

There is the need in more flexible programs which include a command interpreter to provide the batch-mode execution and a FORTRAN interpreter to provide execution as has been realized in e.g. the PAW and OLYMP packages.

Therefore, it was decided to design a new program -ATHENE94- for processing of experimental data using computers with UNIX-like /3/ operational systems and an X-WINDOWS environment.

Work is in progress to develop such a program on the base of a SPARC-station with the operational system SOLARIS. To make the program portable the routines from the standard UNIX library, MOTIF/X11 /4/, CERNLIB packages as well as C++ and Fortran77 languages are used (fig.5). Furthermore, the use of the X11 library will allow to run this program from any remote X-terminal.

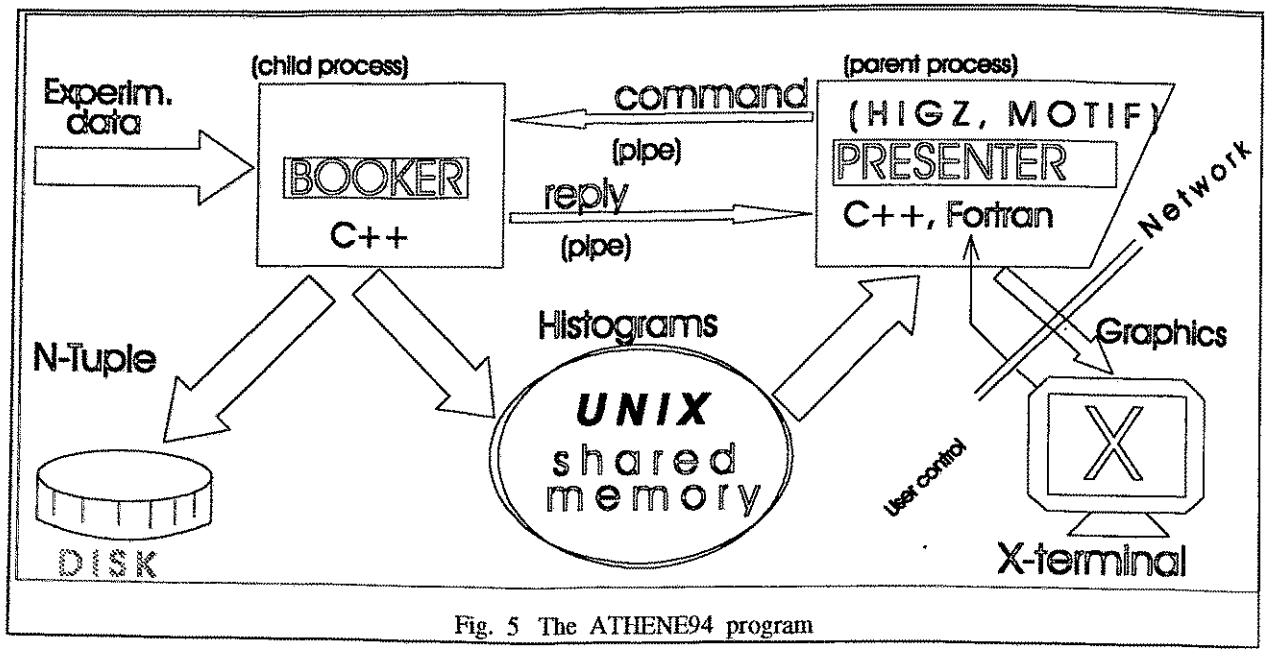

Fig. 5 The ATHENE94 program

To provide real-time data processing the program is subdivided into two UNIX processes connected with each other via UNIX pipes and UNIX shared memory. PRESENTER (fig. 5) provides the interaction (HIGZ /7/ science graphics and the MOTIF /5,6/ user interface) with the user. It also manages the process BOOKER (fig. 5) responsible for conversion of the experimental data, selection and booking into histograms.

It is planned to include into ATHENE94 some useful features of PAW, OLYMP and ATHENE, e.g., the command interpreter, the FORTRAN interpreter and some special FOBOS-oriented tools and algorithms. Great attention will be paid to obtain flexibility and clarity of the code in order to easy modifying or adding further algorithms. For this reason almost all code ATHENE94 is written using the powerful object-oriented language C++ /6,8/.

A preliminary version of ATHENE94 will be created till the end of 1994 and the final version of the program is planned to be created in 1995.

References

/1/ C.-M. Herbach, C. Umlauf, FZR 92-11, Rossendorf, 1992 (Ed. H.-G.Ortlepp, K.-D.Schilling)p.25
/2/ NDP-Fortran Reference Manual, Microway Inc., Kingston, Massachusetts, USA.
/3/ M.I. Belyakov et al, "The Portable Operational System", Radio i svyaz, Moscow, 1991.
/4/ OSF/Motif Programmer's Reference Manual, rev. 1.0, Open Software Foundation, Eleven Cambridge Center, Cambridge, MA 02142, UK.
/5/ OSF/Motif Programmer's Guide, rev. 1.0, Open Software Foundation, Eleven Cambridge Center, Cambridge, MA 02142, UK.
/6/ Bjarne Stroustrup, "The C++ Programming Language", Addison-Wesley, 1986.
/7/ HIGZ User's Guide, CERN Geneva, 1993.
/8/ D.A. Young, "Object-Oriented Programming with C++ and OSF/MOTIF", Prentice Hall, 1992.

(FOBOS Workshop '94, Cracow, June 28–30, 1994)

Activities of the Detector Lab Rossendorf for FOBOS

J. Hutsch, M. Sobiella, K. Heidel, and G. Pausch

Forschungszentrum Rossendorf e.V., Institut für Kern- und Hadronenphysik, Postfach 51 01 19, D-01314 Dresden

1 General tasks and equipment of the Detector Lab

The Detector Lab Rossendorf, belonging to the Institute of Nuclear and Hadronic Physics (Research Center Rossendorf Inc.), had been established during the years 1991-93 as a base for development and assemblage of detector components which are intended for nuclear physics experiments and applied research. The heart of our lab is the precise winding machine [1] designed for an accurate manufacture of multi-wire planes (figure 1). This machine allows to wind wires (diameter range: 10 – 100 μm) with an adjustable constant tension (uncertainty: $< 5\%$) onto a rotating frame with a typical accuracy (characterized by the standard deviation of wire distances) of $\approx 15\mu$m. Wire planes up to 200 cm width and 270 cm length can be produced. A plane large-area granit table sited in a cleanroom beside the winding machine is available for assembling large detectors. The Detector Lab comprises also a small mechanical workshop and an experimental area, equipped with a central vacuum system and a gas supply system for usual counter gases, which is used by the experimentalists for detector tests.
The staff of our lab consists of three engineers an a physicist. Besides the manufacture of wire planes and other detector components, the Detector Lab supports the experimentalists with construction capacity and manpower for detector development and design, including the test of necessary new technologies. Essential contributions have been delivered e.g. for

- the construction of a PET camera for dose localization and beam monitoring in the light-ion tumour therapy which is being established at SIS / GSI Darmstadt [2],
- the construction and manufacture of internal supports and table frames for the EUROBALL CLUSTER detectors [3] within the EUROBALL project [4],
- the development of start detectors for the COSY-TOF collaboration [5] and the COSY 0^0-Facility [6] at COSY / KFA Juelich,
- the revised design and the production of double-grid avalanche counters (DGAC's) [7] for the FOBOS gas-detector ball [8] at the Flerov Laboratory of Nuclear Reactions in Dubna.

2 Production of wire planes for the FOBOS DGAC's

The position-sensitive double-grid avalanche counters (DGAC's) installed at present in the FOBOS gas-detector ball were designed in Rossendorf [7] and produced at the JINR Dubna. One of these detectors is schematically shown in figure 2. A cathode foil, fixed by distance frames, delivers the timing signal. Two wire planes read out via capacitively coupled continuous delay

lines are used to obtain x- and y-information. The grids consist of 50μm W-Au wires, the wire distance is 1 mm. The detector volume is formed by the vacuum-tightened stack of support frames and the entrance/exit windows consisting of thin polyester foils. Preamplifiers for the timing and position signals are mounted on the detector frame. The detector is filled with 3-5 Torr pentane and operated in vacuum.
In 1993 it was decided to revise the design of the DGAC's and to manufacture a series of detectors in our Detector Lab, exploiting the technological progress which was expected to be achieved with the new winding machine and the considerably improved infrastructure in Rossendorf. This revision included a new layout for

- the cathode frames,
- the support frames of the wire planes,
- the support plates of the delay lines for x- and y-readout,
- the x-, y-, and t-preamplifiers and the signal distributor for test signals.

All the support frames listed here consist of printed-circuit boards. The layouts of these frames as well as of the preamplifier and generator boards were designed by using the PC-based P-CAD system [9]. The P-CAD tools provide the flexibility and fine control necessary for the design of such nonconventional boards as e.g. the support frames of the wire planes (figure 3).
A very expensive process of the detector production is the manufacture of the two wire planes delivering the x and y information. In contrary to the previous technology, the wire is wound onto a double-sided winding frame (figure 1) and fixed with glue. As a second step, the wires being located on one half of the winding frame are soldered onto the support frame (figure 4). During this process, the support frame does not touch the wires. This technology guarantees a standard deviation of typically 20μm for the wire distances (figure 6), and a very accurate in-plane adjustment of all wires (figure 7).
Much care was taken to check the quality of the produced wire planes. The wire distances of selected planes were measured and analyzed using a PC-coupled CCD camera and the OPTIMAS software (figure 5). Examples are shown in figure 6. To check the planarity of wires at least qualitatively, wire planes were illuminated with a laser beam. Due to shadowing effects, "runaways" become visible by observing the reflected light with a CCD camera (figure 7). These tests showed clearly the progress achieved with the new technology: The accuracy of the wire distances as well as the in-plane adjustment have been improved considerably (figures 6,7).

3 Status of the detector production for FOBOS

Until the end of August 1994, ten complete pentagons and two complete hexagons have been delivered to the JINR Dubna. The mechanical and electronic components (except for the wire planes and cathode foils) of additional eight hexagons are available, ten additional wire planes for hexagons have already been manufactured. These eight hexagons will be assembled until end of 1994. Together with the DGAC's produced earlier in Dubna, this will allow to assemble the complete gas-detector ball of FOBOS in the beginning of 1995. The production of additional ten hexagons in the Detector Lab Rossendorf is scheduled for 1995. These DGAC's are planned to replace the detectors manufactured in Dubna.

References

[1] M. Sobiella et al.,
Research Center Rossendorf / Inst. of Nuclear and Hadronic Physics,
Annual Report 1992, p.115; Annual Report 1993, p.103.

[2] W. Enghardt et al., Phys. Med. Biol. **37** (1992) 2127.

[3] J. Stephan and M. Freitag,
Research Center Rossendorf / Inst. of Nuclear and Hadronic Physics,
Annual Report 1993, p.89.

[4] J. Gerl, R.M. Lieder (ed.): EUROBALL III – European γ-ray Facility.
GSI Darmstadt, Dec. 1992

[5] P. Michel et al.,
Research Center Rossendorf / Inst. of Nuclear and Hadronic Physics,
Annual Report 1993, p.40.

[6] S. Dienel et al., Subthreshold Production of K-Mesons, Letter of Intent / COSY, KFA Juelich, 1991;
R. Esser et al.,
Research Center Rossendorf / Inst. of Nuclear and Hadronic Physics,
Annual Report 1993, p.86.

[7] W. Seidel et al., Nucl. Instr. and Meth. **A273** (1988) 536.

[8] H.-G. Ortlepp et al., Proc. Intern. Conf. on New Nuclear Physics with Advanced Techniques, Ierapetra, Greece, 1991, p. 302.

[9] P-CAD Productivity Across the Board,
from: ALTIUM, An IBM Company, U.S.A., 7/94 (1994)

[10] Fundamentals of Pro/ENGINEER for release 9.0,
Document No. U06-0392-01, 1992, Parametric Technology Corporation

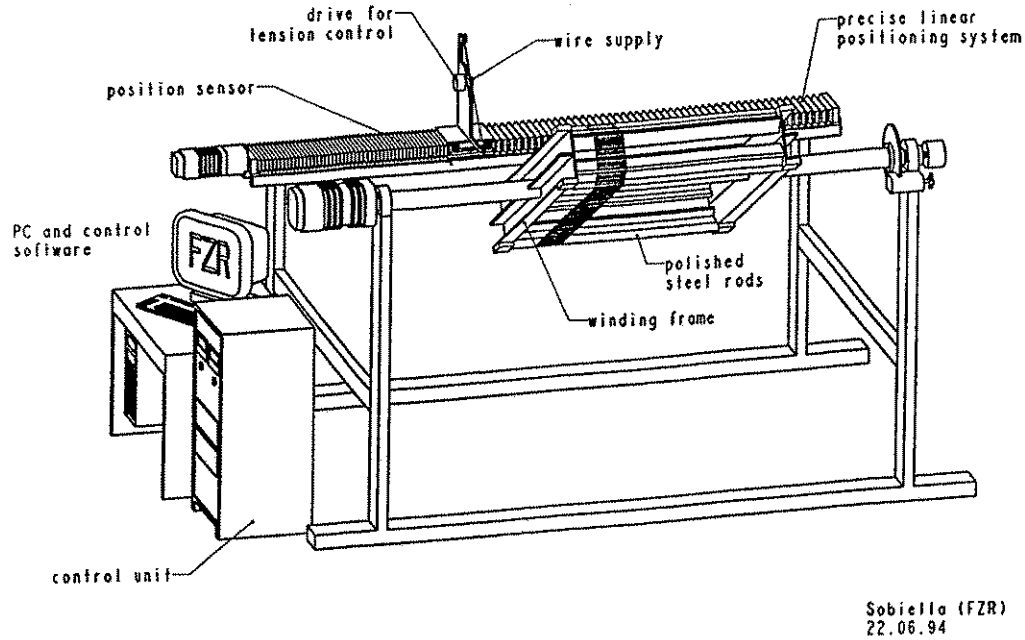

Figure 1: The winding machine for the precise manufacture of multi-wire planes. This drawing was generated with the 3d-CAD system Pro/ENGINEER [10] which is used in the Detector Lab Rossendorf for design and construction of detector components.

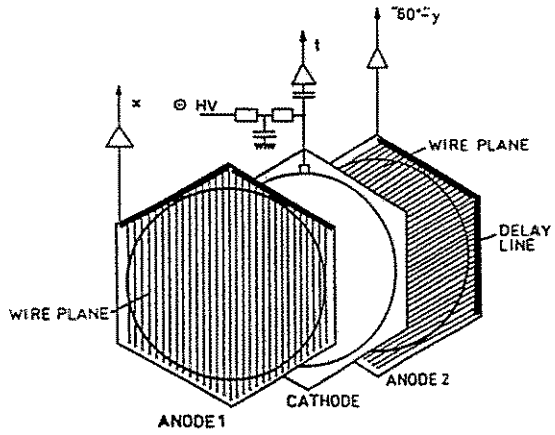

Figure 2: Scheme of a FOBOS double-grid avalanche counter (DGAC) [7]: A cathode foil and two wire planes are housed in a pentane-filled volume. The cathode, supplied with high voltage, delivers the timing signal. Position information is derived from two wire planes. In contrary to this sketch the relative angle between wires of the x- and y-planes is now 90^0.

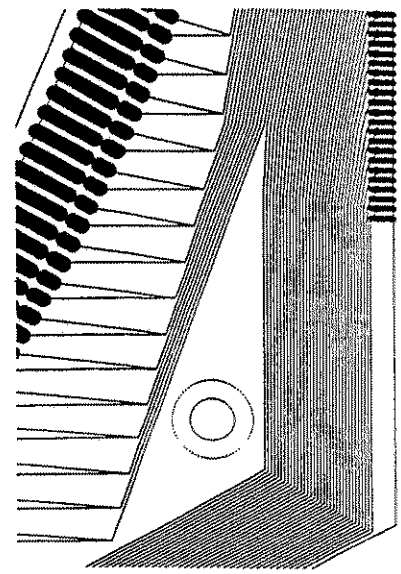

Figure 3: Detail of the layout for a hexagonally shaped wire plane (P-CAD design [9]): A double-sided printed-circuit board is used to connect the wires (soldered onto the left-hand contacts) with the right-hand contacts leading to the delay-line board.

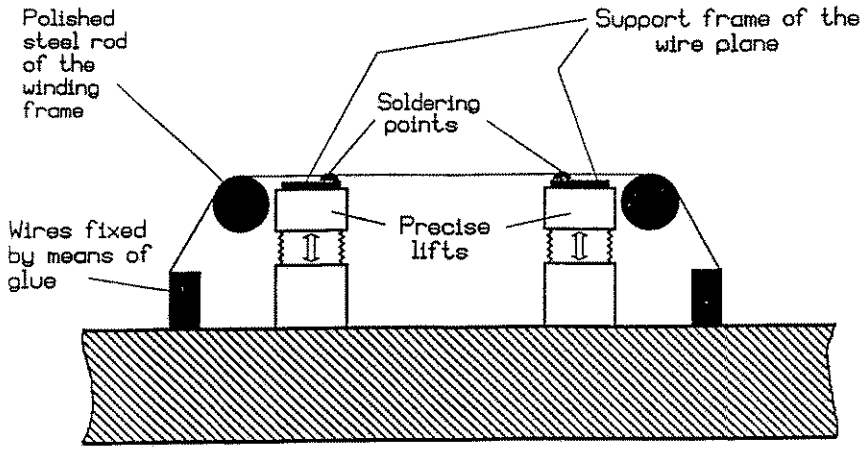

Figure 4: Principle of wire-plane preparation for the FOBOS DGAC's: The wires located on one half of the winding frame (see fig.1) are soldered onto the support frame. During the soldering process the wires do not touch the support frame. This guarantees minimum distortion of the wire positions (see fig.6).

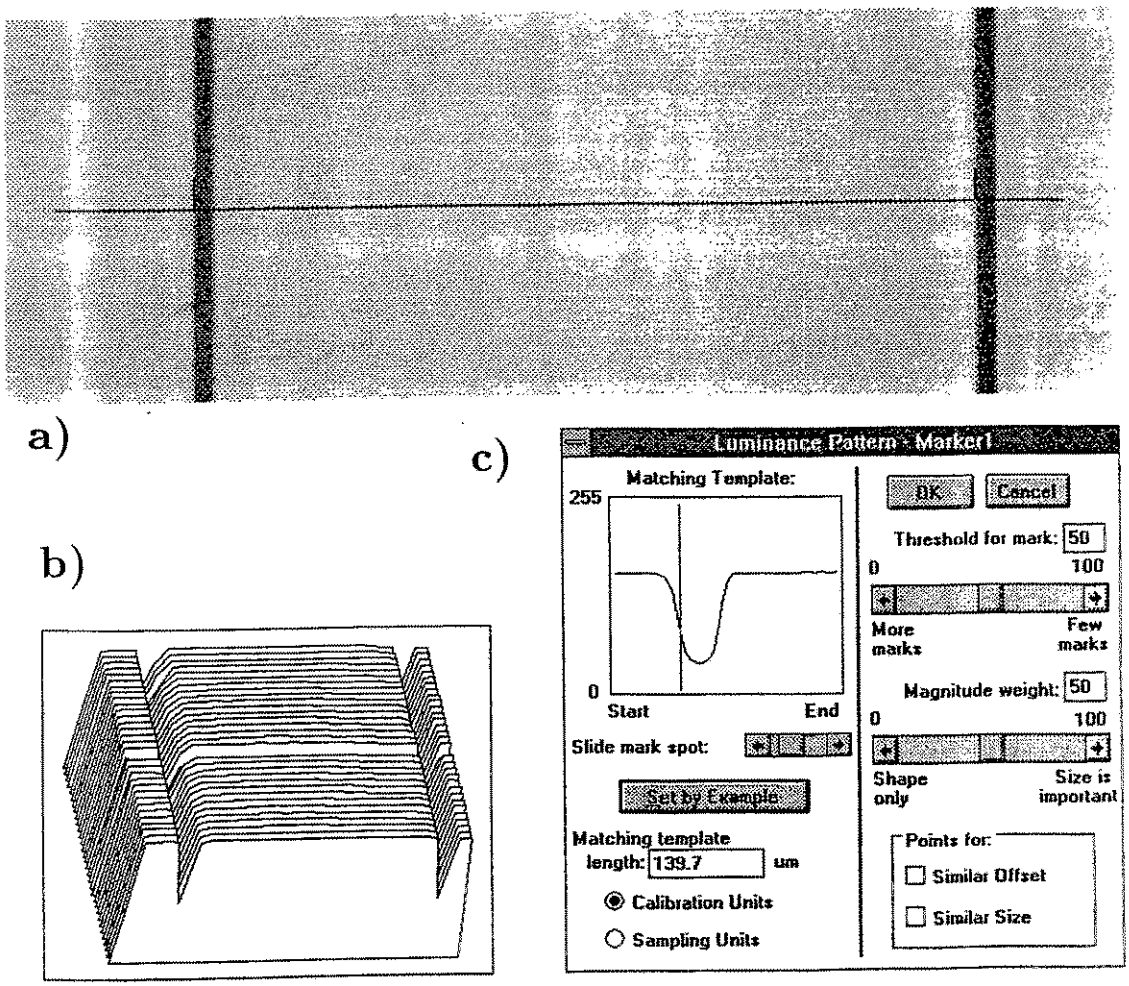

Figure 5: Illustration of the PC-based wire-distance measurement:
a) Two neighboured wires of a DGAC grid as seen by the PC-coupled CCD camera – the solid line indicates the cut used for the distance measurement.
b) Corresponding two-dimensional luminance pattern constructed by the OPTIMAS software.
c) The OPTIMAS menue shows the luminance threshold used for the software-controlled distance measurement.

a)

	A	B
Standardabweichung der Drahtabstände:	18,57	20,10
Durchschnittsfehler der Drahtabstände:	14,44	15,15

- ab hier einfügen -	lauf. Num. n	Werte A	Werte B
Filename: Fo614VI Datum: (A) 17.06.1994 (B) 22.06.1994	1	982	?
	2	992	?
	3	1001	?
	4	961	?
	5	1006	?
	6	1025	?
	7	982	?
Protokoll: (A) 30um, Wolfram vergoldet, 0,55 A Drahtzug 1 Umdrehung pro Minute (B) geloteter Zustand	8	995	989
	9	1006	1015
	10	999	994
	11	983	987
	12	1002	1005
	13		

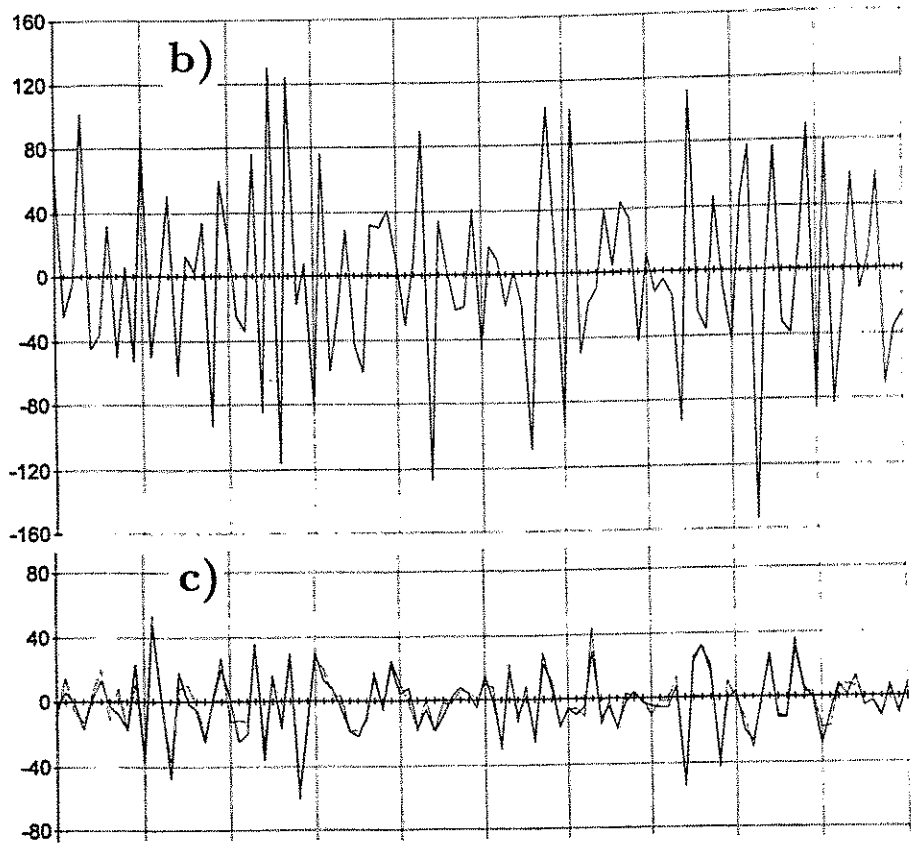

Figure 6: Measured wire distances are transferred into a MS-WORKS table and analyzed with standard procedures:
a) Protocol of a wire-distance measurement.
b) Deviation of measured wire distances (in μm) from the reference value, $d_{ref} = 1000\mu$m, for a DGAC produced in Dubna. The x-axis indicates the wire number.
c) The same for a DGAC grid produced in the Detector Lab Rossendorf. Solid line: Wires on the winding frame. Dotted line: Wires after soldering on the support frame. The dispersion of wire distances is mainly due to the winding process, the influence of soldering is small.

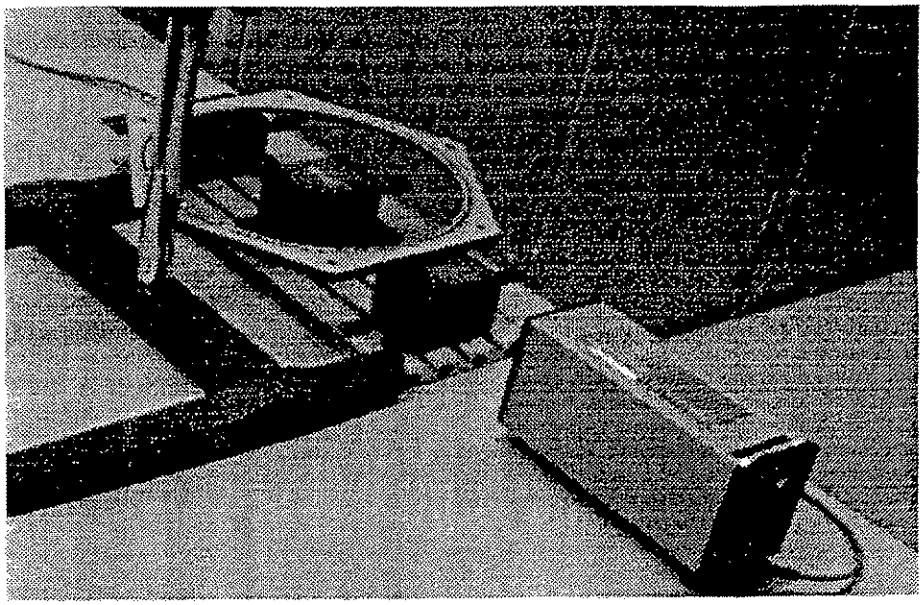

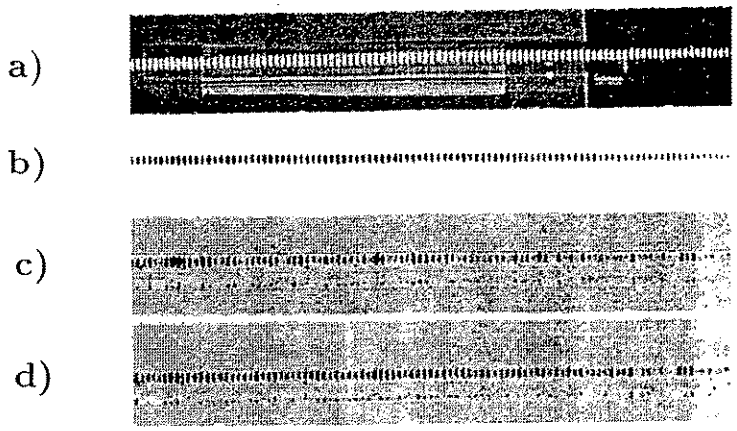

Figure 7: Qualitative test of the in-plane adjustment of wires: The DGAC grid is illuminated by a laser beam, the reflected light registered by a CCD camera. A precisely adjustable glass rod below the wire plane allows to lift misaligned wires.
a) View of a DGAC grid manufactured in the Detector Lab Rossendorf, glass rod does not touch the wires.
b) Negative of fig.7a).
c) View of a DGAC produced in Dubna (negative), glass rod touches the first wires.
d) Same as fig.7c), but glass rod lifted by $+40\mu$m. The misalignment of wires is at least 40μm.

(FOBOS Workshop '94, Cracow, June 28–30, 1994)

Possible ancillary detectors for FOBOS exploiting pulse-shape discrimination for silicon detectors

G. Pausch, H.-G. Ortlepp, W. Wagner

Forschungszentrum Rossendorf e.V., Institut für Kern- und Hadronenphysik, Postfach 51 01 19, D-01314 Dresden

During the last years, substantial progress has been achieved in exploiting pulse-shape discrimination (PSD) for identification of charged particles in silicon detectors [1, 2, 3, 4, 5]. By using a simple scheme of signal processing based on conventional electronics it was possible to identify charge and even mass numbers of heavy ions stopped in a silicon detector of 500μm thickness [5] (figures 1,2). The lower thresholds of element identification were in the order of 3 AMeV and 5 AMeV for carbon and silicon ions, respectively, and thus much lower as e.g. the identification thresholds of the phoswich detectors used in the ARGUS array [6]. A further reduction of these thresholds for IMF's is expected if the detector thickness, the detector bias, and the electronic shaping-times are optimized. This would allow to identify charge numbers of slow IMF's or decay products of nuclear multifragmentation which have low energies in the lab system.
Undoubtedly, the most attractive application would be the construction of a 4π silicon ball similar to the Berlin Si-Ball [7], but with PSD-based particle identification in a wide dynamic range. Such a ball can be combined with 4π neutron- or gamma-ray detectors, which would allow qualitatively new experiments. On the other hand, it is obvious to exploit this method also for ancillary detectors of existing arrays, e.g. FOBOS. Possible applications are:

1. **Alternative forward detectors** (figure 3): For angles larger than the grazing angle of the heavy-ion reaction it is possible to use a combination of a silicon ΔE detector (thickness: 200...500μm) and a usual scintillator (BGO or CsI, read out via photomultiplier or a photodiode). PSD would allow to identify low-energy IMF's and LCP stopped in the Si counter. For high-energy particles penetrating the Si detector, the arrangement is used as a conventional ΔE-E telescope. The thickness of the ΔE detector is then large enough to guarantee excellent charge and mass resolution.

2. **Specialized trigger detectors:** A combination as shown in figure 3 could be used as a trigger on low-energy IMF's at forward angles, where the background of light charged particles is high. The scintillator serves as a veto detector. Slow IMF's are stopped in the ΔE Si-counter and identified by means of PSD.

3. **Filling gaps in FOBOS:** Dead zones of the FOBOS detector caused by the circular active areas of the gas-detector modules (in spite of the polyhedron structure of the FOBOS ball) could be – at least partially – filled with Si detectors. PSD would allow to achieve a charge resolution for IMF's which is comparable with that of the Bragg ionization chambers.

References

[1] J.B.A. England, G.M. Field, and T.R. Ophel,
Nucl. Instr. and Meth. **A280** (1989) 291.

[2] S.S. Klein, and H.A. Rijken,
Nucl. Instr. and Meth. **B66** (1992) 393.

[3] G. Pausch, W. Bohne, H. Fuchs, D. Hilscher, H. Homeyer, H. Morgenstern, A. Tutay, and W. Wagner,
Nucl. Instr. and Meth. **A322** (1992) 43.

[4] G. Pausch, W. Bohne, and D. Hilscher,
Nucl. Instr. and Meth. **A337** (1994) 573.

[5] G. Pausch, W. Bohne, D. Hilscher, H.-G. Ortlepp, and D. Polster,
Preprint FZR–38 (1994), to be published in Nucl. Instr. and Meth. **A**, 1994.

[6] W. Terlau, A. Budzanowski, H. Fuchs, H. Homeyer, W. Kantor, G. Röschert, C. Schwarz, A. Sourell, and L. Zrodlowski,
HMI-Bericht 482 (1990) 93.

[7] W. Bohne, H. Morgenstern, and P. Figuera,
HMI–Bericht 497 (1992) 92,
HMI–Bericht 507 (1993) 79.

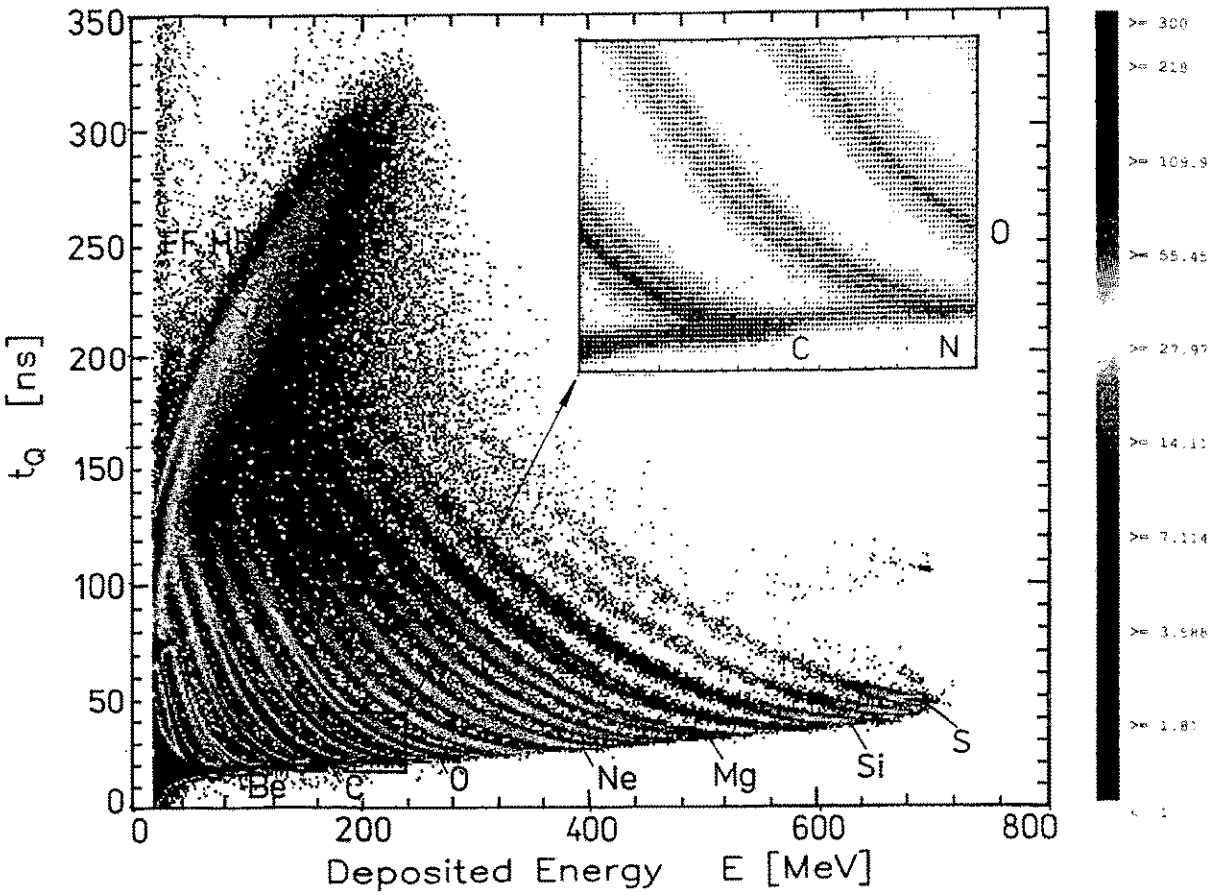

Figure 1: Particle identification based on PSD with a commercial 500μm Si detector (Intertechnique IPH 450-500-20 TM):
Two-dimensional plot of the count rate versus energy deposition E and the particle-sensitive parameter t_Q, which represents a combination of time-of-flight and pulse-shape information. The resolved lines are due to ions with different charge numbers Z. The bump of fission fragments (FF) and heavy residues (HR) determines the lower energy threshold for Z identification, the upper limit is given by the maximum energy deposition of the corresponding ion in the silicon detector.
The zoomed detail of the spectrum shows that isotope lines can be resolved in the element branches.
(Figure taken from ref.[5].)

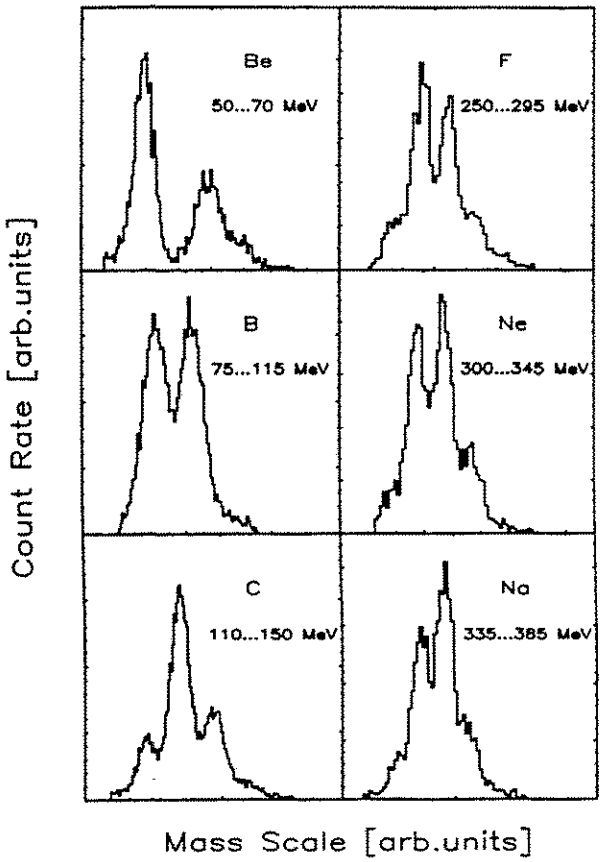

Figure 2: Isotope separation obtained for selected elements: The element branches shown in figure 1 were linearized within the specified energy range, and projected onto an arbitrary mass scale. (Figure taken from ref.[5].)

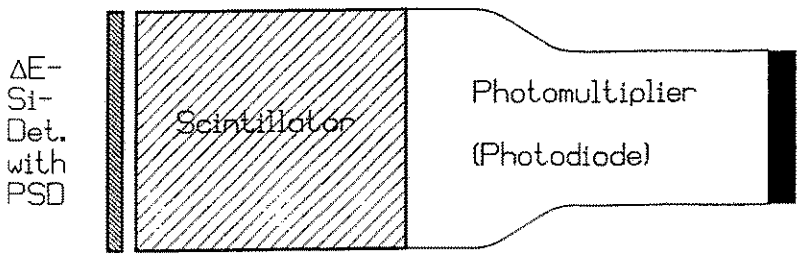

Figure 3: Sketch of the detector combination which could be used as a element of a forward array, or as a specialized trigger detector for slow particles (see text): PSD is applied to the ΔE Si detector and allows to identify slow IMF's which are stopped in this detector. The scintillator is used as a E detector, or as a veto for fast particles penetrating the Si counter.

II. Experiments at FOBOS in 1993 ÷ 1994

First results obtained at FOBOS

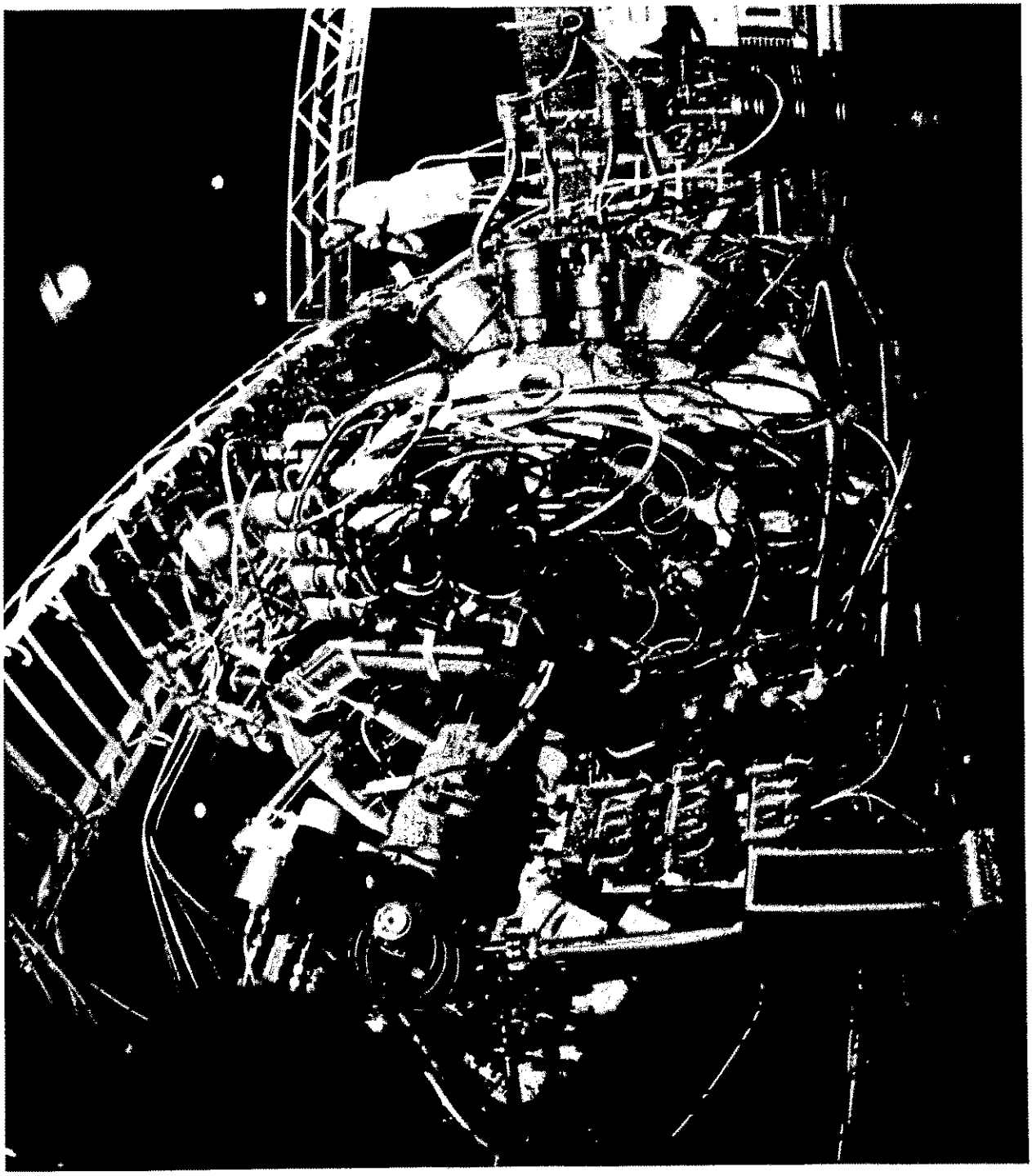

A ^{244}Cm COLD SPONTANEOUS FISSION STUDY AT THE FOBOS SPECTROMETER

Yu.V. Pyatkov [1], A.A. Aleksandrov [1], I.A. Aleksandrova [1], B.I. Andreev [1], P. Gippner [2], C.-M. Herbach [3], E.M. Kozulin, A. Matthies [2], Yu.Ts. Oganessian, H.-G. Ortlepp [2], Yu.E. Penionzhkevich, G. Renz [2], K.-D. Schilling [3], O.V. Strekalovsky, V.M. Vasko, W. Wagner [2]

Joint Institute for Nuclear Research, FLNR, Dubna, Russia
[1] Moscow Physics Engineering Institute, Russia
[2] on leave from Research Centre Rossendorf Inc., Germany
[3] Research Centre Rossendorf Inc., Germany

The method of two velocities was used to measure the mass - energy distribution of fragments originating in spontaneous fission of ^{244}Cm including the regions of cold compact (CCF) and cold deformed fission (CDF). The mass distributions for CCF and CDF products differ cardinally for spontaneous and neutron induced fission of Cm isotopes with roughly similar mass. Possible reasons for the observed differences are discussed.

1. Introduction

Very recent investigations in the field of nuclear fission [1] present an abundant material for a new approach of understanding of this process, especially, for the role of cluster degrees of freedom. One of the most promising ways to get new results is the measurement of the mass and charge spectra of cold fragmentation products. It is well known, that the fragment mass spectra in CCF and CDF are characterized by prominent structures [2] caused by shell and pairing effects.

In recent years a substantial material has been collected on the CCF, but the CDF is much less studied. In particular, there are no data on the CDF fragment spectra for spontaneous fission. The subject of this work is an experimental study of the mass-energy spectrum of the ^{244}Cm(sf) fragments including not only the CCF, but also for the first time the CDF region.

2. The experimental set-up

The experiment was performed at the FOBOS facility of the Flerov Laboratory of Nuclear Reactions at the JINR, Dubna [3]. In its final state, this detector array consists of a "gas-detector ball" of 30 position-sensitive avalanche counters (PSAC) and 30 axial (Bragg) ionization chambers behind them. In the present experiment two groups of 3 PSAC each were used to determine the velocity vectors of complementary fission fragments.

A small transmission avalanche counter near the source delivered the time-reference signal. The flight path amounted to 47 cm. All counters were operated at 3 Torr of pentane in a flow-through regime. A reduced bias of 480 V was applied to effectively discriminate the huge rate of about 10^6 alpha particles per fission.

The ^{244}Cm source consisted of 9.8 μg fissioning material deposited on a 50 μg/cm^2 thick backing of Al_2O_3. It formed a spot of 5 mm in diameter.

In total, about 10^5 events with two registered fission fragments have been collected. The mass ratio and the energy for each event have been determined utilizing an iterative procedure [4] which takes into account all the energy losses. These have been calculated assuming the proton-neutron ratio of a

fragment pair to be equal to that of ^{244} Cm. An absolute time calibration of the spectrometer was not made.

For the evaluation of the calibration parameters for the measured data we used the mean values of the light (A_L) and the heavy (A_H) fission fragment of ^{244}Cm(sf) as well as the total kinetic energies (TKE) known from the literature [5,6,7]. Although only the authors of ref. [6] made use of the two-velocities method, we applied the data of all the three works.

The experimental mass resolution (ΔM) estimated with the help of single-mass peaks in the region of CCF does not exceed 3 amu (fig.1). This well corresponds with the results obtained by simulations where the real thicknesses of the entrance windows of the PSAC as well as the geometry of the FOBOS array have been taken into account. The value of ΔM is mainly determined by the relatively thick window foils of the time-reference detector (altogether 300 $\mu g/cm^2$) .

3. Results

The mass yields of about 10^5 primary fission-fragment pairs of ^{244}Cm(sf) measured are compared with corresponding results [6] in fig.2. Further comparisons are shown in fig.3 and fig.4, namely, for the single-fragment energy before neutron emission and the standard deviation of the single-fragment energy distribution, respectively. In all cases a quite satisfactory agreement is observed.

As an initial result of our measurement, we obtained the yield functions Y(M,E) and Y(M,TKE). Here, M means the mass of the primary fragment and E- its kinetic energy. In order to analyze the fine-structure of the mass yield at different excitation energies (E*) of the fissioning system at the scission point, the distribution Y(M,TKE) has been transformed into a function Y(M,E*), where E* = Q - TKE and Q means the mean reaction energy for the production of fragments with a fixed mass ratio. The calculated Q(M) are weighted mean values over $Q_{Max}(M)$ taken from the tables of ref. [8]. We used a Gaussian weight-function with FWHM = 3 amu, corresponding to the mass resolution obtained.

Three cuts through the Y(M,E*) distribution are presented in fig. 5, namely, at low, medium and high E*. One observe that in the CCF region the yields around the double-magic fragment A_H = 132 are highly suppressed as has been underlined earlier in ref. [9]. These masses, on the other hand, dominate in the yields at high E* values.

Fine structures smoothed at medium E* appear again at diminishing TKE (increasing E*). This is usually interpreted as the appearance of CDF [2]. One should notice, that the mass spectra of cold fragmentation observed in thermal neutron induced fission of the neighboring isotope ^{245}Cm differ substantially from those obtained in our ^{244}Cm(sf) measurement. In CCF dominates the peak at M = 132 amu, whereas for CDF a peak at M = 140 amu prevails [10].

The general tendency of the mass yield for the lighter fission fragment of ^{244}Cm(sf) in dependence on E* can be seen in the three-dimensional plot of fig.6. There, the vertical axis shows the conditional probability P(M | E*) for the formation of a fragment with the mass M at an excitation energy E*. The distribution P(M | E*) has been obtained in correspondence to the theory of probability by the following transformation

$$P(M \mid E^*) = P(M,E^*) / P(E^*) , \qquad (1)$$

where the probability P(M,E*) was evaluated from the measured yield-function Y(M,E*)

$$P(M,E^*) = Y(M,E^*) / \Sigma_{M,E}\, Y(M,E^*) \qquad (2)$$

and P(E*) is the density function of the excitation energy

$$P(E^*) = \Sigma_M Y(M,E^*). \quad (3)$$

The projection of $P(M|E^*)$ on the M - E*- plane illustrated in fig.7 shows contour lines of equal probability. From this figure it is easy to get the function

$$E^*_{Ymax} = \alpha \cdot (M - 96) \quad (4)$$

for the dependence of the excitation energy at maximum yield on the mass of the lighter fragment. This means that E^*_{Ymax} increases linearly with the nucleon number A_L diminished by 96.

Although the distributions P(E*) for the reactions ^{244}Cm(sf) and ^{235}U(n_{th} ,f) show only nonsignificant differences, the functions $P(M|E^*)$ may differ basically (figs. 3÷7). The U(n_{th} ,f) data have been obtained by use of a time-of-flight spectrometer at the reactor of the Moscow Physics Engineering Institute [11].

4. Discussion

The results described above suggest to discuss the following facts:

- The existence of a peak in the yield-function for masses of M ≅140 ÷ 148 amu in the energy region of CCF.
- The inverse appearance of a spherical shell in the mass region around M_H = 132 amu, when the CCF and CDF of ^{244}Cm and of the thermal fission of ^{245}Cm are compared.
- The linear dependence of E* at maximum yield on the mass M_L of the light fragment (4).

Let us interpret these points in the frame of the cluster conception of multi-modal fission, which has been proposed in refs. [12,13]. In this model the following scenario for the two-cluster mechanism of formation of a fission mode is supposed :

At a certain stage of elongation the fissioning system clusterizes into two heavy clusters ($M_I \approx 96$ amu and $M_{II} \approx 132$ amu) and a necklace consisting of alpha particles or other light nuclei (fig.11a). The cluster of M ≈ 96 amu may be caused by the superposition of sufficiently strong shell corrections for protons and neutrons at a deformation of $\beta \approx 0.38$ with the proximity of this deformation to that of the ground state. During separation of these clusters forced by the Coulomb repulsion the alpha particles of the necklace fill the space in-between them forming a neck. The neck rupture may occur at the side of the light cluster (like in the case of spontaneous fission) or at the side of the heavy one (like in the case of thermal neutron induced fission) (figs.11b,c). In the spontaneous fission the neck particles move to the heavy cluster (^{132}Sn) which turns out to be weakly deformed. On the other hand, E* of the lighter cluster increases by a value of about 3.7 MeV/amu (fig.7) when an alpha particle from the neck fuses to it. Therefore, E* of the whole system is mostly concentrated within the light fission fragment. It is obvious from equation (1), that the splitting of a nucleus permits the shells to slightly deviate from the general rule of formation of the mass-energy distribution. This is mainly connected with the function P(E*}.

5. Conclusions

The peculiarities observed here in the fission of Cm are no specific attribute of exclusively this element. An analogous phenomenon has been found for the pair of reactions ^{252}Cf(sf) and ^{249}Cf(n_{th} ,f) [13] by comparison of the mass-energy distributions of this isotopes differing only in the neutron number. For a better understanding of the influence of this parameter, we plan a further investigation of the reactions ^{249}Cm(n_{th} ,f) and ^{250}Cf(sf).

References

[1] Proc. of the II. Int. Conf. on Dynamical Aspects of Nuclear Fission, Smolenice, Slovakia, 1993.

[2] Kaufmann,I., Mollenkopf,W., Gönnenwein,F., Geltenbort,P., Oed,A.: Z. Phys. A 341 (1992) 319.

[3] Ortlepp,H.-G., Andrassy,M., Chubarian,G.G., Danziger,M., Dietterle,L., Fomichev,A.S., Gippner,P., Herbach,C.-M., Ivanenko,A.I., Kolessov,I.V., Matthies,A., May,D., Oganessian,Yu.Ts., Penionzhkevich,Yu.E., Pokrovsky, V.N., Renz,G., Rubinskaya,L.A., Zhuchko,V.E., Strekalovsky,O.V., Trofimov,V.V., Vasko,V.M., Wagner,W., Heidel,K., Schilling,K.-D., Sodan,H.:
Proc. of the Int. School-Seminar on Heavy-Ion Physics, Dubna, Russia, May 10-15, 1993, Vol.2, p.466.

[4] Herbach,C.-M., Trofimov,V.V., Zhuchko,V.E., Dietterle,L., Vakatov,D.V.:
Annual Report 1993, FZR-35, Rossendorf, Germany,1994, p.108.

[5] Alkhazov,I.S., Kostochkin,O.I., Kovalenko,S.S., Malkin,L.Z., Petrzhak,K.A., Shpakov,V.I.:
Sov. Journal of Nucl. Phys. 11 (1970) 281.

[6] Barashkov,Yu.A., Vasiliev,Yu.A., Maslov,A.N., Pavlovsky,R.S., Savaeka,M.K., Sidorov,L.V., Surin,V.M., Terapov,P.V.: Sov. Journal of Nucl. Phys. 13 (1971) 668.

[7] Schmidt,R., Henschel,H.: Nucl. Phys. A395 (1983) 15.

[8] Möller,P., Nix,J.R.: Atomic Data and Nuclear Data Tables 26 (1991) 165.

[9] Caitucoli,F., Asghar,M., Leroux,B., Barreau,G., Hamadache,K., Sicre,A., Doan,T.P., Allab,M.:
Nucl. Phys. A394 (1983) 360.

[10] Pyatkov,Yu.V., Aleksandrov,A.A., Aleksandrova,I.A., Andreev,B.I., Gippner,P., Herbach,C.-M., Kozulin,E.M., Matthies,A., Oganessian,Yu.Ts., Ortlepp,H.-G., Penionzhkevich,Yu.E., Renz,G., Schilling,K.-D., Strekalovsky,O.V., Vasko,V.M., Wagner,W.:
Proc. of the Workshop on Nuclear Fission and Fission-Product Spectroscopy, Château de la Baume, Seyssins, France, May 2 - 4, 1994, Grenoble, 1994, p.144.

[11] Koczon,P., Mutterer,M., Theobald,J.P., Geltenbort,P., Gönnenwein,F., Oed,A.:
Phys. Lett. B191, Nr.3 (1987) 279.

[12] Aleksandrov,A.A., Aleksandrova,I.A., Ermolenko,A.V., Korjuk,Yu.A., Nikulin,D.S., Pevchev,Yu.F., Podchibyakin,S.I., Pyatkov,Yu.V., Sitnikov,S.I., Slyusarenko,A.I., Shemetov,A.N., Shekhmametiev,R.A.:
Nucl. Instr. and Meth. in Phys. Research A303 (1991) 323.

[13] Pyatkov,Yu.V., Shekhmametiev,R.A, Slyusarenko,A.I., Taranenko,A.V.:
Proc.of the Int. Conf. on Nuclear Structure and Nuclear Reactions at Low and Intermediate Energies, Dubna, Russia, 1992, p.347.

[14] Pyatkov,Yu.V., Shekhmametiev,R.A., Slyusarenko,A.I., Naletov,A.A.:
Proc.of the Int. School-Seminar on Heavy-Ion Physics, Dubna, Russia, 1993, vol.1, p.358.

[15] Pyatkov,Yu.V., Shekhmametiev,R.A., Slyusarenko,A.I.: JINR Rapid Communications N2(59), Dubna, Russia, 1993, p.98.

Figure captions

Fig.1: Fragment mass distribution for cold compact fission of ^{244}Cm for excitation energies E* in the region of $0 \div 3$ MeV.

Fig.2: Mass yield of primary fission fragments of ^{244}Cm. The results of this work (triangles) are compared with those of refs. [5,6] (dashed line) and ref. [7] (full points).

Fig.3: Single-fragment energy before neutron emission as a function of the fragment mass. Our results (triangles) are compared with those of ref. [6] (full points).

Fig.4: Standard deviation of the primary single-fragment energy distribution as a function of the fragment mass. Triangles show our results, full points the data of ref. [7].

Fig.5: Mass spectra of ^{244}Cm fission fragments for excitation energies E* of 4 MeV, 30 MeV and 60 MeV. The width of the respective energy windows is 1 MeV.

Fig.6: The conditional probability $P(M \mid E^*)$ for formation of a fission fragment with the mass M at an excitation energy E* in spontaneous fission of ^{244}Cm.

Fig.7: The contour map of $P(M \mid E^*)$ depicted from the three-dimensional plot of fig.6. Equidistant lines are drawn with a step of 1 %.

Fig.8: The conditional probability $P(M \mid E^*)$ of the fission fragment formation in the reaction $^{235}U(n_{th},f)$ [12].

Fig.9: The contour map of $P(M \mid E^*)$ depicted from the three-dimensional plot of fig.8. Equidistant lines are drawn with a step of 1 %.

Fig.10: Comparison of the excitation energy distributions P(E*) for the reactions $^{235}U(n_{th},f)$ [11] and ^{244}Cm(sf) (our results). For convenience the maximum of the function for the ^{244}Cm decay is shifted to the position of the ^{236}U maximum.

Fig.11: Possible cluster configurations of ^{244}Cm at the fission barrier. For explanation see text.

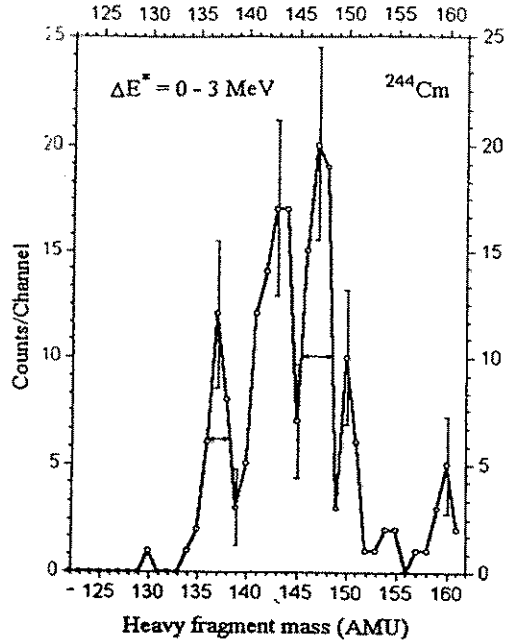

Fig. 1

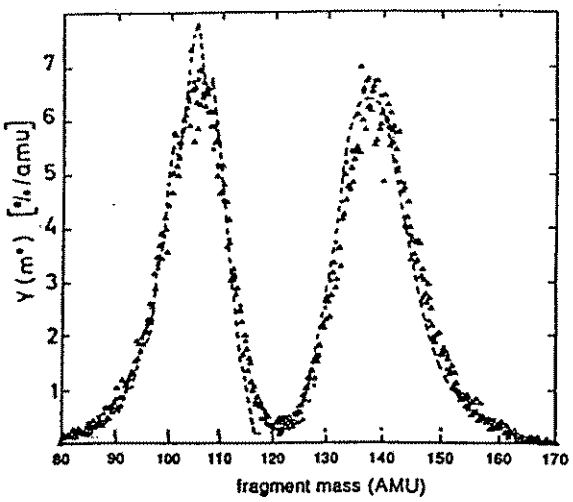

Fig. 2

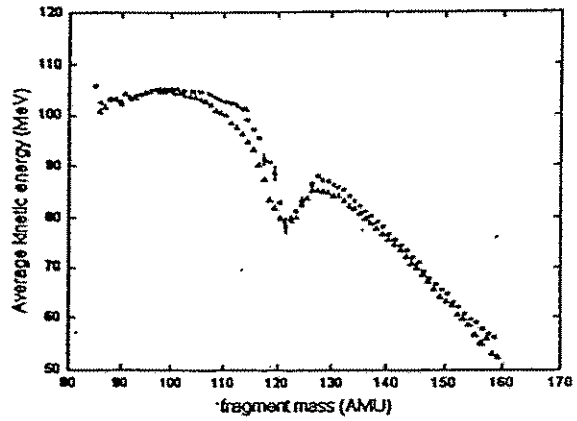

Fig. 3

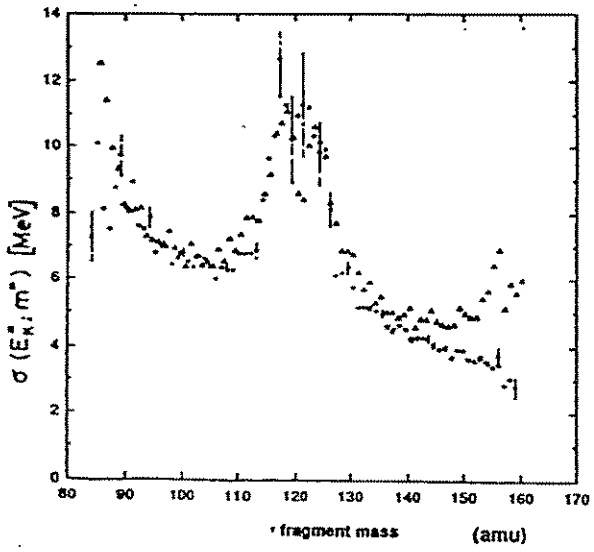

Fig. 4

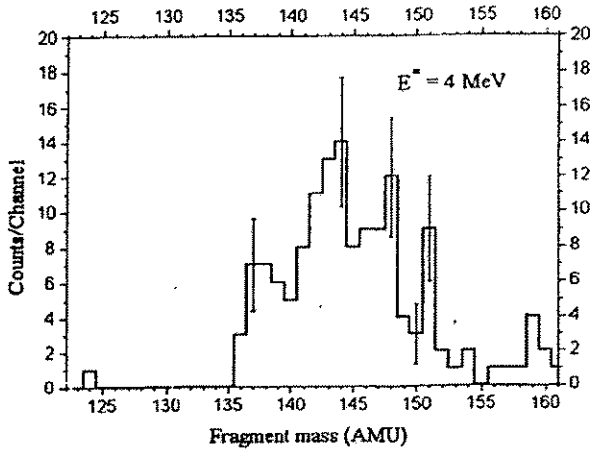

Fig. 5 (a)

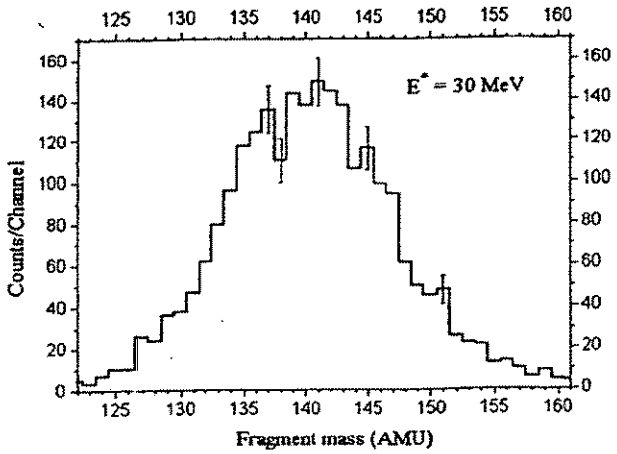

Fig. 5 (b)

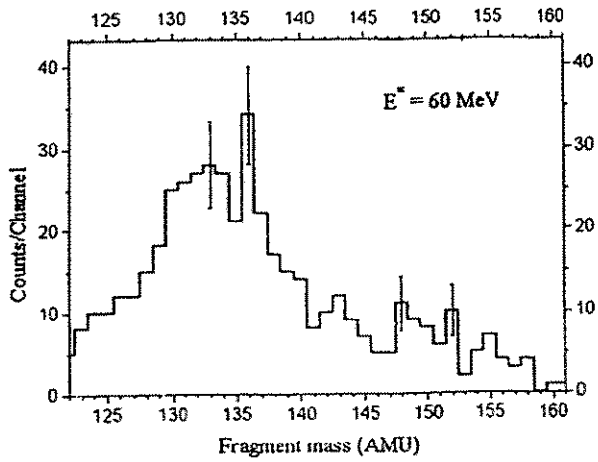

Fig. 5 (c)

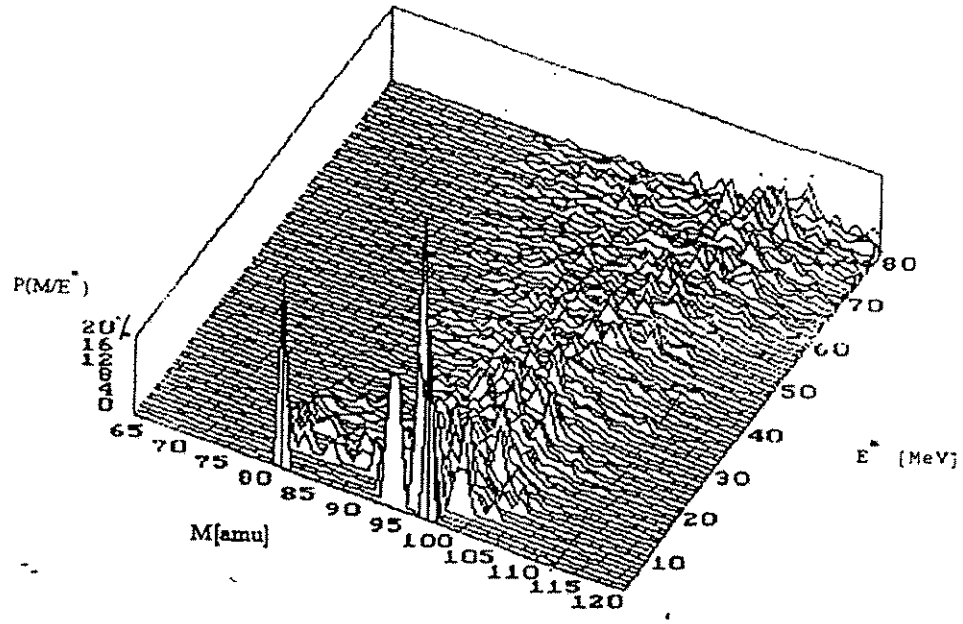

Fig. 6

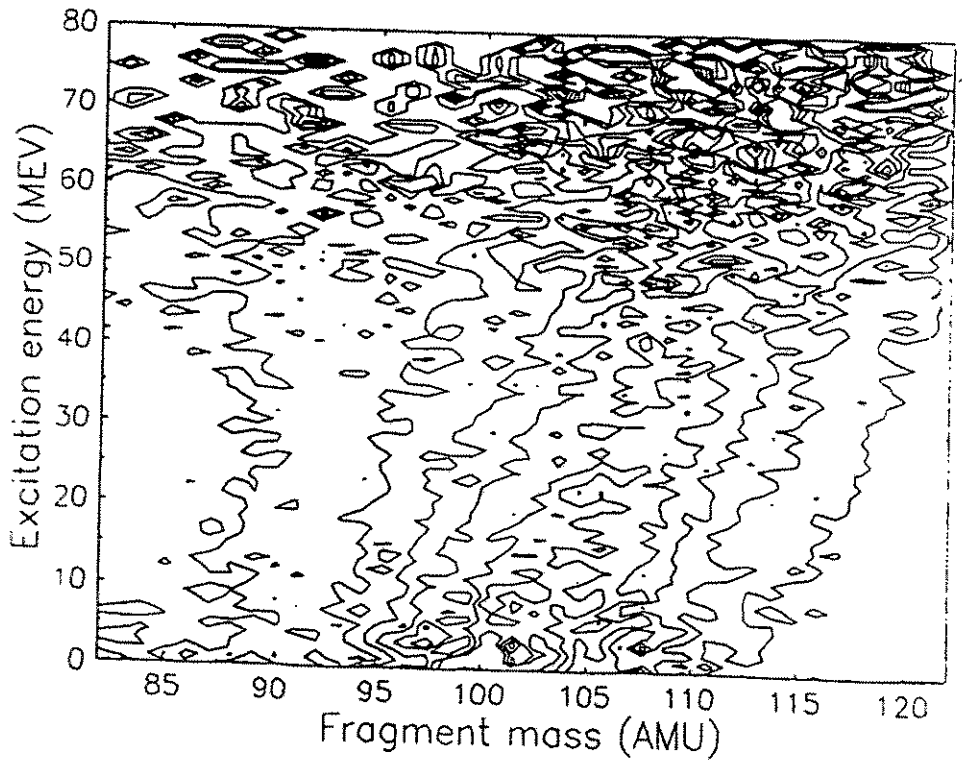

Fig. 7

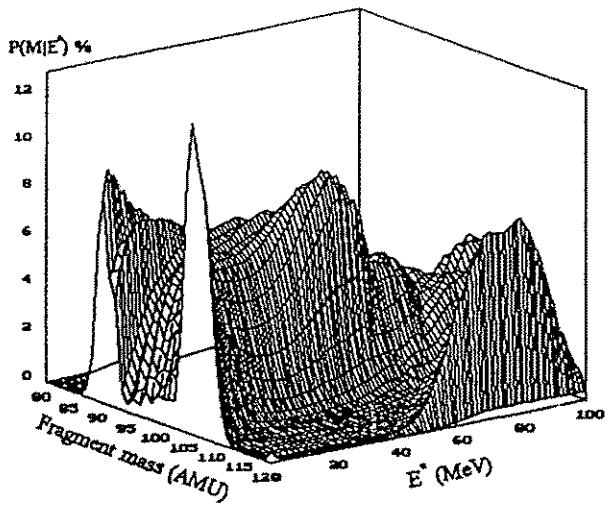

Fig. 8

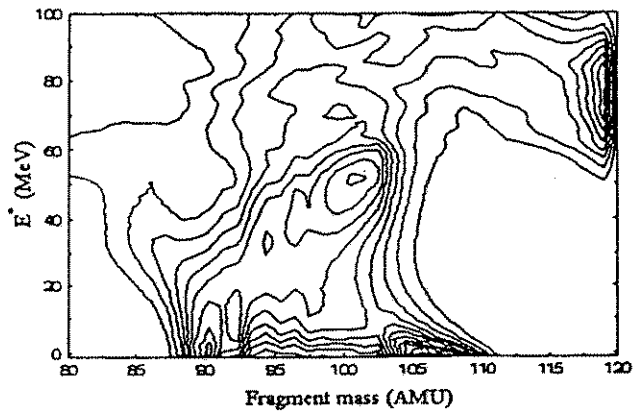

Fig. 9

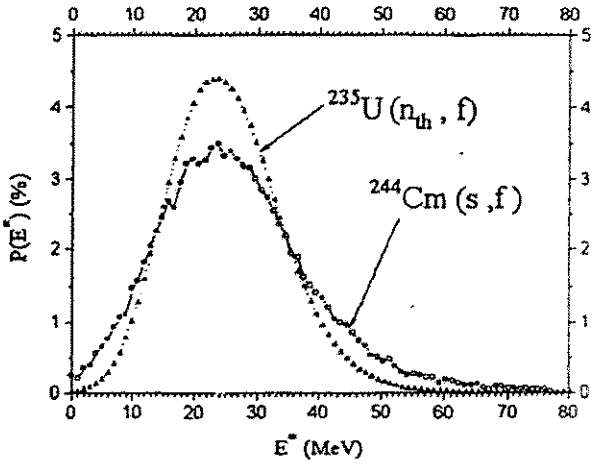

Fig. 10

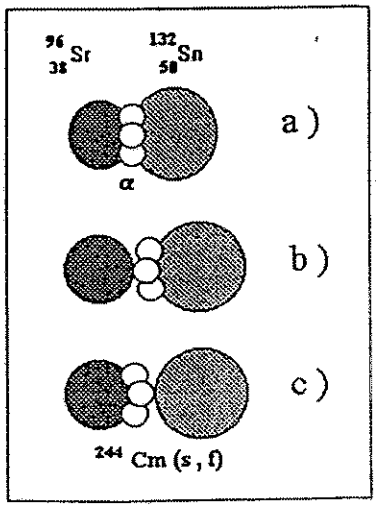

Fig. 11

TERNARY SPONTANEOUS FISSION OF ^{244}Cm

W. Wagner, P.Gippner, C.-M. Herbach, H.-G. Ortlepp

Research Centre Rossendorf Inc., GERMANY

The cold spontaneous fission (sf) of ^{244}Cm has been investigated [1] using a special set-up of the FOBOS array [2].

Six position sensitive avalanche counters (PSAC) were arranged by pairs under 180° to measure the time-of-flight (TOF) of correlated fission fragments (FF) relative to the timing reference signal of a small transmission counter (PAC).

The source consisted of 9.8 µg ^{244}Cm depleted on a thin Al_2O_3 backing.

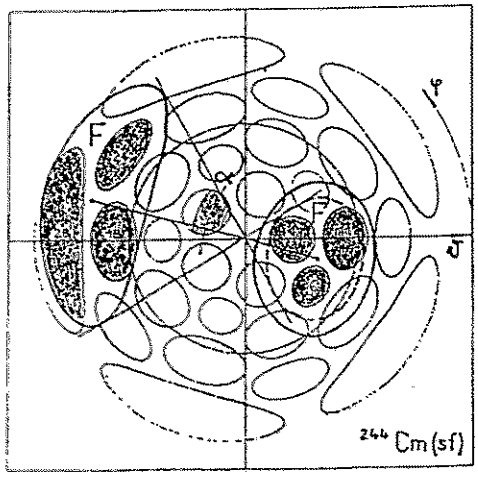

Fig.1 Acceptances (shaded areas) of the FOBOS detectors used in the ^{244}Cm(sf) experiment. The aperture of the PAC (full line) has been calculated.

Parallely ternary events where an additional third particle is emitted should be registered in this experiment. The main component of the light charged particles (LCP) and clusters in ternary sf is due to long-range alpha particles (LRA) emitted from the neck region of the fissioning nucleus at the scission point. They are focused by the Coulomb field of the FF into directions nearly perpendicular to the fission axis. They have a slightly asymmetric energy distribution with a mean value of 16 MeV and a width of 10 MeV [3].

Therefore a CsI(Tl) module of the FOBOS scintillator shell [4] was positioned under ≈90° relative to the symmetry axis of the PAC aperture. The geometrical conditions of the measurement are shown in fig.1.

The CsI(Tl) counters were shielded against the high alpha particle activity of the source by a 40 µm thick Mylar absorber foil what lead to a registration threshold for LRA of ≈6 MeV. Applying the pulse-shape discrimination method [5] LCP were well separated from the prompt fission and background gamma rays (fig.2).

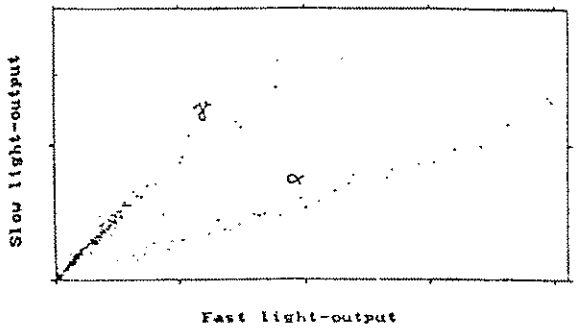

Fig.2 Pulse-shape discrimination matrix for LRA emitted in ^{244}Cm(sf).

Since the main goal of the experiment was to investigate cold sf during the measurement time only 36 triple events could be recorded. The ratio of LRA accompanied sf to binary sf has been corrected for coincidence efficiency and registration threshold and converted into the usually stated ratio of ternary to binary fission relating to the reference ratios of LCP emission probabilities of ^{252}Cf [6].

In result a value of 3.24 ± 0.63 LCP per 10^3 sf has been obtained what is in agreement with the only available data of R.A. Nobles [7] of 3.18 ± 0.20 per 10^3 sf. The dominating part of the uncertainty given is due to poor statistics.

Fig.3 shows a systematics of LCP emission probabilities [6] for several transuranium sf nuclides in dependence on the average Q-TKE value.

Since the difference between the mean Q-value of reaction and the total kinetic energy

(TKE) gives the excitation energy at scission it has been concluded that the LCP emission probability in sf is a measure of the deformation at scission what is mainly connected with the charge asymmetry.

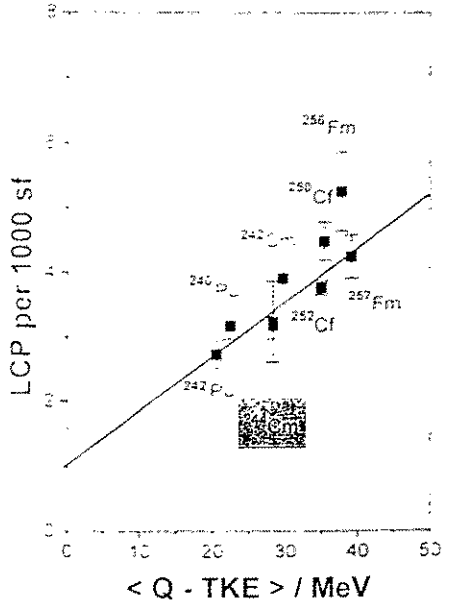

Fig.3 Systematics of LCP emission probabilities in ternary sf (after [6])

We gratefully acknowledge the assistance of E.M. Kozulin who prepared the ^{244}Cm source.

REFERENCES

1) Pyatkov, Yu.V. et al., Proc. of the Workshop on Nuclear Fission and Fission-Product Spectroscopy, Château de la Baume, Seyssins, France, 1994.
2) Ortlepp, H.-G. et al., Proc. of the Internat. School-Seminar on Heavy Ion Physics, v.2, JINR Dubna, Russia, 1993, p.466 (ed. Yu. Ts. Oganessian et al.).
3) Wagner, W. et al., Scientific Report 91/92, Flerov Laboratory of Nuclear Reactions, JINR Dubna, Russia, 1992, p.244.
4) Wagemanns, C., Particle Emission from Nuclei, v.3, CRC Press Inc., 1989.
5) Alarja, J. et al., Nucl. Instr. and Meth. A242, 1986, p.352.
6) Wild, J.F. et al., Phys. Rev. C32, 1985, p.488
7) Nobles, R.A., Phys. Rev., v.126, 1962, p.1508

CORRELATIONS BETWEEN INTERMEDIATE MASS AND FISSION FRAGMENTS IN THE REACTION ^{7}Li (43AMEV) ON ^{232}Th STUDIED AT FOBOS *

A.A. Aleksandrov [1], I.A. Aleksandrova [1], M. Andrassy [2], L. Dietterle [1,2], V.N. Doronin [1], P. Gippner [1,2], C.-M. Herbach [2], D. Hilscher [3], S.I. Ivanovsky [1], A. Matthies [1,2], D. May [1,2], H.-G. Ortlepp [1,2], G. Pausch [2], Yu.E. Penionzhkevich [1], V.N. Pokrovsky [1], G. Renz [1,2], K.-D. Schilling [2], D.I. Shishkin [1], V.E. Shuchko [1], O.V. Strekalovsky [1], V.V. Trofimov [1], C. Umlauf [1,2], D.V. Vakatov [1], V.M. Vasko [1], W. Wagner [1,2]

for the FOBOS - Collaboration

[1] *Joint Institute for Nuclear Research, Dubna, Russia*
[2] *Research Centre Rossendorf e.V., Germany*
[3] *Hahn-Meitner Institute Berlin, Germany*

At present several questions concerning fission of hot nuclei [1] such as the influence of dynamics on time scales, the mechanism of dissipation and others are extensively discussed. One goal of the experiments presently being carried out at FOBOS is the further investigation of neck emission of light and intermediate mass fragments (IMF) observed in ref. [2].

A 270 μg/cm^2 thick ^{232}Th target deposited on a 50 μg/cm^2 Al_2O_3 backing was placed in the center of the FOBOS array [3] and bombarded by a ^{7}Li beam from the U-400M cyclotron of the FLNR. Fission fragments (FF) and IMF were registered by 10 position sensitive avalanche counters (PSAC) measuring the time-of-flight (TOF) and the emission angle and by 12 axial ionization chambers measuring the energy (E) and the Bragg-peak height (Z). Light charged particles (LCP) were registered by 10 CsI(Tl) counters.

Since the U-400M beam parameters did not allow a precise TOF measurement against the RF-signal of the cyclotron two transmission avalanche counters placed near the target in direction of the modules 2 and 5 delivered the timing reference signals.

The geometrical arrangement of the FOBOS modules available at that time has been chosen according to Monte-Carlo simulations of binary and ternary fission after incomplete linear momentum transfer (LMT) (fig. 1).

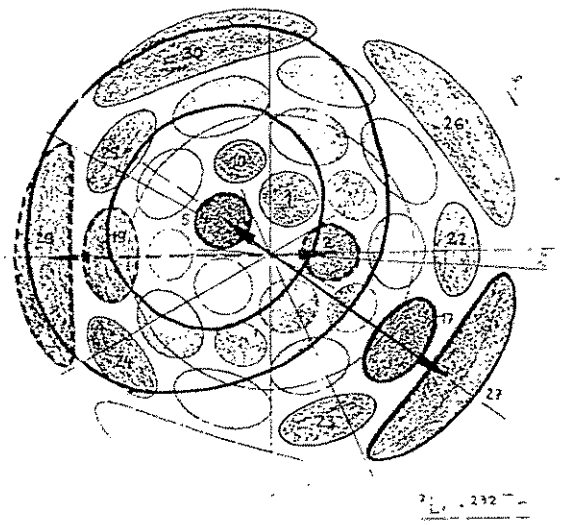

Fig.1 Geometrical acceptances of the FOBOS modules in polar coordinates (ϑ,φ). The modules used are shaded (numbers). The dots are a result of simulation of neck particle emission assuming a mean LMT and considering one FF is registered in module 5, the coincident FF in modules 17 or 27. Expected IMF are distributed within the ring-like region marked by thick full lines.

The BIC and PSAC were operated in a gas flow-through regime at pressures of 200 Torr of P-10 gas mixture and 4 Torr

* The FOBOS project is supported by the BMFT, Germany, under contract N°. : 0 DR 100.

pentane respectively. The PSAC bias set at a value about 5 Volts below the onset of spark discharges guaranteed an efficient registration of fragments from FF down to alpha particles.

Altogether $3.1 \cdot 10^6$ events with two FF have been recorded. They contain 230 triple (IMF-FF-FF) coincidences. The FF and IMF were selected by windows in the TOF-E and E-Z distributions.

As a first result of this experiment yields of IMF accompanied fission related to binary fission have been determined in dependence on the excitation energy (E*) of the intermediate system and the angle between the fission axis and the direction of IMF emission (ϑ_{IMF-FF}). The 230 triple events allow only a rough division into some intervals in E* and ϑ_{IMF-FF} .

The geometrical acceptance factors ε_{ijk} for all combinations with one FF in module i, a second FF in module j and an IMF in module k have been determined with the help of Monte-Carlo simulations. These simulations deliver mean excitation energies (E^*_{ijk}) which were assumed to be proportional to the LMT as well as mean angles (ϑ_{ijk}).

With the numbers $N_{IMF\ (i,j,k)}$ of triple and $N_{FF(i,j)}$ of binary events for a certain combination of FOBOS modules (i,j,k) the measured IMF yield per fission (into the full solid angle 4π) becomes

$$Y_{i,j,k} = N_{IMF\ (i,j,k)} \ / \ (N_{FF\ (i,j)} \cdot \varepsilon_{ijk}) .$$

These yields have been selected into groups of low LMT ($\Delta p \approx 50$ % ; $E^* \approx 150$ MeV) and high LMT ($\Delta p \approx 80$ % ; $E^* \approx 230$ MeV). The yields for five mean angles ϑ_{IMF-FF} are shown in fig. 2.

The $Y_{i,j,k}$ at low LMT do not show any significant variation for ϑ_{IMF-FF} between 35° and 90° . The mean value of this IMF component amounts to $(0.67 \pm 0.08) \cdot 10^{-3}$ IMF accompanied fissions per binary fission. At the higher LMT this value increases to $(2.31 \pm 0.28) \cdot 10^{-3}$.

The enhanced yield near $\vartheta_{IMF-FF} \approx 90°$ for higher E* confirms the existence of a further IMF source, the strength of which increases with E* too. Possibly these IMF were emitted from the neck region of the fissioning system at scission as has been claimed in ref. [2]

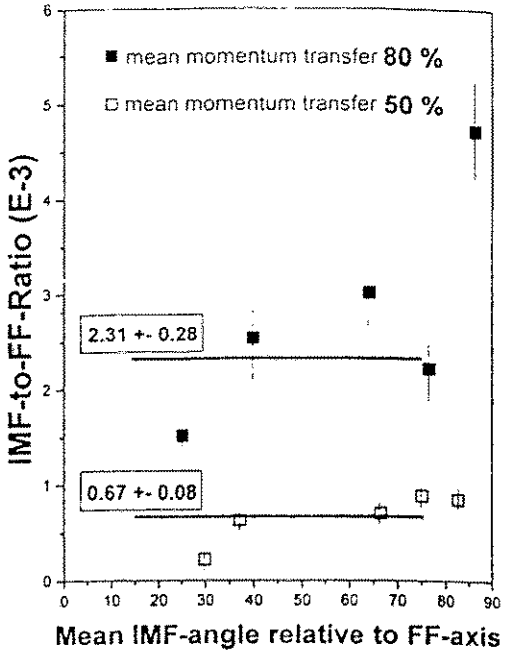

Fig.2 Yields $Y_{i,j,k}$ for certain mean IMF-angles ϑ_{ijk} according to low (open squares) and high (full squares) E^*_{ijk} .

If we consider an interval $\Delta\vartheta_{IMF-FF} = 10°$ around $\vartheta_{IMF-FF} = 90°$ (fig. 2) a rough estimation of the probability for neck emission of IMF results in a value of several units times 10^{-4} per binary fission. It is higher by about one order of magnitude than in the case of low energy (spontaneous or thermal neutron induced) ternary fission [4] .

REFERENCES

1) Hilscher, D. and Rossnèr, H., Ann. Phys. Fr., v.17, 1992 , p.471.
2) Fields, D.E. et al., Phys. Ref. Lett., v.9, 1992 p.3713.
3) H.-G. Ortlepp et al., Proc. of the Internat. School-Seminar on Heavy Ion Physics, v.2, JINR Dubna, Russia, 1993, p.466 (ed. Yu.Ts. Oganessian et al.).
4) Theobald, J.P. et al., Nucl. Phys. A502, 1989, p.343c.

ANALYSIS OF THE FISSION FRAGMENT DISTRIBUTION OBSERVED IN THE REACTION $^{7}Li + ^{232}Th$ AT 43 AMeV BOMBARDING ENERGY

C.-M. Herbach

for the FOBOS-collaboration

Research Centre Rossendorf Inc., Institute of Nuclear and Hadronic Physics, Germany

1. INTRODUCTION

At intermediate bombarding energies of about 10 - 100 AMeV within the Fermi region the experimental data from binary fission following complete and incomplete fusion are usually interpreted within the frame of the massive transfer model (MTM) description (see e.g. ref. [1-9]):

i) The whole excitation energy is deposited into the fused nucleus.
ii) The nucleons of the projectile that are not coupled to the composite system cannot contribute to the momentum and energy transfer.
iii) Any transverse component of the momentum transfer is neglected.

In its simplest manner, the analysis deduces the linear momentum transfer (LMT) from the measurement of the angular correlations between the fission fragments, assumes symmetrical fission and uses relative fission fragment velocities taken from the systematics of ref. [10]. However, this method is strongly restricted to binary events. A more general analysis requires the measurement of the emission directions of the fragments as well as their masses, charges and emission energies. Based on the complete set of the single-particle observables a kinematics analysis can be performed without any further assumption even for events with multiplicities higher than 2.

It is the aim of this work to describe the characteristics of the identification of fission fragments detected by the FOBOS modules [11-14]. The problems of the calibration procedure are discussed in detail. A comparison is made between the results derived, on one hand, from the distribution of the folding angle and, on the other hand, from the balance of the single-particle parameters.

Moreover, some data are presented which can be obtained only by use of a fragment spectrometer as the FOBOS array is. The longitudinal and transversal momentum components of the fissioning system were calculated from the data measured. Single fission fragment masses, the mass sum of both fragments and the relative velocity between the fragments are discussed in terms of the momentum transfer.

2. EXPERIMENTAL SET-UP

The experimental data of the reaction ^{7}Li (43 AMeV) + ^{232}Th which are analyzed in this work, were taken from measurements of the FOBOS spectrometer performed at the U-400M cyclotron of the JINR Dubna. The detector configuration used in these experiments, which were carried out to study the emission of intermediate mass fragments (IMF) before and during fission of excited nuclei [15], is defined by 10 complete gas-filled detector modules. Each of them consists of a position-sensitive avalanche counter (PSAC) placed in front of a axial ionization chamber (BIC) which realizes "Bragg-peak" detection.

The dominant geometrical parameter of the FOBOS 4π-fragment-spectrometer is the relatively large distance between the target and the PSAC (about 50 cm). It guarantees a time-of-flight (TOF) measurement with sufficient relative resolution of 1-3%. Note that this distance is larger than in comparable 4π-arrays [16,17]. In order to achieve a low energy threshold for heavy-fragment detection (about 0.5 AMeV), thin Mylar foils (1.2-1.5 μm) are used for the detector

windows and electrodes. Nevertheless, the fission fragments lose an essential amount of their energy by passing through the detector foils before they are stopped within the BIC. Both the TOF resolution and the energy losses are the main aspects concerning the detection and identification of heavy fragments at FOBOS. The quality of these parameters could only be achieved by using stable supporting grids which reduce the detector transparency to about 66 %.

Taking into account the flight path of 50 cm and the corresponding amount of TOF = 30-80 ns for the fission fragments, the experimental mass resolution of FWHM = 4-7 amu evaluated by the TOF-E-method requires an absolute TOF resolution better than 1 ns. This value could not be guaranteed by the timing referenced to the radio frequency (RF) of the cyclotron. During the runs large shifts of the beam- pulse with respect to the RF were observed which causes a total TOF resolution of FWHM = 10 ns. In order to deduce the time reference independent from the beam-bunch two small parallel-plate avalanche counters (START-PPAC) were mounted at a distance of 7.5 cm from the target. They were positioned to cover the cone of the forward-modules 2 and 5 (fig.1) as complete as possible.

In the measurement runs the data acquisition system was triggered in such a way, that only events with at least one fragment detected by one of the START-PPAC had been written to disk. In this manner the time reference was determined only by the resolution of the avalanche counters, but the available geometrical coincidence efficiency had been reduced.

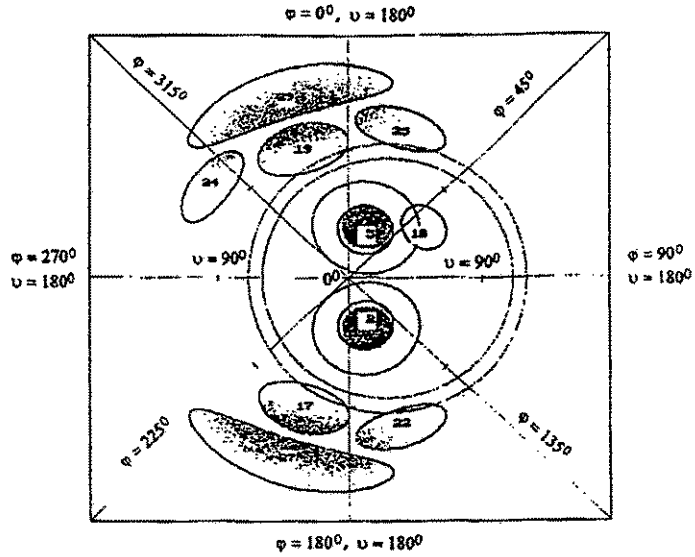

Fig. 1: Geometrical FOBOS set-up for the measurements of ^{7}Li (43 AMeV) + ^{232}Th.

The geometrical positions of the 10 mounted gas-filled modules are shown in fig.1. The radial coordinate of the plot corresponds to the polar angle ϑ and the polar coordinate of the plane displays the amount of the azimuthal angle φ within the three dimensional coordinate system of the FOBOS array. The contours indicate the regions that are covered by the angular cones of the 10 FOBOS modules and the 2 START-PPAC. Additionally, shadowed regions are shown which are caused by the START-PPAC frame and the target-holder system. The points within the effective module cones result from a simulation of fission coincidences considering the center-of-mass velocity of the fissioning system $v_{c.m.}$ = 0.22 cm/ns.

Taking into account the restrictions due to the two START-PPAC, the remaining module combinations for detection of fission fragment coincidences are listed in tab.1. They are classified into three different divisions concerning their positions with respect to the beam axis.

Tab. 1: Detector module pairs used for the measurement of fission fragment coincidences

Type	$\vartheta_1 + \vartheta_2$	$\lvert\varphi_1 - \varphi_2\rvert$	Mod.-No.	ϑ_1	φ_1	Mod. -No.	ϑ_2	φ_2
I	180.0°	180.0°	2	37.4°	162.0°	29	142.6°	342.0°
			5	37.4°	18.0°	27	142.6°	198.0°
II	138.2°	180.0°	2	37.4°	162.0°	19	100.8°	342.0°
			5	37.4°	18.0°	17	100.8°	198.0°
III	154.0°	144.0°	2	37.4°	162.0°	24	116.6°	306.0°
			2	37.4°	162.0°	25	116.6°	18.0°
			5	37.4°	18.0°	22	116.6°	162.0°

3. Folding angle distributions of fission fragment coincidences

The calculations of the detection efficiency with respect to binary fission have been performed for the different module pairs. Thereby $v_{c.m.}$ was varied from zero up to the value of 0.27 cm/ns which corresponds to the maximum LMT. The whole range of folding angles is covered by the module combination of type I. The geometrical acceptance for fission fragment detection of the combinations according to type II and III overlaps at higher momentum transfer only (fig.2).

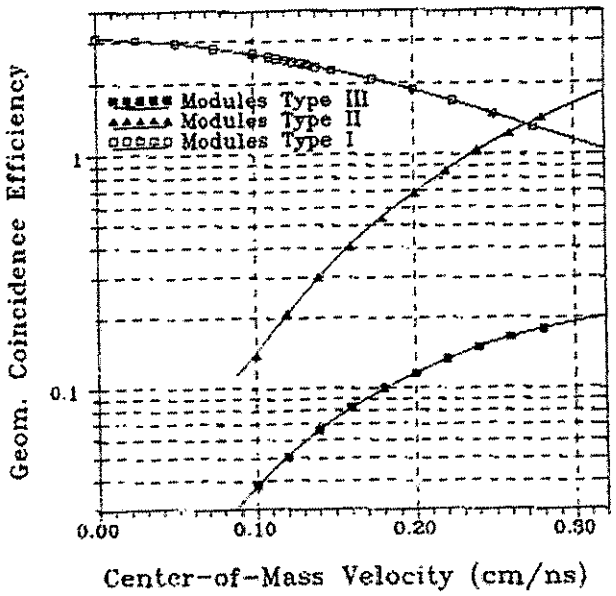

Fig. 2: Geometrical acceptance of the fission fragment detection by the different detector classes. (The data correspond to the TOF-TOF-detection and do not include the transparency loss valid for the measurement of the residual energy)

The efficiency calculations have been performed by use of a Monte-Carlo code assuming an angular distribution of the fission fragments within the frame of the center-of-mass system which is defined by an isotropic recoil from evaporated neutrons to the composite system. For simplification the kinetic energy of the neutrons was fixed to be 6 MeV.

An observable to study the transverse component of motion of the fissioning system is the coplanarity distribution. In contrary to the fission folding angle which is sensitive to the LMT, the coplanarity is not influenced by the longitudinal velocity of the composite system. For a fission fragment detection system with in-plane geometry (type I and II) the mean value is 180^0 and, therefore, the width of the distribution is a measure of the transverse deflection of the fissioning nucleus. However, besides neutron evaporation, other effects can contribute to the broadening of the

coplanarity distribution too, like a transverse momentum transfer during incomplete fusion and the angular straggling of the measured particles within the detector foils.

Nevertheless, a good agreement has been achieved between the simulated and experimental spectra by only varying the number of evaporated neutrons N_n. A comparison for the different fission coincidence detection systems is shown in fig. 3b-5b.

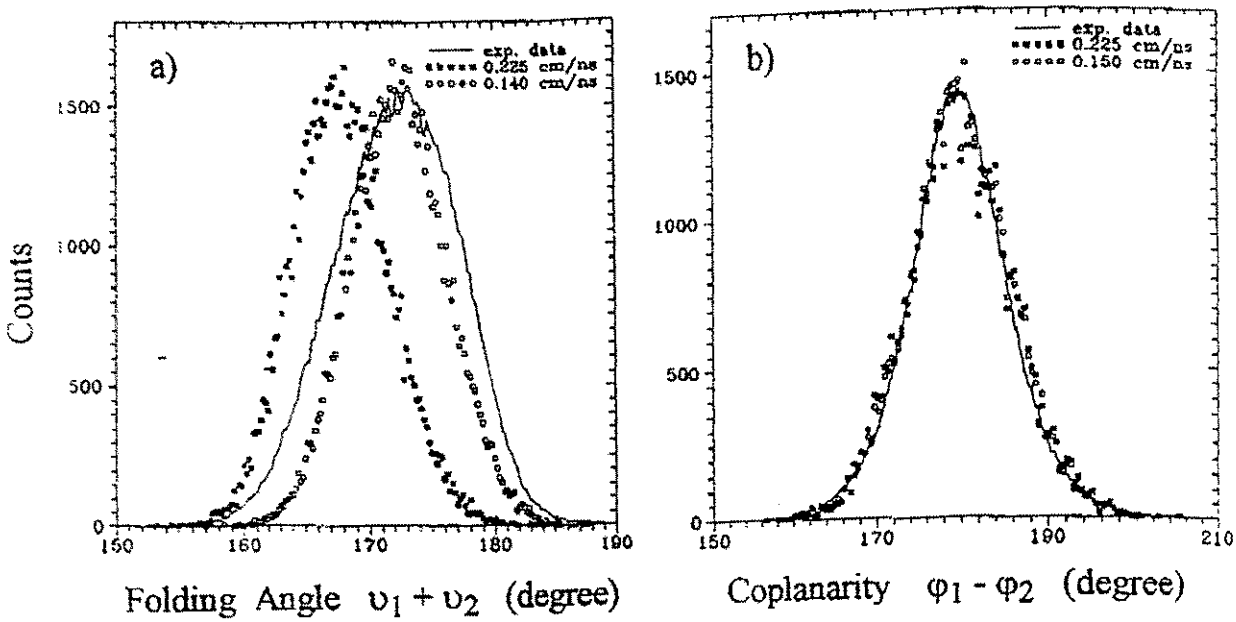

Fig. 3: Measured and simulated distributions for the detection system of type I.
a) fission fragment folding angles $\vartheta_1 + \vartheta_2$; b) of the coplanarity $\varphi_1 - \varphi_2$.

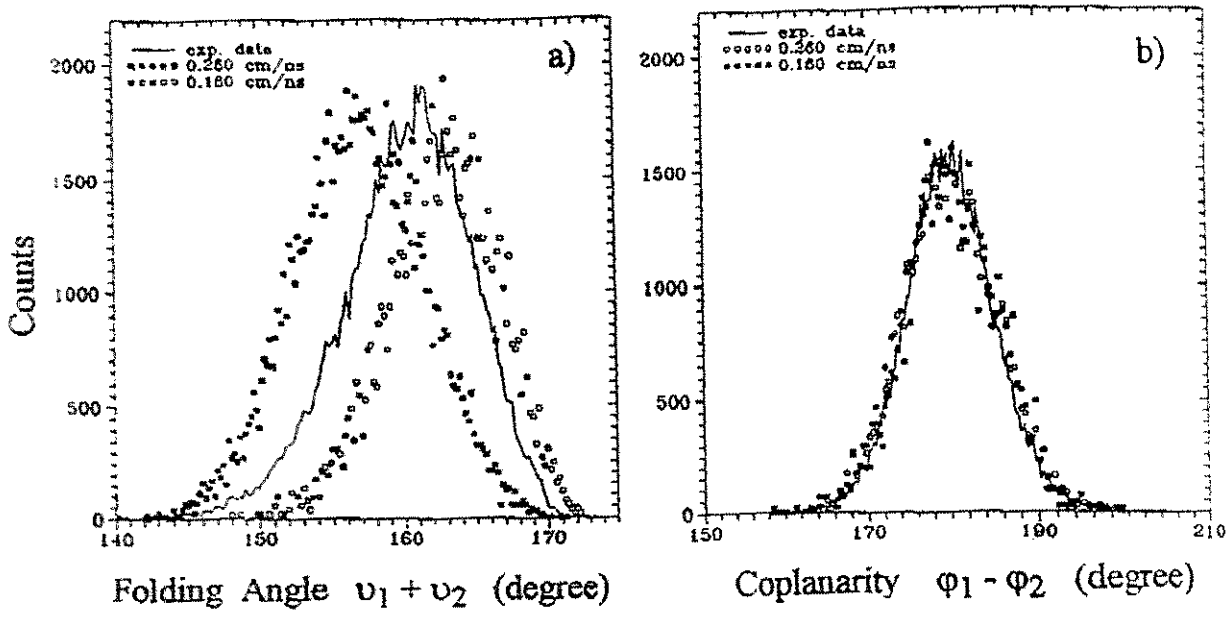

Fig. 4: The same as in fig. 3 but for the detection system of type II.

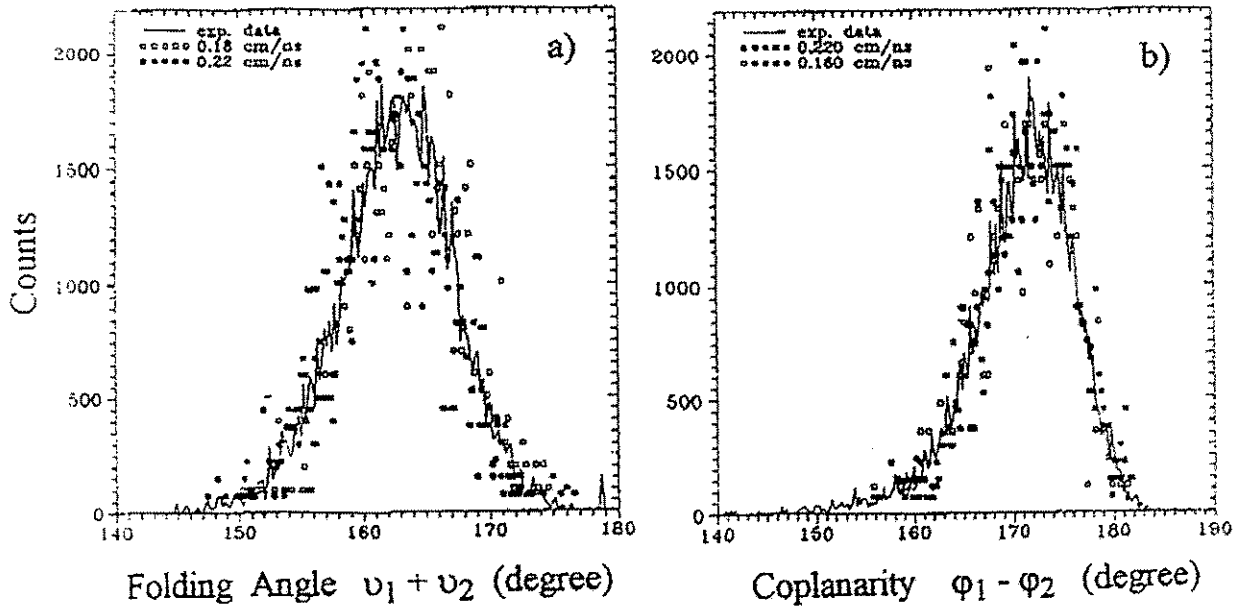

Fig. 5: The same as in fig. 3 but for the detection system of type III.

It should be noticed, that the measured folding angle distribution is reproduced by the simulation also for detection systems mounted out-of-plane (type III) (fig.5a). In this case, fission fragment coincidences can only be detected if the composite system received a strong component of motion in direction perpendicular to the beam.

Optimized parameters of $N_n = 18$ and $N_n = 33$ have been found for fission at mean value of $v_{c.m.} = 0.12$ cm/ns and $v_{c.m.} = 0.24$ cm/ns, respectively. In comparison to this, the number of neutrons emitted with an energy of 6 MeV during an evaporation cascade was determined from the balance of the binding, kinetic and excitation energies as has been proposed by the systematics of ref. [18]. This procedure results in values of $N_n = 11$ and $N_n = 18$ corresponding to the different velocities. The significant discrepancy between these values for a common $v_{c.m.}$ may be caused not only by the slightly simplified simulation code but also by additional contribution from effects listed above. However, the trend of an increasing number of neutrons at a higher LMT is reproduced correctly.

For a further comparison, the angular correlation of the fragments from spontaneous fission of ^{252}Cf is shown in fig.6. There the width of the distribution $FWHM_{sf} = 3^0$ is much smaller than in the case of induced fission ($FWHM_{ind} = 11^0$ -13^0). It is mainly affected by the neutrons emitted from the fragments after fission and from angular straggling. The contribution of the spatial resolution of the PSAC (0.2^0) is negligible.

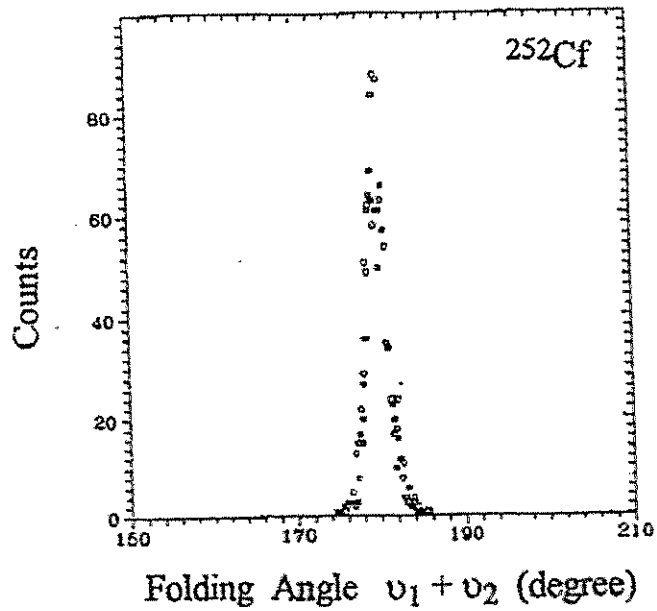

Fig. 6: Folding angle distribution measured with the ^{252}Cf (sf) calibration source.

The longitudinal component of $v_{c.m.}$ was deduced from the measured polar emission angles $\vartheta_1 + \vartheta_2$. Symmetrical fission and a fixed relative fragment velocity is assumed in the relation (1) [2].

$$v_{c.m.} = 1/2 \cdot v_f \cdot (- K \cdot T \; / \; (1 - K \cdot T / 4))^{1/2} \qquad (1)$$

with

$$K = 1 / \tan(\vartheta_1) + 1/\tan(\vartheta_2)$$

$$T = \tan (\vartheta_1 + \vartheta_2)$$

$$v_f = 1.2 \text{ cm/ns} \quad \text{(fission fragment velocity)}$$

By taking into account the geometrical acceptance (fig.2) the determined distribution of $v_{c.m.}$ for the measurements with detection systems of type I and II is shown in fig. 7. The system I covers the total range of LMT, hence, the measured $v_{c.m.}$ distribution represents the complete spectrum of the impact parameter. A considerable part of the spectrum is located at higher velocities than the limit of 0.27 cm/ns for total LMT. This behavior is caused by the deflection effects that contribute not only to the broadening of the coplanarity but also to the folding angle distribution.

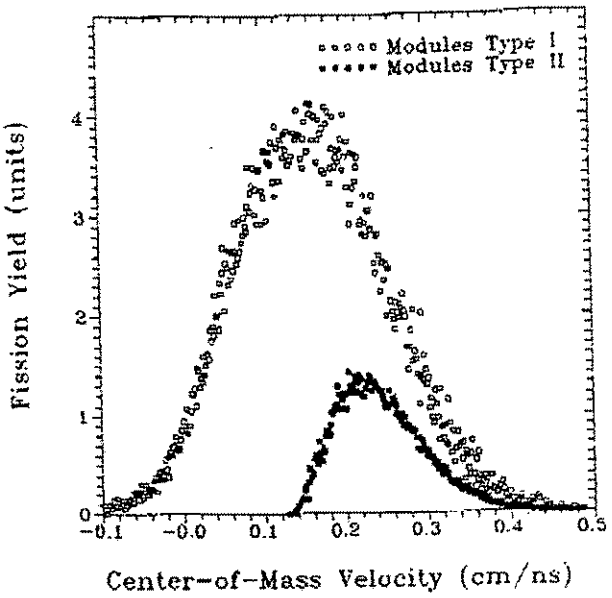

Fig. 7: Velocity distribution of the center of mass of two fission fragments from ^{7}Li (43 AMeV) + ^{232}Th.

The range of acceptance of the detection system II does not include the low LMT region and the measured data are significant only for higher LMT. The difference in the fission yields determined by the detection systems I and II at large LMT is influenced by the asymmetry of the fission process with respect to the beam axis. Both systems differ in concern to the detection angle of the forward emitted fragment. This angle in the laboratory system, e.g., amounts to $\vartheta = 34^{0}$ for the detector type I but to $\vartheta = 49^{0}$ for the type II for coincidences at equal $v_{c.m.} = 0.24$ cm/ns.

The LMT spectrum for fission induced by heavier projectiles of intermediate energy is usually characterized by a double-peaked structure. The two maxima, at low and high LMT, correspond to fission after incomplete and complete fusion. In contrary to this behavior, the data analyzed in this work show a smooth transition from slower to faster composite systems. The maximum amounts to about 0.15 cm/ns what corresponds to 55% of the projectile momentum and an absolute value of 1100 MeV/c. This result is in accordance with the predictions made for the most probable LMT in

central collisions at intermediate energies [19]. There a limit of about 160-180 MeV/c with respect to the LMT per nucleon of the projectile has been found.

4. CALIBRATION PROCEDURE FOR THE DETERMINATION OF THE FRAGMENT MASS

The fragment mass evaluation based on the TOF-E-method requires the determination of the energy losses of the charged particles passing through the foils of the PSAC and the entrance window of the BIC. At the forward modules which include the START-PPAC this energy loss is increased up to more then 50 % of the kinetic energy of the emitted fission fragments. For that reason, the precise knowledge of the foil thicknesses, the use of verified stopping power tables and the exact determination of the calibration coefficients are necessary in order to avoid large systematical errors.

4.1. Time calibration

Measurements with a spontaneous fission source of ^{252}Cf have been performed to determine the zero-point at the time scale. The time referenced from the PPAC made it possible to carry out coincidence measurements with the module pairs of type I. The accessory second module of these detection systems is mounted directly at the opposite side of the trigger. The channel widths of the time-to-digital converters (TDC) used was determined by the help of a precision time calibrator. Using this value the TOF difference between the lighter and the heavier fragment group was converted into physical time units. The result was compared with calculations which simulate the fission fragment emission by taking into account the real geometry of the experimental set-up. Fragment masses and kinetic energy distributions of the $^{252}Cf(sf)$ were taken from ref. [20]. Small discrepancies between the experimental and the calculated results were eliminated by varying a parameter of the geometrical set-up (e.g. the thickness of the target backing). After this procedure the absolute time-scale was derived from the averaged absolute fragment peak positions.

In fig.8 the experimental and simulated data for the fission fragment coincidences of $^{252}Cf(sf)$ have been collected into a TOF_1-TOF_2-matrix. The different positions of the fission fragment groups with regard to the TOF_1 and TOF_2 channel is caused by the additional energy loss of the fission fragments passing through the START-PPAC within the TOF_1 channel.

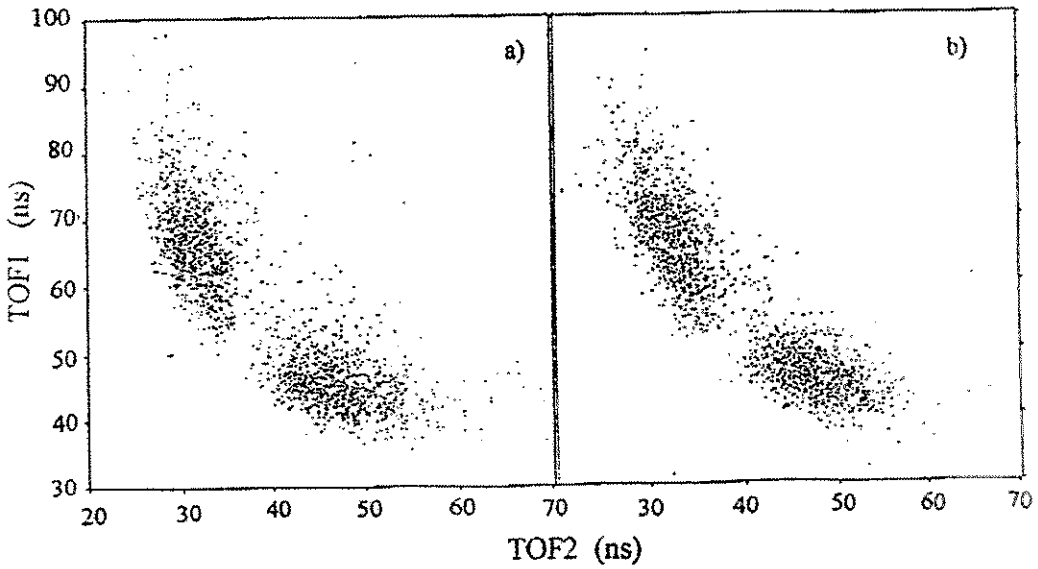

Fig. 8: Measured and simulated TOF_1-TOF_2-coincidences from $^{252}Cf(sf)$.

An evident proof of the calibration was carried out by the TOF_1-TOF_2 data analysis. By analyzing the data from the measurement with $^{252}Cf(sf)$ the total mass sum of the fragments is defined and thereby all fragment parameters are determined from the momentum conservation low. The agreement of the results taken from this analysis with the input data of the fission simulation indicates the consistency of the calibration procedure (fig.9).

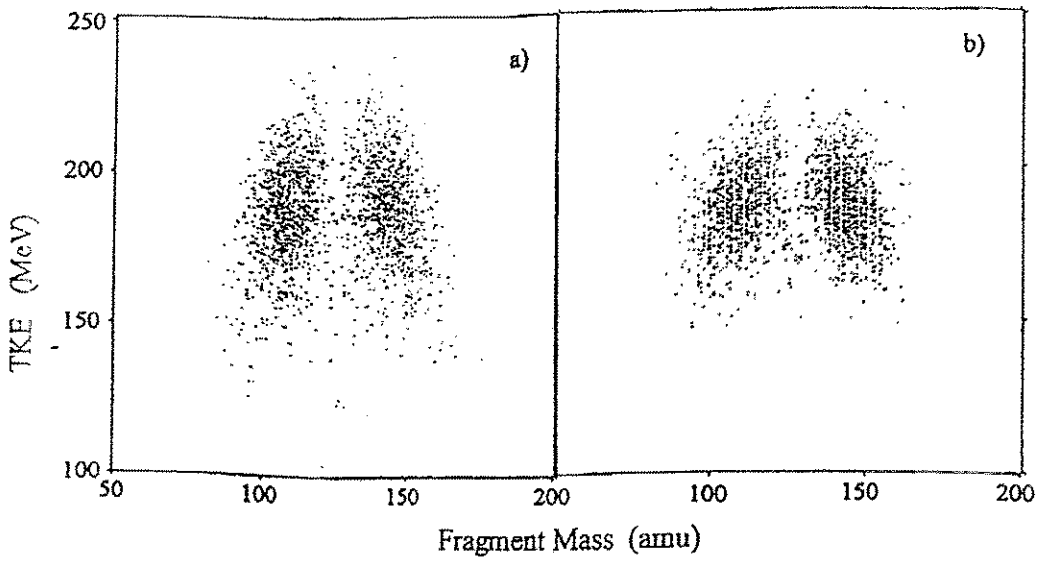

Fig. 9: Measured and simulated TKE - fragment mass distribution from $^{252}Cf(sf)$.

4.2. Energy calibration

The use of the fission fragment events to calibrate the energy spectrum of the BIC is difficult. Besides the large amount of energy losses within the detector foils the residual energy of the fission fragments is not completely converted into the production of free electrons within the chamber gas but also deposited by nuclear interactions. The so called ionization defect known only proximately [21] amounts to about 2-4 MeV for the mixed chamber gas P 10 (90% Ar + 10% CH_4). This value corresponds to 10-30% of the total residual energy of heavy fission fragments (fig.10) and increases the uncertainty of the energy derived from energy loss calculations.

It is a more favored method to identify particles with known kinetic energy directly from the energy loss within the chamber gas. The Bragg ionization chamber not only measures the total energy loss of the fragments within the gas. Additionally, a charge-sensitive signal is derived by storing the maximum-value of the stopping power along the path of the fragment through the chamber. If really the absolute maximum of the stopping power curve (Bragg-peak) has been found, the measured value is independent on the entrance energy of the fragments and scales linearly with its charge. However, the measurement of the Bragg-peak requires a sufficiently large entrance energy of the fragment. This lower threshold depends on the operational parameters of the chamber (electron drift-velocity, gas pressure) and of the signal analysis by the electronics (time constant of the current signal integration, time interval for the integration of the specific energy loss). Taking into account these parameters the lower charge identification limit can be calculated. The comparison of the calculated threshold values for different charges with measured ones makes calibration points

available within the lower energy region. Reaction products of ^{7}Li (43 AMeV) on ^{232}Th and nuclei of the target backing have been used for this purpose.

The maximum energy of the fragments which are stopped within the chamber gas is easier to calculate. For a given fragment this energy threshold depends only on the gas pressure. It can be found within the measured Bragg-peak versus residual energy plot as the maximum of the energy of a certain Z-branch. In contrary to the calibration with an external ^{252}Cf(sf) source, the method described above is not influenced by any energy loss within the detector foils.

The thus calibrated data from ^{252}Cf(sf) are shown in fig.10a. Now, the independent TOF-E-method can be applied for the fragment mass determination. Remaining discrepancies between the results of this evaluation and the distribution known from ref. [20] have been adjusted by varying the asumed thickness of the entrance foil of the BIC.

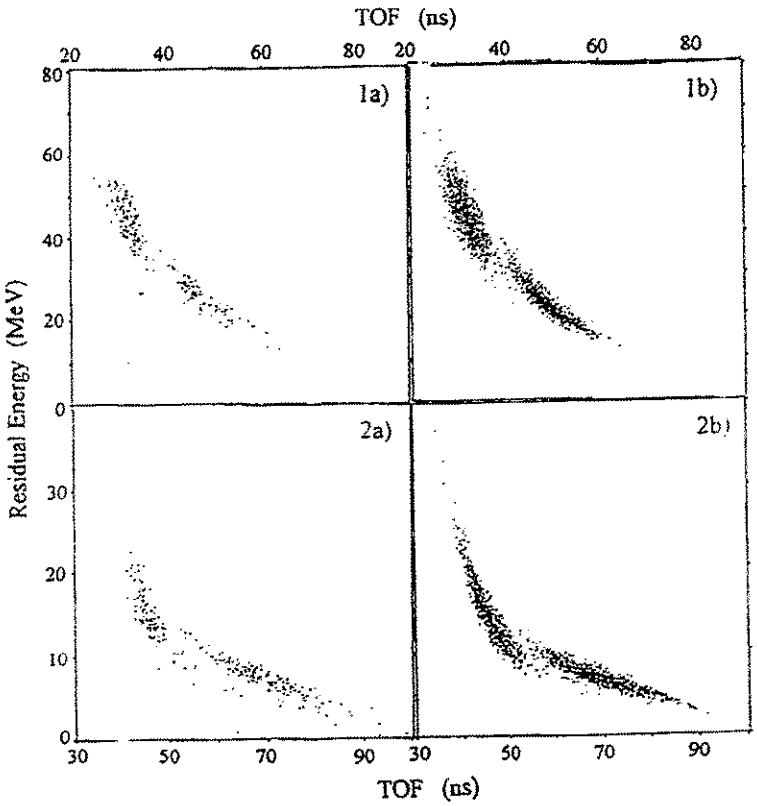

Fig. 10: TOF-E-plots of events from ^{252}Cf(sf) :
a) experimental data ; b) simulated data both for a module without (1) and with START-PPAC (2).

The resulted mass distribution of the single fragments from ^{252}Cf(sf) is shown in fig.11. The distribution of the sum of the independently determined fragment masses has a width of FWHM = 23 amu which indicates the experimental mass resolution (fig.12a) of this measurement. The corresponding value of FWHM = 16 for the single fragment mass resolution is much larger than the FWHM of 8-10 amu achieved in earlier measurements [22,23]. In this experiment some problems occurred with the operation of the BIC deteriorating their energy resolution. Meanwhile these problems have been solved. The relative fission fragment velocity was measured to be 2.42 cm/ns with a FWHM = 0.25 cm/ns (fig.12b).

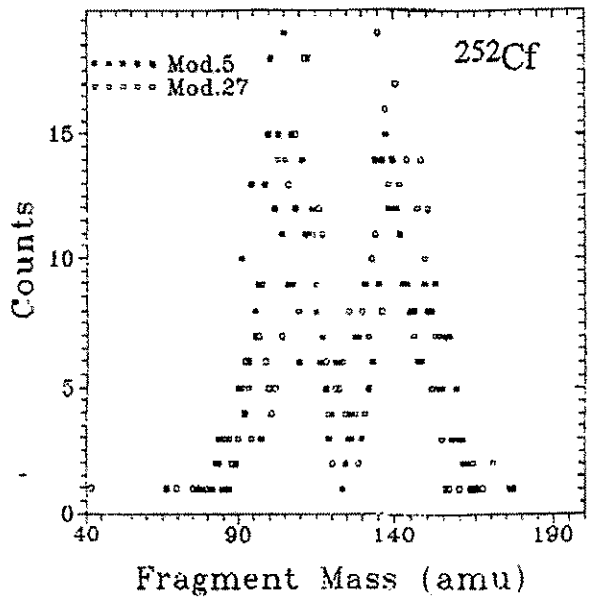

Fig. 11: Mass distribution of fission fragments from ^{252}Cf(sf) evaluated by the TOF-E-analysis.

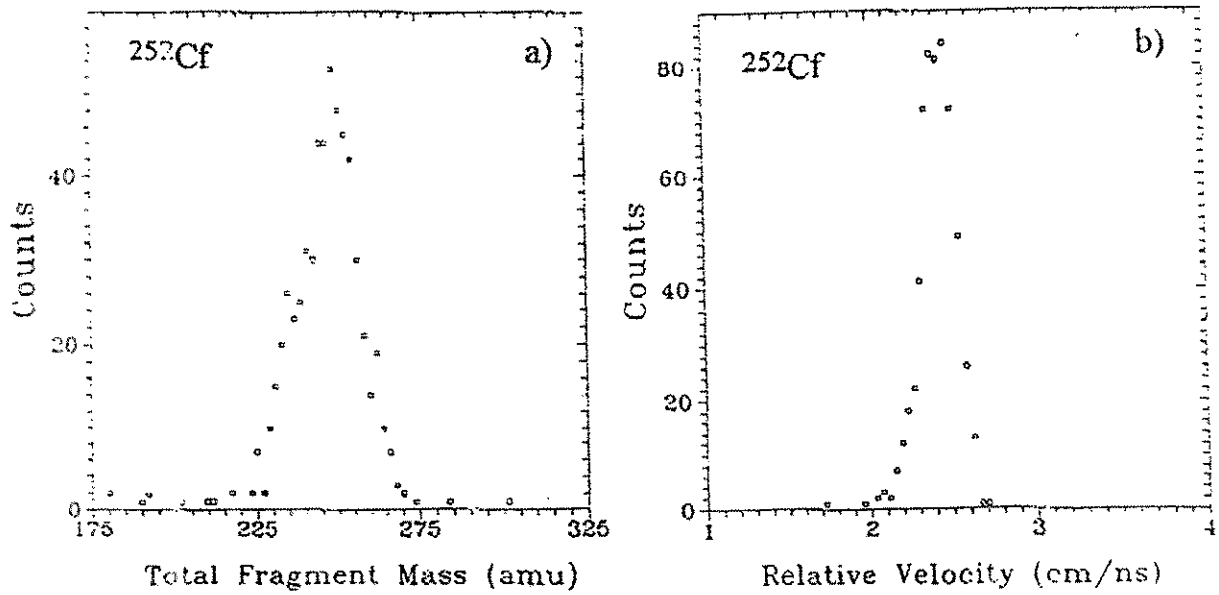

Fig. 12: Results calculated by the TOF-E-analysis of the fission events from ^{252}Cf(sf) : a) sum of the coincident fragment masses ; b) relative fission fragment velocity.

5. MASS AND MOMENTUM BALANCES OF FISSION FRAGMENTS FROM ^{7}Li (43 AMeV) + ^{232}Th

5.1. Modification of the TOF measurement

The absolute time calibration based on the measurement with the ^{252}Cf(sf) source as described in Sect. 4.1. is only applicable for the detector modules which are extended by START-PPAC. By using the time reference signal from the coincident fission fragment also the modules at the opposite side from the trigger detector can be calibrated. In order to determine the zero-time value for the remaining modules the peak position of the events from δ-electrons has been analyzed.

The δ-electrons are produced by the interaction of the projectile and the electrons of the target atoms. A mean TOF = 7.5 ns for the δ-electrons was derived from a measurement with a detector module which was calibrated by ^{252}Cf (sf) and positioned at $\vartheta = 142.6^{0}$ with respect to the beam axis. This amount corresponds to about 70 % of the projectile velocity. Due to the angular dependence of the δ-electron emission the usage of this value is correct only for the modules positioned at the same angle. However, the δ-electrons seen in the TOF spectra were applied also for the other modules to calibrate the time scale absolutely. The error for the modules mounted in the backward hemisphere should not exceed a value of 0.5-1 ns.

The TOF measurements of the different modules were carried out with the timing referenced to the RF of the cyclotron. Only for the trigger modules 2 and 5 a second TOF measurement was related to the signal of the START-PPAC. However, by comparing the two corresponding TOF signals measured by the trigger modules a correction was derived which considers the shifts of the beam pulse relative to the RF. This correction was calculated event by event and applied to all of the registered TOF signals. The time reference of the TOF measurement was transformed from the RF to the START-PPAC and, by this way, the TOF measurement became independently from the beam pulse.

5.2. Distribution of fission events within the TOF-E-matrix

Time-of-flight and residual energy of the fission events are collected into the plot which is shown in fig.13. The positions of the fission fragment groups are nearly the same for the forward-trigger module and for the oppositely positioned backward module. The larger amount of kinetic energy in the forward cone of the laboratory system is completely consumed by the energy loss within the START-PPAC.

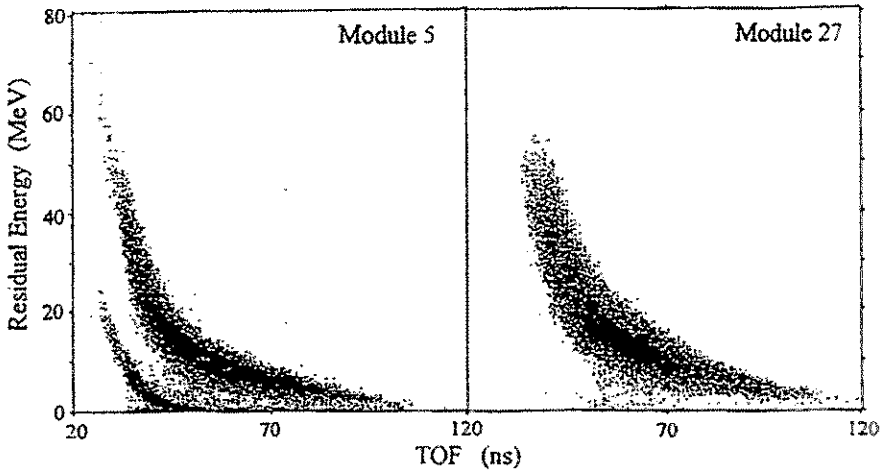

Fig. 13: Residual energy versus time-of-flight of inclusive measurements with a forward (5) and a backward (27) module for ^{7}Li (43 AMeV) + ^{232}Th. (The forward module detects not only fission fragments but also a large amount of lighter reaction products.)

5.3. Fission fragment momentum balance

The fragment mass and the charge determined by the TOF-E-analysis are correlated in accordance to the line of β-stability. At the end of the iterative procedure applied [14] the emission energy of the fragments is evaluated and the complete single-fragment parameters are available for further analysis.

The vector sum of the two single-fragment momenta in the following context is called the *total* momentum. The two transverse components of this vector are shown in fig.14 for the fragments of the nuclear reaction investigated as well as for the ^{252}Cf(sf) calibration source. The width of the distribution of the transverse total momentum for the ^{252}Cf(sf) data is FWHM = 200 - 250 MeV/c. This amounts to about 5 % of the single-fragment momentum. The FWHM = 700 - 800 MeV/c obtained from the data of ^{7}Li (43 AMeV) + ^{232}Th is larger by a factor of about 3.5

.

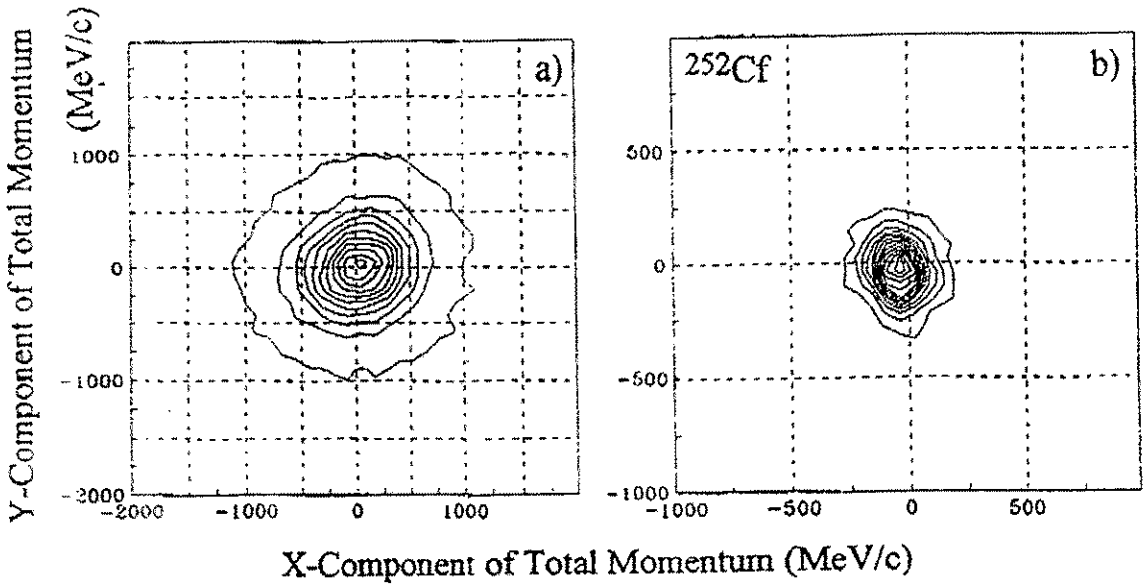

Fig. 14: Transverse components of the total momentum : a) obtained from fission fragments of ^{7}Li (43 AMeV) + ^{232}Th ; b) for the ^{252}Cf(sf) calibration source.

The deflection of the momentum vector of the composite nucleus perpendicular to the beam axis can be explained by the momentum transfer from the projectile to the target in the case of peripheral impacts. Within this frame, the transverse momentum increases at smaller LMT. In contrary to this behavior, the deflection caused by neutron and other light particle evaporation becomes more important at larger LMT.

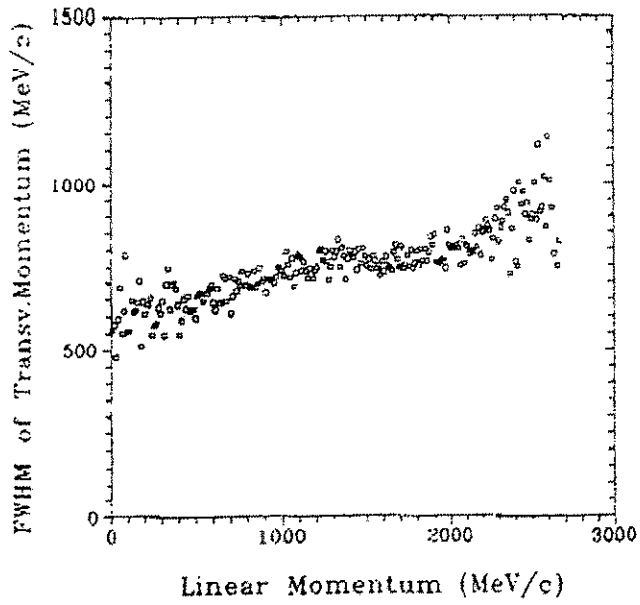

Fig 15: Distribution width of the transverse component of the total momentum as a function of LMT.

The measured FWHM of the transverse component as a function of the LMT is shown in fig. 15. It is characterized by a large amount at small LMT and an increasing at large LMT. This must be interpreted by the dominant influence of the neutron emission. Based on this message, the broad transverse momentum distribution at small LMT can be only explained as resulting from the nuclear reaction if, at peripheral impacts, the composite system receives a transversal kick of several 100 MeV/c.

Using both the sum of the momentum and the fragment masses, the velocity of the composite system has been calculated directly from the single-fragment parameters without any comprehensive assumption. A comparison of its longitudinal component with the results derived from equ. (1) is shown in fig.16. Evidently, with exception of the data at the limits, a good agreement was found which indicates the validity of the assumptions made in equ. (1) as well as the quality of determination of the single-fragment parameters.

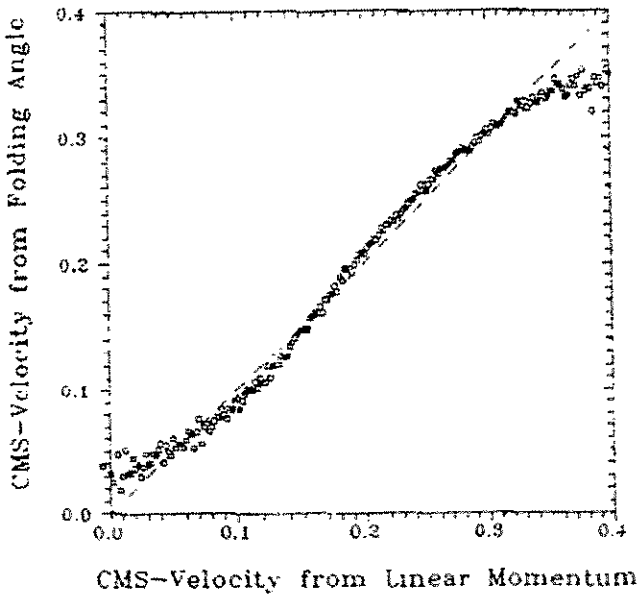

Fig. 16: Longitudinal velocity of the fissioning system determined both from the folding angle (equ. (1)) and from the balance of single-fragment parameters.

5.4. Masses and relative fragment velocities as a function of momentum transfer

The ratio between the amount of the total fragment momentum and the linear momentum of the projectile has been defined as a measure of LMT. This ratio was used to study as the behavior of the mean value and the width of the distribution of the single-fragment mass (fig.17) as of the relative fragment velocity (fig.18) and the total fragment-mass sum (fig.19) in dependence on LMT.

An approximately linear slope of the single-fragment mass with increasing LMT (fig.17a) corresponds to a difference of about 12 amu between the averaged fragment mass at peripheral and central collisions. The distribution width (fig.17b) varies between 35 - 50 amu. It is large compared to the experimental resolution of 16 amu. The increasing width at small LMT results from contributions of asymmetrical fission at low excitation energies. The minimum width is obtained at about 50 % of the projectile momentum, and it increases smoothly up to 50 amu for complete LMT.

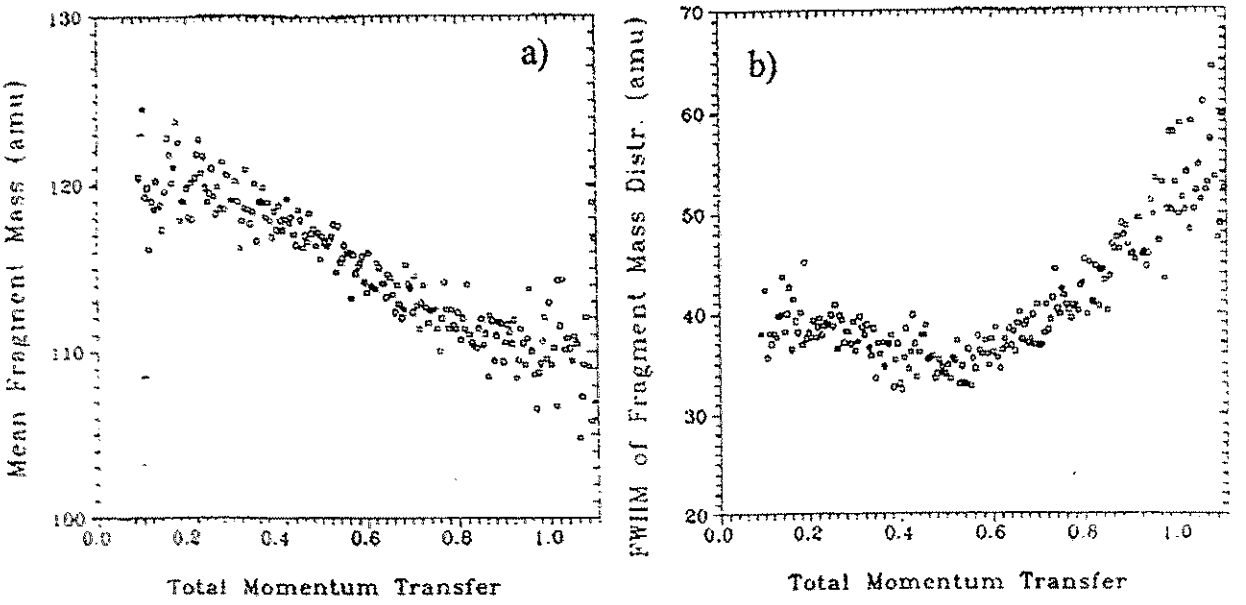

Fig. 17: Single-fragment mass distribution as a function of total momentum transfer.

The measured relative velocities with the averaged value of 2.4 cm/ns and the FWHM = 0.25 cm/ns agree with the results from the calibration measurement using ^{252}Cf(sf). The mean relative velocity (fig.18a) slowly increases at larger LMT. This can be interpreted in the following way: The enlarged velocity is caused by the decreased fragment mass and superposed by the reduction of the total kinetic energy of fission due to evaporation of charged particles. This means, that at large LMT the amount of charged nucleons transferred from the ^{7}Li projectile to the composite system is overcompensated by the emission of charged particles at higher excitation energies. Quantitative estimates will be done.

The larger width of the distribution at higher LMT (fig.18b) can be understood as a result of the increasing distribution widths of mass and charge of the single-fragments as well as of the fissioning system.

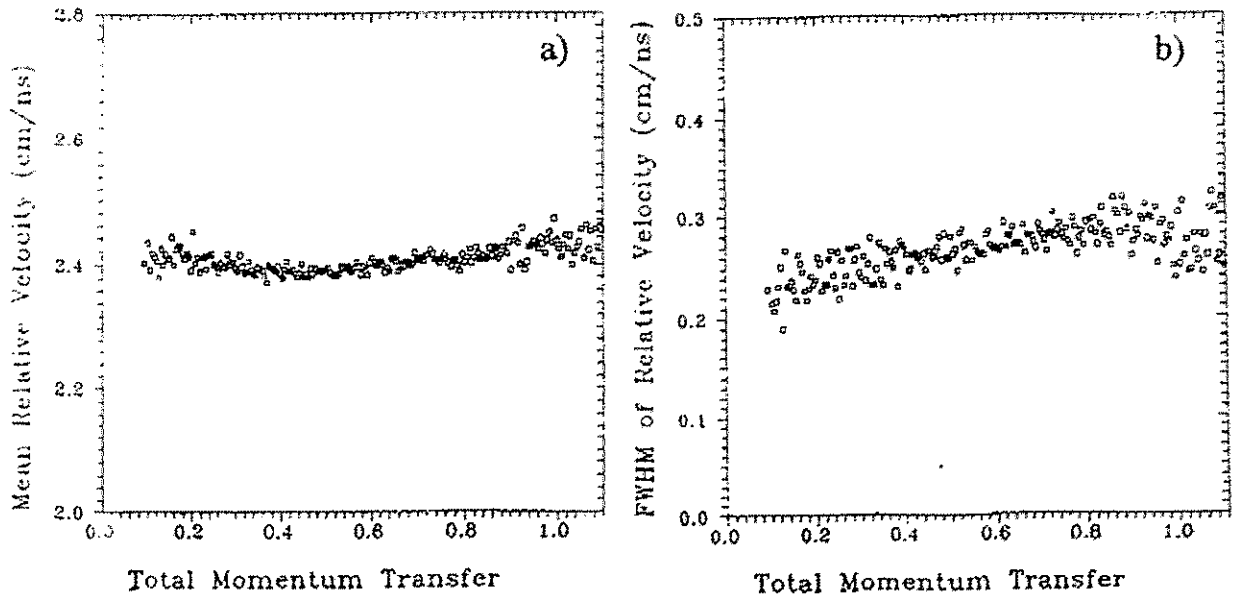

Fig. 18: Relative fission fragment velocity as a function of total momentum transfer.

The sum of the single-fragment mass drops down with increasing LMT. In correspondence with the data of the single-fragment mass analysis, the slope between small and total momentum transfer amounts to about 25 amu. Taking into account the maximum excitation energy of 290 MeV, the averaged energy taken away per evaporated nucleon is about 12 MeV.

The width of the sum mass distribution is strongly influenced by the experimental resolution of 23 amu. Under this condition only the tendency of an increasing width at large LMT can be deduced from the data.

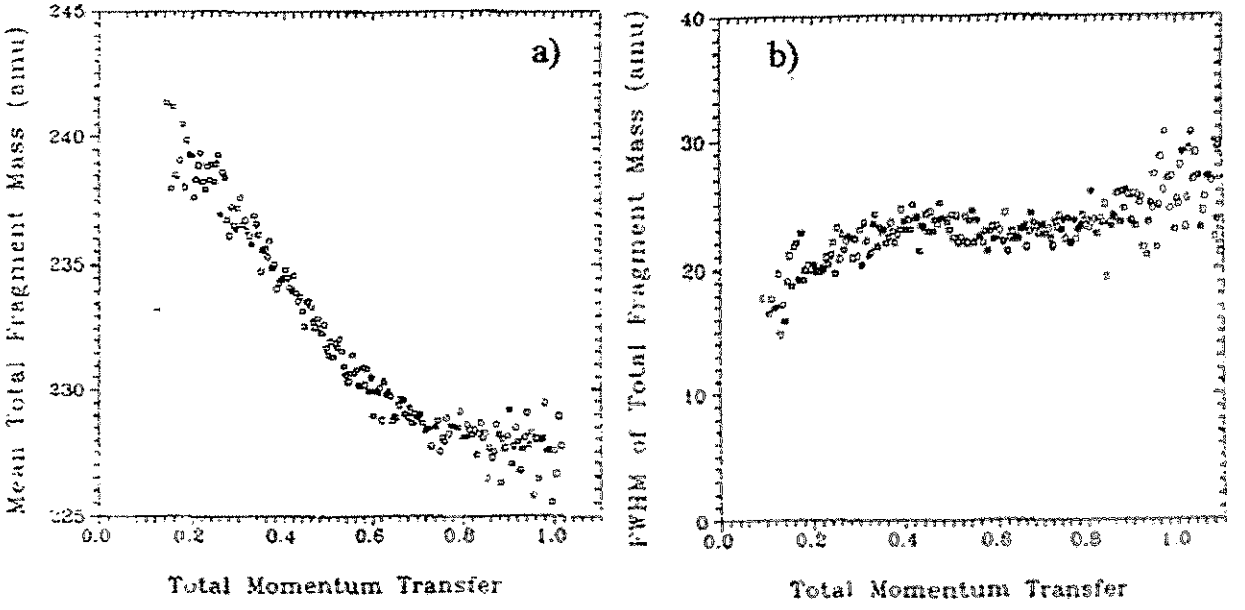

Fig. 19: Mass sum of the coincident fission fragments as a function of total momentum transfer.

SUMMARY

The analysis based on the balance of the single-fragment momenta indicates a large transverse velocity component of the fissioning system in peripheral as well as in central collisions. In correlation to this, a strong influence on the folding angle distribution of fission which is caused, e.g., by the evaporation of neutrons, must be taken into account. For such a very asymmetric projectile-target combination like $^{7}Li + ^{232}Th$, the estimated broadening of the folding angle at a fixed assumed $v_{c.m.}$ amounts to more than 50 % of the total measured width. From this value a large uncertainty must be considered when the momentum transfer and the excitation energy are deduced from the folding angle event by event.

An alternative observable to filter the excitation energy, especially for nuclear reactions with very asymmetric projectile-target combinations, is the determination of the total fragment mass sum. It could be verified that the sum of the fragment masses is approximately linear correlated with the momentum transfer as assumed within the frame of the MTM. The uncertainty of the total mass determination in this experiment (FWHM = 23 amu), compared with the difference of total fragment masses (25 amu) at central and peripheral collisions, was too large for a more detailed analysis. However, with a single-fragment mass resolution of FWHM < 8 amu already achieved in earlier FOBOS-measurements, the sum mass should be a better filter of the excitation energy than the folding angle.

The full advantages of the FOBOS spectrometer can be put into practice only in measurements without START-PPAC. This was not possible in this first FOBOS-experiment at the beam-line of the U-400M cyclotron because of the characteristics of the beam-pulse. In further experiments without use of START-PPAC the geometrical efficiency will be increased essentially. In addition, by replacing the START-PPAC at the forward modules, the energy losses of the fission fragments can be reduced what leads to an improvement of the mass resolution.

The agreement between the results from our independent balance analysis and from the folding angle analysis using the MTM indicates that the TOF-E-method was performed successfully without essential systematic errors even under the conditions of large fragment energy losses.

References

[1] T. Sikkeland et al., Phys. Rev. 125 (1962) 1350
[2] D.Guerreau, Internat. School on Nuclear Physics, "Nuclear Matter and Heavy Ion Collisions", Les Houches, 1989, Report GANIL P89-07.
[3] Fatyga et al., Phys. Rev. Lett. 55 (1985) 1376
[4] M. Conjeaud et al., Phys. Lett. B 159 (1985) 244
[5] C. Volant et al., Phys. Lett. B 195 (1987) 22
[6] E.C. Polacco et al., Proc.of the Third Internat. Conf. on Nucleus-Nucleus Collisions, St. Malo, France, June 1988, p.103.
[7] J. Galin et al., Z. Physik A331 (1988) 63
[8] U. Jahnke et al., Phys. Rev. Lett. 57 (1986) 190
[9] E. Schwinn et al., Nucl. Phys. A568 (1994) 169
[10] V.E. Viola, Nucl. Data Sect. A1 (1966) 391
V.E. Viola et al., Phys. Rev. C32 (1985) 1550
[11] H.-G. Ortlepp et al., "4π-Fragmentspektrometer FOBOS", Report ZfK-734, Rossendorf, 1990.
[12] H.-G. Ortlepp et al., " The FOBOS 4π Detector of Charged Particles at Dubna ", Proc. of the Int. Conf. on New Nuclear Physics with Advanced Techniques, Ierapetra, Crete, June 23-29, 1991, World Scientific, Singapore, 1992.

[13] "FOBOS - a 4π-Fragment Spectrometer for Heavy-Ion Reaction Products", Report FZR 92-11 (Ed. H.-G. Ortlepp, K.-D. Schilling) Rossendorf, 1992.
[14] H.-G. Ortlepp et al., "The 4π Fragment Spectrometer FOBOS - Status and First Preliminary Results-" Proc. Internat. School-Seminar on Heavy Ion Physics, Dubna, Russia, May 10-15, 1993, vol.2, p.466.
[15] A.A. Aleksandrov et al., Fifth Internat. Conf. on Nucleus-Nucleus Collisions,Taormina, Italy, 1994 (Proceedings to be published in Nucl.Phys. A) (see contributions in this report).
[16] G.D. Westfall et al., Nucl. Instr. and Meth. in Phys. Research A 238 (1985) 347
[17] E. Plaguol and the INDRA Collaboration, Nouvelles de Ganil Nr. 44 (Feb.1993).
[18] W.W. Wilcke et al., Atomic Data and Nucl. Data Tab. 25 (1980) 389
[19] C. Gregoire and F. Scheuter, Phys. Lett. 146B (1984) 21
[20] R. Schmidt and H. Henkel, Nucl. Phys. A395 (1983) 15
[21] S. Kahlbitzer et al., Z. Physik A278 (1976) 233
[22] C.-M. Herbach et al., Jahresbericht 1992, Report FZR 93-10, Rossendorf, 1993, p.95.
[23] H.-G. Ortlepp et al., Jahresbericht 1992, Report FZR 93-10, Rossendorf, 1993, p.97.

STUDY OF FISSION AND IMF EMISSION IN THE REACTION ^{14}N (34 AMeV) ON ^{197}Au AT FOBOS *

A.A. Aleksandrov [1], I.A. Aleksandrova [1], L. Dietterle [1,2], V.N. Doronin [1], S. Dshemuchadse [2], P. Gippner [1,2], C.-M. Herbach [2], S.I. Ivanovsky [1], D.V. Kamanin [1], A. Matthies [1,2], D. May [1,2], H.-G. Ortlepp [1,2], G. Pausch [2], Yu.E. Penionzhkevich [1], G. Renz [1,2], K.-D. Schilling [2], D.I. Shishkin [1], , O.V. Strekalovsky [1], V.V. Trofimov [1], C. Umlauf [1,2], D.V. Vakatov [1], V.M. Vasko [1], W. Wagner [1,2], V.E. Zhuchko [1], I.P. Zurin [1]

for the FOBOS - Collaboration

[1] *Joint Institute for Nuclear Research, Dubna, Russia*
[2] *Research Centre Rossendorf e.V., Germany*

After the ^{7}Li + ^{232}Th experiment [1] the investigation of binary and ternary decay of heavy nuclei with excitation energies up to E* ≈ 300 MeV at FOBOS [2] has been continued using another reaction.

A 500 μg/cm^2 thick gold foil has been bombarded by a ^{14}N beam of 34 AMeV delivered by the U-400M cyclotron of the FLNR. A second run at 55 AMeV is planned for 1995.

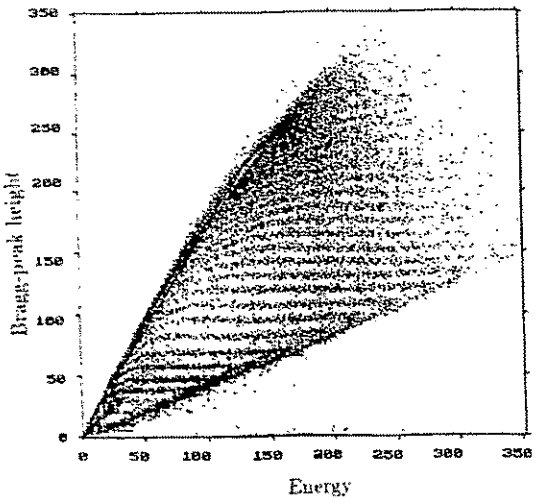

Fig.1 Bragg-peak height over energy plot of particles registered by a BIC at 37°. Z-branches from 2 to 25 are resolved. The transition to unresolved FF is smooth.

16 gas-filled modules of the FOBOS array were used. 80 CsI(Tl) detectors of the FOBOS scintillator shell [3] were operated in a slave-mode with respect to the gas detectors to register light charged particles (LCP) and penetrating light fragments. Two small transmission avalanche counters near the target delivered timing reference signals for the TOF measurement [1]. One remained at ϑ=37° but the second one was positioned at ϑ=101° relative to the beam axis to trigger on backward emitted fragments.

The ionization chambers (BIC) were operated at pressure of 250 Torr of on-line mixed Ar + CH_4 gas, the avalanche counters (PSAC) at 4 Torr of pentane.

Except the time-of-flight (TOF), the direction (ϑ,φ), the energy (E), the Bragg-peak height (Z) and also the PSAC pulse-height (ΔE) of the fragments were measured. Using the ΔE- and TOF-information it was possible to roughly identify slow particles which did not enter the BIC.

About $2.5 \cdot 10^6$ events with two and $2 \cdot 10^3$ events with three fragments hitting the gas modules have been recorded. A first estimate of the ratio of triple (FF+FF+IMF) to binary (FF+FF) decays yields $\approx 2.5 \cdot 10^{-3}$ for events with 80% momentum transfer. This value is comparable with the value obtained for ^{7}Li + ^{232}Th [1]. The larger statistics in this experiment, however, should allow a more detailed analysis. The CsI(Tl) detectors recorded one additional LCP in ≈50 % of the events.

* The FOBOS project is supported by the BMFT, Germany, under contract N° . : 0 DR 100.

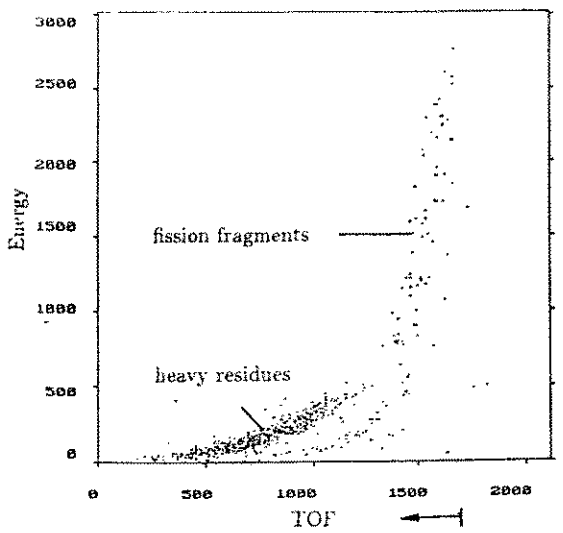

Fig.2 Energy over TOF plot of a module at 37°. Only events in coincidence with IMF at 101° were selected. The two distinct groups can be interpreted as heavy partners of a binary process and fragments of their subsequent fission.

A first scan of the data shows some interesting features to be analyzed in detail :

1. There is a smooth transition from symmetric to very asymmetric fission ($A_1/A_2 \approx 10$) both in the yield and in the fragment energy (fig.1).
2. In coincidence with a sideward emitted light fragment (IMF) we see either a heavy residue or fission fragments (fig.2).
3. Both in symmetric and asymmetric fission there is a considerable probability of LCP emission in backward directions.

After analysis in progress now new information about the competition between binary and ternary decay of hot nuclei with mass $A \approx 190$ at excitation energy $E^* \approx 300$ MeV as well as about the probability for survival of a heavy residue is expected.

REFERENCES

1) Aleksandrov, A.A. et al, "Correlations between intermediate mass and fission fragments.....", this report.
2) Ortlepp, H.-G. et al., Proc. of the Internat. School-Seminar on Heavy Ion Physics, v.2, JINR Dubna, Russia, 1993, p.466.
3) Wagner, W. et al., Scientific Report 91/92, Flerov Laboratory of Nuclear Reactions, JINR Dubna, Russia, 1992, p.244.

IMF-Emission and Projectile Fragmentation in the System $^{32}S + ^{197}Au$ at 30 MeV/u

J. Krüger[1], A. Budzanowski[2], H. Fuchs[3], C.M. Herbach[1], H. Homeyer[3], D. Kamanin[4], A.Matthies[4], H.G. Ortlepp[4], G. Pausch[1], W. Seidel[1], V.Shuchko[4], A. Siwek[3], V. Trofimov[4], A. Tutay[3], W.Wagner[4], L. Zrodlowski[2]

[1] *FZ Rossendorf*
[2] *IPN Krakau*
[3] *HMI Berlin*
[4] *JINR Dubna*

The FOBOS setup will be completed by the ARGUS forward detector system, which consists of 130 phoswich detectors in a cone around the beam axis.
The ARGUS multidetector was built up at the Hahn-Meitner-Institut Berlin [1] and has been used to investigate projectile fragmentation [2] and multiple break-up of nuclei [3] in heavy-ion reactions at 20-30 AMeV.
In 1992, this detector array was modified to investigate the sources of IMF's in the system $^{32}S + ^{197}Au$ at 30 MeV/u [4]. Several phoswich detectors in the midplane were replaced by semiconductors operating in a pulseshape regime [5]. This allows the determination of masses by E-TOF-analysis. For getting charges of IMF's and masses of fission fragments detected in the backward hemisphere, a prototype of a FOBOS gasdetector module [6] was mounted at θ=123^0. During this experiment, which was carried out by the FOBOS collaboration at VICKSI in the HMI Berlin, we also tested the FOBOS data acquisition system [7] and the first-level trigger principle which had to combine the "fast" phoswich detectors with the "slow" gas-detector moduls of FOBOS.
As a first step of data analysis, a folding angle analysis was carried out. We selected pairs of asssociated fission fragments by gates in the plot of the relative velocity versus the sum mass. The relative velocity of fission fragments is given by the VIOLA systematics [8] and approximately 2.4cm/ns.
From the masses and velocities of these fission fragments we computed the velocity vector of the fissioning system (FS) (fig.1). The velocity component in beam direction $v_{||}$ was considered to give a scale for the transferred momentum and the excitation energy of the FS.

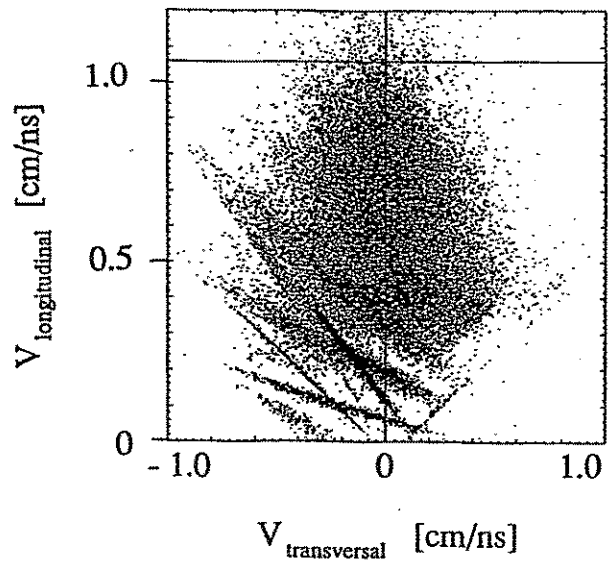

Fig.1
Velocity vectors of the fissioning system.
The line at $v_{||}$=1.06cm/ns indicates full momentum transfer.

Looking at the average multiplicities of hydrogens and heliums in the phoswich detectors,we found that the average multiplicity of hydrogens shows a monotone increase with momentum transfer, whereas the average multiplicity of helium is peaked at medium momentum transfer. It seems to be obvious, that alpha particles play an extraordinary role in the process related to medium momentum tranfer - the projectile fragmentation or dynamical projectile breakup.

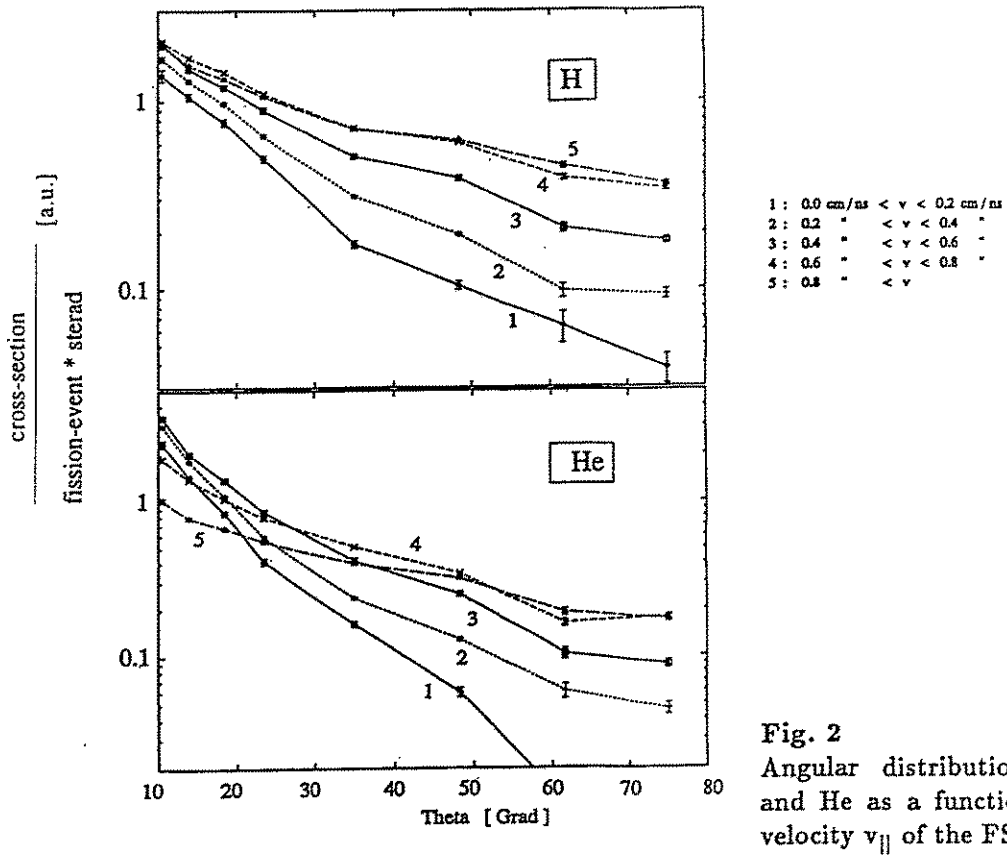

Fig. 2
Angular distributions of H and He as a function of the velocity $v_{||}$ of the FS.

Fig.2 shows the corresponding angular distributions of hydrogens and heliums for five bins of momentum transfer, normalized to the number of fission events and solid angle. For small angles to the beam axis, the yields of alphas decrease with increasing momentum transfer, whereas the yields of protons show a monotone increase. In the model of Möhring [9],the sulfur projectile is treated as a cluster consisting of 8 alpha particles, which are bound in an empirical alpha-alpha-potential. The dynamical projectile breakup is due to an interplay of friction forces on the surface of the target nucleus and the inertial forces acting on the projectile. The angular distributions (fig. 3) show a good agreement with experimental data. For interpretation of the existing differences, the accuracy of the calibration of masses and velocities of fission fragments due to pulse height defect [10] and plasma delay [11] will be improved.

The obtained results from folding angle analysis shall be used to clearify the origin of heavy residues (HR). HR were detected in the semiconductors up to an angle of θ=35^0. Fig. 4 shows the mass spectrum of a semiconductor detector at θ=14^0 in coincidence with a fragment at θ=121^0 and the same mass spectrum with the demand that the particle at θ=121^0 is an IMF . The correlated HR to a backward IMF are well localized. This indicates that IMF are binary partners of HR. By the demand of a detection of an IMF in the backward FOBOS-module, the average multiplicity of fast projectile-like fragments decreases drastically(fig. 5). So we can estimate, that IMF originate from reactions with high momentum transfer. To clearify this question will be the task of further investigations.

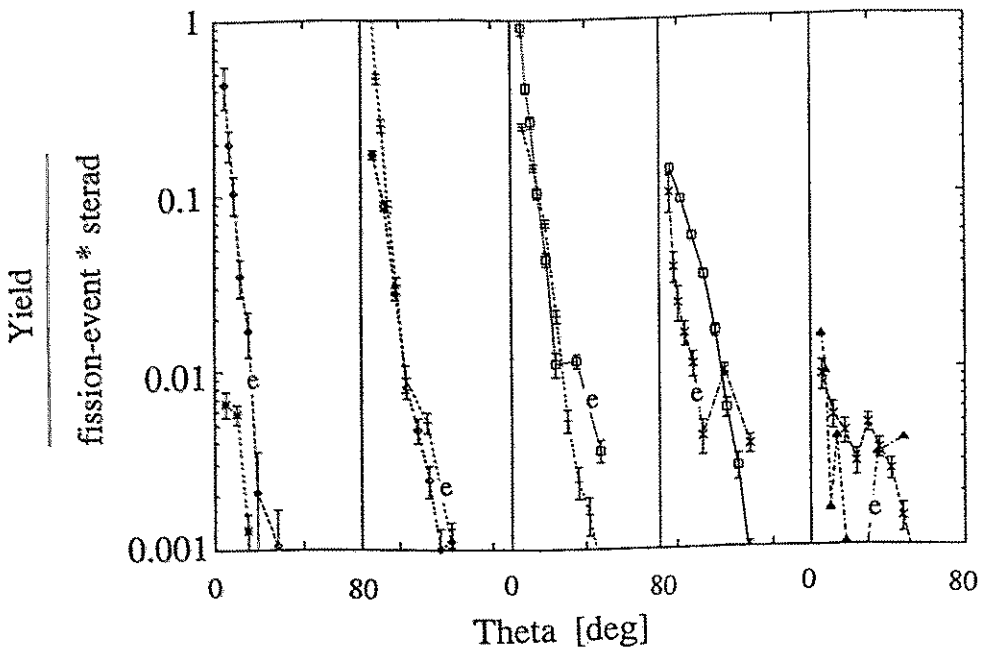

Fig. 3
Comparison of experimental angular distributions of C-Fragments (marked with an "e") with theoretical predictions of Möhring. The bins in $v_{||}$ are from low momentum transfer ($v_{||}$< 0.2 cm/ns) to high momentum transfer ($v_{||}\geq$0.8cm/ns) from left to right

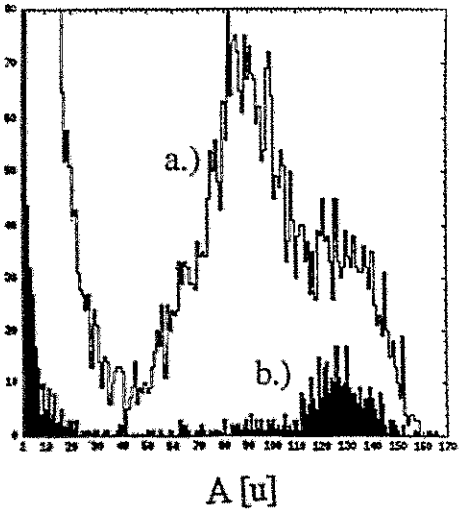

Fig. 4
Mass spectrum at θ=14^0 with the coincidence conditions:
a) registration of a fragment at θ= -121^0.
b) registration of an IMF (4< A $\leq$40) at θ=-121^0.

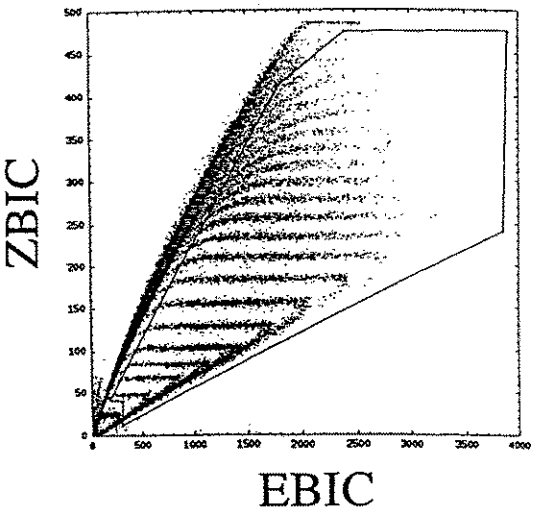

Fig. 5
Raw data scatterplot of the FOBOS module (Bragg peak height vs. residual energy). For the shown IMF-gate the average multiplicity of fast projectilelike fragments (Z>6) decreases from 0.117 (all other events) to 0.013

REFERENCES:

[1] W. Terlau et al., HMI-B 482 (1990), p. 93
[2] C. Schwarz et al., HMI-B 490 (1991), p. 74
[3] A. Siwek et al., Preprint HMI/FK-Fucl (1994), submitted to Zt. f. Physik A
[4] G. Pausch et al., HMI-B 507 (1993), p. 87
[5] G. Pausch et al., Nucl.Instr. and Meth. A337 (1994) 573-587
[6] H.-G. Ortlepp et al., Proc. Int. Conf. on New Nuclear Physics with Advanced Techniques, Ierapetra, Crete, Greece (1991)
[7] C. Beschorner et al., HMI-B 507 (1993), p. 95
[8] V.E. Viola et al.,Phys. Rev. C31 (1985) 1550
[9] K. Möhring et al., Nucl. Phys. A533 (1991) 333
[10] J.B. Moulton et al., Nucl. Instr. and Meth. 157 (1978) 325-331
[11] W. Bohne et al., Nucl.Instr. and Meth. A240 (1985) 145-151

Analysis of light charged particle multiplicities in the reaction ^{32}S(960MeV) + ^{197}Au

D.Kamanin[1], H.Fuchs[2], J.Krueger[3], G.Pausch[3]
([1]JINR, Dubna. [2]HMI, Berlin. [3]FZR, Rossendorf.)

The data of a previous experiment carried out with the extended ARGUS array [1, 2] were analyzed to obtain information about correlations between the multiplicity of light charged particles (LCP) and the decay channel of the targetlike nucleus in the reaction $^{32}S(960MeV) + ^{197}Au$.

For each of the 113 phoswich detectors we defined nine classes of particles by means of gates in the ΔL-L and L-T plots (Fig.1. ΔL - short light component corresponding to the light output of the plastic ΔE scintillator, L - total light output, T - time of flight): H, Li, Be, B, and C particles - which could be identified if their energy was sufficient to pass the ΔE scintillator, PLF - which comprises all ions not stopped in the ΔE scintillator with a charge number Z>6, He particles - which could be identified down to the detection threshold by means of ΔL-L and L-T gates, and two classes of "slow" particles with Z>2 which were stopped in the ΔE scintillator. This classification has also been exploited for other aspects of data analysis [2] . For the 14 semiconductor detectors arranged in the reaction plane [1], three classes of particles were separated by gates in the E-T plane (E - energy deposition in the detector): H, He, and a validation gate for other, heavier particles. Using the particle gates created, the primary data were converted into the so-called New OLYMP Data Structure, which allows to derive angular and multiplicity distributions for the particle classes defined above.

To obtain information on the reaction mechanism we analyzed angular and multiplicity distributions of LCP in coincidence with heavy particles (Z>2) detected in one of the semiconductors. Based on the mass and velocity parameters obtained from the detector calibration [2] we subdivided these heavy ions into two major classes - the intermediate-mass fragments (IMF, with $A = 5-40$ and $v = 0.3-4.0$cm/ns), and the fission fragments (FF, with $A = 40-130$ and $v = 0.3-2.5$cm/ns).

In a first attempt we accumulated angular distributions and multiplicity spectra under the condition of an IMF or FF identified in the semiconductor detector in the backward hemisphere ($\theta = 121°$). By means of an energy threshold we tried to distinguish between high-energy LCP's — originating from projectile breakup or preequilibrium emission — and LCP's evaporated from a slowly moving compound system. A reasonable value for this discrimination level was found to be 50 MeV for alphas and 20 MeV for protons by analyzing energy spectra of LCP's for the forward detectors up to $\theta = 18.5°$ under the coincidence condition described above. All LCP's registered at larger angles were attributed to the evaporation class.

Figure 2 presents the ratio of LCP yields measured in coincidence with an IMF or FF at $\theta = 121°$ as a function of the LCP angle. It is evident that the emission of fast forward-directed LCP's — which carry away part of the momentum and energy of the projectile — is strongly enhanced in coincidence with FF's. This means that IMF production supposes — at least on average — a larger energy dissipation than fission. In accordance with this picture we found an enhanced yield of evaporated LCP's in coincidence with IMF's: The yield ratio in figure 2 is smaller than 1 for the low-energy LCP's, independent of the detection angle. (An exception are very small angles where preequilibrium emission maybe is not completely suppressed).

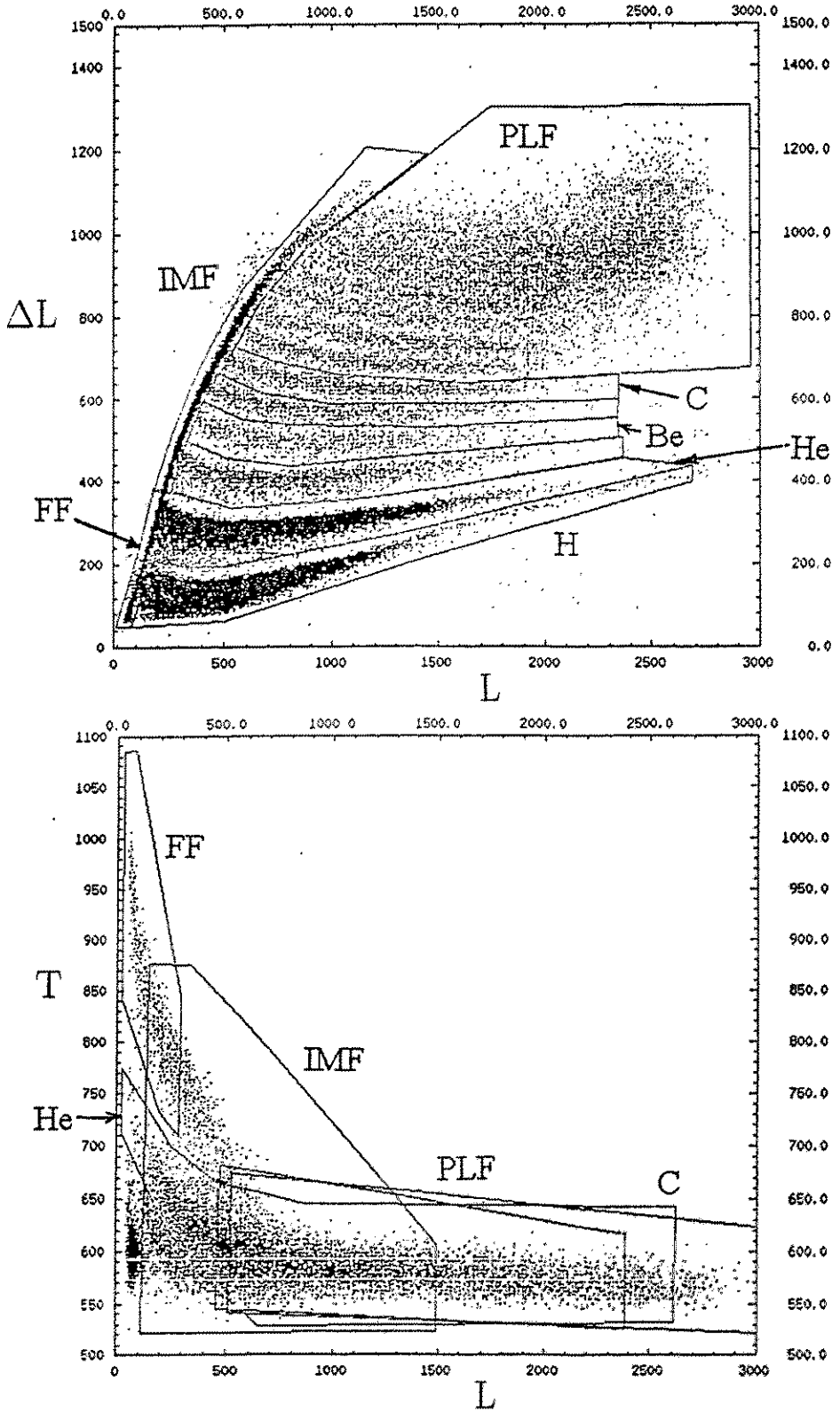

Fig.1. Particle separation by gates.

It is obvious to exploit the LCP multiplicity as a measure of excitation energy. In figure 3, the ratio of FF and IMF counts in the backward semiconductor is plotted versus the multiplicity of the high- and low-energy LCP's. The increase of this ratio with the high-energy LCP multiplicity reflects once again that fission becomes the more dominant compared to IMF emission the more excitation energy is carried away by fast forward-emitted particles. On the other hand, this ratio decreases with the low-energy LCP multiplicity growing with the excitation energy of the heavy (target-like) compound system. One sees how fission progressively cedes to IMF production with rising energy dissipation. The weak increase at multiplicities higher than 5 is probably due to imperfect discrimination against preequilibrium particles.

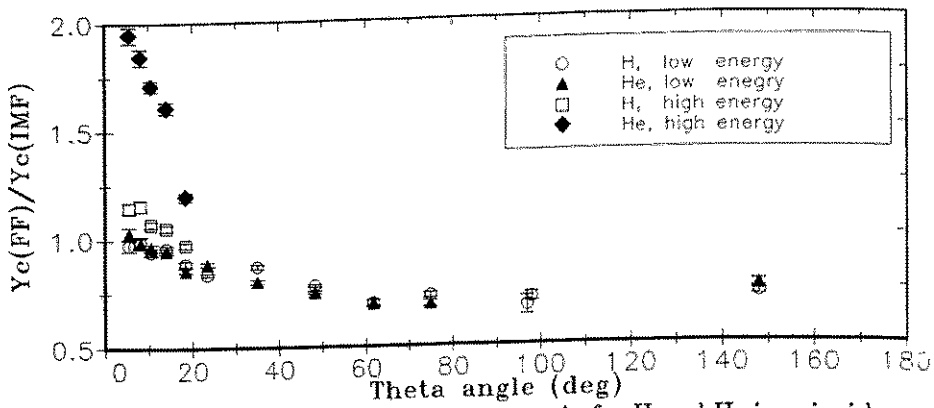

Fig.2. The angular distribution of the count ratio for H and He in coincidences with FF to those with IMF in the backward semiconductor detector.

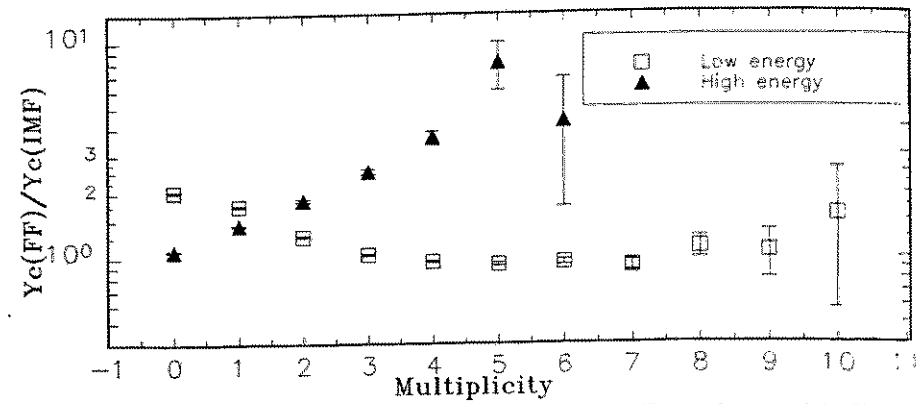

Fig.3. Counts ratio for LCP in coincidences with FF to those with IMF in backward semiconductor detector as function of LCP multiplicity.

These observations reveal anticipated features and make it possible to analyze the mechanism of reaction, in particular the IMF origin, by comparison with theoretical predictions planned as the next step of this work.

References

[1] Pausch G. et al., Annual Report 1992, HMI-B 507(1993)87

[2] Krueger J. et al., Annual Report 1993, HMI-B 520(1994)68

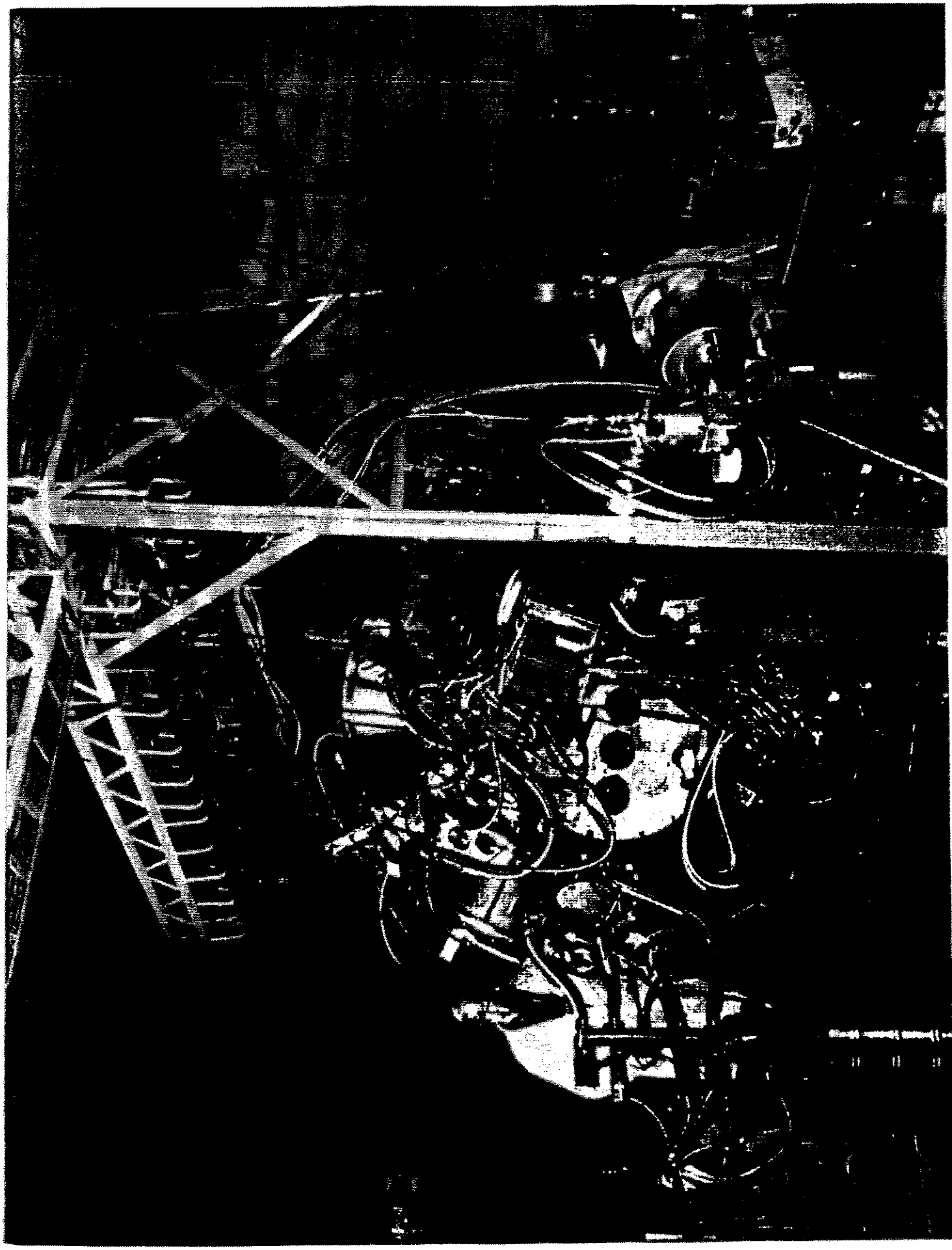

III. Experiment proposals for FOBOS

submitted to the Advisory Committee for Nuclear Physics
of the Joint Institute for Nuclear Research Dubna

November 1994

Proposals for the FOBOS 4π-Fragmentspectrometer

The FOBOS group at the Flerov Laboratory of Nuclear Reactions
Joint Institute for Nuclear Research Dubna

"Instability phenomena of nuclear matter in the Fermi energy domain"

Wolfgang Wagner and Hans-Georg Ortlepp
FZ Rossendorf e.V., Germany and FLNR JINR Dubna

Recent development in the field of investigation of heavy ion induced reactions at "low" intermediate energies (from $\approx$10 up to $\approx$100 AMeV) has been drawn several novel aspects. Since this energy region covers the Fermi energy domain it was expected that new phenomena should be observed connected with the transition from the mean field dominance for motion of nuclear matter to a "real" many body behaviour.
Considerable progress has been made in the dynamical description of nuclear reactions by BUU, QMD, FMD etc. theories. It became possible to simulate the evolution of a colliding system up to a stage where the hot nuclear matter breaks up into several fragments and to understand main features of this processes.
A variety of statistical fragmentation models are able to describe the experimental observations at the final phase of the collision. The dynamical approaches on the other hand consider the nucleon density and their moments in the phase space and include fluctuations which govern the behaviour of the hot nuclear system near its decay. Dynamical instabilities creating large fluctuations are believed to be responsible for the multiple decay mechanism and in general lead to much broader distributions of the experimental observables than in the case of low energy where the single particle motion can be considered as a small perturbation to the collective motion and the behaviour is more adiabatic.

With increasing energy the nuclear reaction looses its binary character and multiple decay channels become possible above the fragmentation threshold.
Shape instabilities responsible for the spontaneous neck rupture of a fissioning nucleus at low energy mix at higher energies with volume instabilities in such regions of the nuclear system where due to expansion or streching a zone of dilute nuclear matter is created and some condensation-like phenomenon takes place beeing a new source of intermediate mass fragments (IMF) and light charged particles (LCP).
A new fragmentation mechanism via intermediate exotic nuclear shapes such as bubbles or toroids has been predicted for certain internal conditions of the hot nucleus. An experimental proof of such phenomena could be of fundamental interest for further understanding of the equation of states of nuclear matter.

The design and buildup of multidetector arrays with different features was the logical consequence folowed up by many laboratories for the last decade to investigate multiple decay processes of hot nuclei.
As has been demonstrated in the first experiments provided at the new 4π-Fragmentspectrometer FOBOS this array is well established for registration and spectrometry of reaction products in a relative wide dynamical range of energy, mass and atomic number. The long flight path of 50 cm guarantees time-of-flight (TOF) measurements with high resolution ($\leq$1.5 ns/m). The gas detector modules have a rather low registration threshold for such devices (<0.5 AMeV) and are position sensitive. These properties allow a sensitive momentum analysis.
The granularities of the gas ball (30 Bragg ionization chambers with avalanche counters in front of them to register IMF and heavy fragments) and of the scintillator shell (210 CsI detectors to register more penetrating particles like LCP) as well as the total solid angle covered ($\approx$0.6 of 4π) have adventage for moderate multiplicities of reaction products as expected in the "low" intermediate energy region.
Therefore we believe that FOBOS should be an appropriate device for a programme of investigation given in the following proposals.

Dubna, October 12 1994

To the JINR Advisory Committee for Nuclear Physics (Dubna, Nov. 24 -25 1994)

Theme 04-5-0889-91/95: Synthesis and Investigation of the Properties of Exotic Nuclei and Nuclear Systems (Yu.E. Penionzhkevich, Yu.P. Gangrsky)

Project 2a: First experiments on FOBOS at the ion beam of U-400M (H.-G. Ortlepp)

Proposal of an experiment at U-400M in 1995

STUDY OF CLUSTER EMISSION IN NUCLEAR REACTIONS NEAR THE FERMI ENERGY

H.-G. Ortlepp, W. Wagner
Research Centre Rossendorf Inc. and FLNR JINR Dubna

1. Physical problem

The emission of intermediate mass fragments (IMF) is an important source of information about the interaction dynamics in heavy ion induced reactions. Especially for very asymmetric systems a competition between IMF emission accompanied with fission or the production of heavy residues has been observed. An exotic source of IMF is found to be the neck region of the separating nuclear system. New theoretical calculations have been provided for semiperipheral collisions of medium heavy nuclei. Evidence of a new reaction mechanism has been found connected with the development of large fluctuations in the overlapping nuclear zone what is assumed to be a novel IMF source

2. Status

Yields of IMF accompanied fission per binary fission have been determined in dependence on the linear momentum transfer for the reaction ^{7}Li + ^{232}Th at 43 AMeV. In the angular correlations there is some evidence of neck emission of IMF. A detailed investigation of this effect requires about two orders of magnitude larger statistics. The investigation of the reaction ^{14}N + ^{197}Au at 34 AMeV allows first evaluations oft he competition between fission and heavy residue production.

3. Proposal

It is planned to study the different sources of IMF emission using the reactions ^{14}N (34 and 55 AMeV) and ^{6}Li (50 AMeV) on ^{197}Au and ^{232}Th.
The following issues will be investigated:

- Yields of sequential IMF and neck IMF in dependence on E*
- N to Z ratio of IMF
- Dependence of IMF characteristics on the mass ratio of fission fragments
- Correlations between light charged particles and fission fragments
- proximity effects

Further calculations are in progress to search for neck instabilities in reactions like e.g. ^{40}Ar (≈40 AMeV) + Mo. They should lead to an increase of the variances of the observables such as mass, charge etc. of the fragments.

4. Experimental set-up

The experiments will be performed at the cyclotron U-400M equipped with an ECR source. The FOBOS spectrometer will be upgraded to ≥ 25 modules each consisting of a position sensitive avalanche counter, an axial ionization chamber and a mosaic of 7 CsI scintillation detectors.

5. Expected results

About 50000 ternary events will be recorded. This allows a detailed investigation of mass and angular correlations between IMF and fission fragments.

Proposal for the FOBOS 4π-Fragmentspectrometer
at the cyclotron U-400M with ECR ion source

Hans-Georg Ortlepp and Claus-Michael Herbach
Forschungszentrum Rossendorf e.V., Germany and FLNR JINR Dubna

"Study of neck emission of IMF in fission of hot nuclei"

1 The physical goal of the experiment

The investigation of neck emission of intermediate mass fragments (IMF) accompanied with fission has been started at FOBOS with the reaction ^{7}Li (43 AMeV) + ^{232}Th. Evidence of the effect reported earlier by Fields et al. /1/ has been found and the relative yield of ternary decays per binary fission has been determined for different folding angle bins /2/. A detailed investigation of the relation between binary fission events and ternary events with accompanied IMF emission, however, requires about two orders of magnitude more statistics.

Especially the dependence of this effect on the fission fragment mass ratio (as proposed by D. Hilscher, HMI Berlin) should give new insights into the process of formation and rupture of the neck.

With the proposed experiment at FOBOS we want to study in detail the neck emission of IMF in fission using the reaction ^{4}He (100 AMeV) or ^{6}Li (50 AMeV) + ^{232}Th.

The following questions will be investigated :

1. Yields of neck IMF and "usual" sequential IMF up to $\approx$300 MeV excitation energy of the compound nucleus.
2. N to Z ratio of neck IMF compared with sequential IMF.
3. Dependence of IMF characteristics on the mass ratio of fission fragments (FF).
4. Light charged particle (LCP)-FF correlations (multisource fits).
5. Other proximity effects than the known Coulomb focusing of fragments emitted from the neck region which should contain information about time scales. Such effects should cause futher structures in the angular correlations between IMF and FF.

2 The experimental setup

The experiment will be performed at the cyclotron U-400M equipped with an ECR ion source. The FOBOS spectrometer should be upgraded to $\geq$25

moduls each consisting of a position sensitive avalanche counter (PSAC), a Bragg ionization chamber (BIC) and a mosaic of 7 CsI scintillation detectors.
In our first experiment (^{7}Li + ^{232}Th) ≈100 ternary events have been recorded per day with a beam duty cycle of 0.1 . This rate can be increased by a factor of ≈10 using a continuous beam. Another factor of ≈5 is gained if the time structure of the beam allows to operate FOBOS without use of time reference detectors and, consequently, with larger number of modules (25 instead of 12 in our first experiment).

In general ≈50 000 ternary events are expected during a beam time of 250 hours. Such statistics allows a detaliled reconstruction of the angular correlation between FF and IMF.

3 Beam characteristics

The beam characteristics demanded are the following:

- ^{4}He (100 AMeV) or ^{6}Li (50 AMeV), ≈5 nA(el)
- Continuous beam with a width of the microbunches of ≤1 ns
- Beam spot of diameter ≤3 mm

One needs about 50 hours for the detector adjustment under beam conditions and 250 hours for data acquisition. Therefore a beam time of two weeks is demanded.

4 Coauthors

D. Hilscher, Hahn-Meitner Institut, Berlin, Germany
G. Pausch, Forschungszentrum Rossendorf e.V., Germany
P. Gippner, Forschungszentrum Rossendorf e.V., Germany
W. Wagner, Forschungszentrum Rossendorf e.V., Germany
A. Matthies, Forschungszentrum Rossendorf e.V., Germany
K.-D. Schilling, Forschungszentrum Rossendorf e.V., Germany

5 References

/1/ D.E. Fields et al., Phys. Rev. Lett. 69 (1992) 3713

/2/ A.A. Aleksandrov et al., Proc. Fiths Int. Conf. on Nucleus Nucleus Collisions, Taormina, Italy, 1994 (to be published in Nucl. Phys.)

Proposal for the FOBOS 4π-Fragmentspectrometer
at the cyclotron U-400M with an ECR ion source

Hans-Georg Ortlepp and Peter Gippner
Forschungszentrum Rossendorf e.V., Germany and FLNR JINR Dubna

"Competition between evaporation residue production and fission in asymmetric colliding systems at excitation energies up to 500 MeV"

1 The physical goal of the experiment

During the last years it has been well established that the fission probability of heavy nuclei drops down if the excitation energy exceeds several hundred MeV, e.g. /1/. This suppression can be explained by the appearance of evaporation cascades which are much faster than the relatively slow fission process. This leads to lighter nuclei which appear as evaporation residues (ER) and do no longer fission.

It is one of the results of the last FOBOS experiment (^{14}N (34 AMeV) + ^{197}Au) that events with sideward emitted intermediate mass fragments (IMF) had been selected. Due to the recoil of these IMFs the remaining heavy system is kicked out of its very forward direction into one of the forward positioned ($\theta \geq 19°$) FOBOS moduls. And indeed, in the respective spectra slow heavy products had been recorded in coincidence with IMFs.

In coincidence with these IMFs also a group of fragments with lighter masses had been observed (fig.1). It is kinematically consistent with fission products from the upper mentioned heavy system. This demonstrates that the FOBOS detector is able to measure the competition between fission and the formation of ER directly.

A new experiment is proposed to study this competition in dependence on the linear momentum transfer (LMT) in the reactions ^{14}N (34 AMeV, 55 AMeV) + ^{197}Au. The LMT which is according to the massive transfer model a good measure of the primary excitation energy of the compound system, can be determined from the sum of momenta of two (IMF+ER) or three (IMF+FF+FF) detected reaction products corrected for the emission of light particles. With increase of LMT a drop of the fission probability is expected as well as a rising yield and higher mean energy of evaporated light charged particles (LCP).

2 The experimental setup

The experiment should be performed at the U-400M cyclotron completed with an ECR ion source. The FOBOS array should be equipped with $\geq$25 moduls each consisting of a position sensitive avalanche counter (PSAC), a Bragg ionization chamber (BIC) and a mosaic of 7 CsI scintillation counters.

The main advantage of FOBOS is the possibility of independent momentum determination for heavy products what enables the total momentum balance mentioned above. Spectra of evaporated LCP should be recorded by the FOBOS scintillator shell in coincidence with FF or ER.

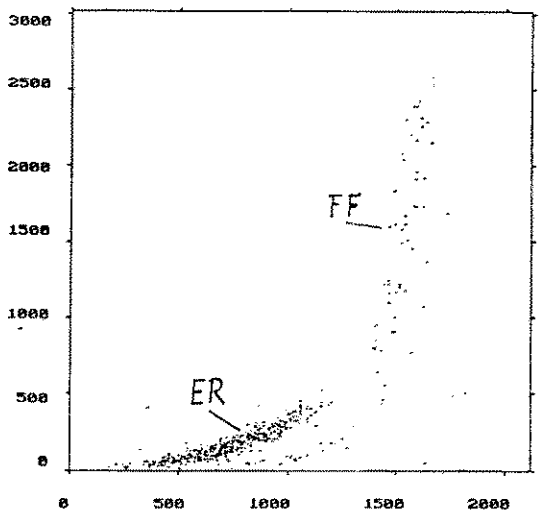

Fig.1:

Energy versus time-of-flight plot of a FOBOS forward module showing ER and FF events (TOF goes from channel 1900 backwards)

3 Beam conditions

The demanded beam characteristics are:
- ^{14}N (34 AMeV and 55 AMeV)
- 5 nA(el) continuous beam
- microbunch width $\leq$1 ns
- beam spot of diameter $\leq$3 mm on the target

The proposed beam time is 3 weeks; one week for beam tuning, detector calibration and adjustment under beam conditions and one week for data acquisition at the two projectile energies respectively.

4 Coauthors

G. Pausch, Forschungszentrum Rossendorf e.V., Germany
C.-M. Herbach, Forschungszentrum Rossendorf e.V., Germany
A. Matthies, Forschungszentrum Rossendorf e.V., Germany
K.-D. Schilling, Forschungszentrum Rossendorf e.V., Germany
W. Wagner, Forschungszentrum Rossendorf e.V., Germany
D.V. Kamanin, FLNR JINR Dubna

5 References

/1/ E. Schwinn et al., Nucl. Phys. A568 (1994) 169

Proposal for the FOBOS 4π-Fragmentspectrometer at the cyclotron U-400M with an ECR ion source

Guntram Pausch
Forschungszentrum Rossendorf e.V., Germany

"Study of the asymmetric binary decay of hot nuclear systems"

1 The physical goal of the experiment

The understanding of the emission mechanism of intermediate mass fragments (IMF) from highly excited nuclear systems is one of the keys to understand the properties of nuclear matter. Usually, IMF emission at excitation energies below the multifragmentation threshold is explained as an evaporation of heavy clusters. On the other hand, evidence has been found for deep-inelastic collisions with complete energy damping even for projectiles in the Fermi energy region /1/. Recent experiments with the ARGUS detector /2/ and with the FOBOS array showed a smooth transition from light IMFs up to fission fragments considering the emission propability as well as the energy spectra peaked near Coulomb energies (fig. 1). Furthermore, for a considerable part of these IMFs heavy partners have been identified in recent FOBOS experiments (fig.2). This would suggest to interpret the IMF emission as a very asymmetric nuclear fission process.

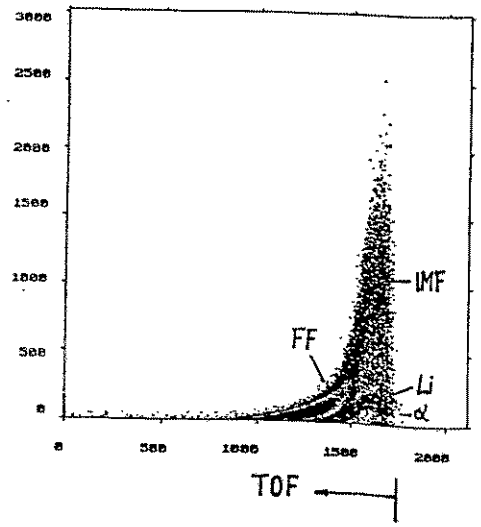

Fig.1: E vs. TOF plot of one FOBOS module at $\theta = 101°$

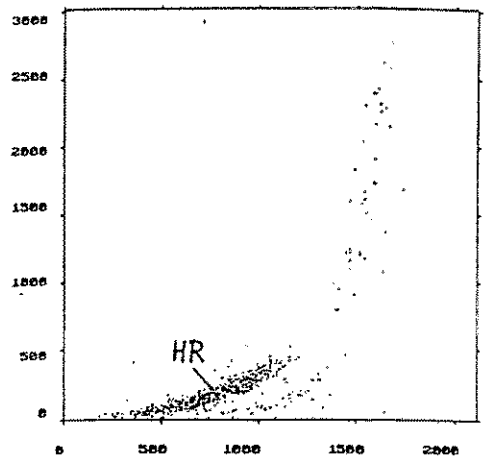

Fig.2: Coincident heavy partners (HR) of IMF shown in Fig.1 registered at $\theta = -37°$ (E vs. TOF)

A new experiment at FOBOS is proposed to study this asymmetric splitting in detail and with sufficient statistics. The reactions ^{14}N (34 AMeV) + ^{197}Au and ^{22}Ne (23 AMeV) + ^{197}Au should allow to investigate the following questions:

1. The TKE distributions for certain mass-splits should be compared with predictions assuming either evaporation or fission. The capability of FOBOS to measure the two masses and also the center-of-mass velocity of the fissioning system allows a TKE determination independent of the preceeding reaction stages.

2. A comparison of the IMF characteristics (charge distribution, emission energy) in both reactions characterized by comparable excitation energies at full linear momentum transfer but for different mass asymmetries should allow to find out, whether the binary partners in the exit channel remember the first reaction stage or not.

3. A distinction between binary decays of compound-like systems and deep inelastic collisions should be possible utilizing the different angular distributions of the outcoming particles.

4. Correlations of light charged particles (LCP) detected in the FOBOS scintillator shell in coincidence with the binary reaction products should give information about reaction times and angular momenta applying a multiple-source fit.

2 The experimental setup

The experiment should be done at the cyclotron U-400M upgraded by an ECR ion source. The FOBOS detector should be equipped with 25 moduls each consisting of a position sensitive avalanche counter (PSAC), a Bragg ionization chamber (BIC) and a mosaic of 7 CsI scintillation detectors.

3 The beam characteristics

The demanded beam characteristics are:

- ^{14}N (34 AMeV) and ^{22}Ne (23 AMeV)
- 5 nA(el) continuous beam
- microbunch widths $\leq$1 ns
- beam spot diameter of $\leq$3 mm at target position

The requested beam time is 3 weeks, one week for detector adjustment and calibration measurements under beam conditions and two weeks for data acquisition with the ^{15}N and ^{22}Ne beams respectively.

4 Coauthors

H. Oeschler, Technische Hochschule Darmstadt, Germany
J. Krueger, Forschungszentrum Rossendorf e.V., Germany
H.-G. Ortlepp, Forschungszentrum Rossendorf e.V., Germany
C.-M. Herbach, Forschungszentrum Rossendorf e.V., Germany
W. Wagner, Forschungszentrum Rossendorf e.V., Germany
D.V. Kamanin, FLNR JINR Dubna

5 References

/1/ H. Oeschler at al, PR 49(1994)1214.

/2/ J.Krueger et al., Annual Report 1993, Institute of Nuclear and Hadron Physics, Forschungszentrum Rossendorf e.V., Germany

Proposal for the FOBOS 4π-Fragmentspectrometer
at the cyclotron U-400M with ECR ion source

Wolfgang Wagner
Forschungszentrum Rossendorf e.V., Germany and FLNR JINR Dubna
Massimo Di Toro
LNS and University of Catania, Italy

"Investigation of instability phenomena in the neck region of breaking hot nuclei near Fermi energy"

1 Physical goal of the experiment

Theoretical studies of the behaviour of the nuclear overlapping zone in semiperipheral heavy ion collisions at intermediate energies show a novel reaction mechanism /1/. For a selected beam energy range (between 40 and 70 AMeV) the onset of dynamical fluctuations has been observed what can give rise to emission of intermediate mass fragments (IMF) from the neck region of the breaking nuclear system (fig.1). The physical background of this effect, calculated for the slightly asymmetric reaction ^{60}Ni + ^{90}Zr using a Bolzmann-Nordheim-Vlasov (BNV) code, is believed to be the development of volume instabilities in the neck region coupled to the shape instabilities already present at lower energies (e.g. in deep inelastic collisions). If the reaction time allows the development of dynamical fluctuations in the neck region what mainly depends on the beam energy and the impact parameter an increase of the variances of observables such as mass, charge, velocity etc. of the fragments is expected. First experimental evidence for this effect already has been reported /2/.

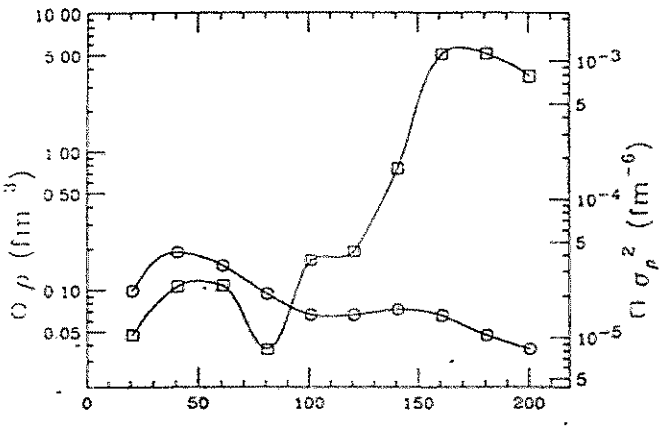

Fig. 1 Time evolution of the mean density ρ (circles) and the density variance σ_ρ (squares) in a sphere of radius 3 fm around the centre of mass for the reaction Ni + Zr at 40 AMeV (from ref. /1/).

The aim of the proposal is to investigate distributions of fragments for triple events with one fragment emitted from the neck region.
Further calculations for more asymmetric systems like e.g. ^{40}Ar + Mo to optimize the required beam energy will be performed.

2 Experimental observations

The FOBOS 4π-Fragmentspectrometer has excellent performance for spectrometry of IMF from neck emmission. Such fragments are focused by the Coulomb fields of the target (TLF) and projectile-like (PLF) fragments into a cone under $\approx 90^{\circ}$ relative to the TLF-PLF-axis.

Similar experimental problems have been solved in one of the last experiments at FOBOS (^{7}Li + ^{232}Th) where evidence of neck emission has been found from ternary fission of hot nuclei /3/.

To select the respective region of impact parameters the correlation between the linear momentum transfer (LMT) and the evaporated light charged particles (LCP) into the backward hemisphere can be used (FOBOS scintillator shell). Forward directed PLF from more peripheral collisions can be registered by the FOBOS forward array.

3 Reaction and beam conditions

- ^{40}Ar ($\approx$40 AMeV) on Mo or Ag target
- Beam current 2-5 nA(el)
- Microbunch width $\approx$1 ns
- Beam time requested $\approx$300 h

4 Coauthors

M. Colonna, LNS Catania, Italy H.-G. Ortlepp, Forschungszentrum Rossendorf e.V., Germany

5 References

/1/ M. Colonna et al., Report GANIL P 94 09, 1994

/2/ W.U. Schroeder, Proc. Int. School-Seminar on Heavy Ion Physics, Dubna, 1993, Vol. 2, p. 166

/3/ A.A. Aleksandrov et al., Proc. Fifth Int. Conf. on Nucleus Nucleus Collisions, Taormina, Italy, 1994 (to be published in Nucl. Phys.)

Proposal for the FOBOS 4π-Fragmentspectrometer
at the cyclotron U-400M with ECR ion source

Wolfgang Wagner and Hans-Georg Ortlepp
Forschungszentrum Rossendorf e.V., Germany and FLNR JINR Dubna
Ed Norbeck
Iowa State University, USA

"Search for formation and decay of exotic (bubble or toroidal) shapes of hot nuclei"

1 Physical goal of the experiment

Recent calculations using BUU transport theory predict for special conditions of heavy ion reactions a surprising phenomenon /1/. In central collisions between nearly equal-mass heavy ions at intermediate beam energies ($\approx$50 AMeV) the hot nuclear matter can form a bubble or toroidal nucleus (fig. 1). Main steps of such an scenario are the compression of the participant matter in the initial stage of the reaction up to 1.3-1.5 of normal density ρ_o, heating and expansion of the system, thermalization and decay. Bubbles also have been seen in BUU simulations of relativistic α-particles hitting a gold nucleus /2/. Here the compression step is absent.

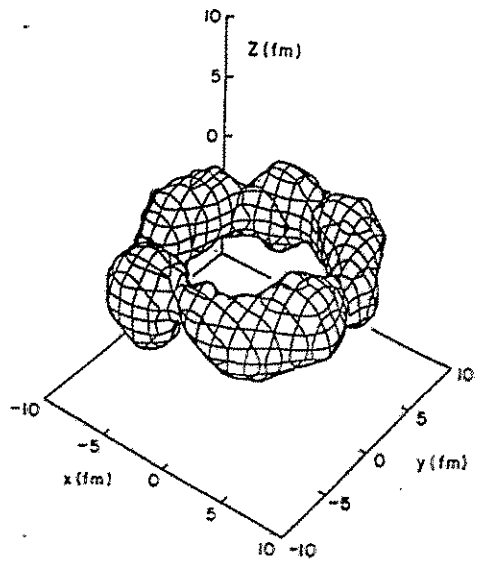

Fig. 1 Surface of constant nucleon number density ρ(x,y,z)=0.3ρ_o for a central ^{93}Nb (60 AMeV) + ^{93}Nb collision at time t=160 fm/c (from ref. /1/)

Several models have been developed to explain the fragmentation of hot nuclei /3,4,5,6/. In the case of central collision the system expands radially.

If a delicate balance between expansion and nuclear binding energy holds the evolution of the system can lead to formation of a dilute central region of lower density ($\approx$ one half of normal). Within times of t $\approx$130 fm/c the system can develop to a bubble or torus of nuclear matter. Later, due to dynamical instabilities, it should break into several IMF. Another possible mechanism is the creation of a spinning ring out of a dinuclear system at larger impact parameters.

The aim of the proposal is to search for signatures of such processes analysing events with several IMFs. BUU calculations presently under progress suggest that bubbles or rings may also be produced if a nucleus in the region ^{14}N..^{20}Ne (50-80 AMeV) hits a heavy one (Ag..Au).

Since the initial compression depends on the parameters of the equation of states (EOS) the observation of such phenomena could give new information about nuclear matter properties.

2 Experimental observations

The signature of a bubble should be a nearly equal, low, Coulomb energy for all the fragments. It is the same for a static ring except that, refered to the center of mass the event is coplanar, perpendicular to the beam axis. For a spinning ring all fragments should be coplanar in a plane containing the beam axis and should have equal velocities in the center of mass system. In the case of volume break-up there are fragments from the central region with very little center-of-mass velocities. These should be absent for rings or bubbles because the central region is empty.

Three facts make the FOBOS array ideally suited for such investigations. First, the velocity distributions in the center of mass system of the break-up products have to be reconstructed to search for the expected lowered overall Coulomb energy and absence of very small velocities. Here the low registration threshold (<0.5 AMeV) and the capability of determination of the center-of-mass system from the measured fragment quantities are essential. Only events with sufficient sum mass should be analysed to be sure that no massive fragment has been lost. Second, a high coordinate resolution as provided by FOBOS is needed for the reconstruction of the expected coplanar multiple decay. Third, the Z determination provided by the FOBOS chambers allows to determine the charge sum of all fragments and therefore to estimate Coulomb energies.

For the selection of central collisions the multiplicity of light charged particles (LCP) registrated by the FOBOS scintillator shell at angles $\theta \geq 50^\circ$ and the FOBOS forward array at angles $\theta \leq 26^\circ$ can be used.

Acceptance simulations and trajectory calculations to account for the respective geometrical measurement conditions are in progress. Furthermore extended BUU calculations have been started to optimize the choice of the reaction to investigate.

3 Reaction and beam conditions

-^{14}N or ^{20}Ne (50-80 AMeV) on a heavy target.
-Beam current 2-5 nA(el)
-Microbunch width $\approx$1 ns
-Beam time in the order of 300-500 h

4 Coauthors

W. Bauer, Michigan State University, USA
C.-M. Herbach, Forschungszentrum Rossendorf e.V., Germany

5 References

/1/ W. Bauer et al., Phys. Rev. Lett. 69 (1992) 1888

/2/ E. Norbeck et al., Proc. of the 9th High Energy Heavy Ion Study. Lawrwnce Berkeley Laboratory (1993) LBL-35984. p.102.

/3/ W.A. Friedman and W.G. Lynch. Phys. Rev. C28 (1983) 16 and Phys. Rev. C28 (1983) 950

/4/ J.P. Bondorf, Nucl.Phys. A387 (1982) 25c

/5/ J. Randrup and S.E. Koonin, Nucl. Phys. A356 (1981) 223

/6/ D.H.E. Gross et al., Z. Phys. A309 (1982) 41

EXPERIMENTAL STUDY OF FISSION REACTION CHARACTERISTICS USING A ^{6}He BEAM

Yu. E. Penionzhkevich, S.V. Stepantsov

The neutron halo of the nucleus is one of the central issues of nuclear structure. Lately also the problem of the existence of a neutron skin in neutron-rich nuclei is being discussed [1]. It is only recently that the neutron skin for radioactive neutron rich nuclei such as ^{6}He and ^{8}He gas been seen experimentally [2]. For ^{6}He radioactive nuclei an interplay appears between the skin and neutron halo effects at energies around the Coulomb barrier. The neutron skin is expected to have a prominent effect on nuclear reactions, for instance, on fusion reactions. The neutrons in the skin are expected to have more mobility than neutrons in normal nuclei, because:

1. a more gradual potential near the surface yields less reflection of incoming waves;

2. the mean free path of the neutron can be longer due to lower density.

In [3] fusion-fission cross sections have been measured for the ^{6}He-^{209}Bi reaction. The ^{6}He beam was produced at FLNR using the primary ion beams of ^{7}Li (35 MeV) of the U-400M cyclotron. One proton stripping from the ^{7}Li ions on a 1.1 mm carbon or hydrogen target was used. The intensity of ^{6}He was about 10^{4} pps for $2\cdot10^{11}$ pps of ^{7}Li ions. The secondary beam purity was up to 96% due to a so called form degrader (1.6 mm Al) positioned between the dipole magnets at an angle of 25° with respect to the beam direction (Fig. 1).

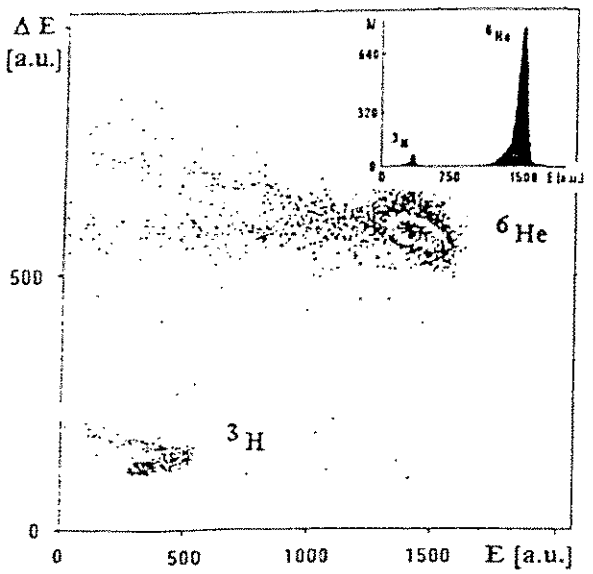

Fig.1. Secondary beam purity of U-400M.

The excitation function for the fission cross section from the ^{6}He + ^{209}Bi reaction is presented in [3]. It was shown that the fission cross section using a ^{6}He beam with an

energy close to the Coulomb barrier is higher than for ^{4}He-ion induced fission. It is most likely that this is connected with the neutron skin of the ^{6}He nuclei. If this is so, any further investigation of the fission process induced by exotic nuclei needs a more detailed measurement of all reaction characteristics - fission fragment angular correlation in the case of complete fusion, fragment angular anisotropy for studying the angular momentum influence on the fission process, fragment mass and energy distributions. Keeping in mind the low intensity of the exotic beams (up to 10^{6} pps), 4π-arrays are necessary. Such a 4π-detector is the FOBOS setup.

We propose to use this setup to investigate the fission characteristics of heavy nuclei, such as ^{232}Th, ^{238}U, using ^{6}He-, ^{8}He-beams. In this case, the beamline leading the primary beam to the FOBOS setup can be used as a separator forming the light radioactive nuclei into a beam. Schematically this beamline is presented in Fig. 2.

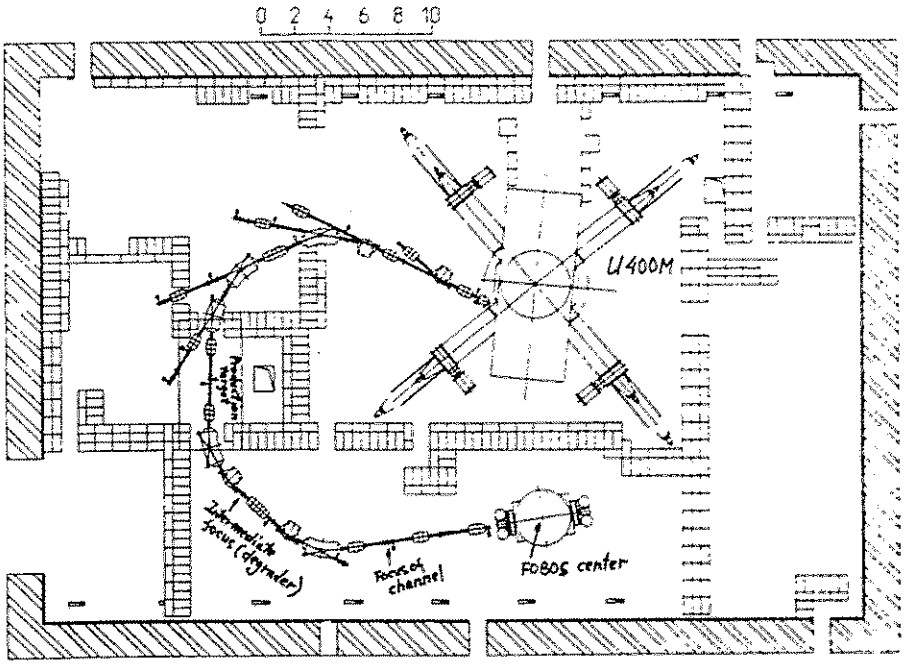

The RIB created in the production target [1] in the primary beam fragmentation reaction is captured by the first doublet of magnetic quadrupole lenses and focused by them onto an intermediate focal plane [2]. The first two dipole magnets produce the space dispersion of the beam in accord with the RIB momentum. In this plane the beam is transported according to the mass per ionic charge (A/q) selection rule (In our case the ionic charge (q) is equal to the nuclear charge (Z) for most not too heavy ions at the energies involved). This place is also suitable for installing a so called energy degrader. Properly profiled the latter gives an opportunity either to monochromatize or to conserve the momentum spread of the RIB ions. In both cases due to the different energy losses of the ions, (these being proportional to the squared charge of the ion) a further purification of the RIB in A and Z will take place.

After passing the intermediate focal plane the momentum dispersion is compensated again down to zero by means of the triplet of quadrupole lenses and the next

Table 1.
Main ion-optical parameters of the FOBOS channel.

Ion source slit size	10x4 mm^2
Solid angle	0.3 msr
Magnetic rigidity	0.15-3.2 Txm
Momentum acceptance:	
-achromatic mode	$2x10^{-2}$
-monokinatic mode	$8x10^{-3}$
Energy resolution:	
-monokinatic mode	$1x10^{-3}$
Beam size at FOBOS target:	
-achromatic mode	15x10 mm^2
-monokinatic mode	40x10 mm^2

two dipole magnets. Then the beam is focused by the second doublet of quadrupoles onto a dispersionless focal plane [3]. The image of the production target in this plane serves as a source for the two last doublets of quadrupoles realizing the focusing of the beam onto the center of the FOBOS spectrometer.

In Table 1 some quantitative results of evaluation of the ion-optical characteristics of the given fragment separator are listed. The beam half-envelopes in both transverse directions along the central path of the facility tuned in an achromatic mode are presented in Fig. 3.

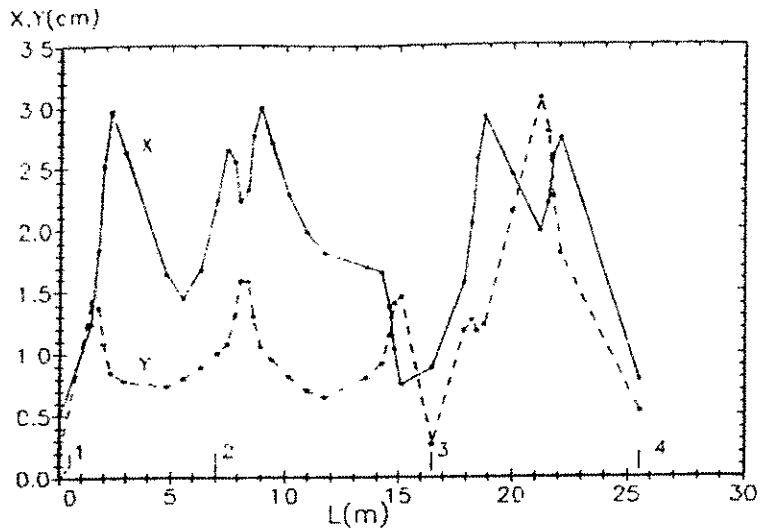

Fig. 3. Transverse beam half-widths (X,Y) along the longitudinal axis (L).

Table 2.

Reaction	RIB	t_{opt} (mg/cm^2)	Bρ (Txm)	E/A (Mev/u)	Transmission (%)	Yield (pps/p$_\mu$A)
^{18}O+Be (56 MeV/u)	$^{16}C^{6+}$	460	2.51	42	1.56	4.2×10^{7}
	$^{14}O^{8+}$	400	1.58	39	0.54	4.7×10^{6}
	$^{6}He^{2+}$	550	2.88	43	0.04	3.6×10^{5}
	$^{8}He^{2+}$	530	3.86	44	0.06	3.4×10^{4}
	$^{9}Li^{3+}$	530	2.87	43	0.09	1.8×10^{5}
	$^{11}Li^{3+}$	500	3.56	44	0.17	6.0×10^{2}
	$^{14}Be^{4+}$	400	3.47	46	0.44	1.1×10^{2}
^{9}Be(^{1}H,2n) (56 MeV/u)	$^{8}B^{5+}$	17 (10^{22}at./cm^2)	1.73	55	1.13	3.5×10^{7}
^{7}Li(^{1}H,n) (45 MeV/u)	$^{7}Be^{4+}$	17	1.69	44	0.52	1.6×10^{7}
^{7}Li(^{1}H,2p) (45 MeV/u)	$^{6}He^{2+}$	17	2.91	44	0.35	1.1×10^{7}
^{11}B(^{1}H,3p) (50 MeV/u)	$^{9}Li^{3+}$	17	3.07	49	0.56	1.8×10^{6}
^{15}N(^{1}H,2n) (56 MeV/u)	$^{14}O^{8+}$	17	1.88	54	5.44	1.7×10^{6}
^{18}O(^{1}H,3p) (56 MeV/u)	$^{16}C^{6+}$	17	2.88	55	3.33	1.0×10^{7}

One can see from Table 2 that the intensity of the ^{6}He-beam can reach 10^{7} pps. Taking into account the solid angle of the system and the value of the transmission coefficient it is expected to get up to 10^{5} ^{6}He nuclei on the FOBOS target. This intensity would allow within 100 hours of beamtime to register about 10^{6} events for the determination of the characteristics of the fission fragments obtained in the ^{6}He-induced fission of heavy nuclei such as ^{209}Bi, ^{238}U and ^{244}Cm.

REFERENCES

1. I. Tanihata et al. Phys. Lett. B289, 261 (1992).
2. Yu. Penionzhkevich. Particles and Nuclei, v. 25(4), 930(1994).
3. A.S. Fomichev et al. JINR Rapid Communications, N4-94 (1994).

Proposal for the FOBOS 4π-Fragmentspectrometer
at the cyclotron U-400M with ECR ion source

Edwin Norbeck
University of Iowa, USA.

"The Direct Reaction $^{24}Mg+^{24}Mg \Rightarrow 3^{16}O$"

1 What are direct reactions?

The direct reaction model calculates the final state of the reaction by means of a matrix element between the initial state and the final state of a simple (usually a delta function) potential between clusters in the beam and the target. The model predicts the complete final state. For the 3 oxygen final state it gives the cross section for all possible points in the 9-dimensional momentum space. This is at the opposite pole from the better known microscopic calculations that follow the reaction through many microscopic steps and end up with predictions for varous inclusive quantities.

2 The reaction to be studied.

The reaction to be studied is $^{24}Mg+^{24}Mg \Rightarrow 3^{16}O$, Q = -13.656 MeV and $4^{12}C$, Q = -27.868 MeV. The cross sections are particularly large when the maximum number of clusters are spectators for which the momentum does not change during the reaction. This leads to sharp peaks in the multi-dimensional phase space that can be easily seen even if the overall cross-section is small. In the $3^{16}O$ case, if an ^{16}O in the target is a spectator, the final state is the same as for slightly inelastic (because of the negative Q value) scattering of $^{16}O+^{16}O$. In the symmetric case the two ^{16}O appear on opposite sides of the beam at an angle between 40 and 45 degrees, with respect to the beam. These two ^{16}O share all of the available energy. If an ^{16}O cluster in the beam is the spectator, the two active ^{16}O share one third of the beam energy, less the 13.7 MeV from the negative Q value. They also share one third of the beam momentum. In the symmetric case the two active ^{16}O appear on opposite sides of the beam at an angle between 55 and 60 degrees. For the $4^{12}C$ final state, the largest cross section occurs when one ^{12}C cluster in the beam and one in the target are spectators. In this case the two ^{12}C share half the beam energy, less 27.9 MeV, and half of the beam momentum. In the symmetic case the two active ^{12}C appear on opposite sides of the beam at an angle between 40 and 45 degrees. If only one ^{12}C cluster in the target is a spectator, the other three ^{12}C share all of the available energy and all of the momentum of the beam. If the only spectator is a ^{12}C in the beam, the three active ^{12}C share all of the energy and momentum not taken by the spectator.

3 Why use FOBOS?

The sharp angular correlations described above can only be demonstrated with an array such as FOBOS that has excellent angular resolution. The two or three active participants need to be identified by Z and their energy measured accurately. In addition, as many other particles as possible that are produced by the beam should be detected and recorded. In the case where only two active ^{12}C are being studied there will be a background of other processes where the unobserved particles are something other than ^{12}C. To reduce this background, any event with particles other than ^{12}C should be discarded. For this purpose the rest of FOBOS serves as an anticoincidence device. For this the low energy threshold is valuable.

4 Why study direct reactions?

It is still a mystery why direct reactions occur at all. From the studies of ^{12}C+^{12}C$\Rightarrow$6^{4}He performed at MSU at beam energies from 660 to 1860 MeV it was found that, as the energy was increased, the cross section decreased but the direct reaction peaks were still there. The careful studies with FOBOS at two different beam energies should help answer some of these questions. The shape of the direct-reaction peaks is highly sensitive to the details of the bound state wave functions. These studies will provide detailed information about the cluster structure of ^{24}Mg. From earlier studies of the direct reaction, ^{2}6Li$\Rightarrow$3^{4}He, it was found that intermediate ^{8}Be states produced coherent interference with the direct reaction peaks. The new studies will provide additional information about such effects. Because of such interference, the direct peaks may not appear at the expected location, but they will still be sharp. Once the energies and angles have been accurately measured, they can serve as a source of calibrations for other detector arrays.

5 Experimental details.

The ^{24}Mg beam energies should be something like 30 and 50 MeV/A. 1.0 particle nA should be adequate. Several days will be required to get adequate statistics. The targets should be as thick as possible without damaging the energy resolution for carbon and oxygen reaction products. Oxygen in the target could provide a serious background. Separated ^{24}Mg metal targets should be used. After preparation in an inert atmosphere, the targets should be dipped into a dilute solution of Formvar to prevent oxidation when the targets are exposed to air. Such solutions are used by people who work with electron microscopes.

PROPOSAL FOR THE FOBOS 4π - FRAGMENTSPECTROMETER AT THE CYCLOTRON U-400M WITH ECR ION SOURCE

MULTIFRAGMENTATION OF MASSIVE FRAGMENTS FORMED IN TERNARY FISSION

V.L. Mikheev

FLNR, JINR, Dubna

1. PHYSICAL GOAL OF THE EXPERIMENT

One of the difficult problems in studying multifragmentation of nuclei is the determination of the real excitation energy.

In experiments performed with 1 GeV protons at Gatchina /1,2,3/ an unusual ternary fission process of ^{238}U has been observed. It has been established that ≈ 1% of fissions were events where two fission fragments were accompanied with more than 8 light charged particles which have a sum mass of ≈ 50 amu. As it follows from a kinematical analysis these particles were formed by the multifragmentation of an unstable third fragment.

In this experiment the fission fragments registered were collinear in the laboratory system. This means that the whole linear momentum of the projectile was transferred to some central part of the target nucleus. In such a case one can speak of a pure central collision with a full transfer of the linear momentum and kinetic energy of the projectile to the fragment formed in the central region of the fissioning nucleus.

Similar effects have been observed by the authors of ref. /4/ who irradiated ^{238}U with 11.5 GeV protons.

In nuclear reactions with heavy ions it was established that high energetic light charged particles emitted in forward directions are associated with central collisions, e.g . in the reaction ^{16}O (20 AMeV) + ^{238}U /5/. This effect can be the result of the action of the radial component of the dissipative force /6/. Hence, one can hope that in central collisions at increasing projectile energy due to the collective nuclear motion an interesting phenomenon of an excited central part and relatively cold fragments could be observed..

Accordingly, the goal of the proposed experiment is the study of multifragmentation of heavy nuclei such as U, Th, Au in ternary fission induced by light heavy ions (^{16}O, ^{20}Ne) with energies of ≈ 80 AMeV. The registration of the two fission fragments being spectators in this process allows to investigate the multifragmentation of the third fragment at well determined values of excitation energy.

2. FEATURES OF THE EXPERIMENT

It is necessary to register two fission fragments in coincidence with particles of atomic number $1 < Z < 10$ for multiplicities up to ≈ 10. The parameters Z, A, E, ϑ, and φ should be determined for every particle. Special attention must be paid to the registration of fission fragments with $\vartheta_1 + \vartheta_2 \approx 180^\circ$ in the laboratory system. One can expect that for reactions like (O; Ne) + (U;Th) at ≈ 80 AMeV all light particles will be focused in the forward hemisphere with $\vartheta < 30^\circ$ relative to the beam direction and that they will have maximum kinetic energy

at ≈ 20 AMeV. Therefore, the registration of the fission fragments has to be performed within an angular interval of $60^\circ < \vartheta < 120^\circ$ in the laboratory system. The 4π fragment spectrometer FOBOS is a well suited set-up for this experiment.

3. REACTION AND BEAM CONDITIONS

^{16}O or ^{20}Ne beam of energy 50 - 80 AMeV
^{232}Th , ^{238}U or ^{197}Au target
Beam intensity $\approx 10^9$ particles per second
Beam time requested ≈ 100 hours

4. CO-AUTHORS

FOBOS-Collaboration, FLNR JINR, Dubna
G.E. Solyakin, St.-Petersburg Institute of Nuclear Physics , Gatchina, Russia

REFERENCES

/1/ G.E. Solyakin, Preprint Nr. 1995, St.-Petersburg Institute of Nuclear Physics, Gatchina, 1994.
/2/ A.I. Obukhov et al., Letters to JETP, v. 57, Nr. 2, 1993, p.73.
/3/ A.A. Zhdanov et al., Letters to JETP, v. 54, Nr. 6, 1991, p.311.
/4/ B.D. Wilkins et al., Phys. Rev. Lett., v. 43, 1979, p.1080
/5/ B.B. Back et al., Phys. Rev. C22, 1980, p.1927.
/6/ D.H.E. Gross and J. Wilczynski, Phys. Lett., v. 67B, 1977, p.1.

PROPOSAL FOR THE FOBOS SPECTROMETER

COLD FRAGMENTATION IN SPONTANEOUS FISSION OF ^{250}Cf

Yu. V. Pyatkov

Moscow Physics Engineering Institute , Russia

1. Introduction

An efficient means of revealing new properties of nuclear matter is its investigation in extreme states of e.g. density, temperature, nucleon structure etc. One of such is realized in a specific fission mode, which has come to be known as cold fragmentation (CF).

In CF the reaction products are formed in a state close to their ground state, i.e. their excitation energy is considerably lower than the neutron binding energy B_n. In a very specific case there seems to appear really true cold fragmentation, namely, if the two fragments are in their ground state and the total reaction heat (Q) is released in the form of kinetic energy (TKE) only [1]. Since more compact scission configurations correspond to higher TKE values, CF, therefore, in this case is defined as *compact* CF.

The fine structures in the fragment mass distribution observed for TKE near the Q value are explained by the influence of shell and pairing effects. Recently, similar structures have been found for the opposite limit of low TKE, i.e. for the case of very large fragment deformations at scission [2,3]. It is assumed that this is *deformed* CF where all available energy has been transformed into deformation.

Data obtained for CF enable us to analyze a number of characteristics which are determined by the dynamics of large amplitude motion of nuclear matter. For example the correlation between the charged odd-even effect and the corresponding theoretical parameter in dependence on TKE is connected with the mechanism of energy dissipation during the descent from the saddle to the scission point, i.e. with nuclear viscosity. Viscosity, on the other hand, is a key parameter for planning of further experiments on the synthesis of superheavy nuclei because existing theoretical estimates are quite unreliable. In this context some fundamental universality of opposite processes, cold fusion and cold fission, is nicely manifested. In deformed CF the fragments achieve extreme deformation being at the same time cold. The comparison of experimental estimates of the deformation energy with corresponding theoretical values obtained from Hartree-Fock calculations with effective forces [4] give the possibility of testing nuclear models using features unavailable from other experiments.

Among general aspects mentioned above a specific problem of fission is still of interest [5]. This is the spontaneous fission of ^{258}Fm where CF with a sharp peaked mass distribution (FWHM ≈ 8 a.m.u.) is prevailing in contrast to the usual broad double-humped mass distributions (FWHM ≈ 50 a.m.u.). The effect, clearly seen in ^{258}Fm(sf), is quickly damped by little excitation even for nuclei with very similar structure. The problem is likely to be the complexity of single-particle effects yet misunderstood up to now [6].

2. Formulation of the problem

As it is evident from existing models [7,8], compact CF occurs closely to the initial stage of descent of the fissioning nucleus from the saddle point. There are theoretical specifications [9,10,11] of the origin of separate fission modes just at this stage. In view of that, compact CF products are something like spectators at this point, and their mass, energy and charge distributions provide information about the fission channels and the cluster degrees of freedom as well [11,12,13].

Hence, the main goal of this proposal is the investigation of the mechanism of formation and evolution of fission modes in low energy (spontaneous) fission of heavy nuclei.

3. Measurement methods

There are at least two alternative techniques of investigation. A first approach is to study plenty of spontaneous fissioning nuclides to create very different single-particle saddle point configurations with varying excitation energies. Conclusions about the CF mechanism then can be drawn from the systematics of corresponding parameters. This way partially still has been developed.

As has been mentioned above, ^{258}Fm(sf) is a limiting case in terms of CF probability because of the sharp mass and charge distributions of the fragments making it dropping out from the systematics. Therefore, it is hard to believe that considerable information can be obtained by systematics only. On the other hand, efforts should be directed to study nuclei in the neighborhood of ^{258}Fm, in particular along the chain of Cf isotopes differing from Fm by two charge units only.

Furthermore, a comparative investigation of CF in the reactions ^{249}Cf(n_{th},f) and ^{250}Cf(sf) should be informative because there the same nucleon configuration is realized, but at different excitation energy, and the initial conditions at the decent from the saddle are similar to that for ^{258}Fm. Data of CF always exist for the reaction ^{249}Cf(n_{th},f) [14].

4. Experimental realization of the proposal

The investigations proposed could be provided at the multi-detector array FOBOS realizing ≈10 % of the solid angle. About $5 \cdot 10^5$ fission events would be registered during a measurement time of 10 days when 50 μg of a mixture of ^{249}Cf and ^{250}Cf (1 % abundance of ^{250}Cf) are used as a source. Sophisticated measurement geometry and necessary calculations can be presented.

References

[1] F. Gönnenwein, Proc. Int. School-Seminar on Heavy Ion Physics, Dubna, USSR, 1987, p. 232.
[2] I.D. Alkhazov et al., Yadernaya Fizika 48 (1988) 655
[3] F. Gönnenwein, Proc. Int. Workshop on Dynamical Aspects of Nuclear Fission, Smolenice, CSFR, 1991.
[4] D. Vauthenin, Phys. Rev. C7 (1973) 296
[5] H.J. Lustig et al., Journ. of Phys. G: Nucl. Part. Phys., v. 6, 1980, p. 25L.
[6] F. Moeller et al., Nucl. Phys. A469 (1987) 1
[7] J.F. Berge et al., Nucl. Phys. A428 (1984) 23C
[8] F. Gönnenwein, "Voprosy Atomnoi Nauki i Techniki", vyp. 1, p. 14 (in Russian).
[9] R.V. Hasse, "Voprosy Atomnoi Nauki i Techniki", vyp. 1, p. 3 (in Russian).
[10] V. Brosa et al., Phys. Reports 197 (1990) 167
[11] A. Sandulescu et al., Journ. of Phys. G: Nucl. Part. Phys., v. 15, 1989, p. 1813.
[12] H.J. Fose and G.A. Jones, Nature 307 (1984) 245
[13] Yu.V. Pyatkov and R.A. Shekhmamet'ev, Proc. Int. School-Seminar on Heavy Ion Physics, Dubna, Russia, 1993, v. 1, p. 358.
[14] Yu.V. Pyatkov et al., JINR Rapid Communications 2[59]-93, Dubna, Russia, 1993, p. 98.

IV. Lectures given on the FOBOS workshop '94

Cracow, June 28 - 30 1994

(The contributions concerning the FOBOS set - up and the results of the first experiments are included into chapters I. and II.)

CHARACTERISTICS OF THE RADIOACTIVE ^{6}HE-BEAM PRODUCED AT THE CYCLOTRON U-400M USING THE PROTON PICK-UP REACTION ^{7}LI (35 AMeV) ON ^{12}C AND $(CH_2)_n$

A.S. Fomichev, I. David, S.M. Lukyanov, Yu.Ts. Oganessian, Yu.E. Penionzhkevich, N.K. Skobelev, N.I. Tarantin and O.B. Tarasov

Joint Institute for Nuclear Research, Dubna, Russia

Besides the well-known projectile fragmentation and the ISOL-method, reactions of the type (p,xn), (p,xp) or (α,xn) are suitable to produce radioactive nuclei (RN) near the drip-line with considerable cross-sections. Due to the kinematics of these reactions the products are peaked forward within a narrow solid angle and, therefore, can be collected and transported with a relative high efficiency. This idea has been realized using the (p,2p) reaction at the lay-out of the beam-transport system of the U-400M cyclotron in the FLNR at the JINR, Dubna (fig.1). Ordinary, this line is used for the transportation of the primary beam to the FOBOS set-up. This transport system could also be successfully used for the production and separation of a radioactive beam.

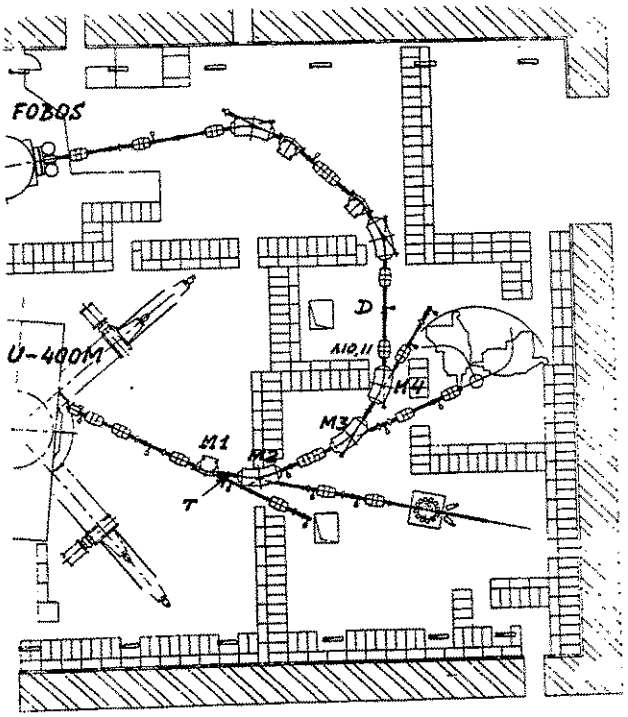

Fig.1 Lay-out of the beam-line system of the U-400M cyclotron.

The most favored position for the insertion of a degrader into the transport line is the beam-diagnostics block situated between the magnets *M3* and *M4*, where the maximum of dispersion was estimated. The calculations of the beam optics have been performed according to the code TRANSPORT [1]. The profile of the secondary beam was scanned using a position-sensitive avalanche counter at the point *D*. It has been found that 90% of the beam intensity are concentrated within these limits.

To produce RN and to estimate the general characteristics of the secondary beam the reaction ^{7}Li (35.5 AMeV) + $(CH_2)_n$ was chosen. A ^{6}He-beam is produced after pick-up of one proton from the projectile. Additionally, the reaction ^{7}Li + ^{12}C has been investigated because of the contents of carbon in the polypropylene target.

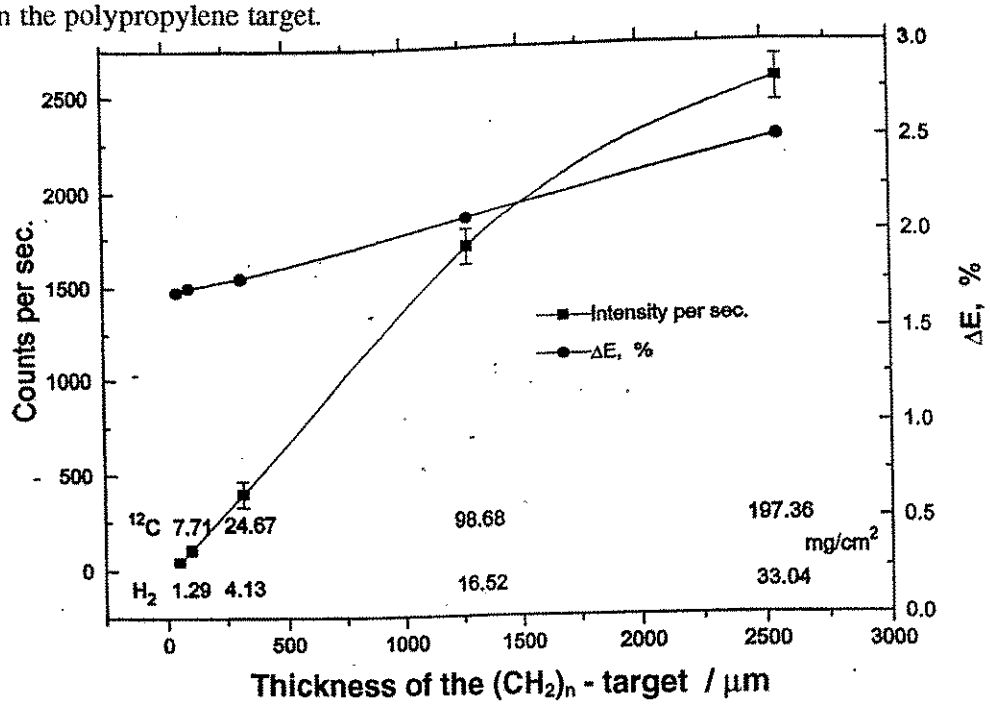

Fig.2 Characteristics of the radioactive ^{6}He beam produced in the proton pick-up reaction ^{7}Li (35 AMeV) + CH_2; Intensity - left axis, energy resolution - right axis.

The ^{6}He yield and the energy spread of the beam in dependence on the thickness of the production target is shown in fig.2. For the first run the primary beam current was 30 nA(e). A linear increase of the yield with target thickness has been observed up to 20 mg/cm^2. At larger target thickness there are losses due to absorption of secondary reaction products in the target layer. The energy spread of the ^{6}He beam is considerably greater at larger target thickness than, e.g., in the case of 50 μm.

One can conclude from our data that a pure hydrogen target of 20 mg/cm^2 thickness would be more optimal for the ^{6}He production than a ^{12}C target. In this case one expect an increase of the relative ^{6}He yield by a factor of 3 and an energy resolution of the secondary beam better than 2%.

With a probability of ≈50 % the ^{7}Li projectile breaks into an alpha particle and a triton. ^{3}H and ^{6}He have the same ratio A/Z=3. Hence, tritons create the main contamination in the secondary ^{6}He beam. The yield ratio between ^{3}H and ^{3}He is shown in fig.3a. The amount of ^{6}He in the secondary beam could be increased up to 96 % by the application of a special degrader (fig.3b). The degrader was a 1.6 mm thick Al sheet located in the beam-line under an angle of 30°. The difference in energy loss leads to different trajectories for ^{3}H- and ^{6}He-ions. A good purification of the secondary ^{6}He beam has been achieved by tuning the magnet *M4*.

The final ^{6}He energy is 180 MeV instead of 210 MeV without a degrader. Actually, the energy spread of about 3 % did not change. The ^{6}He beam intensity was lowered due to the degrader by a factor of two.

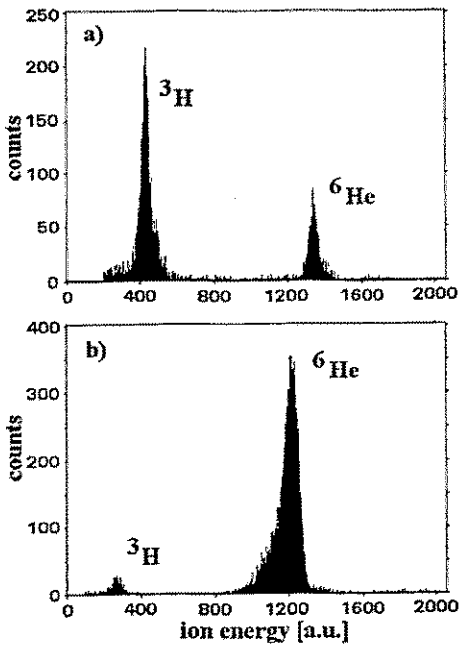

Fig.3 Quality of purification of the secondary ^{6}He beam by use of an Al degrader.

The RN beam was used for the investigation (by *off-line* methods) of ^{6}He-induced fission and evaporation reactions at a bismuth target [2]. The intensity of the purified ^{6}He beam was ≈3000 pps at a primary beam intensity of about $2 \cdot 10^{11}$ pps on the production target ^{12}C (1.1 mm thickness). Taking into account the modernization of the U-400M by installation of an ECR ion source and the manufacturing of a high-pressure hydrogen target, one can expect an essential augmenting of the secondary beam intensity up to 10^6 pps. This opens the real possibility of RN transportation to the FOBOS set-up to study RN-induced fission by *on-line* methods, like, e.g., in ref. [3].

References

[1] K.L. Brown et al., Preprint CERN 80-04, Geneva, Switzerland, 1980.
[2] A.S. Fomichev et al., JINR Rapid Communications N 4 (67), Dubna, Russia, 1994, p.21.
[3] J.L. Sida et al., Fifth Internat. Conf. on Nucleus-Nucleus Collisions, Taormina, Italy, 1994 (to be published in Nucl. Phys. A)

ON THE POSSIBILITY OF USING (HI,αf)-REACTIONS FOR FISSION INVESTIGATIONS

Kalpakchieva R., Muzychka Yu.A, Penionzhkevich Yu.E., Pustylnik B.I.
FLNR, JINR

During the last few years , the interest in studying the fission of weakly excited compound nuclei, produced in heavy ion-induced reactions, has increased. This is connected with the possibility to obtain information about structural effects in fission, fission barriers, fission modes etc. in a wide range of Z and N of the fissioning compound nuclei. Important information on the fission process has been obtained in reactions with light particles (n, p, α) , but only in the region of nuclei situated close to the valley of β-stability. The heavy ion complete fusion reactions essentially extend this region of nuclei, but, as the Coulomb barrier for the fusion is high, the excitation energy of the compound nuclei is more than $\sim$ 25-30 MeV. From this point of view incomplete fusion reactions in which the escape of an α-particle or a heavier nucleus precedes the formation of the compound nucleus are of interest. Such reactions, in principle, allow to produce nuclei with excitation energies as low as desired. The question is just in the probability of such a process. Moreover, these reactions have an advantage over complete fusion reactions in measuring the nuclear fissility, as in this case there is no need to calculate the compound nucleus production cross section with the help of any model, and the fissility is equal to : $P_f = \frac{N_{\alpha f}}{N_\alpha}$, where $N_{\alpha f}$ - is the number of registered coincidences of fission fragments with α-particles, and N_α - the total number of registered α-particles. We can use the given ratio, because, as it has been shown experimentally, the greater part of fast α-particles emitted in forward angles at ion energies near the interaction barrier (E $\sim$ 6-8 MeV/nucleon) is formed in binary reactions [1].

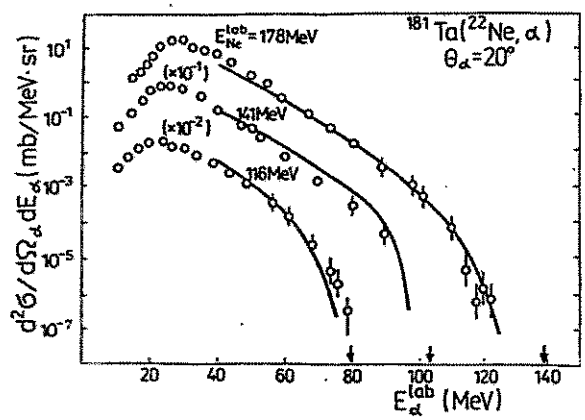

Fig.1 Energy spectra of α-particles measured in the reaction $^{181}Ta(^{22}Ne, \alpha)$ at an angle $\Theta_\alpha = 20°$ for three values of the bombarding energies, 116, 141 and 178 MeV.

The possibility of using incomplete fusion reactions can be illustrated by Fig.1, where energy spectra of α-particles measured in the reaction $^{181}Ta(^{22}Ne, \alpha)$ at an angle $\Theta_\alpha = 20°$ for three values of the bombarding energies, 116, 141 and 178 MeV, are shown [2]. The energies of α-particles corresponding to zero excitation energy of the residual nucleus are shown by arrows. It is seen that the cross section quickly decreases with increasing the α-particle energy. Thus, one should determine the value of the excitation energy up to which the measurement of nuclear fission cross sections is feasible. One should note that low cross

sections define the necessity of registering all fission fragments coinciding with α-particles, i.e. one should use a 4π- setup of the FOBOS-type. As it is evident from the experimental data that the angular distributions of fast α-particles have a sharp maximum at an angle of $\Theta_\alpha = 0°$ [2], then an annular detector situated at forward angles has to be applied. And, at last, it should be pointed out that as seen from the Figure, the higher the beam energy the lower the cross section for formation of the residual nuclei with a given excitation energy. Therefore, the beam energy should not be too high. To estimate it, let us consider the energy of a Ne- ion beam equal to 6 MeV/nucleon. The double differential cross section of α-particle emission at an angle $\Theta_\alpha = 20°$ with an energy corresponding to excitation energy of the residual nucleus E^*=20MeV is equal to (see Fig.1) :

$$\frac{d^2\sigma}{d\Omega_\alpha dE_\alpha} = 2.5*10^{-2}\frac{mb}{MeV*sr}$$

Thus, using a linear approximation for the angular distribution of fast α-particles at small angles it is easy to obtain a cross section value $\sigma \geq 18$ μb for producing residual nuclei with an excitation energy $E^* = 20 \pm 0.5$ MeV if the annular α-particle detector subtends an angular range $3° \leq \Theta \leq 20°$. Similar estimations for $E^* = 15$ MeV provide the value $\sigma \geq 4$ μb. It is a reasonable enough cross section level. By this means, if one uses a target of 200 $\mu g/cm^2$ thickness and ion current I = 10^{10} pps, then with the cross section σ=18 μb one obtains 1 compound nucleus with an excitation energy of 20 MeV in 10 seconds. Let us discuss some problems existing in fission physics which can be solved under these conditions.

One of the ways of obtaining information on fission barrier values is the analysis of excitation functions for different channels of the compound nucleus decay. For a weakly fissioning nucleus it is the fission and evaporation channels - for the effectively fissioning nucleus. A series of experiments has been carried out on the VASSILISSA kinematic separator. The yields of neutron-deficient isotopes in the region of lead-to-uranium elements in xn-, pxn- and αxn-reactions with emission of 4 up to 12 neutrons have been measured. It has been shown that a satisfactory description of the experimental data using the statistical model is obtained taking into accountt shell effects in the level density [3] and in the fission barrier:

$$B_f(Z,A) = C*B_f^{LD}(Z,A) + \Delta W^{exp}(Z,A)$$

where B_f^{LD} is the value of the fission barrier, calculated in the liquid drop model, and $\Delta W^{exp}(Z,A)$ - the shell correction to the mass of the ground state. It appeared that in order to obtain a good agreement between the calculated excitation functions and the experimental ones, it was necessary to decrease the liquid drop part of the fission barrier value by 30 % (C = 0.7). This is true both for closed shell nuclei and for nuclei far from the closed shells [4]. Earlier we showed the possibility of using incomplete fusion reactions in order to determine the influence of shell effects on fission probability of excited nuclei in the region of the compound nuclei $^{201}Tl - ^{222}Ra$ [5]. In this work we propose to study the dependence of compound nucleus fission on the excitation energy for nuclei with small shell corrections to mass and, therefore, to the fission barrier in order to obtain an information on the liquid drop part of the fission barrier. According to calculations the compound nucleus ^{192}Hg which can be produced by the reaction $^{176}Hf(^{20}Ne,\alpha)^{192}Hg^*$ is a suitable nucleus for this purpose, as it has no shell correction, is not very fissionable

and, therefore, is responsive to the fission barrier value .

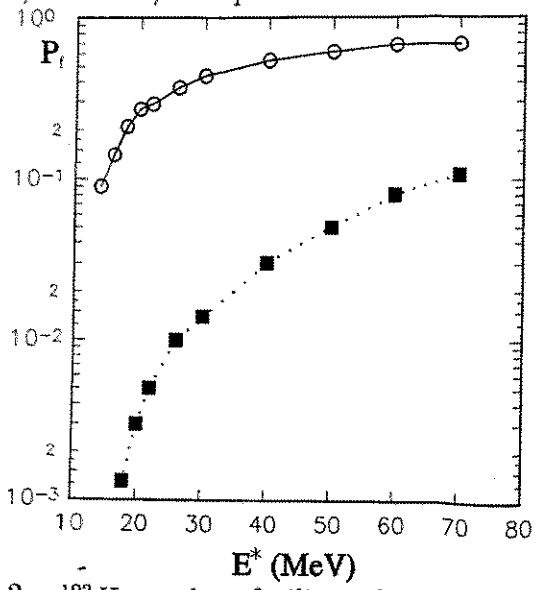

Fig.2 ^{192}Hg nucleus fissility value as a function of the excitation energy

In Fig.2 the results of calculating the ^{192}Hg nucleus fissility value as a function of the excitation energy for two versions of calculation are presented. The dotted curve has been obtained under the assumption that the fission barrier B_f is equal to the value obtained by the liquid drop model with the finite range of nuclear forces B_f^{LD} [6]. The solid curve denotes the results of calculation with $B_f = CB_f^{LD}$, where C = 0.7 according to the results of analysis [4]. From the Figure it can be seen that the difference between the two curves is so great that there is no need to reach excitation energies of 20 MeV so that to clear up the question whether the first or second version corresponds to the experiment, but then one can restrict oneself to higher energies where the cross section level will be essentially higher.

Another problem of fission physics which can be solved using incomplete fusion reactions is the investigation of multimodal structure discovered in recent years in the mass and energy distributions at low energy fission of nuclei in the region of Pb and for the spontaneous fission nearby Fm. Similar data on the fission of neutron-deficient isotopes of thorium have been obtained as well most recently [7]. To perform these investigations nuclei with lower excitation energy have to be produced and neutron-deficient isotopes can be produced only in heavy ion reactions with high Coulomb barriers in the fusion channel. In Fig.3 experimental data (dots) on the fusion cross section in the reaction $^{16}O + ^{204}Pb$ as a function of the excitation energy of the compound nucleus ^{220}Th are presented [8]. Extrapolation of these data (dashed curve) to an excitation energy $E^* = 20$ MeV leads to the cross section value $\sigma = 10\mu$b. Calculations within the statistical model taking into account the competition between fission and neutron evaporation, proton and α-particle emission show that the compound nucleus $^{220}Th^*$ at an excitation energy $E^* = 20$ MeV has a fissility which is equal 1 (2/3 of fission events at this energy will proceed prior

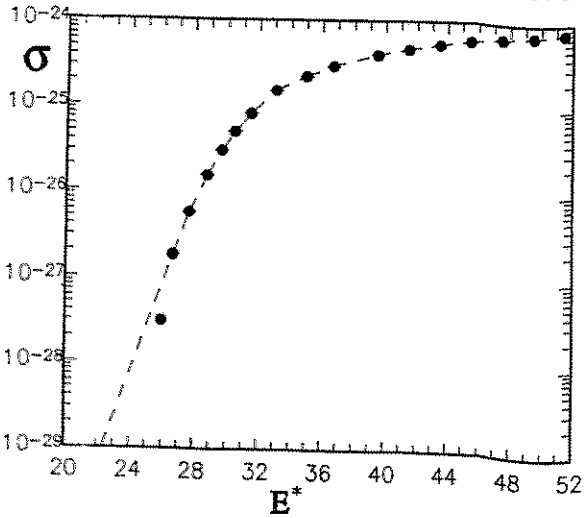

Fig.3 Experimental data (dots) on the fusion cross section in the reaction $^{16}O + ^{204}Pb$

the first neutron escape, and 1/3 of the events - after neutron escape, i.e. at an excitation energy of less than 10 MeV). Thus, the above-mentioned estimations of the cross section and fission fragment yields are true for this reaction. Therefore, the fission cross section for the compound nucleus $^{220}Th^*$ at an excitation energy E^*=22 MeV is to be $\sigma \geq 20\mu b$, this increases the value obtained in complete fusion reactions two times. With decreasing the excitation energy this difference will sharply increases and incomplete fusion reactions are to be the governing factor in studying fission modes of weakly excited nuclei.

REFERENCES

1. Kamanin V.V. et al., Nucl. Phys., A431 (1984) 545
2. Borcea et al., Nucl. Phys., A415 (1984) 169
3. Ignatyuk et al., Yad. Fiz., 37 (1983) 485
4. Andreev et al., Nucl. Phys., A568 (1994) 323
5. Bogdanov D.D. et al., Proc. of the Int. Workshop "Dynamical Aspects of Nucl. Fission", Smolenice 1991, JINR Report E7-92-95, Dubna, 1992, p.86
6. Krappe H.J. et al., Phys. Rev., C20 (1979) 992
7. Itkis M.G. et al., JINR Rapid Commun. 3(66)-94, Dubna, 1994, p.19
8. Murakami T. et al., Phys. Rev., C34 (1986) 1353

TIME MEASUREMENTS IN THE HEAVY IONS COLLISIONS

M. Aboufirassi[1], A. Badala[1,α], B. Bilves[2], G. Bizard[1], R. Bougault[1], R. Brou[1], A. Buta[1], J. Colin[1], F. Cosmo[2], D. Durand[1], Y. El Masri[6], A. Genoux-Lubain[1,ß], D. Guerreau[3], T. Hamdani[1], F. Hanappe[7], D. Horn[1,γ], J. Galin[3], J.L. Laville[1,δ], C. Le Brun[1], J.F. Lecolley[1], F. Lefebvres[1], O. Lopez[1], D. Jacquet[4], M. Louvel[1], M. Mahi[1], M. Morjean[3], T. Motobayashi[5], A. Péghaire[3], J. Péter[1], R. Régimbart[1], G. Rudolf[2], F. Saint-Laurent[3], F. Scheibling[2], J.C. Steckmeyer[1], L. Stuttge[2], B. Tamain[1], S. Tomasevic[2]

1. Laboratoire de Physique Corpusculaire - ISMRA - 14050 CAEN CEDEX - France
2. CRN Strasbourg - BP 20 - 67037 STRASBOURG CEDEX - France
3 - GANIL, BP 5027 - 14021 CAEN - France
4 - IPN Orsay - BP 1 - 91406 ORSAY - France
5 - Rikkyo University, Toshima-Ku, Tokyo 171, Japan
6 - U.C.L. Louvain La Neuve, Belgique
7 - U.L.B. Bruxelles, Belgique
α – On leave from INFN Catania - Italia
β - Now at Laboratoire de Physique Corpusculaire - Clermont-Ferrand - France
γ – On leave from CRL (AECL) - Canada
δ – Now at Laboratoire de Physique Nucléaire - Nantes - France

ABSTRACT

The formation and decay of excited nuclei with masses around A = 200 are studied for excitation energy, ε^* ranging from 0 to 6 MeV/u. For ε^* values up to 6 MeV/n, the various decay channels ending with one (evaporation), two (fission) or more (3, 4, 5) fragments still compete. In case of multifragment emission, we find that :
- the life-time of the excited nucleus before breaking is equal to 100-150 fm/c for ε^* values around 5 MeV/u
- the emission time (i.e. the interval between the emission of two fragments) evolves from a large value (τ > 1000 fm/c, sequential decay) when ε^* equals 2-3 MeV/u to a very small value (τ < 50 fm/c, simultaneous decay) for ε^* values around 5 MeV/u.

1. Introduction

A major objective of the study heavy ion collisions is to probe the static and dynamic properties of nuclear matter out of equilibrium[1,2]. In this paper, we will concentrate on two points : Firstly in our domain of interest where the excitation energy per nucleon ranges between 0 and 7 MeV/u, the emission of massive fragments plays an important role. Beyond the fragment

multiplicity , we have measured the characteristics of the emitted fragments and used them to analyze the collision, reconstruct the primary products and extract various physical quantities of interest. Secondly, we have made special efforts to derive the various time-scales which characterize the collisions. They are closely related to the questions of physical interest : limit of stability, lifetime of the excited nuclei, fragment emission timescale and the signatures and characteristics of multifragmentation.

To investigate these points we have used the Nautilus set-up at GANIL. Fragments were detected in the DELF[3] and XYZT[4] detectors. These two detectors constitute an ensemble of 30 position sensitive parallel plate avalanche counters (PPAC), each followed by an ionisation chamber. The angular range covered was 3°-150° with a geometrical acceptance of 55%. Full detection efficiency for atomic numbers equal to or larger than 8 was obtained. The set-up had a low velocity threshold : .5 cm/ns (.13 MeV/u) for DELF and 2 cm/ns (2.07 MeV/u) for XYZT in the forward direction. The measured parameters were the atomic number, Z, the fragment velocity, V, and the angle (with a resolution better than one degree). Light charged particles (not to be discussed here) were also detected with two complex arrays : the Mur and Tonneau. The data presented in this paper concerns the fate of excited nuclei (whose mass are around A = 180-220) produced by a variable impact parameter-dependent transfer of linear momentum, mass and energy from the projectile to the target. The results have been obtained by bombarding Au targets with Ne, Ar, Kr, Xe and Pb projectiles at incident energies ranging from 27 to 60 MeV/u. We will not discuss here the mechanisms but we have observed that, for the lightest systems and the highest energies (Ne at 60 MeV/u, Ar at 30 and 60 MeV/u, Kr at 43 and 60 MeV/u) the collisions end with only one piece of excited nuclear matter which then deexcites, whereas for the largest systems and the lowest energies (Kr+Au at 27 MeV/u, Xe+Au at 44 MeV/u, Pb+Au at 29 MeV/u) the system remains dinuclear at the end of the collision. In the first case, the excitation energy was derived on the basis of the massive transfer hypothesis whereas in the second situation the excitation energy was deduced from the total kinetic energy loss (TKEL) between the two partners.

2. Decay mode probability

The number of massive fragments detected for each collision Pb+Au at 29 MeV/u varied between 2 and 7. When we analysed the multifragment distribution we clearly observed two sources. From the relative velocity between the two sources we deduced the TKEL and the excitation energy per nucleon. We were then able to deduce the fragment multiplicity as a function of the excitation energy. The values for each multiplicity have been corrected for

contamination events where at least one fragment has been missed. The resulting distribution is shown in figure 1.

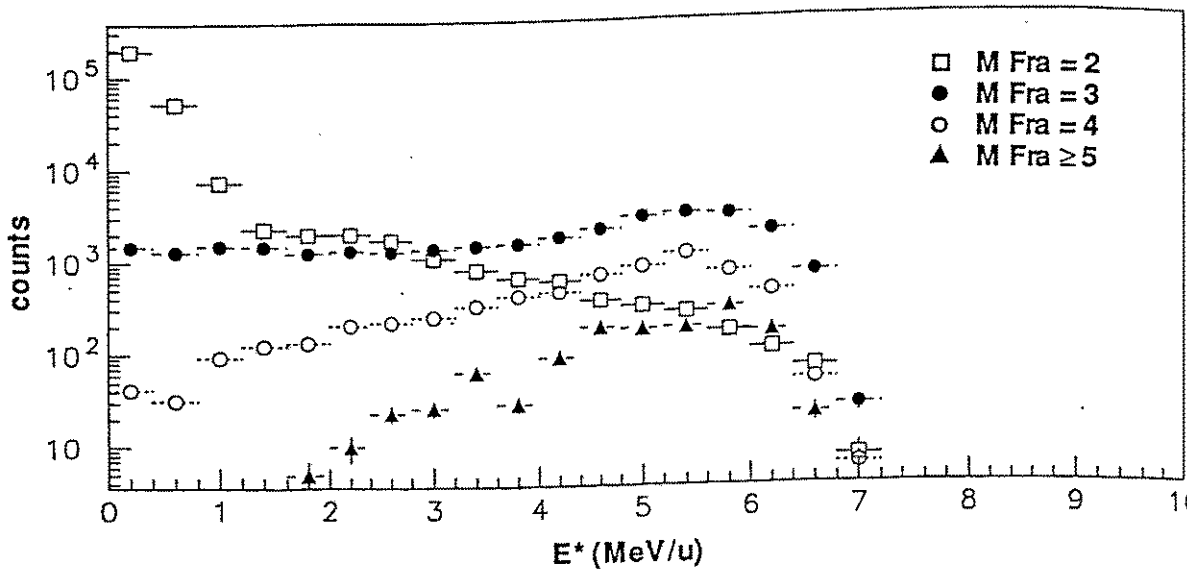

Fig. 1 : Fragment multiplicity , M Fra,as a function of the excitation energy per nucleon ,ε^*.

The two body decay channel is still present for excitation energy as high as 6 MeV/u, indicating that the two excited primary partners evaporate only light particles and that the nuclei can sustain without disassembling excitation energies up to 6 MeV/u. This is a value larger than that given by nuclear matter calculations[5]. The five-body final state corresponds to a situation where one of the primary partner disassemblies into at least 3 fragments. This occurs for excitation energies between 2 and 3 MeV/u.

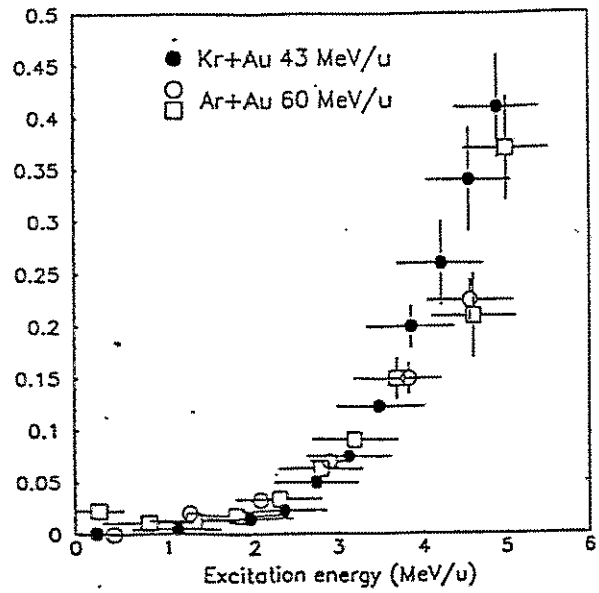

Fig. 2 : Evolution of the two-fold versus three-fold fragment production as a function of the excitation energy per nucleon E. Symbols correspond to different methods for estimating E* and to the two systems studied .*

The transition between two-body and three-body breakup has been also studied for the excited nuclei formed in the Ar+Au and Kr+Au collisions using the kinematic coincident method[6]. The excitation energy has been calculated by various methods and the results are given in the figure 2. As seen in the previous figure three-body decay starts to set-in around ε^*=2-3 MeV/u and dominates for ε^*=5 MeV/u.

3. Fragment emission : from long to short time-scales

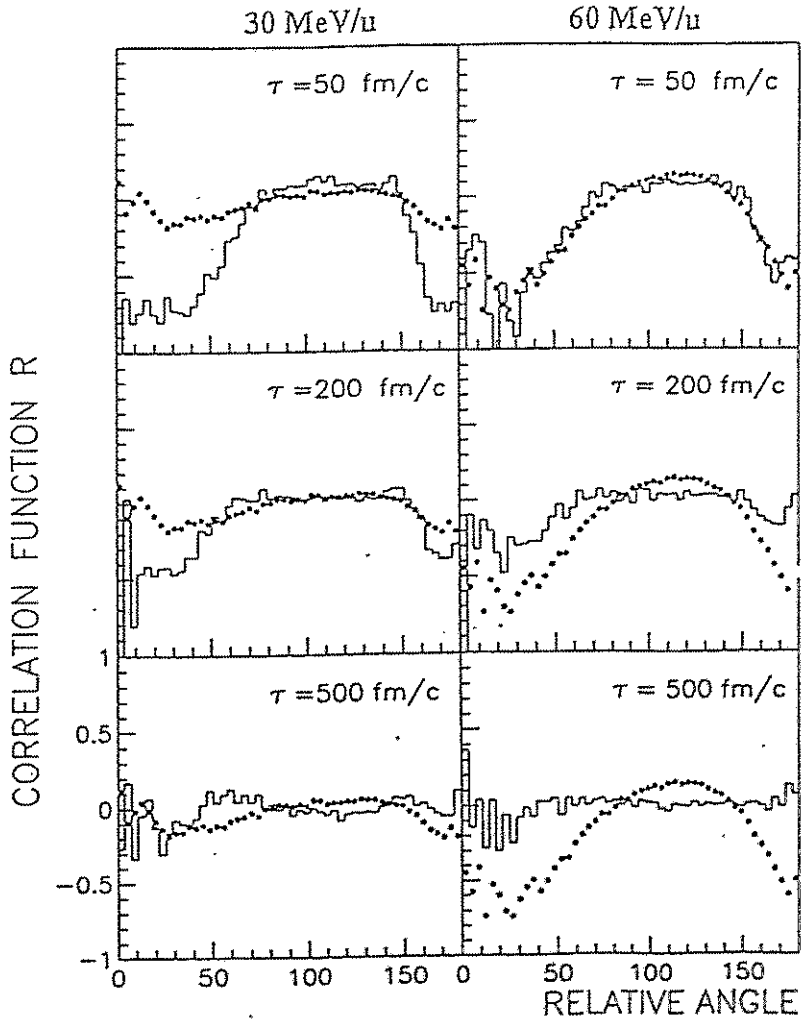

Fig. 3 : Correlation function for the relative angle distributions. The dots are the experimental results and the histograms are the results of the calculations for various spliting times. At 30 MeV/u on the left, the decay is clearly sequential (τ > 500 fm/c) whereas at 60 MeV/u, it is simultaneous ($\tau \leq$ 50 fm/c).

The occurence of multi-body decay is, however, not enough to characterize properly the process of multifragmentation. Indeed, one must investigate in detail the fragment emission time-scales since "true" multifragmentation is generally defined as a fast process. This aspect of the process may be studied with the help of the angular correlations between the fragments taken two-by-two[7,8]. In particular, when dealing with all the emitted fragments, the angular correlations are very different depending on whether the emission is simultaneous or sequential. It is even possible to derive, in the case of sequential decay, the time-scales between each splitting by comparing the experimental angular correlations to the results of trajectories calculated using various values of the time. The first value, obtained for the excited nuclei (3 MeV/u) formed in the Ne+Au collisions at 60 MeV/u was 300 fm/c[9].

The method has been and is presently being used for various systems and an illustration is given in figure 3 for Ar+Au collisions at 30 and 60 MeV/u[10,11,12].

The results for the different systems are given as a function of excitation energy in the figure 4.

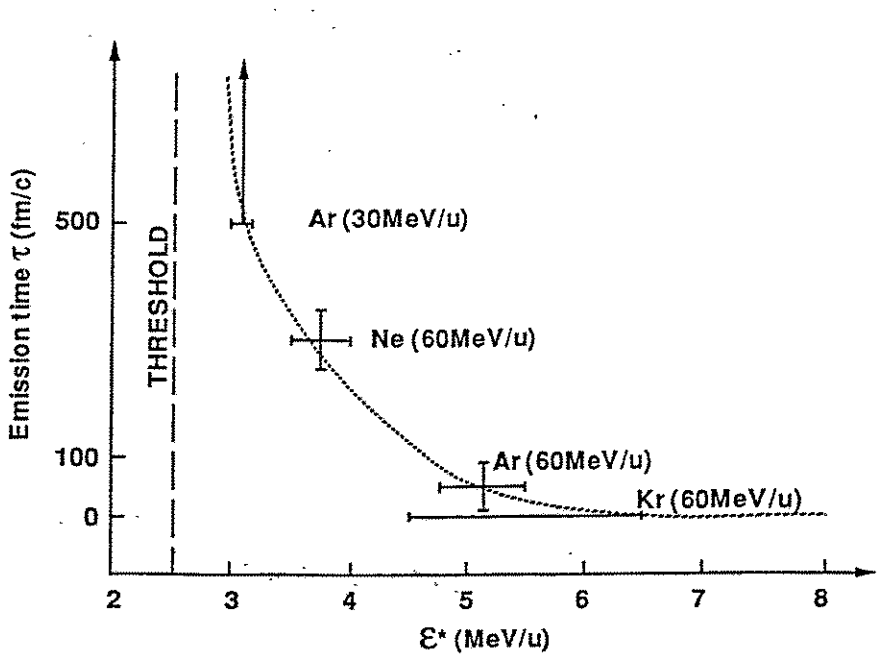

Fig. 4 : Fragment emission time as a function of the excitation energy .

For each system, it is possible to observe a time signature for the multifragmentation which clearly occurs for excitation energy larger than 5 MeV. By studying the charge evolution, in the case of three-body decay by means of Dalitz plots (fig. 5), we observe a clear evolution from fission with an additional light fragment to the multifragmentation where we observe identical charge distributions for each fragment. For the multifragmentation events in the Kr+Au

collisions at 60 MeV/u, the average fragment kinetic energy as a function of atomic number is given in figure 6 and compared with the calculations described in reference [13]. There is no need for any expansion energy.

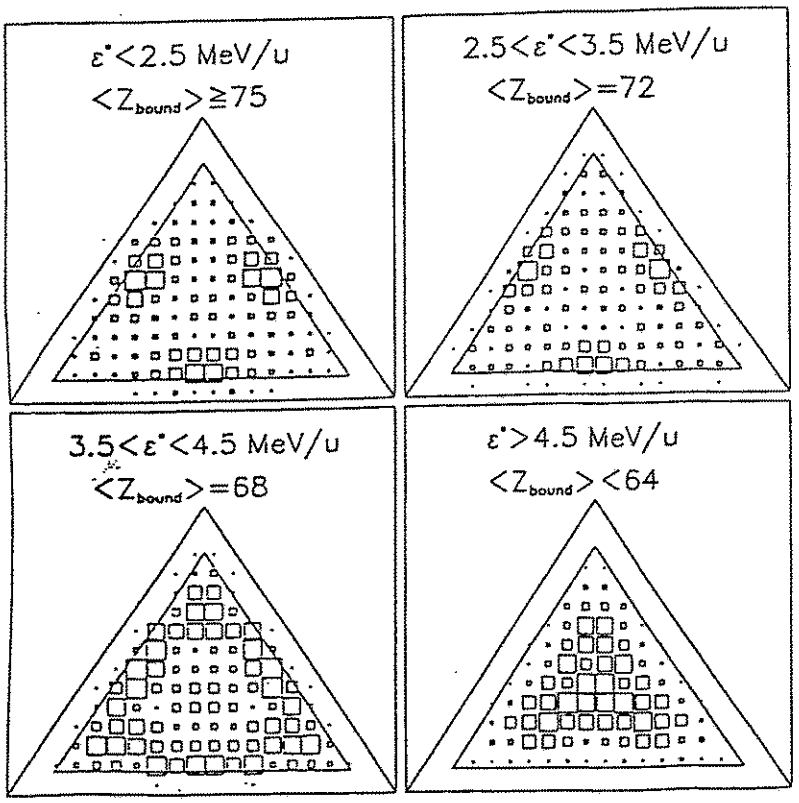

Fig. 5 : Dalitz plots for the three fragments for the Kr+Au system. The events have been sorted according to the excitation energy per nucleon. For each bin, the average Zbound = $Z_1+Z_2+Z_3$ is indicated. The interior triangle shows the limits due to the detection system (lowest detectable charge is 8).

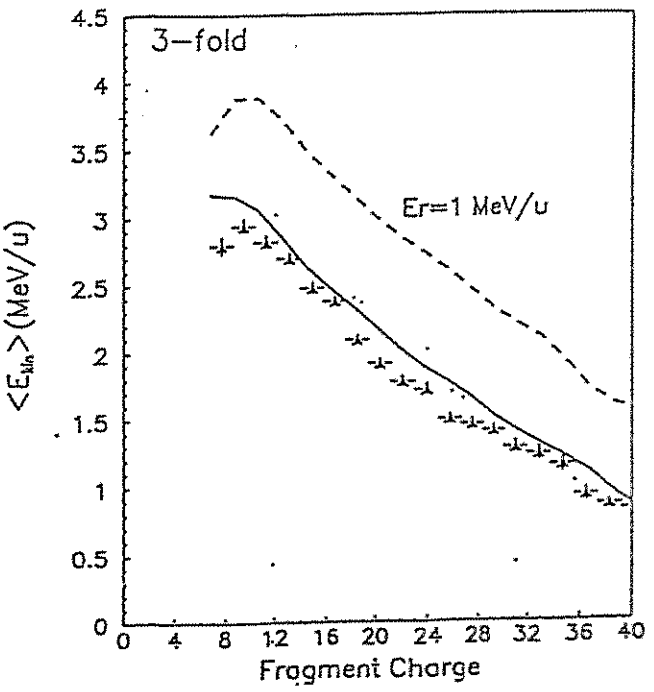

Fig. 6 : Average fragment kinetic energy as a function of atomic number for three target-emitted fragments in the reaction Kr+Au at 60 MeV/u. Black triangles : experimental points. Curves : statistical multifragmentation model [13] with two different initial conditions ; no expansion energy (solid line) and 1 MeV/u radial expansion energy (dashed line).

4. Measurement of lifetimes

Whereas the emission time measurement allows one to obtain a signature of multifragmentation and to study the excited nuclei, the measurement of the lifetime of the excited nuclei between the end of the collision and the beginning of the disassembly is a key parameter for the understanding of the collision mechanisms. Roughly speaking the knowledge of this time provides information on the origin of the disassembly. In case of very short times, as given by semi-classical codes, we are probably dealing with bulk instabilities related to a spinodal decomposition and we would be testing the equation of state at low density. On the other hand, a "long" lifetime would be related to surface and Coulomb instabilities and the system probably evolves with large deformation up to the breakup (simultaneous for high excitation energies and sequential for lower excitation energies). In that case we are measuring the viscosity and its temperature dependance. The measurement of such a lifetime is made possible when the collision fulfills the two following conditions : the primary collision has a deep inelastic character and ends with two excited nuclei which fly away before decay and, secondly, only one of these nuclei disassemblies into fragments. The disassembly products have their trajectories influenced by the large Coulomb field induced by the partner which has not broken up. This point is illustrated in the figure 7 which also displays the trends of the expected angular distributions with respect to the main axis of the collision. The characteristics of the angular distribution of the fragments, especially the dip around zero degree is directly related to the lifetime of the excited nucleus prior to breakup.

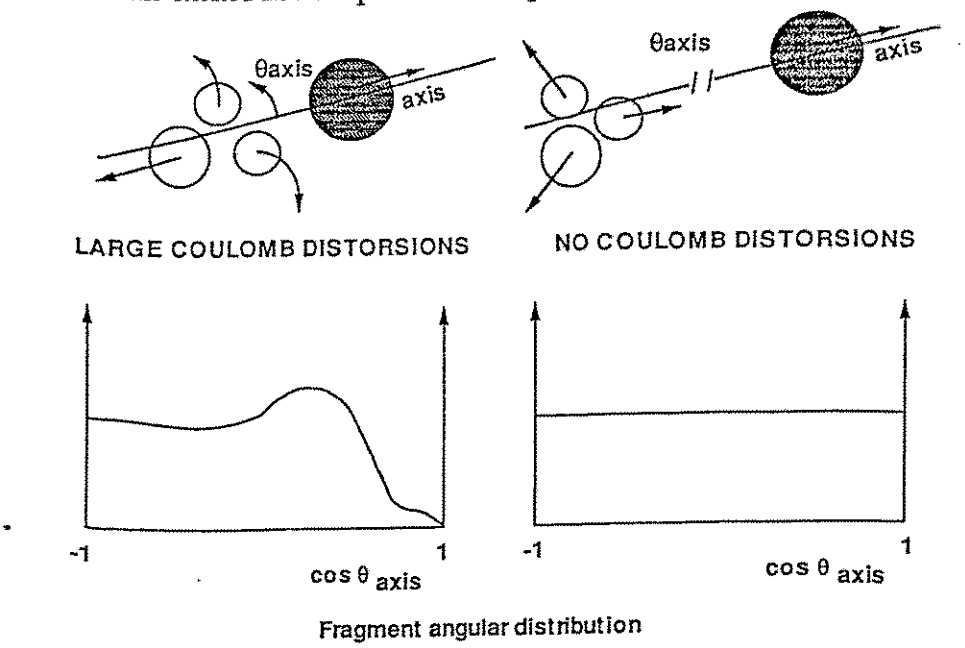

Fig. 7 : Proximity effects between the two partners when only one disassemblies

The experimental distributions for the collisions Pb+Au at 29 MeV/u are displayed in figure 8 for several bins of TKEL. We see a clear evolution from the low excitation energies where we do not see any dip at zero degree and only angular momentum effects, to the highest excitation energies where we can clearly see the dip and thus a sizeable influence of the heavy partner indicating a short separation at the time of breakup.

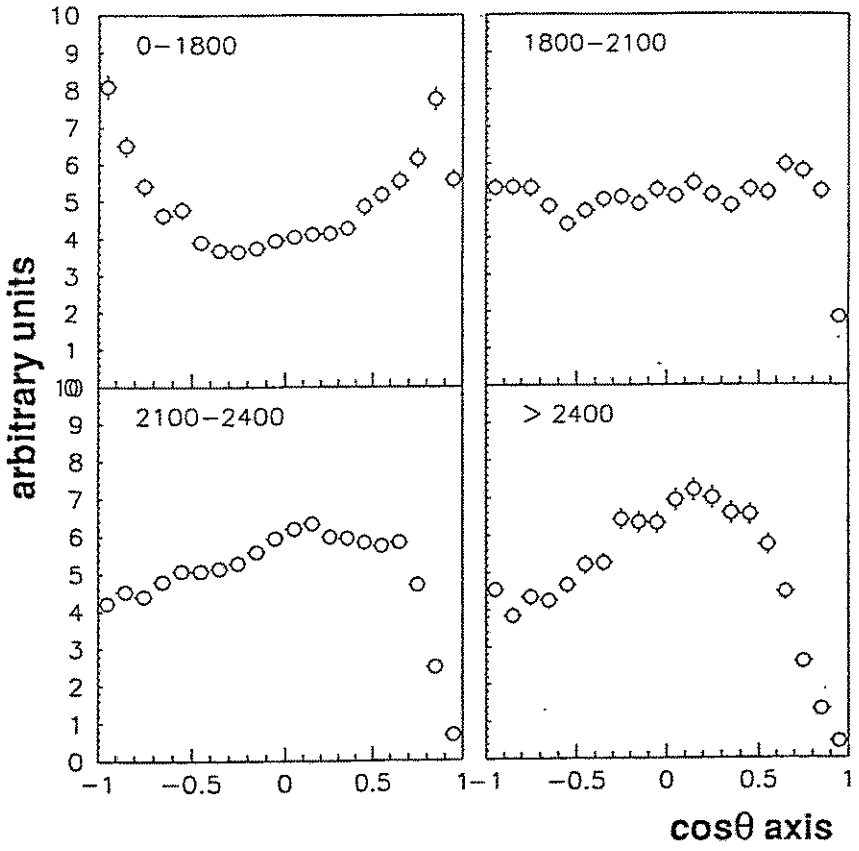

Fig. 8 : Cos θ axis distributions for various TKEL bins. The fragment multiplicity of the selected events is 4, one of them corresponding to one primary fragments and the other to the disassembly of the second primary fragment.

To obtain the lifetime we have to know the separation and the velocity. This can be done by use of a simulation taking into account the collision as described by a simple diffusion model giving the velocities at scission before Coulomb acceleration. The results of the influence of the lifetime on the angular distribution is given on the figure 9 for these different values and compared to the experimental distribution corresponding to the highest excitation energy and thus the shortest life time. The best fit is found for 150 fm/c.

The results are still preliminary and more complete calculations able to reproduce all the characteristics of the collisions are needed before given definitive values and evolution with excitation energies may be given. Nevertheless, we have already observed that for heavy ion collisions at 30 MeV/u, where fusion does not occur even for the highest excitation energies (> 5 MeV/u) the lifetime is larger that the one given by rather dynamical models. Thus seems

indicate that we are dealing with statistical decay rather than with dynamical decay. This conclusion is strengthened by the observation of the mixing of the various decay modes over a large range of excitation energy.

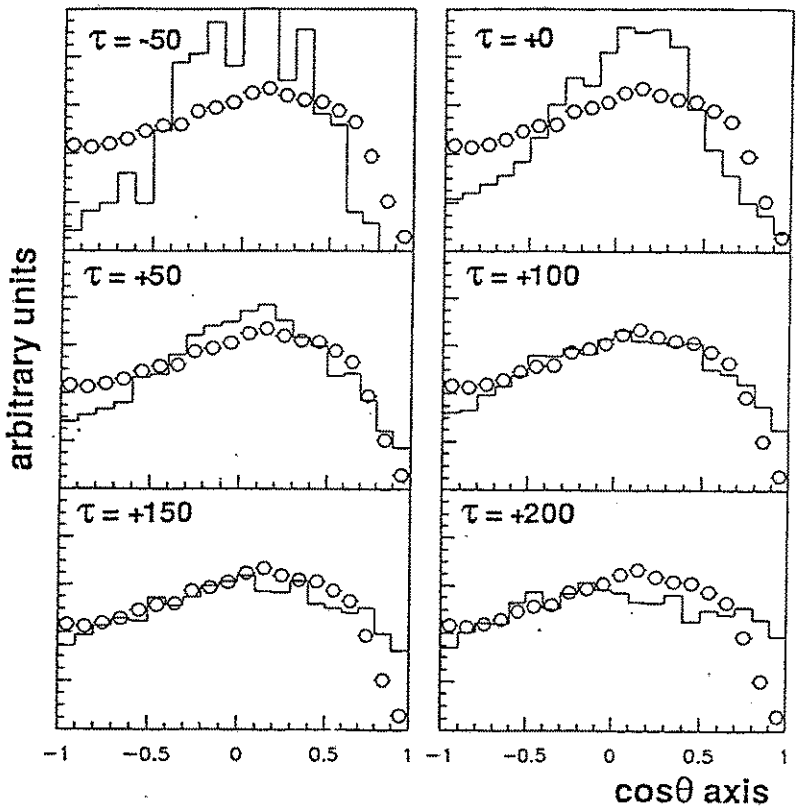

Fig. 9 : Cos θ axis distribution
points : experimental results for the highest TKEL (> 2100 MeV).
Histogram : Results of trajectory calculations under various lifetime conditions.

5. Conclusions

The results presented here are based on an analysis using the characteristics of all the massive fragments produced in heavy -ion collisions. We observe that evaporation processes (only one massive fragment at the end) still exists for excitation energies as large as 6 MeV/u and that the various decay modes are present over the whole range of excitation energies.

By using the Coulomb effects between the various massive fragments, we are also able to measure various characteristic time-scales.

Firstly we have measured the emission time between fragments and for various systems we have observed the evolution from sequential decay, where the fragments are produced by several splitting separated by time intervals larger than 1000 fm/c, to the simultaneous decay, for ε* larger than 5 MeV/u. We obtain in the latter case a clear signature of multifragmentation, as confirmed by the charge distributions.

Secondly, for collisions retaining a binary character (as observed in the Pb+Au collisions at 29 MeV/u) and by using events where only one of the primary partners disassemblies, we have measured the lifetimes of nuclei with excitation energies larger than 5 MeV/u. The measured value at this excitation energy is 150 fm/c (5 10^{-22} s). This value, obtained for a bombardment energy of 30 MeV/u, is rather long with respect to what is expected from dynamical effects alone and seems to indicate that in this case, we are observing a fast statistical decay.

The same kind of analysis will be used in the future with the results obtained with the INDRA detector for several other systems.

References

1 - G. Bertsch, S. Das Gupta, Phys. Rep. 160 (1988) 189

2 - E. Suraud, B. Tamain, C. Grégoire, Prof. of Nucl. and Part. Science 23 (1989) 357

3 - R. Bougault et al, NIM A259 (1987) 473

4 - G. Rudolf et al, NIM A307 (1991) 325

5 - E. Suraud, Nuclear Physics A462, 109,1987 and references therein

6 - G. Bizard et al, Phys. Letters B302 (1993) 162

7 - R. Trockel et al, Phys. Rev. Lett. 59 (1987) 2844

8 - Y.D. Kim et al, Phys. Rev. Lett. 67 (1991) 14

9 - R. Bougault et al, Phys. Letters B232 (1989) 291

10 - G. Bizard et al, Phys. Letters B276 (1992) 413

11 - M. Louvel et al, Nucl. Phys. A559 (1993) 137

12 - M. Louvel et al, LPCC93-12 accepted by Physics Letters

13 - O. Lopez et al, Phys. Lett. B 315 (1993) 34

DEEP INELASTIC COLLISIONS IN THE SYSTEM ^{40}AR + ^{232}TH AT 31 MeV/NUCLEON

V. Lips, R. Barth, G. Klotz-Engmann, H. Oeschler
Institut für Kernphysik, Technische Hochschule Darmstadt, D-64289 Darmstadt, Germany

Y. Cassagnou, M. Conjeaud, R. Dayras, S. Harar[1], R. Legrain, E.C. Pollacco and C. Volant
DAPNIA/SPhN, CE Saclay, F-91191 Gif-sur-Yvette Cedex, France

Abstract

The charge, velocity and angular distributions of three coincident fragments measured for the system ^{40}Ar on ^{232}Th at an incident energy of 31 MeV/nucleon evidence a deep inelastic collision process followed by fission. The estimated total kinetic energy loss is about 600 - 800 MeV which represents roughly 60% - 80% damping of the initial kinetic energy.

In heavy-ion reactions with incident energies below 10 MeV/nucleon deep inelastic collisions (DIC) are a well-known phenomenon. These reactions are interpreted as collisions in which the projectile follows an orbital trajectory around the target nucleus. This trajectory is governed by the balance between attractive nuclear and repulsive Coulomb forces. The long contact time between projectile and target allows for a large mass transfer and a high energy dissipation. The collision system ^{40}Ar + ^{232}Th, studied in this article, has previously been investigated at energies close to the Coulomb barrier and the typical behaviour of the DIC has been well demonstrated [1,2].

In the medium energy regime (above 20 MeV/nucleon) a new reaction class has been found in which intermediate mass fragments (IMF) are emitted. The reaction mechanism of peripheral collisions is often described in

[1]Present address: GANIL, BP 5027, F-14021 Caen Cedex.

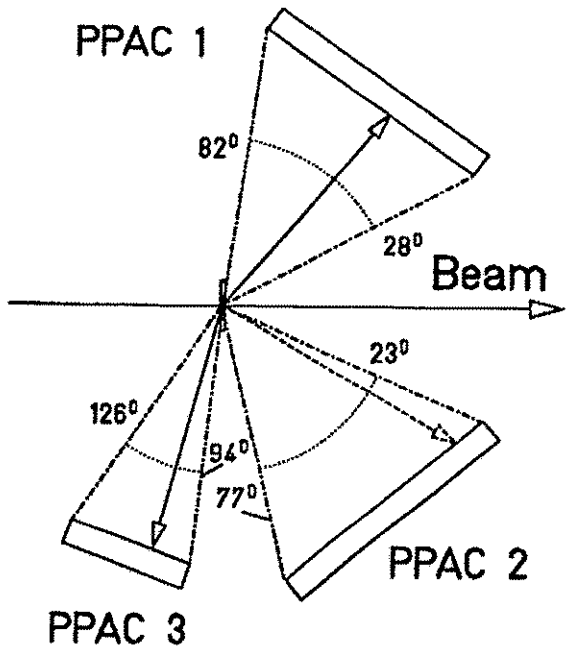

Figure 1: *Experimental setup consisting of three large-area parallel-plate avalanche counters (PPAC).*

terms of the participant-spectator picture where the nucleons of the overlapping region of the two nuclei form a highly excited subsystem while the remaining parts of the projectile and target continue on their way with almost beam velocity or stay at rest in the laboratory system, respectively [3]. The energy spectra of the IMF's have been analysed in this framework by decomposition into a target-like, a projectile-like and an intermediate component. Only recently an attempt has been made to take DIC into account as a production mechanism for the IMF's at 27 MeV/nucleon [4]. In an experiment where the circular polarization of γ-rays emitted in coincidence with IMF was measured [5], negative deflection angles were observed for the fragments. The polarizations measured in coincidence with fragments with $A \geq 4$ were comparable to the polarizations observed for DIC at much lower incident energies. This report is focused on the existence of DIC at 31 MeV/nucleon [6].

The reaction ^{40}Ar + ^{232}Th has been previously studied at medium en-

ergies and gave evidence for a rapid disappearance of fission in central collisions with increasing incident energy [7]. For a closer inspection of the evolution of central collisions a second experiment had been performed at GANIL, Caen (France). Analyzing these new data we found an interesting event class: triple coincidences with two medium-mass fragments and a third rather light nucleus. The part of the experimental setup which is relevant for discussing these events, is shown in Fig. 1. It consisted of three position-sensitive parallel-plate avalanche counters (PPAC's). Two of them (PPAC 1 and PPAC 2), sized 30×30 cm^2 [8], were mounted at a distance of 30 cm from the target, covering angular ranges of 28^0 to 82^0 and 23^0 to 77^0, respectively. PPAC 3, sized 17×15 cm^2, spanned an angular range of 94^0 to 126^0. The energy loss and the velocity of the fragments were measured with the PPAC's, using the time signal of the accelerator. From these two quantities an estimate of the atomic number of the fragments was obtained using an iterative procedure [9] yielding a charge resolution of about 30%. The amplitude of the ΔE signal was calibrated using a ^{252}Cf source. This allowed to calculate the efficiency of the PPAC which was limited by the threshold applied to the ΔE signal. With this method an efficiency of 100% was determined for fragments with Z > 10. Since the precise determination of the lower threshold in Z is of big importance for the charge distributions shown in this paper it has been verified by increasing the ΔE threshold offline and controlling its influence on the resulting charge distributions.

The main characteristics of the triple coincidences are summarized in Fig. 2. Part (a) - (d) show the velocity and charge distributions at 31 MeV/nucleon incident energy for PPAC 1 and PPAC 2. The detection of a third fragment in PPAC 3 introduces a strong asymmetry in the spectra of PPAC 1 and PPAC 2 despite their symmetric position relative to the beam. The fragments detected in counter 1 show a narrow velocity distribution, centered at 1.4 cm/ns, their charge distribution is peaked at Z≈40. In Fig. 2(e) the relative velocity between the fragments detected in PPAC 1 and PPAC 3 is shown. The narrow distribution, centered at the Viola velocity, together with the charge and velocity distribution of the fragment detected in counter 1 and 3 (not shown) indicate that coincidences between two fission fragments were observed with these counters. In PPAC 2 fast (v≈3 cm/ns) and light fragments are detected. The dotted line in Fig. 2(d) marks the lower threshold for full detection efficieny of the PPAC. The peaked structure of the measured distribution reflects therefore the efficiency loss of the

counter, folded with the resolution of the analysis method used for the charge measurement. A small fraction of events was observed, with two fission fragments detected in PPAC 1 and PPAC 2, together with an IMF in PPAC 3. These events were removed in the analysis by suppressing fission in PPAC 2 by a v_2 - ΔE_2 cut.

The velocity and charge distributions observed for the fragments detected in counter 2 show properties characteristic of inelastically scattered projectiles as observed in the low-energy regime. Namely, (i) their charges are close to the projectile charge, (ii) the velocities are well below those of the beam (7.7 cm/ns), (iii) the angular distribution is strongly forward peaked (Fig.2(f)), and finally (iv) the fragments in counter 2 lye preferentially in the plane spanned by the two fission fragments. In the picture of a deep inelastic collision, this results from the transferred angular momentum in the primary collision. The subsequent fission process of the target-like fragment occurs preferentially in the plane perpendicular to the spin axis. The width of this out-of-plane distribution is significantly smaller than the geometrical acceptance of the respective PPAC ($\phi = \pm 30^0$). All these observations lead us to conclude that the projectile-like partner (or the remaining part) of a DIC is observed.

To calculate the total kinetic energy loss (TKEL) of the reactions leading to the triple coincidences a detailed momentum balance of all fragments was done, including the momentum caried away by preequilibrium particles. The masses of the detected fragments were calculated using the iterative method for kinematical coincidences from Casini [10]. This method takes advantage of the overdetermined kinematics for three fragments and yields the primary velocities. Required input for the calculations – besides the angles and velocities of the fragments – are the total mass of the three-body system, which depends on the number of preequilibrium particles assumed for the respective calculation and its center-of-mass velocity. The center-of-mass velocity was determined by comparing the masses deduced from the kinematical coincidence analysis to the charges calculated from the velocity and ΔE information of the PPAC's. The momentum balance finally allowed to determine the velocity and kinetic energy of the preequilibrium particles. Their number has been varied between 20 and 30 such that their velocities fall in the range of 0.5 – 1 times the beam velocity. With this assumption TKEL values of 600 MeV to 800 MeV are obtained which corresponds to 60% - 80% damping of the available kinetic energy.

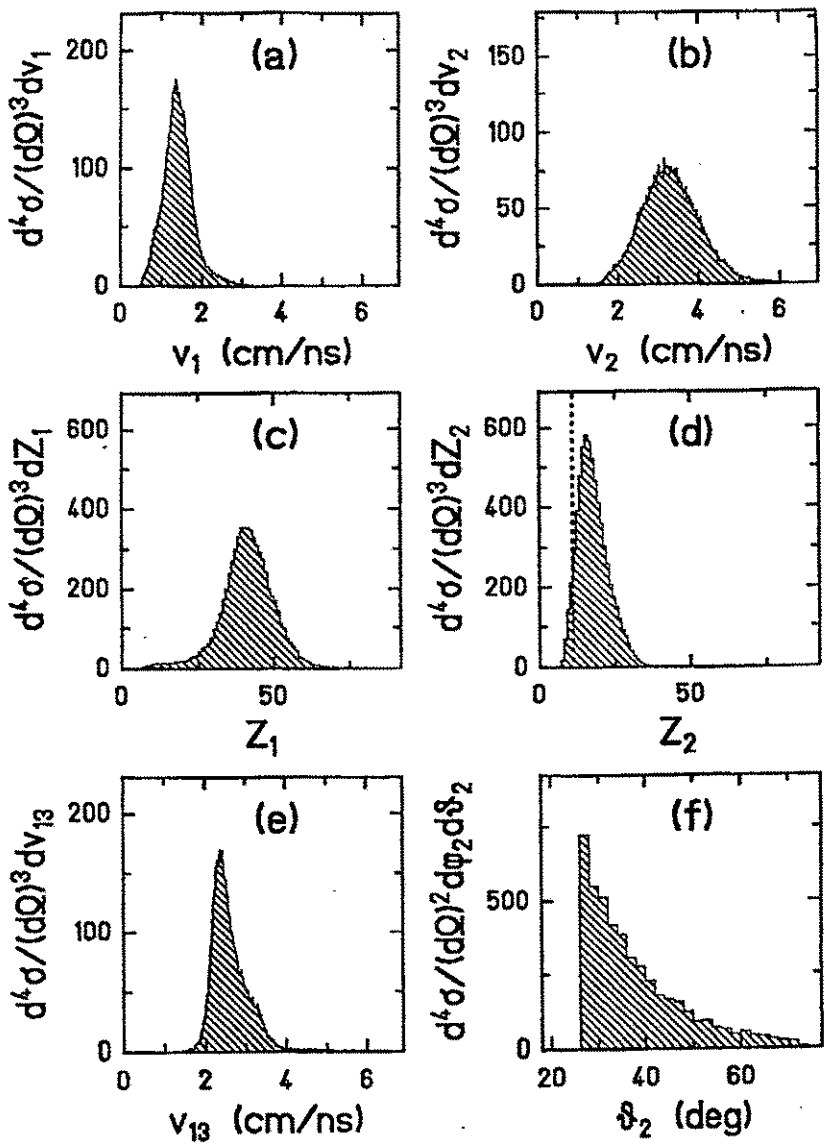

Figure 2: *Properties of triples coincidences in PPAC 1, 2 and 3. (a) Distribution of fragment velocities measured with PPAC 1. (b) The same quantity measured with PPAC 2. (c) Fragment-charge distribution measured with PPAC 1. (d) The same quantity measured with PPAC 2. The dotted line marks the threshold for full detection efficiency. (e) Distribution of relative velocities between fragments detected in PPAC 1 and PPAC 3. (f) Angular distribution of the fragments detected in PPAC 2.*

It is interesting to compare our results with the 4π neutron detector data for the system $^{40}Ar + ^{197}Au$ at 44 MeV/nucleon incident energy [11,12] High neutron multiplicities are observed in reactions triggered by projectile-like fragments at 20^0, yielding similar TKEL values as in our case. Also, BUU-calculations performed for nearly the same incident energy, evidence typical binary deep-inelastic collisions from the grazing impact parameter up to half its value [13]. For strongly damped collisions the contact times are very similar to those obtained in experiments close to the Coulomb barrier.

The experimental data show no dependence of the deduced TKEL value upon the deflection angle of the projectile fragments, in the angular range between 30^0 and 70^0 studied here, i.e. at values larger than the grazing angle (9^0). A similar observation has been made for the system $^{40}Ar + ^{nat}Ag$ where such a correlation was seen only in the vicinity of the grazing angle [4]. This suggests that the projectile-like fragment is deflected towards negative angles, as observed for the system $^{14}N + ^{154}Sm$ at similar incident energies [5].

To get an estimate of the cross section, a Monte-Carlo calculation was performed to obtain the efficiency of our setup for triple coincidences. In the angular range of 30^0 to 60^0, a contribution of around 100 mbarn is estimated for IMF's to originate from DIC (followed by fission).

In summary, the triple coincidences observed in the system $^{40}Ar + ^{232}Th$ are interpreted as projectile-like fragments issuing from DIC followed by fission of the target-like partners. This process has been identified by the charge, energy and angular distribution of the light fragments and the relative velocity and charges of the two other fragments. TKEL values were estimated to about 600 – 800 MeV corresponding to a rather strong damping of the initial motion. This high energy loss which is independent of the emission angle indicates negative deflection angles for these collisions .

The presence of DIC shows that, even at Fermi energies, nuclei behave collectively. This process must be taken into account when studying multiplicities and cross sections for IMF production in this regime.

We would like to thank H. Folger and the GSI target laboratory for preparing the targets and the staff of the GANIL accelerator for providing an excellent beam.

References

[1] A.G. Arthuk, G.F. Gridnev, V.L. Mikeev, V.V. Volkov and J. Wilczynski, Nucl. Phys. A215, 91 (1973).

[2] J.C. Jacmart, P. Colombani, H. Doubre, N. Frascaria, N. Poffé, M. Riou, J.C. Roynette, C. Stéphan and A. Weidinger, Nucl. Phys. A242, 175 (1975).

[3] R. Dayras, A. Pagano, J. Barrette, B. Berthier, D.M. De Castro Rizzo, E. Chavez, O. Cisse, R. Legrain, M.C. Mermaz, E.C. Pollacco, H. Delagrange, W. Mittig, B. Heusch, R. Coniglione, G. Lanzano and A. Palmeri, Nucl. Phys. A460, 299 (1986).

[4] B. Borderie, M. Montoya, M.F. Rivet, D. Jouan, C. Cabot, H. Fuchs, D. Gardès, H. Gauvin, D. Jacquet, F. Monnet and F. Hanappe, Phys. Lett. B205, 26 (1988).

[5] M.B. Tsang, W.G. Lynch, R.M. Ronningen, Z. Chen, C.K. Gelbke, T. Nayak, J. Pochodzalla, F. Zhu, M. Tohyama, W. Trautmann and W. Dünnweber, Phys. Rev. Lett. 60, 1479 (1988).

[6] V. Lips, R. Barth, G. Klotz-Engmann, H. Oeschler, Y. Cassagnou, M. Conjeaud, R. Dayras, S. Harar, R. Legrain, E.C. Pollacco and C. Volant, Phys. Rev. C 49 (1994) 1214.

[7] M. Conjeaud, S. Harar, M. Mostefai, E.C. Pollacco, C. Volant, Y. Cassagnou, R. Dayras, R. Legrain, H. Oeschler and F. Saint-Laurent, Phys. Lett. 159B, 244 (1985).

[8] H. Stelzer, H.W. Daues and N. Shenhav, GSI Scientific Report 1984, p. 293.

[9] V. Lips, Diploma thesis, Technische Hochschule Darmstadt 1989; GSI Scientific Report 1987, p. 309.

[10] G. Casini, P.R. Maurenzig, A. Olmi and A.A. Stefanini, Nucl. Instrum. Methods A277, 445 (1989).

[11] J. Galin, J.L. Charvet, B. Cramer, E. Crema, H. Doubre, J. Frehaut, B. Gatty, D. Guerreau, G. Ingold, D. Jacquet, U. Jahnke, D.X. Jiang, B. Lott, C. Magnago, M. Morjean, J. Patin, E. Piasecki, J. Pouthas, F. Saint-Laurent, E. Schwinn, A. Sokolov and X.D. Wang, Proceedings of the Symposium on Nuclear Dynamics and Nuclear Disassembly, Dallas 1989, edited by J.B. Natowitz (World Scientific, Singapore) p. 320.

[12] A. Sokolov, D. Guerreau, J.L. Charvet, B. Cramer, H. Doubre, J. Fréhaut, J. Galin, B. Gatty, G. Ingold, D. Jacquet, U. Jahnke, D.X. Jiang, B. Lott, C. Magnago, M. Morjean, Y. Patin, E. Piasecki, J. Pouthas, E. Schwinn, Nucl. Phys. A562(1993)273.

[13] M.F. Rivet, B. Borderie, C. Grégoire, D. Jouan and B. Remaud, Phys. Lett. B215, 55 (1988); D. Jouan, B. Borderie, M.F. Rivet, C. Cabot, H. Fuchs, H. Gauvin, C. Grégoire, F. Hanappe, D. Gardès, M. Montoya, B. Remaud and F. Sébille, Z. Phys. A340, 63 (1991).

Flow and Multifragmentation in Heavy-Ion Collisions at Intermediate Energies

H.W. Barz [a,b] and B. Heide [b,a]

[a] Institut für Theoretische Physik, Technische Universität Dresden,
Mommsenstr. 13, D-01062 Dresden, Germany

[b] Institut für Kern- und Hadronenphysik, FZ Rossendorf,
Pf 510119, D-01314 Dresden, Germany

Abstract: The occurrence of flow in heavy-ion reactions is briefly reviewed. The influence of radial flow on the energy spectra is investigated for nearly central collisions of Au on Au at 150 MeV per nucleon.

1. Introduction

With the present day heavy ion accelerators heavy ion collisions can be studied in a wide range of bombarding energies. The search for collective behaviour of matter is important if one tries to gain informations about the equation of state.

The occurrence of flow in heavy ion reactions is now well established. The possibility to treat hot nuclear matter by hydodynamics was anticipated earlier [1]. The side flow was the first phenomenon which was observed [2] and later the sqeeze-out effect [3] was established. The side flow is observed in nearly central collisions with finite impact parameter. It is best visualized by the energy-flow tensor Θ within the reaction plane defined by the so-called flow angle. The energy contained in this flow amounts to 5 MeV per nucleon for a collision of Au on Au at 200 MeV bombarding energy. The side flow is usually measured by the change of the mean side flow as a function of rapidity y as the reduced flow $\frac{d}{dy} < p_x/p_\perp >$ with p_x and $p_\perp$ being the side and the total tranverse momentum. This ratio is sensitive to the properties of the matter. If one describes the scattering process within the frame of transport theories based on the Boltzmann-Ühling-Uhlenbeck (BUU) approach it turns out that the side flow depends not only on the strength of the attractive mean field and the repulsive Coulomb field but also on the in-medium nucleon-nucleon cross sections. Especially the balance energy which marks the point at which the side flow changes its sign is an interesting quantity [4].

A careful analysis of the side flow as a function of the fragment mass reveals that the flow rises with increasing mass. So in a plane perpendicularly to the beam direction heavier fragments show a much larger asymmetry then nucleons [5]. This can be explained as follows. All particles flow with the same velocity as the surrounding matter in the direction of the flow angle. In addition, the particles have thermal velocity which is proportional to $\sqrt{T/A}$ with T and A being the temperature and the mass of the particles, respectively. For composite fragments the thermal velocity becomes smaller and therefore with increasing mass number the distribution becomes more concentrated around the flow direction.

The side flow is observable with a single type of particles. This is not the case for the radial flow. The reason is that a thermal source of nucleons, without any flow at the beginning, will form a radial velocity field after a sufficiently long time. If there is in addition a radial flow it cannot be disentangled if only nucleons are detected.

However the presence of composite particles allows one to identify both components of the velocity field by measuring the kinetic energy of fragments with different mass. The thermal motion contributes a constant energy of $\frac{3}{2}T$ to the fragment energy while the contribution of the radial velocity field contributes an energy which is proportional to the mass:

$$E_{kin} = \frac{3}{2}T + A\,E_{flow}, \quad (1)$$

from which E_{flow} is easily extracted.

Radial flow was detected in very central collisions, where the matter can easily be compressed. In reactions of Ar on Ag/Br at 60 MeV a value of 3 MeV was extracted [6], similarly to those reported by J. Peter at this meeting. Using heavier target and projectile combinations and higher energies big flow values were extracted ranging up to 40 MeV [7, 8, 9, 10].

2. Analysis of BUU calculations

To gain insight in the reaction mechanism we apply the BUU approach for the collision of *Au* on *Au* at 150 MeV per nucleon. This approach, described in detail in ref. [11], generates the phase space distribution $f(\mathbf{r}, \mathbf{p}, t)$ by averaging over parallel ensembles of pseudo-nucleons.

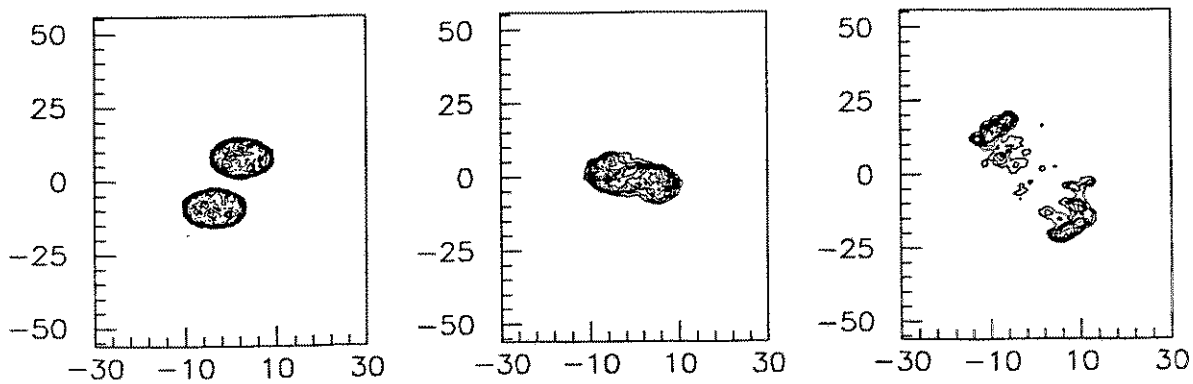

Fig. 1. Density plot in the reaction plane for Au on Au collision at 150 A·MeV for an impact parameter of 6 fm. The plots are calculated for collision times of 0, 40, and 90 fm/c.

We use this approach to calculate the density profile (see fig. 1) as well as energy and momentum distributions of the matter in different regions of the coordinate space at a certain break-up time after which we assume that the fragmentation process sets in. Following the time evolution we recognize that a considerable number of fast particles leave the collision zone early and move within highly diluted matter. These pre-equilibrium particles are too far away from each other to participate in the fragmentation process. These particles are excluded by introducing a limiting density n_{limit} at break-up time. The pre-equilibrium particles take away a large part of the energy. Therefore, the excitation energy of the remaining matter becomes moderate (see fig. 1). This is an important fact since it explains why so many intermediate mass fragments (IMFs) with charges $Z > 2$ are observed at this high bombarding energy.

To account for the side flow we choose a coordinate system given by the principle axes

of the energy flow tensor $\Theta_{ij} = \frac{1}{2mN}\sum_n p_i^{(n)} p_j^{(n)}$, where the sum runs over all N nucleons with $p_i^{(n)}$ being the i-th component of the nucleon momentum.

In this new frame we determine the energy which is contained in the flow in the direction of the axis i via

$$F_i = \frac{1}{2m} \frac{\left[\frac{1}{A}\sum_n (p^{(n)} e^{(i)})(r^{(n)} e^{(i)})\right]^2}{\frac{1}{A}\sum_n (r^{(n)} e^{(i)})^2}. \qquad (2)$$

These definitions generalize the radial flow F_{radial} which is a convenient measure in nearly spherically expanding systems. In general the unequality relation $\sum F_i \geq F_{radial}$ holds.

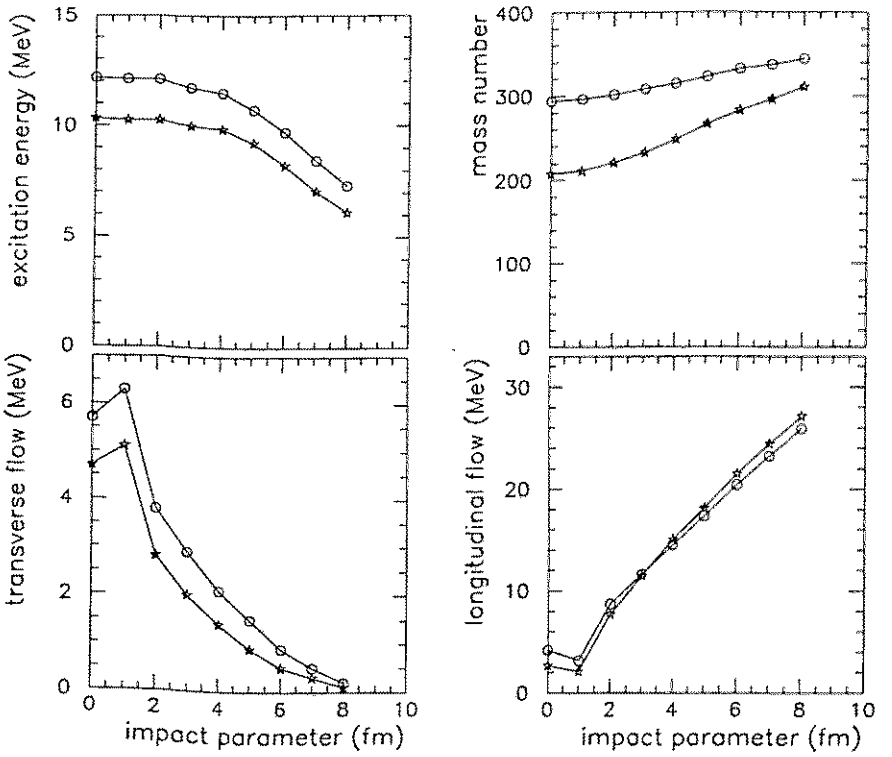

Fig. 2. Calculated excitation energy E^*, mass number A, transverse flow $(F_1 + F_2)/2$ and longitudinal flow F_3 as a function of the impact parameter for two limiting densities of 0.08 n_0 (circles) and 0.15 n_0 (stars), respectively.

From the BUU calculations we extract further the excitation energy per particle E^* as sum of the potential energy, the Coulomb energy and the kinetic energy in the co-moving mean velocity-field.

In fig. 2 we have represented the excitation energy, the mass number, the transverse and the longitudinal flow energy as a function of the impact parameter for two different limiting densities $n_{limit} = 0.08 n_0$ and $0.15 n_0$ at a time of 70 fm/c. The flow pattern for impact parameters smaller than 1.5 fm has an oblate shape. Between 4 fm and 6 fm the system becomes prolate, and the one-source picture changes eventually into a two-source one which is clearly seen in fig. 1.

3. Energy spectra

In the experiment [8, 10] we are analysing multiplicity cuts were used to select central collisions corresponding to impact parameters smaller than 3.5 fm.

To describe the fragment formation we employ the Copenhagen statistical multifragmentation model [12] to the inner zone. This model starts with the situation at break-up time given by the parameters corresponding to fig. 1. The break-up density was chosen to be one fourth of normal nuclear matter density. In the average the system decays into 35 hot fragments among them are approximately 23 IMFs. Next, we incorporate the flow by giving the fragments an initial velocity. Each velocity component v_i is taken to be proportional to the distance from the centre and the amount is chosen such that the flow energies F_i are obtained. Further, a random thermal velocity given by the kinetic temperature of 15 MeV is superimposed.

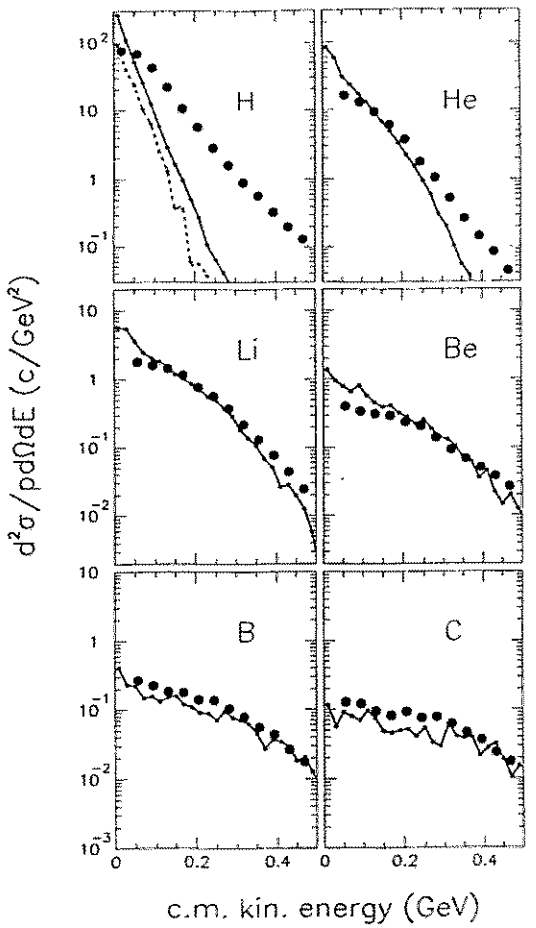

Fig. 3. Calculated energy spectra in the centre-of-mass system (small dots connected by line) compared to data [10] (big dots) for light elements. The dashed line in the first frame shows the spectrum of pre-equilibrium protons.

The time evolution of these hot sources is calculated taking into account the influence of the Coulomb force and the continuous evaporation of light particles. At the end of the expansion the final multiplicity is increased to about 100 particles while the number of IMFs is reduced to about seven.

One of the characteristic features which appear from our scenario are the fragment spectra measured as a function of the cm-energy. In analysing these data [10] we found that the flow obtained for the fragments was somewhat too large. This might be caused

by the fact that in BUU calculations only the nucleonic flow can be obtained reliably. Fragment formation is not well described. If IMFs are formed preferentially in the central region the flow could be smaller. To achive agreement with experiment we reduce the flow by 33 %. The results are shown in fig. 3 for several light isotopes. No agreement is reached for hydrogen isotopes. In our model most of the hydrogen isotopes are evaporated from hot fragments. However, it is known that the pre-equilibrium protons coalescence with neutrons to deuterons and tritons. This mechanism gives the hydrogen isotopes a larger kinetic energy and produces a flatter spectrum.

The flow at break-up amounts to 11 MeV. In the course of the expansion this flow increases due to Coulomb repulsion and particle evaporation to about 18 MeV. A value which agrees well with the one derived from eq. (1).

4. Conclusions

The measurement of IMFs is an important tool to detect collective flow effects in heavy ion collisions. As an example we analysed central *Au* on *Au* collisions combining the BUU approach with the statistical multifragmentation model. We found that a central region consisting of roughly half of the total number of nucleons has a sufficient small excitation energy of about 10 MeV giving a charge distribution being compatible with the measured one. The nucleonic flow was not fully transferred to the fragments as we have obtained by comparing the energy spectra of the IMFs with experiment.

The authors acknowledge support by the German BMFT under contract 06DR107.

References

[1] W. Scheid. B. Müller and W. Greiner, Phys. Rev. Lett. 32 (1974) 741;
M. Sobel, P. Siemens, J. Bondorf and H. Bethe, Nucl. Phys. A251 (1975) 302.

[2] H.-A. Gustafsson et al., Phys. Rev. Lett. 52(1984)1590.

[3] H.Gutbrod et al., Phys. Lett. B218(1989)267.

[4] G.D. Westfall et al., Phys. Rev. Lett. 71(1993)1986.

[5] K.G.R. Doss et al., Phys. Rev. Lett. 59(1987)2720.

[6] H.W. Barz et al., Nucl. Phys. A531 (1991) 453.

[7] D.R. Bowman *et al.* Phys. Rev. C46 (1992) 1834;
W. Bauer et al., Phys. Rev. C47 (1993) R1838.

[8] S.C. Jeong et al., Phys. Rev. Lett. 72(1994)3468.

[9] B. Kämpfer, R. Kotte, J. Mössner, W. Neubert, D. Wohlfahrt and FOPI, Phys. Rev. C48 (1993) R955.

[10] W. Reisdorf, Proc. Int. Workshop XXII on Gross Properties of Nuclei and Nuclear Excitations, Edt. H. Feldmeier, W. Nörenberg, Hirschegg, Austria, Jan. 17-22, 1994, p. 93;
B. Kämpfer et al., ibda., p. 113.

[11] W. Bauer et al., Phys. Rev. C 34 (1986) 2127.

[12] J.P. Bondorf, R. Donangelo, I.N. Mishustin and H. Schulz, Nucl. Phys. A444 (1985) 460.

J. Łukasik*, J. Cibor, T. Kozik and Z. Majka

Jagellonian University, Institute of Physics, Reymonta 4, 30-059 Kraków
*Present address: Institute of Nuclear Physics, Radzikowskiego 152, 31-342 Kraków

ABSTRACT

A microscopic model based on a molecular dynamics concept is presented. The model simulates some quantum effects and thus enables studies of large fermionic systems. It was devised to investigate the dynamics of heavy ion collisions at intermediate energies and in particular to study the early phase of the $^{84}Kr + ^{159}Tb$ reaction at 45 MeV/nucleon. The model confirms the experimentally observed binary character of this reaction (the output channel with 2 heavy fragments takes about 80-90% of the total cross section). It predicts a maximum of the multiplicity of intermediate mass fragments (IMF) at intermediate impact parameters in the early phase of the reaction. This maximum is more pronounced in the soft EOS case (up to 5 IMFs per event). The initial discrepancy between soft and hard EOS disappears during the long time scale evaporation phase as far as the simplest observables are concerned (Z and angular distributions, energy spectra). The IMFs produced in the early phase ($t \leq$ 300 fm/c) originate mainly from the hot elongated interaction zone formed for intermediate impact parameter collisions and are focussed in the forward direction. The model predicts equilibration of the system after 100-200 fm/c. The comparison of the asymptotic characteristics with the experimental data is quite reasonable. The linear momentum transfer observable calculated for various systems seems to favour the soft EOS.

The model, or rather its numerical implementation dubbed CHIMERA, is a compilation of two recently devised models which utilize the molecular dynamics concept to describe the intermediate (20-200 MeV/nucleon) energy nuclear reactions. These are the Quantum Molecular Dynamics (QMD) model of Aichelin and Stöcker [1] and the Quasi-Particle Dynamics (QPD) model of Boal and Glosli [2,3]. The code is described in detail elsewhere [4,5] and here we shall specify its important characteristics only:

- The nucleons are represented by constant width Gaussian wave packets obeying the minimal requirement of the uncertainty relation. The centroids of the Gaussians are assumed to evolve along classical trajectories.
- The hard core scattering of the nucleons is treated as if they were free (stochastic isotropic scattering with the nucleon-nucleon cross section $\sigma_{NN} = 41$ mb). The collisions are statistically independent and the interference between two different collisions is neglected. The collision is allowed provided the post scattering states are not already occupied by the like nucleons. Otherwise the collision is blocked and the two nucleons continue their movement in the effective potential. The occupancy of phase space around the final states is assumed to be the overlap of the Gaussians representing the phase space distribution of the nucleons. The angular momentum of the scattering nucleons is not conserved during the collision.
- The real part of the transition matrix is replaced by an effective potential. The nuclear effective potential was derived from a Skyrme parametrization of the potential energy density and was supplemented with the Coulomb potential and the momentum dependent Pauli potential. The bell shaped Pauli potential was implemented to simulate the fermionic nature of the nucleons. It introduces repulsion among the nucleons of the same kind whenever they come too close in phase space. It is also crutial during construction of the ground state configurations of the nuclei. It causes the nucleons to have non vanishing momenta in spite of their vanishing

Code for Heavy Ion Medium Energy ReActions

CHIMERA ← QPD/QMD + ...

Cold projectile and target

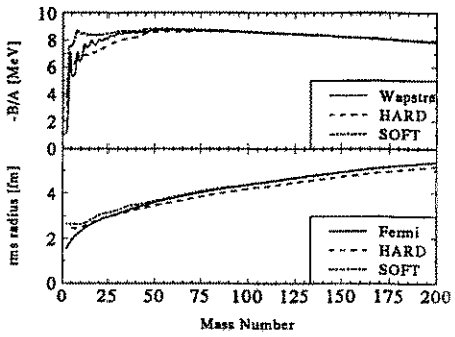

Figure 1: Binding energies and rms radii of the model nuclei. The line labeled "Fermi" is a best fit to the experimental root mean square radii assuming the Fermi distribution of nuclear density.

Initial conditions

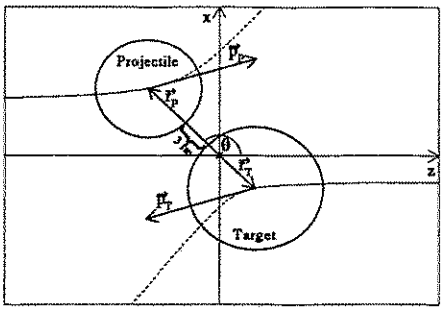

Figure 2: Initial positions and momenta of colliding ions.

Time evolution of $A_P + A_T$ particles

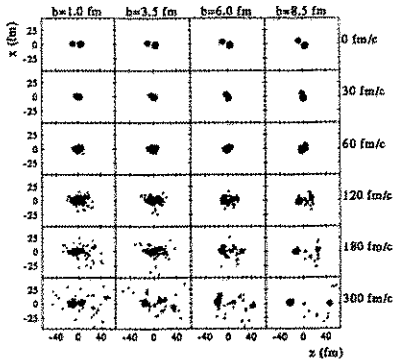

Figure 3: Time evolution of the mean positions of the nucleons predicted by the soft EOS CHIMERA calculation for the 45 MeV/nucleon $^{84}Kr+^{159}Tb$ reaction at 1.0, 3.5, 6.0 and 8.5 fm impact parameter values.

Cluster search

A set of hot fragments

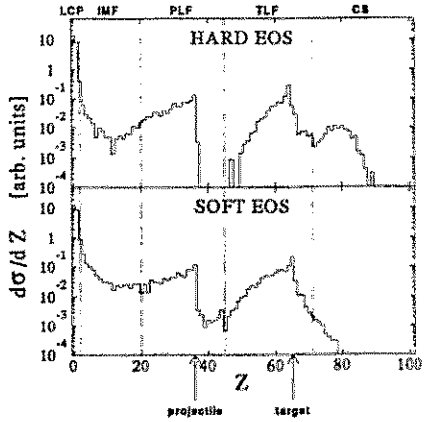

Figure 4: Charge distributions taken at 300 fm/c for the 45 MeV/nucleon ^{84}Kr + ^{159}Tb reaction for the hard (upper panel) and the soft (lower panel) EOS. The dotted lines separate the respective classes of fragments specified at the top of the figure (light charged particles (LCP), intermediate mass fragments (IMF), projectile like fragments (PLF), target like fragments (TLF) and compound systems (CS)).

COOLER
statistical deexcitation

A set of cold fragments

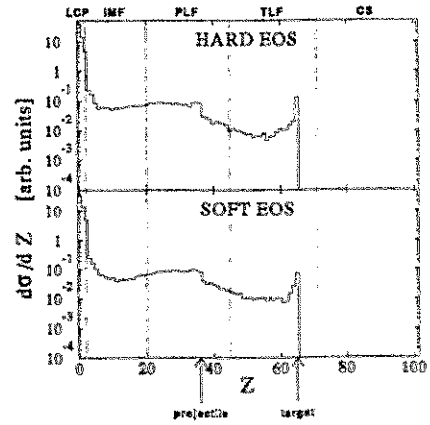

Figure 5: Same as Fig. 4, but for cold fragments (CHIMERA+COOLER).

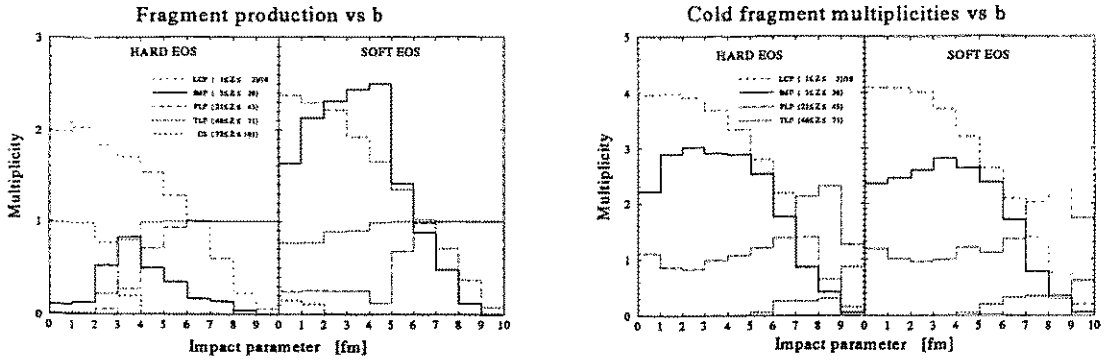

Figure 6,7: Mean multiplicities of various classes of fragments (specified in the legend) versus the impact parameter for the 45 MeV/nucleon $^{84}Kr + ^{159}Tb$ reaction for the hard and the soft EOS. The multiplicities of LCPs were divided by 10. The multiplicities in the figure on the left handside were calculated **after 300 fm/c**, while the multiplicities on the right handside were calculated **for cold fragments**.

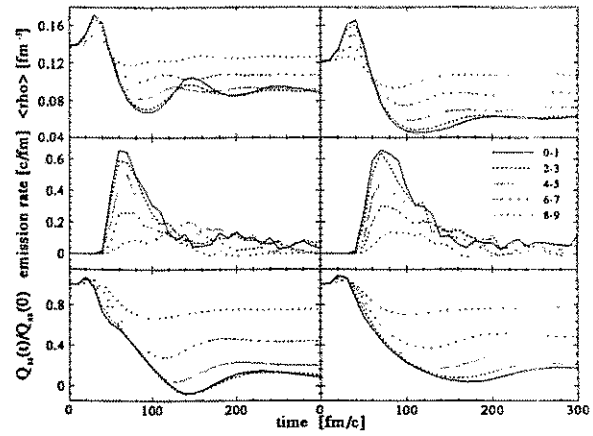

Figure 8: Time evolution of three observables for the 45 MeV/nucleon $^{84}Kr + ^{159}Tb$ reaction for hard (left part) and soft (right part) EOS. The top panels present the evolution of the mean density, the middle panels show the evolution of the emission rates of fragments with $Z \leq 20$ and the bottom panels visualize the evolution of the relative zz-th component of the quadrupole moment tensor in momentum space.

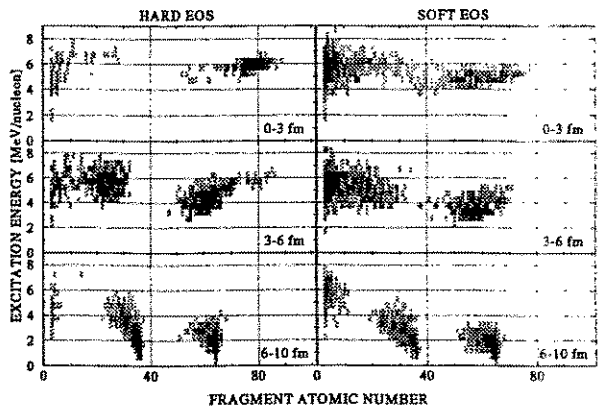

Figure 9: Excitation energy per nucleon of the 45 MeV/nucleon $^{84}Kr + ^{159}Tb$ reaction products versus Z number of the fragment. The energies were calculated at 300 fm/c, for central ($0 \leq b \leq 3$ fm), semi-central ($3 < b \leq 6$ fm) and peripheral ($6 < b \leq 10$ fm) collisions. The left part of the figure represents calculation with the hard EOS while the right part for the soft EOS. The shades of grey scale logarithmically with the number of fragments.

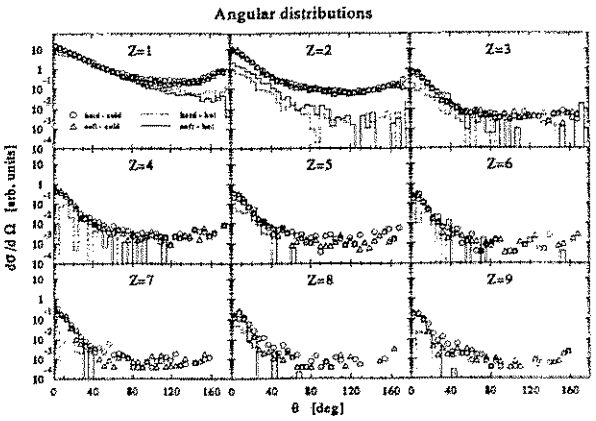

Figure 10: Angular distributions of fragments with Z from 1 to 9. Open circles and triangles represent the asymptotic CHIMERA+COOLER predictions for the hard and soft EOS, respectively, and the dotted and solid histograms present the results of the CHIMERA calculations taken after 300 fm/c.

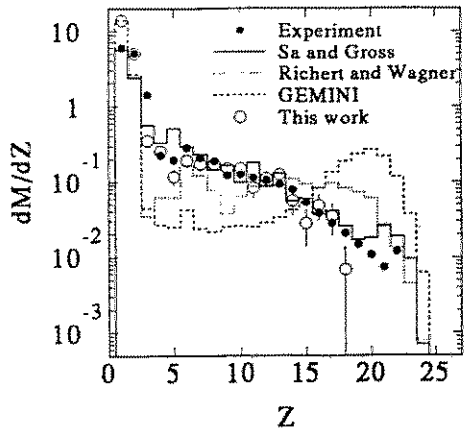

Figure 11: Charge distributions for the ^{40}Ca + ^{40}Ca reaction at 35 MeV/nucleon - experiment and the model calculations. The solid points represent the data taken from the ref. [8], the solid line represents the simultaneous multi-fragmentation calculation of Sa and Gross [9], which assumes an expanded starting nucleus with $\rho \cong 1/6\ \rho_0$, the dotted line represents the binary decay calculation of Richert and Wagner [10], the dashed line represents the statistical code GEMINI [11] calculation, which also treats the fragment emission as sequential and the open circles represent the prediction of the hybrid CHIMERA plus COOLER for central collisions ($b \leq 2$ fm).

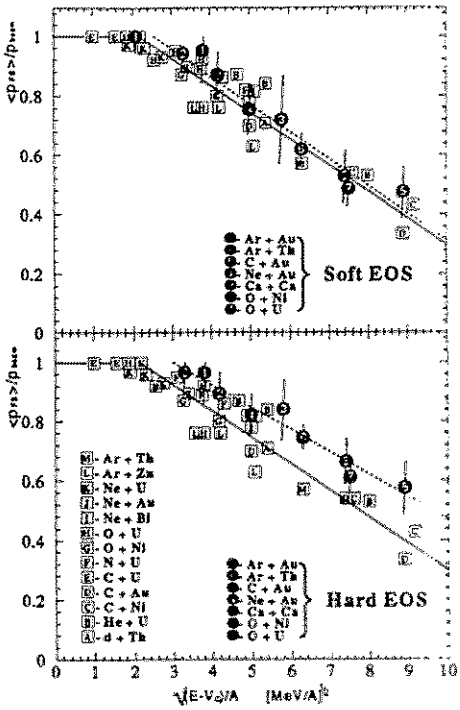

Figure 12: Linear momentum transfer to the heavy residue for various systems. The letters in squares represent the available experimental data. The solid line is the best linear fit to the experimental data. The black circles with digits represent the results of CHIMERA calculations for the specified systems and with the use of the soft (upper part) and hard (lower part) EOS, respectively. The dashed lines are the best fits to the model predictions.

velocities. The actual form of this potential was adopted from the work of Boal and Glosli [2]. Calculations were performed for the nuclear potential corresponding to the hard and soft equation of state (the nuclear matter compressibility K ≅ 380 and 200 MeV, respectively).

- Application of the frictional cooling method [6,2,3] to finding the ground state configurations allowed to reproduce very well the experimental values of the ground state binding energies and rms radii of the nuclei by the model calculations [5] (see also Figure 1). The proper values of the binding energies allowed to calculate the excitation energies of hot fragments.
- The two colliding ions are assumed to move along classical Coulomb trajectories until the distance between their surfaces is 3 fm. This distance was found to be the best compromise between the consequence of neglecting the nuclear force at such a separation, and the requirement to save as much as possible the computer time. Later on the A_P+A_T body dynamics is switched on.
- After a specified time the dynamical evolution is stopped. Now a cluster search routine is called. It is assumed that all the nucleons which are separated in the configuration space by less then d = 3 fm form a single cluster. Each cluster has then assigned a mass number, atomic number, CM position, linear momentum, binding energy, temperature and spin.

Since the reaction products are still hot at the end of the early phase of the reaction (300 fm/c) and may decay in the time scale of the order of 10^7 fm/c, which is out of scope of the CHIMERA code, the microscopic model was supplemented with a statistical dynamical one - COOLER [7]. This code uses the hot fragments produced by CHIMERA as an input and cools them down statistically. It also traces the Coulomb trajectories of all charged fragments.

The asymptotic characteristics of the reaction products could be thus compared with the experimental data. In Fig. 11 such a comparison with the 35 MeV/nucleon ^{40}Ca + ^{40}Ca experiment [8] is presented.

BIBLIOGRAPHY

[1] J. Aichelin and H. Stöcker, *Phys. Lett.* **176B**, 14(1986), G. Peilert, H. Stöcker, W. Greiner, A. Rosenhauer, A. Bohnet, and J. Aichelin, *Phys. Rev.* **C 39**, 1402(1989), C. Hartnack, Li Zhuxia, L. Neise, G. Peilert, A. Rosenhauer, H. Sorge, J. Aichelin, H. Stöcker and W. Greiner, *Nuc. Phys.* **A495**, 303c(1989), L. Neise, M. Berenguer, C. Hartnack, G. Peilert, H. Stöcker and W. Greiner, *Nuc. Phys.* **A519**, 375c(1990), J. Aichelin, G. Peilert, A. Bohnet, A. Rosenhauer, H. Stöcker and W. Greiner, *Phys. Rev. C* **37**, 2451(1988), J. Aichelin, *Phys. Rep.* **202**, 233(1991).

[2] D.H. Boal and J.N. Glosli, *Phys. Rev. C* **38**, 1870(1988),

[3] D.H. Boal and J.N. Glosli, *Phys. Rev. C* **38**, 2621(1988), D.H. Boal, J.N. Glosli and C. Wicentowich, *Phys. Rev. C* **40**, 601(1989), D.H. Boal and J.C.K. Wong, *Phys. Rev. C* **41**, 118(1990).

[4] J. Łukasik and Z.Majka, *Acta Phys. Pol.* **B24,** 1959(1993).

[5] J. Łukasik, Ph.D. Thesis, Jagellonian University, Kraków (1993), unpublished.

[6] L. Wilets, E.M. Henley, M. Kraft and A.D. MacKellar, *Nuc. Phys.* **A282**, 341(1977), L. Wilets, Y. Yariv and R. Chestnut, *Nuc. Phys.* **A301**, 359(1978), D.J.E. Callaway, L. Wilets and Y. Yariv, *Nuc. Phys. A327*, 250(1979).

[7] T. Kozik, to be published, T. Kozik, J. Buschmann, K. Grotowski, J.J. Gills, N. Heide, J. Kiener, H. Klewe-Nebenius, H. Rebel, S. Zagromski and A.J. Cole, *Z. Phys.* **A326**, 421(1987), K. Grotowski, J. Ilnicki, T. Kozik, J.Łukasik, S. Micek, Z. Sosin, A. Wieloch, N. Heide, H. Jelitto, J. Kiener, H. Rebel, S. Zagromski and A.J. Cole, *Phys. Lett.* **223B**, 287(1989).

[8] K. Hagel, M. Gonin, R. Wada, J.B. Natowitz, B.H. Sa, Y. Lou, M. Gui, D. Utley, G. Nebbia, D. Fabris, G. Prete, J. Ruiz, D. Drain, B. Chambon, B. Cheynis, D. Guinet, X.C. Hu, A. Demeyer, C. Pastor, A. Giorni, A. Lleres, P. Stassi, J.B. Viano and P. Gonthier, *Phys. Rev. C* **68**, 2141(1992).

[9] Sa Ban-Hao and D.H.E. Gross, *Nuc. Phys.* **A437**, 643(1985).

[10] J. Richert and P. Wagner, *Nuc. Phys.* **A517**, 399(1990).

[11] R.J. Charity at. al, *Nuc. Phys.* **A483**, 371(1988).

One Step Production of Six Alpha Particles

E. Norbeck[a], L.B. Yang[a], Y.W. Cheng[a], J. Lauret[b], R. Lacey[b], A. Elmaani[b], D. Craig[c], E. Gualtieri[c], S. Hannuschke[c], D. Klakow[c], T. Li[c*], T. Reposeur[c†], A.M. Vander Molen[c], G.D. Westfall[c], J.S. Winfield[c], J. Yee[c], S.J. Yennello[c‡], and A. Nadasen[d]

[a]Dept. of Physics and Astronomy, Univ. of Iowa, Iowa City, IA 52242 USA
[b]Dept. of Chemistry, SUNY-Stony Brook, Stony Brook, NY 11794 USA
[c]NSCL, Michigan State University, East Lansing, MI 48824 USA
[d]Dept. of Physics, Univ. of Michigan at Dearborn, Dearborn, MI 48128 USA

For the reaction, $^{12}C + ^{12}C \rightarrow 6\,^4He$, the Born approximation allows the calculation of the cross section for all possible final states in the 18 dimensional phase space of the 6α particles. The largest cross sections occur when there are spectators, that is particles for which the original momentum is not changed by the reaction. The largest spectator peak is expected to be the one for which two α particles from the beam and two from the target are spectators. In this case one third of the momentum of the beam and one third of the energy of the beam, less the breakup energy of about 15 MeV, are shared by the two active α particles. Figure 1 shows such a peak at 605 MeV (with an 1860 MeV ^{12}C beam). Because the spectators have no transverse momentum, the two active α particles must appear on opposite sides of the beam. With the condition that the azimuthal angle between the two observed α particles is greater than 120°, the peak is clearly visible (Fig. 1a). If the azimuthal angle is less than 100°, the peak is much reduced (Fig. 1b).

Peaks similar to those in Fig. 1 were found, with about the same ratio to background, for carbon beams of energies from 660 to 1860 MeV. The beams were produced by the National Superconducting Cyclotron at Michigan State University. The particles were detected with the MSU 4π Array. For details of the experiment see [1].

The model has been tested extensively for the reaction $^6Li + ^6Li \rightarrow 3\,^4He$ [2–4]. With $^6Li + ^6Li$, the reaction accounts for a large fraction of the total reaction cross section. With $^{12}C + ^{12}C$ there are many more competing reactions. If the experiment is not specifically designed to study this reaction, the large background allows only the largest peaks from the direct process to be seen. Most of the background in Fig. 1 is from events with α particles along with other particles that are not observed. A smaller part of the background comes from events in which some of the active α particles are not observed.

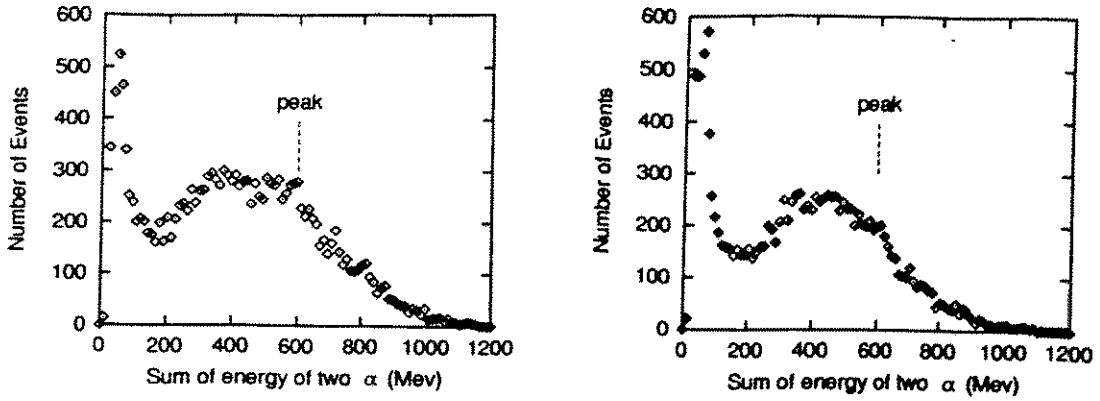

Figure 1. (a) Number of two α-particle events as a function of the sum of the energies of the two α particles when the azimuthal angle between them is greater than 120°. (b) Same as (a) but with the azimuthal angle less than 100°.

THE MODEL

The peak shown in Fig. 1a is actually the coherent sum of the one step process with the two step process $^{12}C+{}^{12}C \rightarrow 2\,{}^{4}He+2\,{}^{8}Be \rightarrow 6\,{}^{4}He$. Here we are concerned with only the α particles from the first of the two steps. The 4-body calculation is simpler than the full 6-body calculation and will be presented first.

The differential cross section according the Born approximation is

$$\frac{d\sigma^n}{dp^n} = \frac{2\pi}{\hbar^2}\frac{\mu}{k}\rho(p^n)|\langle\psi_f|V|\psi_i\rangle|^2$$

in which n is the number of independent parameters (angles and energies), 8 for a 4-particle final state and 14 for a 6-particle final state. The reduced mass of the beam and target is μ and $\hbar k$ is their relative momentum. For the first step of the $^{12}C+{}^{12}C$ reaction the phase-space factor, ρ, is given by R. E. Warner [5] who used it for the identical, except for a factor of two in the masses, $^{6}Li+{}^{6}Li \rightarrow 2\,{}^{4}He+2\,d$ reaction. The phase-space factor is nearly constant in the region of phase space where the cross section is varying rapidly.

The rapid variation is in the matrix elements $\langle\psi_f|V|\psi_i\rangle$ in which ψ_f is the final state with each particle expressed as a plane wave. The initial state ψ_i contains the motion of the beam and target (as plane waves) times the bound state wave functions. The interaction potential, V, is the sum of the interactions between every pair of particles. The matrix elements will be evaluated here only for the parts of the potential that give rise to the peaks of interest. The $^{6}Li+{}^{6}Li$ studies showed that a delta-function interaction

gives about the same results as a longer range interaction [4]. To simplify the calculation of relative cross sections, all of the constant, or slowly varying, multiplicative factors will be set to unity. The coordinates of the nuclei and clusters are indicated in Figs. 2 and 3.

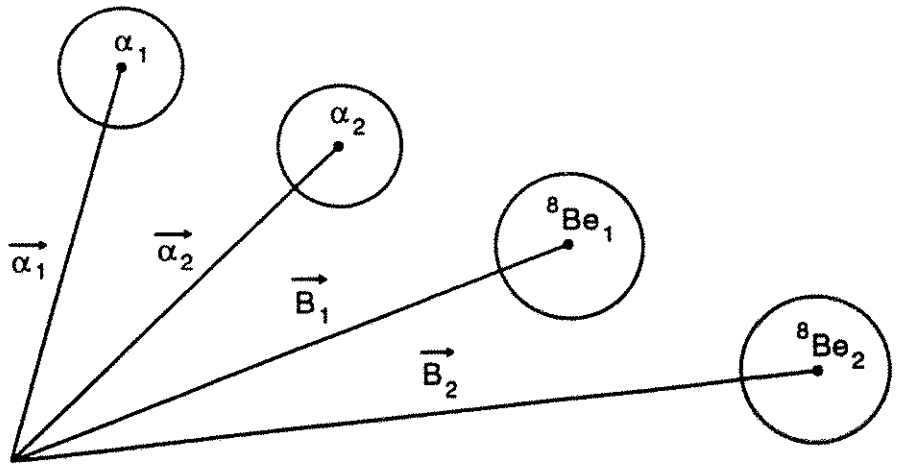

Figure 2. Final state coordinates for $^{12}C + {}^{12}C \rightarrow 2\,{}^4He + 2\,{}^8Be$.

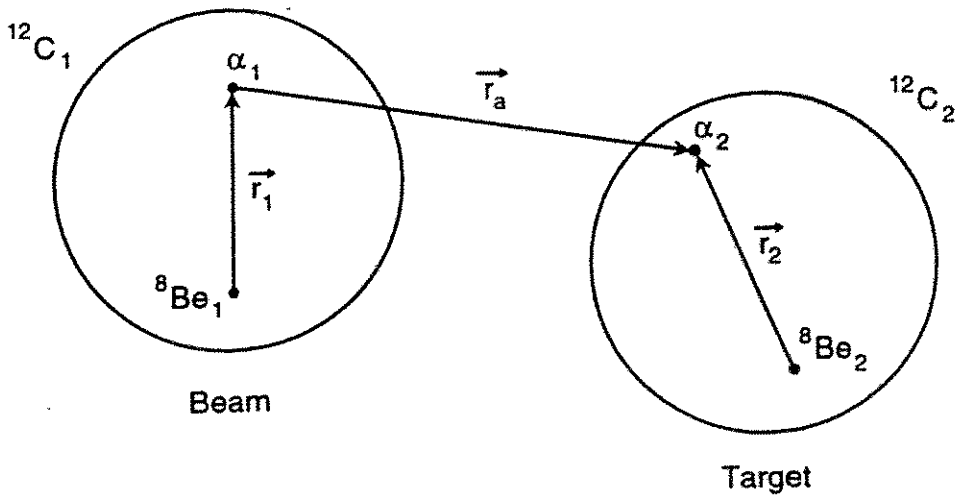

Figure 3. Initial state coordinates. The coordinates of the beam and target are $\vec{r_B}$ and $\vec{r_T}$.

$$\psi_f = \exp(i\overrightarrow{k_{\alpha 1}} \cdot \overrightarrow{\alpha_1} + i\overrightarrow{k_{\alpha 2}} \cdot \overrightarrow{\alpha_2} + i\overrightarrow{k_{B1}} \cdot \overrightarrow{B_1} + i\overrightarrow{k_{B2}} \cdot \overrightarrow{B_2})$$

$$\psi_i = \exp(i\overrightarrow{k_B} \cdot \overrightarrow{r_B} + i\overrightarrow{k_T} \cdot \overrightarrow{r_T})\,\phi_B(\overrightarrow{r_1})\,\phi_T(\overrightarrow{r_2})$$

$$V = \delta(\overrightarrow{r_a})$$

in which $\overrightarrow{r_B} = \dfrac{\overrightarrow{\alpha_1} + 2\overrightarrow{B_1}}{3}$ and $\overrightarrow{r_T} = \dfrac{\overrightarrow{\alpha_2} + 2\overrightarrow{B_2}}{3}$.

The meaning of the various $\overrightarrow{k}$ can be seen from the final and initial wave functions. The initial momentum of the target nucleus, $\hbar\overrightarrow{k_T}$, is given explicitly and is not set to zero. The advantage of plane waves is that the coordinates can be separated so that the integrals can be evaluated. It is first necessary to write the various coordinates in terms of the arguments in the bound state wave functions ϕ_B and ϕ_T and the potential V. The following relations can be deduced from an examination of Fig. 3.

$$\overrightarrow{\alpha_1} = \overrightarrow{\alpha_2} - \overrightarrow{r_a}$$

$$\overrightarrow{B_1} = \overrightarrow{\alpha_2} - \overrightarrow{r_a} - \overrightarrow{r_1}$$

$$\overrightarrow{B_2} = \overrightarrow{\alpha_2} - \overrightarrow{r_2}$$

After collecting the various terms, the matrix element can be written as

$$\begin{aligned}\langle\psi_f|\delta(\overrightarrow{r_a})|\psi_i\rangle = \int d\overrightarrow{\alpha_2} \exp(-i\overrightarrow{k_{\alpha 1}} - i\overrightarrow{k_{\alpha 2}} - i\overrightarrow{k_{B1}} - i\overrightarrow{k_{B2}} + i\overrightarrow{k_B} + i\overrightarrow{k_T}) \cdot \overrightarrow{\alpha_2} \\ \times V \int d\overrightarrow{r_a}\,\delta(\overrightarrow{r_a}) \exp(i\overrightarrow{k_{\alpha 1}} + i\overrightarrow{k_{B1}} - i\overrightarrow{k_B}) \cdot \overrightarrow{r_a} \\ \times \int d\overrightarrow{r_1}\,\phi_B(\overrightarrow{r_1}) \exp(i\overrightarrow{k_{B1}} - \tfrac{2}{3}i\overrightarrow{k_B}) \cdot \overrightarrow{r_1} \\ \times \int d\overrightarrow{r_2}\,\phi_T(\overrightarrow{r_2}) \exp(i\overrightarrow{k_{B2}} - \tfrac{2}{3}i\overrightarrow{k_T}) \cdot \overrightarrow{r_2}\ .\end{aligned}$$

The first integral contains the requirement for conservation of momentum in the reaction. The second integral is a constant. If the particles are assumed to be bound in square wells the last two integrals are the same and can be evaluated analytically. The value of this integral is [2]

$$I(\Delta) = \left(\frac{2\beta}{1+\beta R}\right)^{1/2} \frac{1}{\Delta}\left\{\frac{\Delta \sin\gamma R \cos\Delta R - \gamma \cos\gamma R \sin\Delta R}{\gamma^2 - \Delta^2}\right.$$
$$\left. + \frac{\sin\gamma R}{\beta^2 + \Delta^2}\left(\beta \sin\Delta R + \Delta \cos\Delta R\right)\right\}$$

in which Δ is the magnitude of the coefficient of the integration variable in the exponential term. The coefficients β and γ appear in the wave functions, ϕ_B and ϕ_T, as a factor in $\exp(-\vec{\beta} \cdot \vec{r})$ for $r > R$ and in $\sin(\vec{\gamma} \cdot \vec{r})$ for $r < R$.

If we assume the α particle is bound in a $3S$ state (to satisfy the Pauli principle) in a square well of radius $1.2(12)^{1/3}$ with a separation energy of 7.37 MeV, the matrix element is completely determined. The bound state integral is similar to $\frac{\sin\Delta}{\Delta}$ with a maximum at $\Delta = 0$. For $\Delta = 0$ the ^{8}Be in the beam (or target) ends up with two thirds of the initial beam (or target) momentum. This is the condition for being a spectator. The width of $I(\Delta)$ is such that a ^{8}Be target spectator can acquire a kinetic energy of about 1.0 MeV. However, the same energy in the center of mass of a ^{8}Be beam spectator corresponds to a kinetic energy of about 70 MeV in the laboratory system. The spread in energy of the spectators produces a corresponding spread in the total kinetic energy of the active particles.

For the direct break up into 6α particles, the calculation is about the same. The relative location of the three α particles in each carbon are given by Jacobi coordinates whose relation to the absolute locations, $\vec{\alpha}$, of the α particles is shown in Fig. 4.

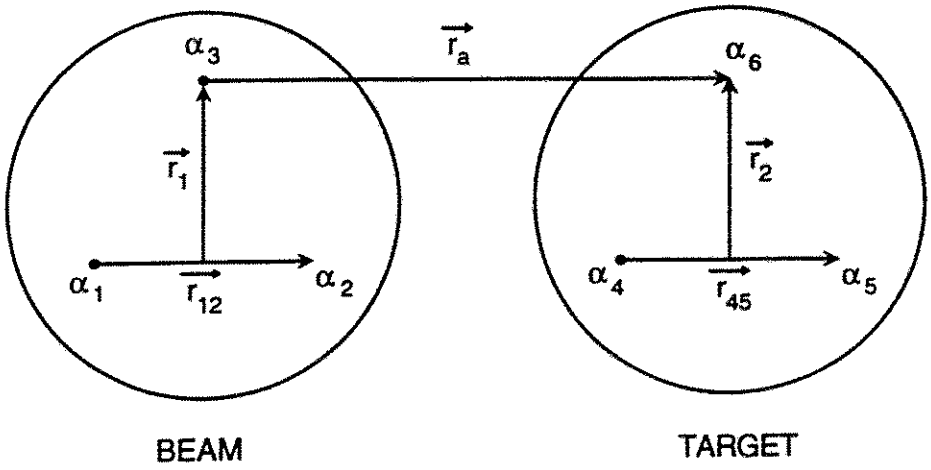

Figure 4. Initial state coordinates for ^{12}C as three α clusters.

$$\alpha_1 = \alpha_6 - r_a - r_1 - \tfrac{1}{2}r_{12}$$
$$\alpha_2 = \alpha_6 - r_a - r_1 + \tfrac{1}{2}r_{12}$$
$$\alpha_3 = \alpha_6 - r_a$$
$$\alpha_4 = \alpha_6 - r_2 - \tfrac{1}{2}r_{45}$$
$$\alpha_5 = \alpha_6 - r_2 + \tfrac{1}{2}r_{45}$$

$$\psi_f = \exp(i\vec{k_{\alpha 1}}\cdot\vec{\alpha_1} + i\vec{k_{\alpha 2}}\cdot\vec{\alpha_2} + i\vec{k_{\alpha 3}}\cdot\vec{\alpha_3} + i\vec{k_{\alpha 4}}\cdot\vec{\alpha_4} + i\vec{k_{\alpha 5}}\cdot\vec{\alpha_5} + i\vec{k_{\alpha 6}}\cdot\vec{\alpha_6})$$
$$\psi_i = \exp(i\vec{k_B}\cdot\vec{r_B} + i\vec{k_T}\cdot\vec{r_T})\,\phi_B(\vec{r_{12}},\vec{r_1})\,\phi_T(\vec{r_{45}},\vec{r_2})$$
$$V = \delta(\vec{r_a})$$
$$\vec{r_B} = \frac{\vec{\alpha_1}+\vec{\alpha_2}+\vec{\alpha_3}}{3} \qquad \vec{r_T} = \frac{\vec{\alpha_4}+\vec{\alpha_5}+\vec{\alpha_6}}{3}$$
$$\vec{r_B} = \vec{\alpha_6} - \vec{r_a} - \tfrac{2}{3}\vec{r_1} \qquad \vec{r_T} = \vec{\alpha_6} - \tfrac{2}{3}\vec{r_2}$$

$$\langle t|V|i\rangle = \int d\vec{\alpha_6}\exp i(\vec{k_B}+\vec{k_T}-\vec{k_{\alpha 1}}-\vec{k_{\alpha 2}}-\vec{k_{\alpha 3}}-\vec{k_{\alpha 4}}-\vec{k_{\alpha 5}}-\vec{k_{\alpha 6}})\cdot\vec{\alpha_6}$$
$$\times \int d\vec{r_a}\,\delta(\vec{r_a})\exp(i\vec{k_{\alpha 1}}+i\vec{k_{\alpha 2}}+i\vec{k_{\alpha 3}}-i\vec{k_B})\cdot\vec{r_a}$$
$$\times \iint d\vec{r_{12}}\,d\vec{r_1}\,\phi_B(\vec{r_{12}},\vec{r_1})\exp(\tfrac{i}{2}\vec{k_{\alpha 1}}-\tfrac{i}{2}\vec{k_{\alpha 2}})\cdot\vec{r_{12}}\exp(i\vec{k_{\alpha 1}}+i\vec{k_{\alpha 2}}-\tfrac{2}{3}i\vec{k_B})\cdot\vec{r_1}$$
$$\times \iint d\vec{r_{45}}\,d\vec{r_2}\,\phi_T(\vec{r_{45}},\vec{r_2})\exp(\tfrac{i}{2}\vec{k_{\alpha 4}}-\tfrac{i}{2}\vec{k_{\alpha 5}})\cdot\vec{r_{45}}\exp(i\vec{k_{\alpha 4}}+i\vec{k_{\alpha 5}}-\tfrac{2}{3}i\vec{k_T})\cdot\vec{r_2}$$

In the integrals over the bound states, the integrals over $\vec{r_1}$ and $\vec{r_2}$ correspond to the same integrals in the ^{8}Be + ^{4}He calculation. The difference is that the final momentum of each ^{8}Be cluster is replaced by the sum of the momenta of a pair of α particles. The form of the other integrals over the bound states suggests that the peak in the cross section is large when the difference of the two momenta is small. The coefficient of $\vec{r_{12}}$ (and $\vec{r_{45}}$) in the exponential is zero when the momenta of the two α particles are the same. The two relations together are equivalent to having a ^{8}Be spectator.

COMMENTS

The one-step, direct reaction model is at the opposite pole from the classical dynamical α-cluster model [6] that follows the microscopic details of the collision process. However, both models predict a large production of spectator α-particles.

If the potential acts between the two ^{8}Be clusters the cross section is large when the two α particles are spectators. The calculation is the same as above but with some relabeling of the coordinates. Because of the symmetry of the calculation, one should expect a large peak in the sum of the energy for 4α particles at two thirds of the beam energy. In fact, the number of 4α particle events was two orders of magnitude smaller than the number of two α particle events. Because the detectors in the 4π Array are quite large, both particles from the break up of ^{8}Be usually go into the same detector and are recorded as a pile-up event.

Using a different relabeling of the coordinates so that the potential acts between an α particle in one carbon nucleus and a ^{8}Be in the other, the cross section is large when one α particle and one ^{8}Be are spectators. This results in peaks in the sum of the energy of three α particles at energies of one third and two thirds of the beam energy. Such peaks do appear in the data, but the total number of counts is small and is mostly background.

The calculations presented here show the essential features of the Born approximation method. There are many improvements that would make small changes in the predicted cross sections. The wave functions need to be symmetrized with respect to all of the α particles. Relativistic corrections should be observable at the beam energy used in the experiment. Better wave functions would give better predictions.

The same kind of calculation can be applied to many nuclear reactions, but the peaks are large and distinct only when the reaction has considerable symmetry. We plan to study $^{24}\mathrm{Mg} + {}^{24}\mathrm{Mg} \rightarrow$ both $3\,{}^{16}\mathrm{O}$ and $4\,{}^{12}\mathrm{C}$.

The $^{12}\mathrm{C} + {}^{12}\mathrm{C}$ data was originally processed with the goal of finding the energy for the disappearance of flow [1]. We are currently reprocessing the data in a different way to reduce the backgrounds that interfere with the direct reaction studies.

REFERENCES

* Present address: SuperNova International, 5712 Shaw St., Haslett, MI 48840 USA

† Present address: University of Nantes, Nantes, France

‡ Present address: Texas A & M University, College Station, TX 77843 USA

[1] G.D. Westfall et al. *Phys. Rev. Lett.* **71**, (1993) 1986.

[2] L.L. Gadeken and E. Norbeck *Phys. Rev. C* **6**, (1972) 1172.

[3] L.L. Gadeken and E. Norbeck *Phys. Rev. Lett.* **27**, (1971) 952; M. Lattuada et al. *Z. Phys. A* **330**, (1988) 183.

[4] E. Norbeck et al. *Phys. Rev. C* **23**, (1981) 2557.

[5] R.E. Warner *Nucl. Phys. A* **379**, (1982) 191.

[6] A. Szczurek, A. Budzanowski, L. Jarczyk, A. Magiera, K. Möhring, R. Siudak, and T. Srokowski *Z. Phys. A* **338**, (1991) 187.

POSSIBLE MECHANISM OF LIGHT NUCLEI PRODUCTION IN FUSION OF HEAVY IONS

N.V.Antonenko[1,2], R.V.Jolos[1,2] and W.Scheid[1]

[1] *Institut für Theoretische Physik der Justus–Liebig–Universität, D–35392 Giessen, Germany*

[2] *Joint Institute for Nuclear Research, 141980 Dubna, Russia*

Abstract

A possible mechanism of the production of light nuclei in fusion reactions is considered. It is shown that the decay of the dinuclear system evolving to a compound nucleus yields a substantial rate for the production of light nuclei. The cross section of this process is calculated for reaction ^{58}Ni+^{58}Ni. The coupling of modes of motion causes an increase of asymmetric decay of the dinuclear system.

1. INTRODUCTION

Two mechanisms can contribute to the production of light nuclei with $Z > 2$ in fusion reactions of heavy ions at low energy. One of them is a cluster evaporation from the compound nucleus [1] and the other is the decay of a dinuclear system (DNS) at a preequilibrium stage of reaction [2,3]. The last mechanism plays a significant role in the process of compound nucleus formation if it proceeds through an increase of the mass asymmetry of the DNS. In this case the fusion is interpreted in the following way: the dinuclear system formed after a capture stage evolves to a compound nucleus via the nucleon transfer from a light nucleus to a heavy one.

It is possible of course that after the capture stage the neck between the nuclei grows quite quickly and a deformed united system is formed. The further processes are determined by the evolution of this nuclear system. Its form will approach the equilibrium one if the initial distance between the nuclei is less then the value corresponding to the saddle point of the compound nucleus. Otherwise the formation of the compound nucleus is not possible and the system goes to the quasifission channel. Both mechanisms are combined in reality and their relative role can change from reaction to reaction.

In the reactions with heavy nuclei the deformed compound nucleus at the saddle point is more compact than a dinuclear system. So, the channel connected with the increase of the neck radius contributes mainly to the quasifission cross section. The channel connected with the increase of the mass asymmetry becomes important for the description of the fusion cross section. For example, this was confirmed by the calculation of fusion cross sections in the reactions ^{100}Mo+^{100}Mo and ^{110}Pd+^{110}Pd [4].

In reactions with light nuclei the channel connected with the increase of neck radius contributes mainly to the compound nucleus formation. However, the competition of two channels is possible. The decay of very asymmetric configurations of the DNS can enhance the yield of light nuclei. Therefore, the investigation of the production of light nuclei gives us additional, although indirect, information on the fusion reaction mechanism.

In this work we investigate the preequilibrium light particle production in the reaction ^{58}Ni+^{58}Ni. This reaction is interesting due to its intermediate place between the reaction with heavy and light nuclei. The compound nucleus formation goes here mainly through the change of a united system form. Nevertheless, the channel of the DNS evolution contributes to the production of light nuclei with $Z > 2$.

2. MODEL

2.1. Charge distribution

Nuclei fusion proceeding through an increase of the mass asymmetry of the DNS appears to be consistent with the following qualitative picture [4]: (i) after total dissipation of the initial kinetic energy the rotating DNS is formed. (ii) A diffusion process leads to the nucleon exchange between two touching fragments, thus generating a time-dependent distribution in the charge (mass) asymmetry of the DNS. The DNS evolves to a compound nucleus by the nucleon transfer from a light nucleus to a heavy one. (iii) There is a certain decay probability of the DNS evolving to a compound nucleus. Just the asymmetric DNS decay contributes to the production of light nuclei with $Z > 2$ in fusion of heavy ions at low energies. In comparison with deep inelastic transfer reactions, where the DNS decays inevitably, in the fusion reactions the decay probability of the DNS is smaller than 1.

As a result of the above stated, the cross section of the production of light nuclei depends on the formation probability P_Z of the DNS configuration with the charge number Z of the light fragment and on the decay probability Λ_Z. Thus, our task is to calculate P_Z and then to determine Λ_Z. To calculate P_Z, a diffusion equation can be used [5]. The values of Λ_Z can be calculated by a classical treatment of the DNS using two macroscopic degrees of freedom (the distance between the nuclei centers R and the mass asymmetry of the DNS η) [3].

We determine the cross section of the production of light nuclei by the expression similar to that used in [5]

$$\frac{d\sigma}{dZ} = \frac{\pi}{E_p m A_p} \int_0^\infty dt \int_0^\infty dJ\, J\Phi(J) P_Z(J,t) G(t) \Lambda_Z(J), \qquad (1)$$

where A_p and E_p are the mass number and the energy of the projectile, respectively. The factor $G(t)$ represents the probability that the interaction time is t. $\Phi(J)$ is the probability of defined reaction class (deep inelastic transfer, fusion and so on) at the angular momentum J. Choosing $\Phi(J)$ in (1) we can obtain the contribution of the defined reaction class to the observed charge distribution. The time integration in (1) gives the cross section averaged over

possible interaction times. The factor $\pi(E_p m A_p)^{-1} J dJ$ defines the element of the geometric cross section.

Putting $\Lambda_Z(J) = 1$ in (1) we get the known expression used for the calculations of the charge distributions in the deep inelastic transfer reactions [5]. Since these reactions occur mainly for J near the critical angular momentum J_{crit}, then we may use the following parameterizations

$$\Phi(J) = \exp\left(-\frac{|J_{crit} - J|}{\Delta J}\right), \tag{2}$$

$$G(t) = \frac{1}{\tau_0}\exp\left(-\frac{t}{\tau_0}\right), \tag{3}$$

where τ_0 is a mean life time of the DNS. The expressions (1–3) allow one to obtain the contribution of the deep inelastic transfers to the light nuclei production.

If Z is far from the projectile charge the formation probability P_Z is small for trajectories with $J > J_{crit}$. For J near J_{crit} it increases because of the increase of the interaction time. For $J < J_{crit}$ the interaction time becomes larger and we can simplify (1)

$$\left(\frac{d\sigma}{dZ}\right)_{J<J_{crit}} = \frac{\pi}{E_p m A_p}\int_0^{J_{crit}} J P_Z(J, \tau_{int})\Lambda_Z(J) dJ. \tag{4}$$

At this point we suppose that all trajectories with $J < J_{crit}$ have the same interaction time τ_{int}. The value of J_{crit} for the reaction ^{58}Ni+^{58}Ni practically coincides with the value of momentum $J_{B_f=0}$ which corresponds to the vanishing of the fission barrier of the compound nucleus ^{116}Ba. Therefore, at $J < J_{crit}$ the fusion reaction takes place and we can put $\Phi(J) = 1$. Using (4) the cross section of the production of light nuclei in fusion of heavy ions can be calculated.

It has been assumed above that factors P_Z and Λ_Z can be considered separately. This is possible because the characteristic time for nucleon transition from one nucleus to other one is less than the decay time of the DNS. In the forthcoming publication we shall consider the nucleon transfer and the DNS decay simultaneously.

2.2. Formation probability P_Z

To calculate P_Z we use the master equation

$$\frac{d}{dt}P_Z(J,t) = \Delta^{(-)}_{Z+1}(J)P_{Z+1}(J,t) + \Delta^{(+)}_{Z-1}(J)P_{Z-1}(J,t) - (\Delta^{(+)}_Z(J) + \Delta^{(-)}_Z(J))P_Z(J,t), \tag{5}$$

which is indeed a suitable tool to describe the evolution of the DNS. In (5) $\Delta^{(\pm)}_Z(J)$ are the transport coefficients which can be calculated microscopically [6] or can be parameterized [5]. Since the transport coefficients obtained in both these approaches are similar [7], we use the following parameterization [5]

$$\Delta^{(\pm)}_Z(J) = kf\exp\left(\frac{U(Z,J) - U(Z\pm1,J)}{2T}\right). \tag{6}$$

Here $U(Z,J)$ is the potential energy of the DNS (driving potential) with the charge number Z of the light fragment at angular momentum J. We have used $U(Z,J)$ instead of the ground state energy of the DNS in accordance with the results of [7]. In the calculation of $U(Z,J)$, the distance R for each Z corresponds to a position of the potential pocket minimum (see Sec. 3). The local thermodynamic temperature T is calculated by means of the expression $T = \sqrt{(U(Z_0,J) + E_0^*(J) - U(Z,J))/a}$, where $a = A/8$ MeV^{-1}, $U(Z_0,J)$ is the potential energy of the initial DNS and A is the nucleon number of the DNS. The excitation energy of the initial DNS $E_0^*(J)$ is the difference between the energy in c.m.s. $E_{c.m.}$ and the value of the nucleus-nucleus potential for R corresponding to the bottom of the pocket. Note that the values of $E_{c.m.}$ above the Coulomb barrier are considered in the present paper. In (6) f is the geometric factor

$$f = 2\pi \frac{R_1 R_2}{R_1 + R_2} d \qquad (d = 1.0\text{fm}), \tag{7}$$

where R_1, R_2 are the radii of the interacting nuclei. The value k in (6) defines the time scale ($k = 0.5 \cdot 10^{20}\text{s}^{-1} \cdot \text{fm}^{-2}$).

Solving the equations (5) we obtain the dependence of charge distribution on time. To obtain the measurable charge distribution we should multiply P_Z by the decay probability.

2.3. Decay probability of the DNS

As it was mentioned above the decay probability Λ_Z for the collisions with $J < J_{crit}$ is smaller than 1 and has to be calculated. In the notation of [3], we take the collective Hamiltonian of the DNS in the following form

$$H_{coll} = \frac{1}{2}\mu\dot{R}^2 + \frac{1}{2}B_{\eta\eta}\dot{\eta}^2 - B_{R\eta}\dot{R}\dot{\eta} + U(R,\eta,J), \tag{8}$$

where $\mu = mA_1A_2/(A_1 + A_2)$ is the reduced mass. The mass asymmetry is defined by $\eta = (A_1 - A_2)/(A_1 + A_2)$, where A_1 and A_2 are the fragment mass numbers. $U(R,\eta,J)$ is the potential energy of the DNS depending on R, η and J. One-to-one correspondence between η and Z is assumed. The mass coefficients have the form

$$B_{\eta\eta} = \mu\xi^2 + \tilde{B}_\eta, \qquad B_{R\eta} = \xi\mu, \tag{9}$$

where

$$\begin{aligned} \tilde{B}_\eta &= \frac{mA^2}{12} \sum_{i=1,2} \frac{R_i^2}{A_i} \sum_{\lambda=2}^{\infty} \frac{2\lambda+1}{\lambda} \left(\frac{I_{\lambda+1/2}(2R_i^2/r_w^2)}{I_{1/2}(2R_i^2/r_w^2)} \right)^2, \\ \xi &= -\frac{A}{2} \left[\frac{R_1}{A_1} \left(1 - \frac{r_w^2}{2R_1^2} \right) - \frac{R_2}{A_2} \left(1 - \frac{r_w^2}{2R_2^2} \right) \right]. \end{aligned} \tag{10}$$

Here, $A = A_1 + A_2$, r_w is the radius of the window between the nuclei and $I_{\lambda+1/2}(x)$ is the modified Bessel function. Expressions (10) have been obtained in [3].

It is well seen that at $\xi = 0$ $A_1 = A_2$ and that $B_{R\eta}$ is negligible around the symmetric configuration. However, for the configurations with large mass asymmetry $B_{R\eta}$ is not small and should be taken into account. Due to this nondiagonal coupling the energy contained in the mass asymmetry mode is transferred to the radial mode of motion. Therefore, the DNS approaches the radial potential barrier when moving from the Businaro–Gallone (η_{BG}) maximum of the potential $U(R, \eta, J)$ to more asymmetric configurations. This leads to an increase of the decay probability.

To obtain $\Lambda_Z(J)$, we have to determine the distribution function $f(R, \eta, p_R, p_\eta, t)$ of collective coordinates and conjugated momenta by solving the Fokker–Plank equation for f [3]. The distribution function of the distances between the fragment centers is of a particular interest for us.

$$\begin{aligned} P(R, J, t) &= \int f(R, \eta, p_R, p_\eta, t) d\eta dp_R dp_\eta \\ &= (2\pi\chi_{RR}(t))^{-1/2} \exp\left(-\frac{(R - \bar{R}(t))^2}{2\chi_{RR}(t)}\right). \end{aligned} \tag{11}$$

Here $\bar{R}(t)$ and $\chi_{RR}(t)$ are the average value of R and the variance of the radial distribution, respectively. Due to our assumption on the classical motion along η we can write

$$P(R, J, t) = P(R, J, \bar{\eta}(t)).$$

Using (11) the decay probability can be obtained as follows way

$$\Lambda_Z(J) = \int_{R_b}^{\infty} P(R, J, \bar{\eta}) dR, \tag{12}$$

where $\bar{\eta}$ corresponds to Z, and R_b defines the barrier position of the nucleus–nucleus potential for given Z. The main advantage of use the Fokker–Planck equation for the dynamic description of the DNS is the possibility to include the penetration through the potential barrier and the influence of thermal and quantum fluctuations.

3. RESULTS

3.1. Potential energy of the DNS

The calculation of the potential energy of the DNS is needed in order to obtain the transport coefficients (6) and to solve the Fokker-Plank equation. Let us consider here only the interaction of spherical fragments, neglecting a possible deformation. The value of $U(R, Z, J)$ is defined as

$$U(R, Z, J) = B_1 + B_2 + V_{coul}(R) + V_n(R) + V_{rot}(R, J) - (B_{12} + V'_{rot}(J)), \tag{13}$$

where B_1, B_2 and B_{12} are the binding energies of the fragments and the compound nucleus, V_n, V_{coul} and V_{rot} are the nuclear, Coulomb and centrifugal parts of the nucleus–nucleus

potential, respectively. The value of U in (13) is normalized on the energy of the rotating compound nucleus by $B_{12} + V'_{rot}$.

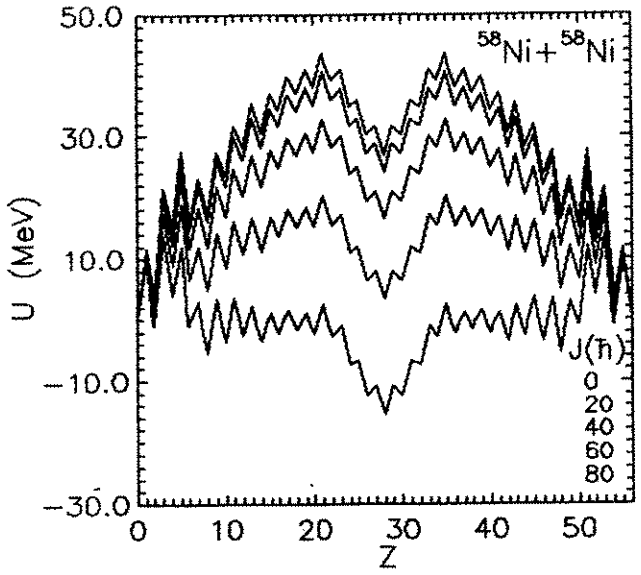

Fig.1. Driving potential (13) for the system ^{58}Ni+^{58}Ni as a function of Z for different values of J. The distance R for each configuration corresponds to the position of potential pocket minimum. The energy scales are normalized to the total energy of the rotating compound nucleus. The sequence $J = 0,\ 20,\ 40,\ 60,\ 80\hbar$ is assigned to curves from top to bottom.

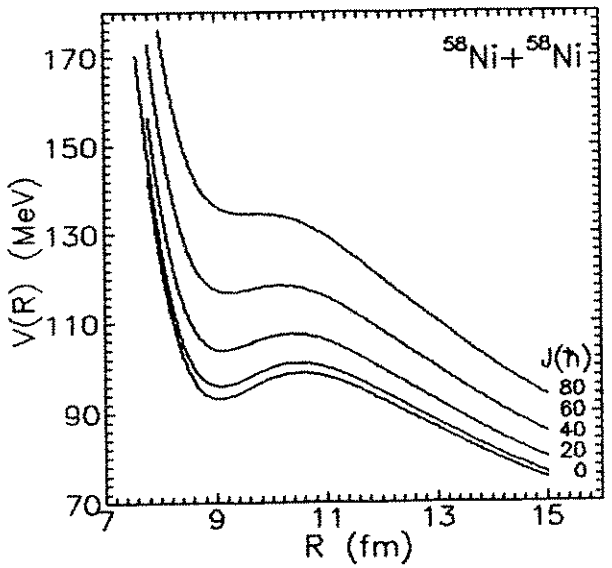

Fig.2. Radial dependence of nucleus-nucleus potential for the system ^{58}Ni+^{58}Ni at different values of J. The sequence $J = 0,\ 20,\ 40,\ 60,\ 80\hbar$ is assigned to curves from bottom to top.

The dependence of $U(R, Z, J)$ on Z is presented for different angular momenta in Fig.1. The distance R for each configuration corresponds to the position of the potential pocket minimum. Binding energies were taken from [8,9]. The mass number of the light nucleus was extracted from the minimization condition of $U(R, Z, J)$. A large influence of the shell structure of the interacting nuclei on $U(R, Z, J)$ can be seen. This is in agreement with the strong influence of the structure of the light nucleus on the nucleon exchange between the nuclei [6].

At high values of J the energy of the symmetric configuration approaches the energy of the compound nucleus and then becomes less than this energy. At low bombarding energies and high J the DNS can not overcome the BG maximum and the channel of compound nucleus formation is closed. Instead of compound configurations quasimolecular configurations with a sufficiently long lifetime can occur [10,11]. If we consider neutron deficient nuclei far from stability line which have relatively small binding energies, then some of their excited states can be imagined as formed by two strongly bound interacting fragments. Constituent fragments are strongly bound because, being lighter, they have such an N/Z-ratio that corresponds to stability line. Due to the balance in binding energies these cluster-type states can appear at relatively low excitation energies. The investigation of the relationship between the DNS configurations and exotic nuclear shapes is a separate interesting problem [12].

As it is seen in Fig.2 the potential pocket disappears for $J > 60\,\hbar$. The fission barrier of the compound nucleus is equal to zero at $J > 60\,\hbar$. Therefore, at high angular momenta ($\Lambda_Z(J) = 1$) only deep inelastic transfers contribute to the production of light nuclei.

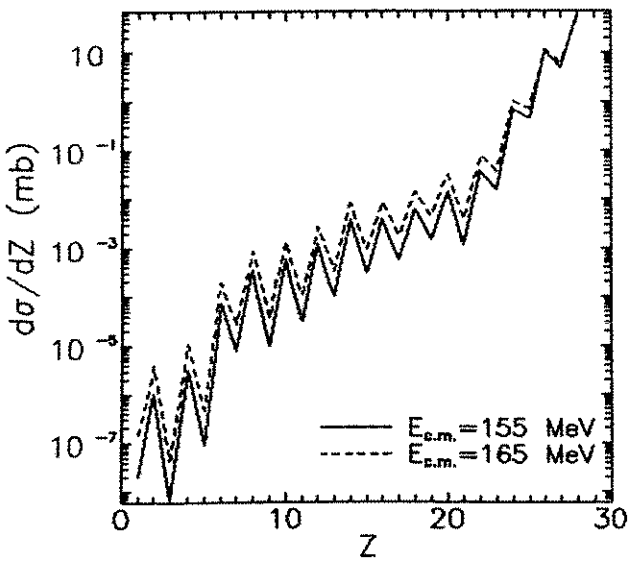

Fig.3. Calculated cross sections of deep inelastic transfers products in the reaction ^{58}Ni+^{58}Ni at E_{cm} = 150 MeV (solid line) and E_{cm} = 165 MeV (dashed line) (see text).

3.2. Deep inelastic transfers contribution

Using (1–3) and (5–7) we have calculated the charge distribution for deep inelastic transfers. The results for the reaction ^{58}Ni+^{58}Ni at $E_{c.m.} = 150$ MeV and 165 MeV are shown in Fig.3. The set of parameters $\bar{J} = 60\hbar$, $\Delta J = 10\hbar$, $\tau_0 = 2.5 \cdot 10^{-21}$s has been used. With increasing collision energy the yield of light nuclei increases and a larger number of partial waves contribute to the deep inelastic transfers. Comparing the results in Fig. 3 with the experimental data it is necessary to have in mind that for $Z > 21$ (Businaro–Gallone maximum) the contribution of the highest partial waves is not taken into account (although it exists) because they do not contribute to the cross section at smaller Z.

3.3. Contribution of the trajectories with $J < J_{crit}$

If at $J < 60\hbar$ the kinetic energy is large enough, the DNS can overcome the Businaro–Gallone maximum. After this point the system goes to the compound nucleus and its asymmetry increases. At $\eta > \eta_{BG}$ $\Lambda_Z(J)$ increases with decreasing Z (Fig.4). The thermal and quantum fluctuations rule the value of $\Lambda_Z(J)$ near the Businaro–Gallone maximum. The calculated cross sections $(d\sigma/dZ)_{J<J_{crit}}$ (2) are presented in Fig.5. The dependence of $\Lambda_Z(J)$ on Z is very important and leads to enhanced yields for light nuclei in heavy ion collisions. If we compare our results with the typical ones of the evaporation model, we shall see that our calculations give the same cross section for the production of ^{12}C and ^{16}O, although the evaporation cross section for ^{12}C is usually an order of magnitude as large as that for ^{16}O [13]. Thus, our results show that the cross section of the preequilibrium decay of the DNS can be an order of magnitude as large as that given by statistical predictions of light nuclei evaporation from a compound nucleus. Therefore, this mechanism has to be taken into account in the analysis of experimental data.

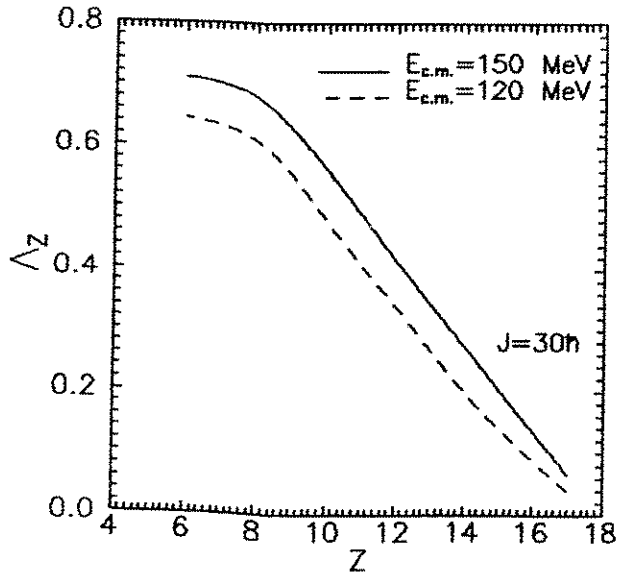

Fig.4. Probability decay of the dinuclear system Λ_Z as a function of Z in the reaction ^{58}Ni+^{58}Ni at $J = 30\hbar$.

4. CONCLUSION

We have calculated the cross sections of the production of light nuclei in the reaction ^{58}Ni+^{58}Ni. Preequilibrium decay of the DNS gives a large contribution to the light nucleus emission. Therefore, careful measurement of the charge distributions in the reaction ^{58}Ni+^{58}Ni at different collision energies will allow us to estimate the relationship between the increase of charge asymmetry and the growing neck radius in the DNS. Enhanced experimental yields of light nuclei in comparison with the statistical model predictions will demonstrate the presence of the fusion channel connected with the DNS evolution along charge (mass) asymmetry. The angular distribution of light nuclei, which are the result of

the DNS decay, should be close to the symmetric one. The energies of these nuclei assume to be close to the corresponding Coulomb barriers. To distinguish the products of the DNS decay and the evaporation from the compound nucleus, the best way is the use of few reactions with different mass asymmetries in the entrance channel but leading to the same compound nucleus. The decay probabilities of the asymmetric DNS should depend on the entrance channel. After the preequilibrium decay of the asymmetric DNS the heavy fragment has smaller excitation energy than the compound nucleus. Therefore, it can reduce the yield of the fission products in comparison with the case where the DNS decay is not considered.

We should mention also that if the energy of the symmetric DNS is smaller than the compound nucleus energy, the molecular-like states at high angular momenta are formed.

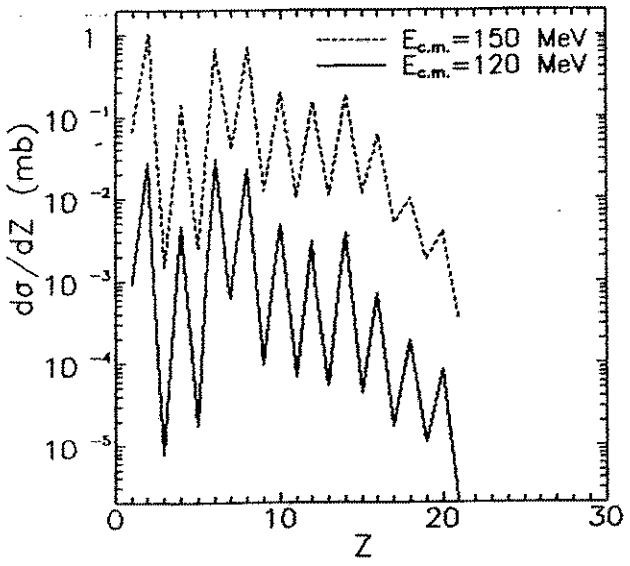

Fig.5. Calculated charge distribution $(d\sigma/dZ)_{J<J_{crit}}$ in the reaction ^{58}Ni+^{58}Ni at E_{cm} = 150 MeV (dashed line) and E_{cm} = 120 MeV (solid line).

References

[1] M. Blann and T.T. Komoto, Phys. Rev. C 24, 426 (1981).

[2] V.V. Volkov, S.N. Ershov and S.P. Ivanova, Sov. J. Nucl. Phys. **43**, 874 (1986).

[3] N.V. Antonenko and R.V. Jolos, Z. Phys. **A339**, 453 (1991); Z. Phys. **A341**, 459 (1992).

[4] N.V. Antonenko, E.A. Cherepanov, A.K. Nasirov, V.P. Permjakov and V.V. Volkov, Phys. Lett. **B319**, 425 (1993).

[5] L.G. Moretto and J.S. Sventek, Phys. Lett. **B58**, 26 (1975).

[6] N.V. Antonenko and R.V. Jolos, Z. Phys. **A338**, 423 (1991).

[7] G.G. Adamian, N.V. Antonenko, R.V. Jolos and A.K. Nasirov, Nucl. Phys. **A551**, 321 (1993).

[8] A.M. Wapstra and G. Audi, Nucl. Phys. **A432**, 1 (1995).

[9] S. Liran and N. Zeldes, At. Data and Nucl. Data Tables **17**, 431 (1976).

[10] U. Abbondanno, G. Vannini, M. Bettiolo, L. Vannucci, R.A. Ricci, M. Bruno, M. D'Agostino, P.M. Milazzo and N. Cindro, (unpublished) (1992).

[11] W. Scheid, H.J. Fink and H. Müller, Lecture Notes in Physics **22**, 144 (1973).

[12] G.G. Adamian, N.V. Antonenko, R.V. Jolos, S.P. Ivanova and O.I. Melnikova, Sov. J. Nucl. Phys. (in print) (1994).

[13] Yu.A. Muzychka, B.I. Pustylnik and V.V. Avdeichikov, *Proceedings of the International School-Seminar on Heavy Ion Physics, 1986* (JINR, Dubna, 1987).

THE MECHANISMS OF LIGHT PARTICLE FORMATION AND NUCLEUS - NUCLEUS INTERACTION

V. Zagrebaev

Department of Theoretical Physics, Chuvash State University, Cheboksary, 428900 Russia (zagreb@chgu.chci.chuvashia.su)

1. Introduction

Now we may more or less confidently affirm that extensive experimental and theoretical studies on heavy ion collisions for more than twenty years do not fully justify our hopes of not only thoroughly clarifying the dynamics of the nucleus–nucleus interaction, but also revealing the quite novel properties of nuclear matter. On the one hand, extremely interesting and sometimes unexpected experimental data are accumulated. On the other hand, we have rather poor information on the dynamical properties and the structure of complex nuclei from the processing of these data. Up to now, however surprising it is, we have not determined the very fundamental characteristics of the nucleus-nucleus interaction. We do not know, as before, the ion-ion potential forces near and behind the Coulomb barrier. Clearly observing a high-rate process of kinetic energy dissipation into an internal excitation of colliding nuclei we still have not determined unambiguously either the mechanism responsible for this process or the value and the character of the dissipative forces. Experimentally studying the massive transfer reactions and the heavy-ion radioactivity (the spontaneous emission from the 'cold' nuclei of such ions as ^{14}C or ^{24}Ne), we have only vague idea about multi-nucleon clustering, i.e., about potentials, formfactors, and spectroscopy of heavy fragments inside nuclei. It is not difficult to continue the list of our ignorance.

There are both experimental and theoretical reasons for such a state. The inclusive character of the most interesting experimental data does not allow us to 'discern' and to fix unambiguously the mechanism of the process under study. The absence of adequate theoretical models capable of describing all the sets of experimental data only redoubles this uncertainty.

In 'pre-heavy-ion' nuclear physics one could single out experimentally and use for the study of one or another nucleus property two limit (and, therefore, clear enough) mechanisms of nuclear reactions – the process of the compound-nucleus formation and the direct process. It was the direct reactions and elastic scattering, with the help of which such fundamental characteristics as the nucleus mean field and the single-particle states, an existence and behaviour of the few-nucleon clusters inside nuclei, etc. were determined quantitatively. However, with the increase of the colliding nuclei masses the role of direct processes and of reactions going through the formation of a compound nucleus, becomes noticeably smaller. As a result, it is not only difficult to single out the direct one-step reactions in heavy-ion collisions, but they are also 'poor-informative'. The latter is due to the very strong coupling of the channels that leads to the strong absorption in an elastic one. As a consequence, such processes are localized in an extremely peripheral region and do not allow us to look inside the nucleus.

Thus, in heavy ion collisions we have to study very many reaction mechanisms, some of which are badly defined and can be hardly distinguished experimentally from each other. In my view, for the highly informative data, just the detection of the particles formed on the *initial stage* of reaction (the products of few-nucleon transfer, pre-equilibrium light particles, high-energy γ-rays, etc.) is of the most interest.

Note, for example, that the cross section of light particle production is very large (comparable to the total reaction cross section) and therefore their formation is a common feature of nucleus - nucleus collisions. A complete understanding of these cannot be obtained without an understanding of the formation mechanisms of the light particles. Secondly, as experiments show, the properties of mass, energy, and angular distributions of the ejected light particles are quite unexpected and (in some cases) are very difficult to explain. Finally, it is well established that a considerable part of these particles (sometimes - the largest one) is emitted just

in the initial stage of nucleus - nucleus interaction, and therefore it contains immediate information about the dynamics of this interaction, in contrast to the decay products of the compound nucleus which have no memory of its formation.

Here I would like to formulate several problems concerning the mechanisms of heavy-ion-induced nuclear reactions and the nucleus-nucleus potential and dissipative forces which remain unsolved. Some of them could be clarified in experiments with (coincident) detection of pre-equilibrium light particles, in particular, with the FOBOS facility.

2. The questions concerning reaction mechanisms

There are obviously a lot of undecided questions concerning the mechanisms of heavy-ion-induced nuclear reactions. Here, I'll briefly touch only some of them connected with the fusion dynamics, transfer reactions, and break-up process.

2.1 Fusion dynamics

It is generally assumed that the fusion process dominates the total reaction cross section at low energies in collisions of not so heavy ions with the nuclei. Just because of this this process is worthy of particular attention. However, in spite of numerous experiments and theoretical papers devoted to this process, we have not got a complete notion about fusion dynamics up to now.

(1) Why do the nuclei retain their 'personalities' at the large spatial overlap of them in deep inelastic collisions and why don't they fuse in this case? What keeps nucleons within two nuclei and what prevent them from the 'collectivization'? It may be due to the 'reluctance' of nucleons to change sharply their single-particle states, i.e., to change the character (n,l) of single-particle wave functions, i.e., to change the character of their single-particle motion. This would mean the steadiness of single-particle trajectories in a common multi-dimensional phase space, in spite of the large dissipation of relative motion kinetic energy into the internal excitation energy of both nuclei.

(2) What happens with the increase of the nuclear masses: why does the fusion cross section decrease sharply at $A \geq 220$? Does the fission barrier of compound nucleus regulate significantly the fusion process or not? What is the real multi-dimensional potential energy surface of di-nuclear system? What and where is the potential pocket on this surface? Why does the fission fragment distribution depend on the way of compound nucleus formation? Are there the different modes of the mass relaxation process? What is the real 'trajectory' of di-nuclear system in multi-dimensional (distance, deformations, mass asymmetry,...) space?

(3) What is the mechanism of sub-barrier fusion and what is the role of dissipative forces in this case? Is there the real dissipation of kinetic energy in the under-barrier region and what does it mean? What is the correct interpretation of the 'barrier' distribution and its structure observed in sub-barrier fusion reactions?

(4) The last question is mainly to the theorists. Is it possible to reduce at last the related processes of fusion and fission to the unified problem within the frame of the common quantum - mechanical model with a friction (i.e., with a strong channel coupling)?

2.2 Transfer reactions

Of course, there are many quite different mechanisms of transfer reactions: beginning from the quasi-elastic few-nucleon transfer and up to the overdamped massive transfer reactions. Here I list only a few principal questions concerning the transfer processes.

(1) What is energy dependence of the massive transfer cross section near the Coulomb barrier? How can we distinguish at all the massive transfer process (I identify it with incomplete fusion) from the complete fusion with subsequent evaporation of light particle? It would be very interesting to measure an excitation function of ICF reaction. Is there low-energy threshold of it? Is there high-energy limit of it? We found that situation may be as shown schematically in Fig.1. The Fermi motion of light particle inside the projectile and emission of it into the backward angles may significantly increase the cross section of incomplete fusion at sub-barrier energies.

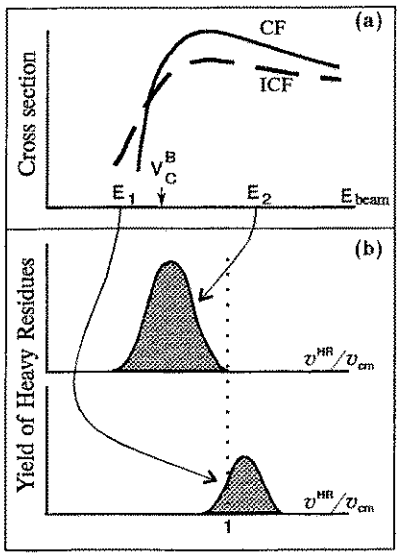

Fig.1. Excitation functions of complete and incomplete fusion reactions - (a) and velocity distributions of heavy residual nuclei at different (above- and sub-barrier) energies - (b).

(2) It is well known that just the binary transfer reactions dominate at the energies up to 40 MeV/nucleon at least. We know also that at higher energies the multi-particle exit channels dominate. However, at high energies we detect, as a rule, not the primary reaction products but the products of their decay. The two questions arise in connection with it. Do the binary transfer reactions survive at high energies? Do the transfer processes survive at all at high energies?

The displacement of two Fermi spheres at high relative velocity of colliding nuclei is the main reason against the possibility for transfer reactions at high bombarding energy (see Fig.2). However, if at 100 MeV/nucleon beam energy the dissipative phenomena still take place, then the previous argument is not quite correct, because, firstly, Fermi distribution of both nuclei will be washed away at high excitation energy, and, secondly, the separation of the Fermi spheres will be not so large due to a decrease of relative motion velocity at contact.

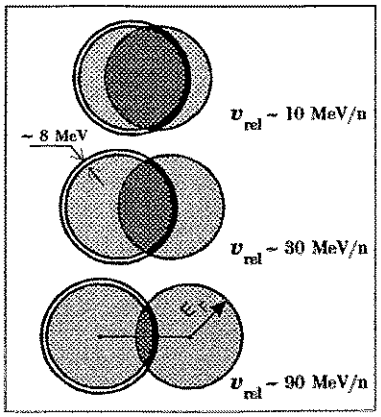

Fig.2. Displacement of the two Fermi spheres showing the momentum distribution of nucleons within the projectile and the target for different relative velocities at contact of them. The radius of the largest circle corresponds to the highest bound state in the target ($\approx E_F + 8MeV$). The disappearing narrow black strip shows the vacant bound states, which can be occupied by the transferred nucleons (from [1]).

2.3 Break-up process

(1) All the processes of break-up of the incident ion can be devided onto *elastic* and *inelastic* (depending on the total kinetic energy dissipation) and onto *direct* and *sequential*. The direct (prompt) break-up happens just in the vicinity of the target nucleus and is regulated by the 'three-body dynamics', i.e., depends on the interaction of all the fragments with each other and with the target nucleus. The sequential break-up (decay) of the primary excited projectile like nucleus is caused by 'two-body interaction' and occurs far from the target. In experiments we may more or less clear decompose the total break-up cross section onto *elastic*

and *inelastic* parts (see Fig.3). But the decomposition onto the *direct* and *sequential* mechanisms is more difficult. The detections of angular correlations of the fragments or their relative motion energy spectra do not answer unambiguously this question. Note, that determination of the break-up mechanism is of principal for correct choise of the theoretical model for description both the low-energy two-body break-up and the high-energy multi-fragmentation of the projectile.

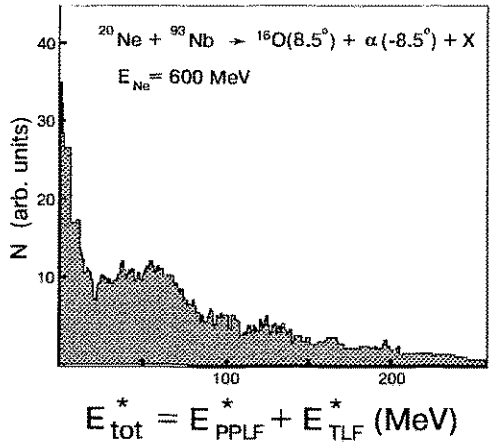

Fig.3. Total energy excitation spectra obtained for the reaction $^{20}Ne+^{93}Nb \rightarrow \alpha(8.5^{\circ})+^{16}O(-8.5^{\circ})+X$ at E=600 MeV assuming the three-body kinematics of exit channel (from [2]).

(2) As experiments show, even at the beam energy of 30 MeV/nucleon just the *two-body break-up* exit channels dominate the total yield of the projectile like fragments (PLF) in coincidence with the light particles (Fig.4).

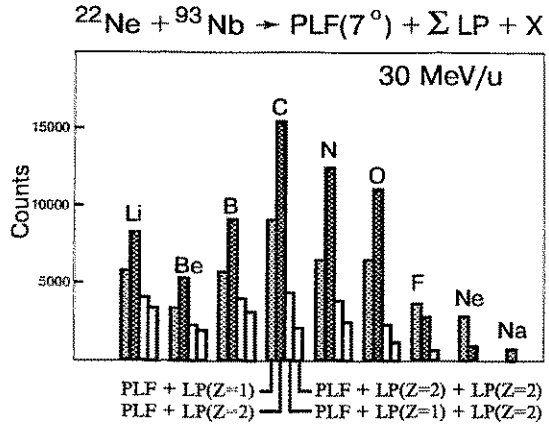

Fig.4. Histogram of the successive correlation yield for a fragment detected at 7.3° in coincidence with only: one (Z=1) LP (hatched); one (Z=2) LP (checked); one (Z=1) LP + one (Z=2) LP (third bars); two (Z=2) LP (fourth bars) (from [3]).

Up to what bombarding energy does this situation take place? How does it depend on the projectile mass? This should also depends on the primary excitation of the projectile like nucleus. Is this excitation high or low? In a case of high excitation of the projectile its decay should not depend strongly on the ground state masses of decay products, and, in a case of low excitation, such dependence should be observed. As can be seen from Fig.5, there is not unambiguous answer this question. It would be interesting to clarify this fact at lower beam energies and for different projectiles.

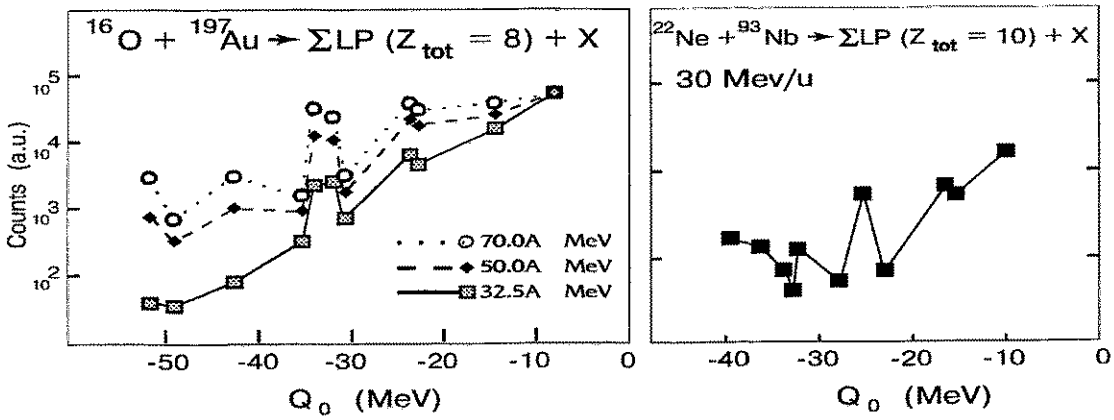

Fig.5. Relative yields of the different projectile dissociation channels as a function of their Q_0-values.
To the left: (1) C He, Q_0 =-7.16 MeV; (2) He He He He, -14.44; (3) C H H, -22.34; (4) B He H, -23.13; (5) B Li, -30.89; (6) Li He He H, -31.80; (7) He He He H H, -34.25; (8) Li Li He, -35.35; (9) B H H H, -42.93; (10) Li Li H H, -49.15; (11) Li He H H H, -51.60 [4].
To the right: (1) O He, Q_0 =-9.7 MeV; (2) F H, -15.3; (3) C He He, -15.9; (4) N Li, -23.0; (5) N He H, -25.5; (6) Be He He He, -27.9; (7) O H H, -33.2; (8) C Li H, -33.2; (9) B Li He, -34.0; (10) B He He H, -36.5; (11) C He H H, -39.7 [3].

3. The questions concerning the nucleus-nucleus interaction

Besides unknown nature of many heavy-ion-induced reaction mechanisms, there is another aspect of our ignorance connected with badly determined character of nucleus-nucleus interaction. Instead of great number of nucleon degrees of freedom we usually try to introduce a few collective variables to describe the global properties of nucleus-nucleus interaction. But, as a rule, the global (collective) degrees of freedom (even such clear as the distance between the centers of two nuclei) can be used (and clear defined) only within some limited regions of their values. A strong coupling of these global variables with the internal degrees of freedom complicates significantly the corresponding equations of motion. At last, the quantum effects redouble the uncertainty and make the problem almost quite unsolvable.

3.1 Potential forces

The potential energy of two approaching nuclei is one of the most fundamental and important characteristics of their dynamics. In a nucleon-nucleus interaction the role of the nuclear mean field is sufficiently clear, but for nucleus-nucleus collision both the collective potential energy of their relative motion and the potential energy of the separate nucleons are unknown to us in explicit form. Determining the heights of the Coulomb barriers with accuracy of a few MeV, we have a very vague idea about their form. We even cannot say with certainty if two nuclei accelerated or hindered in the region behind the barrier. Up to what distances can we speak at all about the potential energy of *two separate* nuclei, when they penetrate into each other? If we use the multi-dimensional potential energy, then what collective degrees of freedom have to be taken into consideration and what have to be not? What is the role of the potential forces in the heavy ion collisions and in the light particle formation? There are different points of view: from the total disregard of these forces up to the statement, that the light particles and the projectile like fragments are deflected predominantly into the negative angles due to the nuclear mean field. The disappearance of transverse flow of light particles at the beam energy $\sim 70 \div 80$ MeV/nucleon is also explained by the balance between the attractive nuclear mean field on one side and nucleon-nucleon collisions on the other side: deflection to the negative angles due to the attractive forces at low energies gives place to predominant repulsion due to the large compression at higher energies.

Undoubtedly, the determination of the nucleus-nucleus potential forces is quite necessary if we want

to attain the quantitative understanding of the heavy ion induced nuclear reactions. All the theoretical models contain these forces, which define the classical trajectories (including the caustic surfaces and nucleon focusing), local momenta, distorted waves, barrier penetration, and so on. Strong absorption in an elastic channel does not allow us to look behind the absorption radius in experiments on elastic scattering. Thus, we need to look for some other reactions the cross section of which are sensitive to the value of the nucleus-nucleus potential forces at the relatively small distances behind the Coulomb barrier.

3.2 Dissipative forces

Nuclear friction is no less important for an understanding the nucleus-nucleus interaction dynamics. However, the value and the nature of the dissipative forces are determined even more poorly than those of the potential ones. Note, that the friction forces are much more informative (and physically clearer) than the imaginary part of the optical potential. They not only substitute for the absorption $iW(r)$ defining the exhaustion of the flux in the elastic channel, but also allow us to keep watching the distribution of this flux over other channels. It substantially reduces the uncertainty when evaluating an absolute value of one or another reaction cross section. In my opinion, it should be refused in heavy ion physics where possible the use of an umaginary part of optical potential and introduce more general quantity - the dissipative forces.

The experimental and theoretical investigations of heavy ion deep inelastic reactions have not aloowed us till now to deduce unambiguously the value of nuclear friction forces. Parameters of friction forces obtained by different authors vary over a wide range. Moreover, we cannot answer very principal questions concerning friction forces. What are the main reasons and mechanisms of nuclear viscosity: one-body excitations inside a time-depended mean field [5], two-nucleon collisions [6], chaotic motion of nucleons in asymmetric deformed nucleus [7], excitations of collective degrees of freedom [8], nucleon exchange [9], chaotization of coupling matrix elements [10] or single-particle energy spectra [11],...? If there are several mechanisms, then what are their relative contributions depending on mass and energy of interacted nuclei? May a simple quantum system of only one degree of freedom display a dissipative response? Does the energy dissipation need a minimal time interval or there is some fast dissipation mechanism? Do the dissipative processes survive (it meens the transfer processes do) at high energies? Is it possible at all to distinguish correctly the dissipative and potential forces in heavy ion experiments? At last, how can we consider the friction forces within quantum theory of collisions?

3.3 Light particle emission as a probe of nucleus-nucleus interaction

Now I would like to underline again that just the detection of pre-equilibrium fragments and light particles emitted on initial stage of nucleus-nucleus collision with subsequent analysis of the cross section within more or less adequate theoretical model can help us to answer some questions listed above.

In Fig.6 the angular distribution of fast α-particles formed in the reaction $^{181}Ta(^{22}Ne,\alpha)$ is shown in comparison with the corresponding calculations fulfilled within the multi-step (dissipative) massive transfer mechanism [12]. The angular distribution of the light particles was found very sensitive to the value of the nucleus-nucleus potential forces at the range behind the Coulomb barrier (see inset in Fig.6).

Estimated yield of pre-equilibrium neutrons formed in the reaction $^{20}Ne+^{181}Ta \rightarrow n+X$ at bombarding energy of 10 MeV/nucleon is shown in Fig.7 depending on the value of friction forces in the entrance channel. The simple three-body classical model with the standard proximity nucleus-nucleus potential forces is used for calculation the neutron emission in the break-up and incomplete fusion processes. We see again that pre-equilibrium light particle spectra are extremely sensitive to the dynamics of nucleus-nucleus relative motion in entrance channel.

Of course, we need more systematic analysis of light particle spectra fulfilled over a wide range of the beam energies and over a wide range of the projectile masses to determine more or less reliably the nucleus-nucleus potential and dissipative forces.

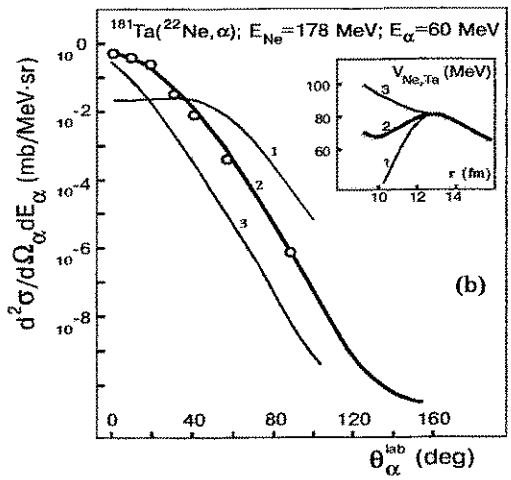

Fig.6. Angular distribution of α-particles in the $^{181}Ta(^{22}Ne,\alpha)$ reaction at E_{lab} = 178 MeV and E_α = 60 MeV [13]. The solid lines (obtained within the dissipative massive transfer model [12]) indicate the sensitivity of the light particle distribution to the value of nucleus-nucleus potential forces in the region behind the Coulomb barrier. In the inset the corresponding potentials are shown.

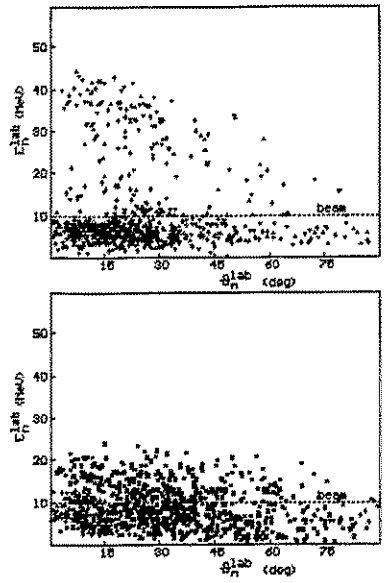

Fig.7. Simulated distributions of pre-equilibrium neutrons emitted in the reaction $^{181}Ta(^{20}Ne,n)$ at E/A = 10 MeV. Top - without friction in the entrance channel, bottom - overdamped collision.

References

1. D.Guerreau, *Nucl.Phys.*, 1985, **A447**, p.37c.
2. M.Stern et al., *Z.Phys.*, 1988, **A331**, p.323.
3. M.Stern et al., *Nucl.Phys.*, 1993, **A559**, p.401.
4. J.Pouliot et al., *Phys.Rev.*, 1991, **C43**, p.735.
5. D.M.E.Gross, *Nucl.Phys.*, 1975, **A240**, p.472
   H.Hofman, P.J.Siemens, *Nucl.Phys.*, 1976, **A257**, p.165.
6. G.Mantzouranis, H.C.Pauli, *Phys.Rev.*, 1980, **C22**, p.1550.
   S.Pal, N.K.Granguly, *Nucl.Phys.*, 1981, **A370**, p.175.
7. W.J.Swiatecki, *Nucl.Phys.*, 1988, **A488**, p.375c.
8. R.A.Broglia et al., *Phys.Rev.Lett.*, 1978, **41**, p.25.
   F.Catara, U.Lombardo, *Nucl.Phys.*, 1986, **A455**, p.158.
9. J.Randrup, *Ann.Phys.*,1978,**112**,p.356; *Nucl.Phys.*,1979,**A327**,p.490.
10. M.C.Nemes, H.A.Weidenmuller, *Phys.Rev.*, 1981, **C24**, p.450.
11. V.I.Zagrebaev, *Z.Phys.*, 1994, **A345**, in print.
12. V.I.Zagrebaev, *Ann.Phys.*, 1990, **197**, p.33.
13. C.Borcea et al., *Nucl.Phys.*, 1984, **A415**, p.169.

V. References

to publications starting from 1991

(The publications issued prior to 1991 are partially included or cited in the status report "**FOBOS - Ein 4π - Fragmentspektrometer** " - Zweite Ausbaustufe - ZfK - 734, Zentralinstitut für Kernforschung, Rossendorf, 1990)

References

H.-G.Ortlepp, H. Sodan, M. Andrassy, W.-D. Fromm, C.-M. Herbach, K.-H. Kaun, G. Pausch, W. Seidel, W. Wagner, H. Homeyer, H. Fuchs, T. Dietterle, G. Renz , M. Danziger, F. Gleisberg, W. Meiling, A.S. Fomichev, A.I. Ivanenko, I.V. Kolesov, Yu.E. Penionzhkevich, Yu.Ts. Oganessian, L.A. Rubinskaya, O.V. Strekalovsky, V.M. Vasko, A. Budzanowski

FOBOS - Ein 4π- Fragmentspektrometer (Zweite Ausbaustufe)
Report ZfK - 734, Zentralinstitut für Kernforschung Rossendorf, Deutschland, November 1990.

Experimentvorschläge für das 4π - Fragmentspektrometer FOBOS
Berichte der Arbeitstagung der FOBOS - Kollaboration, Dresden, Deutschland, April 1991, Report ZfK - 751, Zentralinstitut für Kernforschung Rossendorf (Ed. H. Sodan) Rossendorf, Dezember 1991 (Nachdruck Juni 1992).

H.-G. Ortlepp, M. Andrassy, G.G. Chubarian, M. Danziger, T. Dietterle, A.S. Fomichev, Sh.M. Heinitz, C.-M. Herbach, A.I. Ivanenko, I.V. Kolesov, D. May, Yu.Ts. Oganessian, Yu.E. Penionzhkevich, G. Renz, L.A. Rubinskaya, O.V. Strekalovsky, V.M. Vasko, W.-D. Fromm, K. Heidel, H. Sodan, W. Wagner, B.A. Burova, S.V. Radnev, I.D. Sandrev
The FOBOS 4π - Detector of Charged Particles at Dubna
Proc. of the Internat. Conf. on Exotic Nuclei, Foros, Crimea, Ukraine, October 1 - 5, 1991 (Ed. Yu.E. Penionzhkevich, R. Kalpakchieva) World Scientific, Singapore, 1991.

M. Andrassy, B.A. Burova, M. Danziger, T. Dietterle, A.S. Fomichev, W.-D. Fromm, K. Heidel, Sh.M. Heinitz, C.-M. Herbach, A.I. Ivanenko, I.V. Kolesov, H.-G. Ortlepp, Yu.Ts. Oganessian, Yu.E. Penionzhkevich, S.V. Radnev, G. Renz, L.A. Rubinskaya, I.D. Sandrev, H. Sodan, O.V. Strekalovsky, V.M. Vasko, W. Wagner
Present status of the FOBOS 4π - array
Scientific Report 1989 - 1990, Laboratory of Nuclear Reactions, Joint Institute for Nuclear Research, Dubna, Russia, JINR E7 - 91 - 75 (Ed. B.I. Pustylnik) Dubna, 1991, p.171.

W.-D. Fromm, K. Heidel, H.-G. Ortlepp, O.V. Strekalovsky
Electronics of the FOBOS gas - filled detector modules
ibid., p.173.

M. Andrassy, H.-G. Ortlepp, Sh.M. Heinitz, V.M. Vasko
The FOBOS fragment detector subsystem
ibid., p.175.

G. Renz
The computer controlled evacuation and gas - supply system of "Mini - FOBOS"
ibid., p.177.

C.-M. Herbach, P. Gippner, H.-G. Ortlepp, D. Wohlfarth
HERAKLES - an algorithm for fission fragment mass identification in TOF - E measurements with large energy loss corrections
ibid., p.179.

Software developments for FOBOS :
G. Renz, T. Ihle
"PRESS"
A. Stendal, C.-M. Herbach, G. Renz
"FOIL"
R. Engel, G. Renz
"FLASHADC"
E. Will, U. Sodan
"PCMESS"
R. Engel, G. Renz
"COM1INT"
C.-M. Herbach, H.-G. Ortlepp, D. Wohlfarth, P. Gippner
"HERAKLES"
C.-M. Herbach, C. Umlauf
"ATHENE"
C.-M. Herbach
"ORION"
M. Danziger, St. Herpich, H. Perner
"DETEC"
ibid., p.293 - 295.

H.-G.Ortlepp, H. Sodan, M. Andrassy, W.-D. Fromm, C.-M. Herbach, K.-H. Kaun, G. Pausch, W. Seidel, W. Wagner, H. Homeyer, H. Fuchs, T. Dietterle, G. Renz , M. Danziger, F. Gleisberg, W. Meiling, A.S. Fomichev, A.I. Ivanenko, I.V. Kolesov, Yu.E. Penionzhkevich, Yu.Ts. Oganessian, L.A. Rubinskaya, O.V. Strekalovsky, V.M. Vasko, A. Budzanowski
The 4π - Fragment spectrometer FOBOS
Frühjahrstagung DPG e.V., Darmstadt, Deutschland, ... 1991, Verhandl. DPG (..) .. (1991) S. ...

G. Pausch, H. Fuchs, H. Homeyer, G. Röschert, C. Schwarz, A. Siwek, W. Terlau, A. Tutay, B. Bochev, W. Wagner, A. Matthies, W. Kantor
Production of intermediate mass fragments in 960 MeV ^{32}S + Au
Annual Report 1991, HMI - 497, Hahn - Meitner - Institut GmbH, Berlin, Deutschland, 1992, p.83.

C. Beschoner, B. Drescher, T. Kiehne, C. Kluge, G. Röschert, V.V. Trofimov, P. Ziem
Rechnergestützte Erfassung und Auswertung von experimentellen Daten
ibid., p.101.

H.-G. Ortlepp, M. Andrassy, G.G. Chubarian, M. Danziger, T. Dietterle, A.S. Fomichev, Sh.M. Heinitz, C.-M. Herbach, A.I. Ivanenko, I.V. Kolesov, D. May, Yu.Ts. Oganessian, Yu.E. Penionzhkevich, G. Renz, L.A. Rubinskaya, O.V. Strekalovsky, V.M. Vasko, W.-D. Fromm, K. Heidel, H. Sodan, W. Wagner, B.A. Burova, S.V. Radnev, I.D. Sandrev
The FOBOS 4π - detector of charged particles at Dubna
Proc. of the Int. Conf. on New Nuclear Physics with Advanced Techniques, Ierapetra, Crete, Greece, June 23 - 29, 1991 (Ed. F.A. Beck, S. Kossionides & C.A. Kalfas) World Scientific, Singapore, 1992, p.302.

H. Fuchs, H. Homeyer, G. Pausch, W. Terlau, C. Schwarz, A. Siwek, B. Bochev, W. Wagner, A. Budzanowski, W. Kantor
Multiple break - up of nuclei : Experiments with ARGUS at the Hahn - Meitner - Institut Berlin
Proc. of the 10th Internat. School on Nuclear Physics, Neutron Physics and Nuclear Energy, Varna, Bulgaria, October 14 - 19, 1991.

FOBOS - a 4π - Fragment spectrometer for heavy - ion reaction products
Report FZR 92 - 11, Forschungszentrum Rossendorf e.V., Germany (Ed. H.-G. Ortlepp, K.-D. Schilling) 1992.

A.S. Fomichev, H.-G. Ortlepp, Yu.E. Penionzhkevich, C.-M. Herbach, I. David, W. Wagner, G. Pausch, H. Sodan, V.A. Vitenko
Basic characteristics of the scintillation phoswich detectors of the 4π - set - up FOBOS
Preprint P15 - 92 - 50, Joint Institute for Nuclear Resarch, Dubna, Russia, 1992 (in Russian).

H. Fuchs, H. Homeyer, G. Pausch, G. Röschert, C. Schwarz, A. Sourell, W. Terlau, A. Tutay, A. Budzanowski, W. Kantor, A. Siwek, W. Wagner
Study of intermediate - mass fragment emission and multifragmentation with 30 AMeV ^{32}S projectiles
Frühjahrstagung DPG e.V., Salzburg, Österreich, 24.- 28. 2 1992, Verhandl. DPG (..) .. (1992) S. ..

H.-G. Ortlepp, M. Andrassy, G.G. Chubarian, M. Danziger, A.S. Fomichev, C.-M. Herbach, A.I. Ivanenko, I.V. Kolesov, Yu.Ts. Oganessian, Yu.E. Penionzhkevich, G. Renz, O.V. Strekalovsky, V.M. Vasko, A. Matthies, W. Wagner, H. Fuchs, D. Hilscher, H. Homeyer, W. von Oertzen, G. Pausch
The 4π - Fragment spectrometer FOBOS
Book of Abstracts of the **Internat. Nucl. Physics Conf., Wiesbaden, Germany, July 26 - August 1, 1992, Nr. 5.2.**

G. Pausch, W. Bohne, H. Fuchs, D. Hilscher, H. Homeyer, H. Morgenstern, A. Tutay, W. Wagner
Particle identification in solid - state detectors by exploiting pulse - shape information
(Preprint HMI - P / 92 / P2 - Pau1, Hahn - Meitner - Institut GmbH, Berlin, Deutschland, 1992)
Nucl. Instr. and Meth. in Phys. Research A 322, 1992, p.43.

H.-G. Ortlepp, M. Andrassy, G.G. Chubarian, M. Danziger, L. Dietterle, A.S. Fomichev, P. Gippner, C.-M. Herbach, I.A. Ivanenko, I.V. Kolesov, A. Matthies, D. May, Yu.Ts. Oganessian, Yu.E. Penionzhkevich, V.N. Pokrovsky, G. Renz, L.A. Rubinskaya, O.V. Strekalovsky, V.V. Trofimov, V.M. Vasko, K. Heidel, K.-D. Schilling, W. Seidel, H. Sodan, W. Wagner, H. Fuchs, D. Hilscher, W. von Oertzen, G. Pausch, P. Ziem, V.E. Zhuchko
Status of the 4π - Fragment spectrometer FOBOS
a) **Annual Report 1992, Institute of Nuclear and Hadronic Physics, Forschungszentrum Rossendorf e.V., Germany, FZR - 93 - 10 (Ed. F. Dönau, H. Prade) Rossendorf, 1993, p.93.**
b) **Scientific Report 1991 - 1992, Flerov Laboratory of Nuclear Reactions, Joint Institute for Nuclear Research, Dubna, Russia, JINR E7 - 93 - 57 (Ed. B.I. Pustylnik) Dubna, 1993, p.242.**

W. Wagner, A.S. Fomichev, C.-M. Herbach, A. Matthies, H.-G. Ortlepp, O.V. Strekalovsky, V.A. Vitenko, G. Pausch
The scintillator shell of the FOBOS 4π - array
ibid., a) **p.124,** b) **p.244.**

C.-M. Herbach, M. Andrassy, G.G. Chubarian, P. Gippner, A. Matthies, H.-G. Ortlepp, G. Renz, K.-D. Schilling
Nuclear reactions at the Coulomb barrier induced by ^{84}Kr (4.3 AMeV) on ^{116}Sn and ^{118}Sn
ibid., a) **p.95.**

H.-G. Ortlepp, M. Andrassy, G.G. Chubarian, P. Gippner, C.-M. Herbach, A. Matthies, G. Pausch, G. Renz, K.-D. Schilling
Model independent balance analysis of fission fragments produced by $^{40}Ar + ^{194}Pt$ at energies of 5.5 AMeV and 10 AMeV
ibid., a) **p.97.**

G. Pausch, J. Krüger, W. Seidel, W. Wagner, C.-M. Herbach, A. Matthies, H.-G. Ortlepp, V.V. Trofimov, H. Fuchs, H. Homeyer, G. Röschert, A. Tutay, P. Ziem, A. Budzanowski, A. Siwek, L. Zrodlowski, V.E. Zhuchko
Extension of the ARGUS phoswich - array by a FOBOS gas - detector module and test of the FOBOS data acquisition system
ibid., a) **p.99.**

J. Krüger, G. Pausch, W. Seidel, W. Wagner
Yields for IMF - production of the reaction ^{32}S (960 MeV) + ^{197}Au
ibid., a) **p.100.**

G. Renz, P. Gippner, C. Umlauf, V.M. Vasko, D. May
Status of the evacuation and gas - supply system of FOBOS
ibid., a) **p.122.**

G. Pausch, W. Bohne, H. Fuchs, D. Hilscher, H. Homeyer, H. Morgenstern, A. Tutay, W. Wagner
Particle identification in solid - state detectors by exploiting pulse - shape information
ibid., a) **p.125.**

K. Heidel, H.-G. Ortlepp
Development of data acquisition electronics for FOBOS
ibid., a) **p.136.**

K. Heidel, H.-G. Ortlepp, A.P. Sirotin
Complete test of the Bragg digital processor BDP 5385
ibid., a) **p.137.**

M. Andrassy, H.-G. Ortlepp, Sh. Heinitz, V.M. Vasko
Progress in gas - filled detector development for FOBOS
ibid., b) **p.243.**

H.-G. Ortlepp, M. Andrassy, G.G. Chubarian, C.-M. Herbach, G. Renz
Calibration test of gas detectors from the FOBOS spectrometer
ibid., b) **p.251.**

C.-M. Herbach, H.-G. Ortlepp
Fragment mass identification using gas detector modules of the FOBOS array
ibid., b) **p.253.**

M. Andrassy, G.G. Chubarian, A.S. Fomichev, P. Gippner, Sh. Heinitz, C.-M. Herbach, A. Matthies, H.-G. Ortlepp, G. Renz, O.V. Strekalovsky, W. Wagner, G. Pausch
Pilot experiments using detectors of the FOBOS array
ibid., b) **p.255.**

C.-M. Herbach
Response of the FOBOS spectrometer concerning events from multifragmentation
ibid., b) **p.240.**

A.V. Daniel, D. Hilscher, E.M. Kozulin, Yu.E. Penionzhkevich, A.P. Tonchev, S.R. Voronin
Possibilities of the neutron measurement on the FOBOS set-up
ibid., b) **p.258.**

G. Renz, M. Andrassy, P. Gippner, C. Umlauf
The computer controlled evacuation and gas - supply system of FOBOS
ibid., b) **p.246.**

D. May, H.-G. Ortlepp, G. Renz, O.V. Strekalovsky
Electronics and data acquisition at the FOBOS detector test stand
ibid., b) **p.248.**

P. Ziem, T. Kiehne, L. Dietterle, C.-M. Herbach, S.A. Ivanovsky, O.V. Strekalovsky, V.V. Trofimov, V.E. Zhuchko,
Development of data acquisition and analysis software for FOBOS
ibid., b) **p.249.**

C.-M. Herbach, C. Umlauf
ATHENE - a program for data analysis of multi - parameter measurements
ibid., b) **p.250.**

G. Pausch, J. Krüger, W. Seidel, W. Wagner, C.-M. Herbach, A. Matthies, H.-G. Ortlepp, V.V. Trofimov, V.E. Zhuchko, H. Fuchs, H. Homeyer, G. Röschert, A. Tutay, P. Ziem, A. Budzanowski, A. Siwek, L. Zrodlowski
Extension of the ARGUS phoswich - array by a FOBOS gas - detector module and test of the FOBOS data acquisition system
Annual Report 1992, HMI - 507, Hahn - Meitner - Institut GmbH, Berlin, Deutschland, 1993, p.87.

A. Tutay, H. Fuchs, H. Homeyer, G. Pausch, G. Röschert, C. Schwarz, A. Siwek, A. Sourell, W. Terlau, A. Budzanowski, W. Kantor
.....
ibid., p.70.

M. Wilpert, Th. Wilpert
Anwender - Programme für Experimentsteuerung und -auswertung
ibid., p.93.

C. Beschoner, B. Drescher, T. Kiehne, C. Kluge, G. Röschert, V.V. Trofimov, T. Weigert, P. Ziem
Rechnergestützte Erfassung und Auswertung von experimentellen Daten
ibid., p.95.

G. Pausch, W. Bohne, H. Fuchs, D. Hilscher, H. Homeyer, H. Morgenstern, A. Tutay, W. Wagner
Particle identification in solid - state detectors by exploiting pulse - shape information
ibid., p.81.

G. Pausch, W. Bohne, D. Hilscher
Simulation of pulse - shapes in silicon detectors for heavy - ion spectroscopy
ibid., p.83.

G. Pausch, T. Funk
Measurement of charge - carrier mobilities in silicon detectors by means of pulse - length analysis
ibid., p.85.

M. Andrassy, G.G. Chubarian, A.S. Fomichev, P. Gippner, Sh. Heinitz, C.-M. Herbach, A. Matthies, H.-G. Ortlepp, G. Renz, O.V. Strekalovsky, G. Pausch, K.-D. Schilling, W. Wagner
Heavy - ion reaction experiments at the Dubna U - 400M cyclotron using detectors of the FOBOS array
ibid., p.75.

M. Andrassy, G.G. Chubarian, M. Danziger, P. Gippner, L. Dietterle, A.S. Fomichev, H. Fuchs, K. Heidel, C.-M. Herbach, D. Hilscher, H. Homeyer, I.A. Ivanenko, I.V. Kolesov, A. Matthies, D. May, Yu.Ts. Oganessian, W. von Oertzen, H.-G. Ortlepp, G. Pausch, Yu.E. Penionzhkevich, G. Renz, K.-D. Schilling, H. Sodan, O.V. Strekalovsky, V.V. Trofimov, V.M. Vasko, W. Wagner, P. Ziem
FOBOS - ein 4π – Detektor mit niedriger Energieschwelle für Schwerionenreaktionsprodukte
Frühjahrstagung DPG e.V., Mainz, Deutschland, 22. - 26. 3. 1993, Verhandl. DPG (VI) 28 (1993) S.565.

M. Andrassy, G.G. Chubarian, P. Gippner, C.-M. Herbach, A. Matthies, H.-G. Ortlepp, G. Pausch, G. Renz, K.-D. Schilling, W. Wagner
Analyse der Massen- und Impulsbilanz bei Messungen von Fragmenten aus Schwerionenreaktionen
Frühjahrstagung DPG e.V., Mainz, Deutschland, 22. - 26. 3. 1993, Verhandl. DPG (VI) 28 (1993) S.634.

G. Pausch, W. Bohne, H. Fuchs, D. Hilscher, H. Homeyer, H. Morgenstern, A. Tutay, W. Wagner
Identifikation schwerer Ionen in Halbleiterdetektoren durch Impulsformanalyse
Frühjahrstagung DPG e.V., Mainz, Deutschland, 22. - 26. 3. 1993, Verhandl. DPG (VI) 28 (1993) S.565.

A.S. Fomichev, W. Wagner, I. David, Z. Dlouhy, J.M. Corre, M. Lewitowicz, S.M. Lukyanov, A. Matthies, L. Nosek, H.-G. Ortlepp, Yu.E. Penionzhkevich, I. Pecina, M.G. Saint-Laurent, N.K. Skobelev, O.B. Tarasov
The resonse of a CsI(Tl) counter to light and intermediate mass fragments in the energy range 2 - 77 MeV/A
Preprint JINR P13 - 93 - 114, Joint Institute for Nuclear Research, Dubna, Russia, 1993.

A.S. Fomichev, I. David, S.M. Lukyanov, Yu.E. Penionzhkevich, N.K. Skobelev, O.B. Tarasov, A. Matthies, H.-G. Ortlepp, W. Wagner, M. Lewitowicz, M.G. Saint-Laurent, J.M. Corre, Z.Dlouhy, I.Pecina
The response of a large CsI(Tl) detector to light particles and heavy ions in the intermediate energy range
Report GANIL P 93 23, Laboratoire Commun IN2P3 (CNRS) - D.S.M (CEA), Caen, France, 1993.

W. Wagner, A.S. Fomichev, H.-G. Ortlepp, C.-M. Herbach, A. Matthies, G. Pausch, O.V. Strekalovsky, M.A. Milovidov, V.A.Vitenko
A large area CsI(Tl) detector for the scintillator shell of FOBOS
JINR Rapid Communications 4 [61] - 93, Joint Institute for Nuclear Research, Dubna, Russia, 1993, p.49.

H.-G. Ortlepp, M. Andrassy, G.G. Chubarian, M. Danziger, P. Gippner, L. Dietterle, A.S. Fomichev, C.-M. Herbach, A.I. Ivanenko, I.V. Kolesov, A. Matthies, D. May, Yu.Ts. Oganessian, Yu.E. Penionzhkevich, V.N. Pokrovsky, G. Renz, L.A. Rubinskaya, O.V. Strekalovsky, V.V. Trofimov, V.M. Vasko, K. Heidel, K.-D. Schilling, W. Seidel, H. Sodan, W. Wagner, V.E. Zhuchko, H. Fuchs, D. Hilscher, H. Homeyer, P. Ziem, G. Pausch, B.A. Burova, S.V. Radnev, I.D. Sandrev
The 4π – Fragment spectrometer FOBOS - Status and first preliminary results -
Proc. of the Internat. School-Seminar on Heavy Ion Physics, Dubna, Russia, May 10 - 15, 1993, JINR E7 - 93 - 274, vol. 2 (Ed. Yu.Ts. Oganessian, Yu.E. Penionzhkevich, R. Kalpakchieva) Dubna, 1993, p.466.

A.A. Aleksandrov, I.A. Aleksandrova, M. Andrassy, L. Dietterle, V.N. Doronin, P. Gippner, C.-M. Herbach, D. Hilscher, S.A. Ivanovsky, J. Krüger, A. Matthies, D. May, H.-G. Ortlepp, G. Pausch, Yu.E. Penionzhkevich, V.N. Pokrovsky, G. Renz, K.D. Schilling, D.I. Shishkin, O.V. Strekalovsky, V.V. Trofimov, C. Umlauf, D.V. Vakatov, V.M. Vasko, W. Wagner, V.E. Zhuchko
Fission and IMF emission in the reaction 43 AMeV ^{7}Li on ^{232}Th studied with FOBOS
Annual Report 1993, Institute of Nuclear and Hadronic Physics, Forschungszentrum Rossendorf e.V., Germany, FZR - 35 (Ed. F. Dönau, H. Prade) Rossendorf, 1994, p.55.

A.A. Aleksandrov, I.A. Aleksandrova, M. Andrassy, L. Dietterle, V.N. Doronin, P. Gippner, C.-M. Herbach, E.M. Kozulin, A. Matthies, D. May, H.-G. Ortlepp, Yu.V. Petkov, G. Renz, K.-D. Schilling, D.I.Shishkin, O.V. Strekalovsky, V.V. Trofimov, C. Umlauf, D.V. Vakatov, V.M. Vasko, W. Wagner, V.E. Zhuchko
Measurement of ^{244}Cm(sf) at FOBOS
ibid., p.57.

W. Wagner, P. Gippner, C.-M. Herbach, H.-G. Ortlepp
Ternary spontaneous fission of ^{244}Cm
ibid., p.59.

J. Krüger, A. Budzanowski, H. Fuchs, C.-M. Herbach, H. Homeyer, D.V. Kamanin, A. Matthies, H.-G. Ortlepp, G. Pausch, G. Röschert, W. Seidel, A. Siwek, V.V. Trofimov, A. Tutay, W. Wagner, R. Wolski, P. Ziem, V.E. Zhuchko,
Investigation of IMF emission and projectile fragmentation in the system ^{32}S (960 MeV) + ^{197}Au with the extended ARGUS detector
ibid., p.61.

G. Renz, V.M. Vasko, P. Gippner, M. Andrassy, V.N. Doronin, D.I. Shishkin
The gas - supply system of the FOBOS avalanche counters
ibid., p.90.

G. Renz, V.M. Vasko, P. Gippner, A. Matthies, M. Andrassy, V.N. Doronin, D.I. Shishkin, Sh. Heinitz
The gas - supply system of the FOBOS Bragg ionization chambers
ibid., p.91.

W. Wagner, H.-G. Ortlepp
The light output of CsI(Tl) for low - energy alpha particles
ibid., p.93.

G. Pausch, W. Bohne, D. Hilscher, H.-G. Ortlepp, D. Polster
Particle identification in a wide dynamic range based on pulse - shape analysis with solid - state detectors
ibid., p.99.

C.-M. Herbach, V.V. Trofimov, V.E. Zhuchko, L. Dietterle, D.V. Vakatov
Software development for FOBOS
ibid., p.108.

O.V. Strekalovsky, S.A. Ivanovsky, H.-G. Ortlepp, G. Pausch, G. Renz, V.V. Trofimov, W. Wagner, V.E. Zhuchko
The FOBOS data acquisition system in 1993
ibid., p.109.

C. Umlauf, D. May, G. Renz
Status of the software development for the FOBOS gas - vacuum system
ibid., p.111.

K. Heidel, H.-G. Ortlepp
Development of data acquisition electronics for FOBOS
ibid., p.113.

M. Andrassy, L. Dietterle, V.N. Doronin, P. Gippner, K. Heidel, C.-M. Herbach, D. Hilscher, S.A. Ivanovsky, J. Krüger, A. Matthies, D. May, H.-G. Ortlepp, G. Pausch, Yu.E. Penionzhkevich, G. Renz, K.-D. Schilling, D.I. Shishkin, O.V. Strekalovsky, V.V. Trofimov, C. Umlauf, D.V. Vakatov, V.M. Vasko, W. Wagner, Th. Wilpert, V.E. Zhuchko
Analyse von leichten, intermediären und Spaltfragmenten in der Reaktion ^{7}Li (43 AMeV) + ^{232}Th mit dem Multidetektorsystem FOBOS
Frühjahrstagung DPG e.V., München, Deutschland, 21. - 25. 3. 1994,
Verhandl. DPG (VI) 29 (1994) S.1888.

J. Krüger, A. Budzanowski, H. Fuchs, C.-M. Herbach, D. Hilscher, H. Homeyer, D. Kamanin, A. Matthies, H.-G. Ortlepp, G. Pausch, W. Seidel, A. Siwek, V.V. Trofimov, A.Tutay, W. Wagner, R. Wolski, L. Zrodlowski, V.E. Zhuchko
Untersuchung der Projektilfragmentation und IMF - Emission im System ^{32}S (960 MeV) + ^{197}Au am erweiterten ARGUS - Detektor
Frühjahrstagung DPG e.V, München, Deutschland, 21. - 25. 3. 1994,
Verhandl. DPG (VI) 29 (1994) S.1945.

G. Pausch, W. Bohne, H. Hilscher, H.-G. Ortlepp, D. Polster
Weiterentwicklung der Impulsformmethode zur Identifikation schwerer Ionen in Halbleiterdetektoren
Frühjahrstagung DPG e.V., München, Deutschland, 21. - 25. 3. 1994,
Verhandl. DPG (VI) 29 (1994) S.1883.

A.S. Fomichev, I. David, S.M. Lukyanov, Yu.E. Penionzhkevich, N.K. Skobelev, O.B. Tarasov, A. Matthies, H.-G. Ortlepp, W. Wagner, M. Lewitowicz, M.G. Saint-Laurent, J.M. Corre, Z. Dlouhy, I. Pecina, C. Borcea
The response of a large CsI(Tl) detector to light particles and heavy ions in the intermediate energy range
Nucl. Instr. and Meth. in Phys. Research A 344, 1994, p.378.

G. Pausch, W. Bohne, D. Hilscher
Particle identification in solid - state detectors by means of pulse - shape analysis
- Results of computer simulations -
(Preprint HMI - P /93/P2 - Pau1, Hahn - Meitner - Institut GmbH, Berlin, Deutschland, 1993)
Nucl. Instr. and Meth. in Phys. Research A337, 1994, p.573.

G. Pausch, W. Bohne, D. Hilscher, H.-G. Ortlepp, D. Polster
Particle identification in a wide dynamic range based on pulse - shape analysis with solid - state detectors
(Preprint FZR - 38, Forschungszentrum Rossendorf e.V., Germany, 1994)
Nucl. Instr. and Meth. in Phys. Research A 349, 1994, p.281.

A. Siwek, A. Sourell, A. Budzanowski, H. Fuchs, H. Homeyer, G. Pausch, W. Kantor, G. Röschert, C. Schwarz, W. Terlau, A. Tutay
Multifragmentation study on 30 AMeV ^{32}S + ^{58}Ni
Preprint HMI / FK - Fuc1, Hahn - Meitner - Institut GmbH, Berlin, Deutschland, 1994.

H.-G. Ortlepp, M. Andrassy, G.G. Chubarian, M. Danziger, T. Dietterle, A.S. Fomichev, Sh.M. Heinitz, C.-M. Herbach, A.I. Ivanenko, I.V. Kolesov, D. May, Yu.Ts. Oganessian, Yu.E. Penionzhkevich, G. Renz, L.A. Rubinskaya, O.V. Strekalovsky, V.M. Vasko, W.-D. Fromm, K. Heidel, H. Sodan, W. Wagner, B.A. Burova, S.V. Radnev, I.D. Sandrev
The FOBOS 4π - detector of charged particles at Dubna
Proc. of the Internat. Workshop on Physical Experiments and First Results on the Heavy Ion Storage and Cooler Rings, Smolenice, Slovakia, June 1 - 5, 1992, JINR E 7 - 94 - 270, Dubna, Russia,1994, p.388.

Yu.V. Pyatkov, A.A. Aleksandrov, I.A. Aleksandrova, B.I. Andreev, P. Gippner, C.-M. Herbach, E.M. Kozulin, A. Matthies, Yu.Ts. Oganessian, H.-G. Ortlepp, Yu.E. Penionzhkevich, G. Renz, K.-D. Schilling, O.V. Strekalovsky, V.M. Vasko, W. Wagner
Two-velocities measurements of fragment spectra in ^{244}Cm cold spontaneous fission on the FOBOS spectrometer
Internat. Workshop on Nuclear Fission and Fission Product Spectroscopy, Château de la Baume, Seyssins, France, May 2 - 4, 1994 (Ed. H. Faust & G. Fioni) Grenoble, 1994, p.144.

A.A. Aleksandrov, I.A. Aleksandrova, M. Andrassy, L. Dietterle, V.N. Doronin, P. Gippner, C.-M. Herbach, D. Hilscher, S.A. Ivanovsky, A. Matthies, D. May, H.-G. Ortlepp, G. Pausch, Yu.E.Penionzhkevich, V.N. Pokrovsky, G. Renz, K.-D. Schilling, D.I. Shishkin, O.V. Strekalovsky, V.V. Trofimov, C. Umlauf, D.V. Vakatov, V.M. Vasko, W. Wagner, V.E. Zhuchko
First experiments with FOBOS
Proc. of the 5th Internat. Conf. on Nucleus-Nucleus Collisions, Taormina, Italy, May 30 - June 4, 1994 (to be published as special issue of Nucl. Phys. A).

O.V. Strekalovsky, K. Heidel, S.A. Ivanovsky, D. May, H.-G. Ortlepp, G. Pausch, G. Renz, V.V. Trofimov, I.P. Tsurin, W. Wagner, V.E. Zhuchko
The front - end electronics and the data acquisition system of the FOBOS 4π - array
Proc. of the 16th Internat. Symp. on Nuclear Electronics, Varna, Bulgaria, September 12 - 18, 1994 (to be published).

O.V. Strekalovsky, H.-G. Ortlepp, V.V. Trofimov, V.E. Zhuchko
The data acquisition system of the FOBOS 4π - array
Proc. of the Internat. ESONE Conf. on Real - Time Data Systems, Dubna, Russia, August 1994 (to be published).

O.V. Strekalovsky, H.-G. Ortlepp, V.V. Trofimov, V.E. Zhuchko,
The data acquisition system of the FOBOS 4π - array
Conf. .. St. Petersburg, Russia, September 1994.

W. Wagner, H.-G. Ortlepp, D.V. Kamanin, A. Matthies, O.V. Strekalovsky, V.E. Zhuchko
Status of the FOBOS scintillator shell
a) **Scientific Report 1993 - 1994, Flerov Laboratory of Nuclear Reactions, Joint Institute for Nuclear Research, Dubna, Russia (to be published at JINR Dubna).**
b) **Annual Report 1994, Institute of Nuclear and Hadronic Physics, Forschungszentrum Rossendorf e.V., Germany (to be published)**

W. Wagner, A. Budzanowski, B. Czech, D. Hilscher, J. Holik, H. Homeyer, W. Janczur, H.-G. Ortlepp, G. Pausch, O.V. Strekalovsky, L. Zrodlowski
The FOBOS forward array
ibid. a) and b)

Yu.V. Pyatkov, A.A. Aleksandrov, I.A. Aleksandrova, B.I. Andreev, P. Gippner, C.-M. Herbach, E.M. Kozulin, A. Matthies, Yu.Ts. Oganessian, H.-G. Ortlepp, Yu.E. Penionzhkevich, G. Renz, K.-D. Schilling, O.V. Strekalovsky, V.M. Vasko, W. Wagner
Cold spontaneous fission of ^{244}Cm studied at FOBOS
ibid. a) and b)

W. Wagner, P. Gippner, C.-M. Herbach, H.-G. Ortlepp
Ternary spontaneous fission of ^{244}Cm
ibid. a)

A.A. Aleksandrov, I.A. Aleksandrova, M. Andrassy, L. Dietterle, V.N. Doronin, P. Gippner, C.-M. Herbach, D. Hilscher, S.A. Ivanovsky, A. Matthies, D. May, H.-G. Ortlepp, G. Pausch, Yu.E. Penionzhkevich, V.N. Pokrovsky, G. Renz, K.D. Schilling, D.I. Shishkin, O.V. Strekalovsky, V.V. Trofimov, C. Umlauf, D.V. Vakatov, V.M. Vasko, W. Wagner, V.E. Zhuchko
Correlations between intermediate mass and fission fragments in the reaction ^{7}Li (43 AMeV) on ^{232}Th studied at FOBOS
ibid. a) and b)

A.A. Aleksandrov, I.A. Aleksandrova, L. Dietterle, V.N. Doronin, S. Dshemuchadse, P. Gippner, C.-M. Herbach, S.A. Ivanovsky, D.V. Kamanin, A. Matthies, D. May, H.-G. Ortlepp, G. Pausch, Yu.E. Penionzhkevich, G. Renz, K.D. Schilling, D.I. Shishkin, O.V. Strekalovsky, V.V. Trofimov, I.P. Tsurin, C. Umlauf, D.V. Vakatov, V.M. Vasko, W. Wagner, V.E. Zhuchko
Study of fission and IMF emission in the reaction ^{14}N (34 AMeV) on ^{197}Au at FOBOS
ibid. a) and b)

G. Renz, V.M. Vasko, P. Gippner, A. Matthies, V.N. Doronin, D.I. Shishkin, C. Umlauf, M. Gebhardt
Status of the evacuation and gas - supply system of FOBOS
ibid. a) and b)

M. Gebhardt, V.N. Doronin, P.Gippner, H.-G. Ortlepp, G. Renz, D.I. Shishkin, W. Wagner
Test measurements performed with a Bragg ionization chamber
ibid. b)

Yu.V. Pyatkov, A.A. Aleksandrov, I.A. Aleksandrova, B.I. Andreev, P. Gippner, C.-M. Herbach, E.M. Kozulin, A. Matthies, Yu.Ts. Oganessian, H.-G. Ortlepp, Yu.E. Penionzhkevich, G. Renz, K.-D. Schilling, O.V. Strekalovsky, V.M. Vasko, W. Wagner
^{244}Cm cold spontaneous fission study on the FOBOS spectrometer
(submitted to Zeitschrift für Physik)

H.-G. Ortlepp, W. Wagner, A.A. Aleksandrov, I.A. Aleksandrova, L. Dietterle, V.N. Doronin, P. Gippner, C.-M. Herbach, D. Hilscher, S.A. Ivanovsky, A. Matthies, Yu.Ts. Oganessian, G. Pausch, Yu.E. Penionzhkevich, G. Renz, K.-D. Schilling, D.I. Shishkin, O.V. Strekalovsky, V.V. Trofimov, C. Umlauf, D.V. Vakatov, V.M. Vasko, V.E. Zhuchko, A.G. Artukh, G.F. Gridnev, M. Grushezki, J. Szmider, Yu.G. Teterev, M.G. Nagaenko, Yu.M. Sereda, I.N. Vishnevski,S.G. Genchev

The COMBAS - fragment - separator of radioactive nuclei and the FOBOS - 4p - detector for charged particles

Proc. of the Internat. Workshop on Physics with Recoil Separators and Detector Arrays, New Delhi, India, January 30 - February 2, 1995 (Allied Publishers Ldt.) New Delhi, 1995. (submitted to the publisher)

H.-G. Ortlepp, C.-M. Herbach, W. Wagner, P. Gippner, A. Matthies, G. Pausch, Yu.E. Penionzhkevich, G. Renz, K.-D. Schilling, O.V. Strekalovsky, V.E. Zhuchko

Fission and emission of intermediate - mass fragments in asymmetric heavy - ion collisions

Internat. Nuclear Physics Conference, Beijing, China, August 21 - 26, 1995. (submitted abstract)

(end of redaction , December 1994, W. W.)